UNIVERSIDAD AUTÓNOMA DE MADRID
FACULTAD DE CIENCIAS
DEPARTAMENTO DE BIOLOGÍA

DOCTORAL THESIS
Biology PhD

"LIPID METABOLISM ALTERATIONS IN COLORECTAL CANCER: POTENTIAL CLINICAL RELEVANCE IN THE PROGNOSIS OF THE DISEASE"

INSTITUTO MADRILEÑO DE ESTUDIOS AVANZADOS EN ALIMENTACIÓN (IMDEA FOOD INSTITUTE)

SILVIA CRUZ GIL

Madrid, 2018

UNIVERSIDAD AUTÓNOMA DE MADRID
FACULTAD DE CIENCIAS
DEPARTAMENTO DE BIOLOGÍA

DOCTORAL THESIS
Biology PhD

"LIPID METABOLISM ALTERATIONS IN COLORECTAL CANCER: POTENTIAL CLINICAL RELEVANCE IN THE PROGNOSIS OF THE DISEASE"

INSTITUTO MADRILEÑO DE ESTUDIOS AVANZADOS EN ALIMENTACIÓN (IMDEA FOOD INSTITUTE)

Memoria presentada por: **Silvia Cruz Gil**
Para optar al grado de: DOCTOR EN BIOLOGÍA

Directoras:
Ana Ramírez de Molina
Ruth Sánchez Martínez

Tutora:
Ana Ramírez de Molina

Doña Ana Ramírez de Molina, Doctora en Bioquímica y Biología Molecular por la Universidad Autónoma de Madrid, y Doña Ruth Sánchez Martínez, Doctora en Biología por la Universidad Autónoma de Madrid, investigadoras del Instituto IMDEA Alimentación, informan favorablemente la solicitud de autorización de defensa de la tesis doctoral con el Título: **"LIPID METABOLISM ALTERATIONS IN COLORECTAL CANCER: POTENTIAL CLINICAL RELEVANCE IN THE PROGNOSIS OF THE DISEASE**" por **COMPENDIO DE PUBLICACIONES**, presentada por Dª **Silvia Cruz Gil** para optar al grado de Doctor en Biología. Este trabajo ha sido realizado en el Instituto Madrileño de Estudios Avanzados en Alimentación (IMDEA Alimentación) bajo su dirección, y cumple satisfactoriamente las condiciones requeridas por el Departamento de Biología de la Universidad Autónoma de Madrid para optar al Título de Doctor.

Y para que así conste, firman el presente informe:

Dª Ana Ramírez de Molina

Dª Ruth Sánchez Martínez

This work was developed in the framework of two Spanish State Program projects:

- **Ministerio de Economía y Competitividad del Gobierno de España (MINECO, Plan Nacional I+D+i AGL2013-48943-C2 and AGL2016-76736-C3),**

- **Community of Madrid (Gobierno regional de la Comunidad de Madrid):P2013/ABI-2728, ALIBIRD-CM,**

- And with the support of **EU Structural Funds**.

The doctoral candidate got the opportunity to enjoy a European grant for a short research stage thanks to:

- Boehringer Ingelheim Fonds. Foundation for Basic Research in Medicine

and

- Universitätsklinikum Carl Gustav Carus, TU Dresden, Gastro-intestinal stem cell biology group under the supervision of Dr. Med. Daniel Stange, MD, PhD.

This doctoral thesis is based on the following research publications:

- **Publication I:** Ruth Sánchez-Martínez, Silvia Cruz-Gil, Marta Gómez de Cedrón, Mónica Álvarez-Fernández, Teodoro Vargas, Susana Molina, Belén García, Jesús Herranz, Juan Moreno-Rubio, Guillermo Reglero, Mirna Pérez-Moreno, Jaime Feliu, Marcos Malumbres, Ana Ramírez de Molina "A link between lipid metabolism and epithelial-mesenchymal transition provides a target for colon cancer therapy". **Oncotarget**, 2015. doi: 10.18632/oncotarget.5340

- **Publication II:** Ruth Sánchez-Martínez, Silvia Cruz-Gil, María Soledad García-Álvarez, Guillermo Reglero, Ana Ramírez de Molina. "Complementary ACSL isoforms contribute to a non-Warburg advantageous energetic status characterizing invasive colon cancer cells". **Scientific Reports**, 2017. doi: 10.1038/s41598-017-11612-3

- **Publication III:** Silvia Cruz-Gil, Ruth Sánchez-Martínez, Marta Gómez de Cedrón, Roberto Martín-Hernández, Teodoro Vargas, Susana Molina, Jesús Herranz, Alberto Dávalos and Ana Ramírez de Molina. "Targeting the lipid metabolic axis ACSL/SCD in colorectal cancer progression by therapeutic miRNAs: miR-19b-1 role". **The Journal of Lipid Research**, 2017. doi:10.1194/jlr.M076752

- **Publication IV:** Silvia Cruz-Gil, Dr. Ruth Sánchez-Martínez, Sonia Wagner-Reguero, Dr. Kristin Werner, Dr. Sebastian Schölch, Dr. Daniel Stange and Dr. Ana Ramírez de Molina. "A more physiological approach to lipid metabolism alterations in cancer: CRC-like organoids assessment" **(submitted for publication)**

And on the following review publication:

- Silvia Cruz-Gil, Dr. Ruth Sánchez-Martínez and Dr. Ana Ramírez de Molina. "Insights into fatty acid metabolism blockade in cancer development: ACSL/SCD axis" **(submitted for publication)**

Contributions to congresses and conferences during the PhD period:

- A link between lipid metabolism and epithelial-mesenchymal transition provides a target for colon cancer therapy.
  Ruth Sánchez-Martínez, Silvia Cruz-Gil S, Marta Gómez de Cedrón, Mónica Álvarez-Fernández, Teodoro Vargas, Susana Molina, Belén García, Jesús Herranz, Juan Moreno-Rubio, Guillermo Reglero, Mirna Pérez-Moreno, Jaime Feliu, Marcos Malumbres, Ana Ramírez de Molina. **Frontiers in Stem Cells & Cancer. EMBO/EMBL symposium**. 29-31 March, 2015. Heidelberg, Germany.

- Complementary ACSL isoforms contribute to a non-Warburg advantageous energetic status characterizing invasive colon cancer cells.
  Ruth Sánchez-Martínez, Silvia Cruz-Gil, María Soledad García-Álvarez, Guillermo Reglero and Ana Ramírez de Molina. **Beatson International Cancer Conference. FEEDING THE BEAST - The Metabolic Landscape of the Tumour and its Host**. 2-5 July, 2017. Glasgow, Scotland.

- Targeting the metabolic axis ACSL/SCD in colorectal cancer progression by therapeutic miRNAs: miR-19b-1 role.
  Silvia Cruz-Gil, Ruth Sánchez-Martínez, Marta Gómez de Cedrón, Roberto Martín-Hernández, Teodoro Vargas, Susana Molina, Jesús Herranz, Alberto Dávalos, Guillermo Reglero and Ana Ramírez de Molina. **Beatson International Cancer Conference. FEEDING THE BEAST - The Metabolic Landscape of the Tumour and its Host**. 2-5 July 2017. Glasgow, Scotland.

Comienza haciendo lo que es necesario, después lo que es posible y de repente estarás haciendo lo imposible

San Francisco de Asís

ACKNOWLEDGEMENTS

En primer lugar me gustaría dar las gracias a mis directoras de tesis: Ana, gracias por darme la oportunidad de entrar en el grupo y por confiar en mí para este proyecto de tesis. Eres un ejemplo de la cada vez mayor necesidad del papel de liderazgo de la mujer en la ciencia. Ruth, según me habían explicado, creo que te podría definir como todo lo contrario de una directora de tesis, y digo esto porque ha sido todo realmente fácil contigo. Gracias por tus incansables explicaciones, consejos y correcciones, porque tienes madera para enseñar de verdad, y porque gran parte de este trabajo es gracias a ti. Doy inmensas gracias por la suerte que he tenido de contar con vosotras.

A la dirección de IMDEA, en primer lugar al director Guillermo Reglero, porque tu motivación en este gran proyecto IMDEA me contagia siempre y me ha hecho querer formar parte de él desde el principio de manera activa. A la gerente, Inmaculada Galindo, gracias por tu trabajo, porque gestionar ciencia y científicos no debe resultar nada fácil. Gracias también al resto del grupo de administración, gracias por sacarnos de más de un aprieto.

A mi grupo de Oncología Molecular, un verdadero grupo de investigación, con verdadera dedicación y pasión por lo que hacen: Marta, Lara, Jorge, Lamia, Su, Mónica, Sonia, Marina y Adrián y los que formaron parte, de todos puedo decir que he aprendido mucho. Gracias por tener siempre tiempo para resolver un problema técnico, discutir de Ciencia, o de no-ciencia, dar nuevas ideas o alentar en los momentos más flojos. ¡Creo que formamos un gran equipo!

En especial quiero agradecer a mis compañeras pero sobre todo amigas Monica, Lara, Cris, Ruth y Sonia, gracias por las risas de cada día, por las interminables historias de cada una, por vuestras recetas de cocina, por aguantar mis tonterías, por siempre tener el consejo del día… Estos cuatro años no habrían sido igual sin vosotras

También al resto de compañeros de IMDEA. Su, es admirable tu forma de trabajar. Me llevo para siempre tus técnicas y consejos. También a nuestras innovadoras, María y Josune, incansables trabajadoras para todos nosotros. A Víctor, Ruth B, Lidia, Paloma,… como dan de sí las comidas del comedor. A Carmen, por animarme tanto en este año y ayudarme con las gestiones de la tesis. A mi compañera de box, Judit, por sus galletas de chocolate en las tardes interminables. Y a los demás grupos de investigación de IMDEA, plataforma GENYAL, servicio de estadística y bioinformática. ¡Sois grandes compañeros y grandes científicos!

A mis amigos de siempre, Ángeles, Iván, Sánchez, Isaac, Cris, César, a ellos por ser parte de mi camino. Por ser también parte de mis elecciones, por estar en todos los momentos pero no como espectadores sino involucrándose desde el corazón y haciendo también suyos mis pequeños logros. Gracias por hacerme ver que os interesaba mi investigación; por intentar

entender qué hacía exactamente en un laboratorio y en qué consistía, por venir corriendo de viaje a cambiar mis “androides”, por participar en *La noche de los Investigadores* y echar carreras de ADN. Gracias, por ser vosotros, y por hacerme sentir una amiga afortunadísima.

A mi familia, en especial a mis padres, sin ellos no sería quien soy ni habría llegado hasta aquí. Porque plantar una semillita cada día desde pequeña enseñándome el valor del esfuerzo, la constancia, y el trabajo duro ha dado sus frutos. Gracias papá porque parte de emprender esta aventura en la ciencia se la debo al inmenso entusiasmo que tienes por tu trabajo. Gracias mamá por confiar siempre en mis capacidades y alentarme a dar siempre lo mejor de mí. A mis hermanos pequeños, Víctor y Clara, por ser un gran equipo y apoyarnos siempre mutuamente. A Raquel, porque no es casualidad que la vida me haya llevado a hacer investigación en el campo del cáncer. Siempre mi ángel. A ti, especialmente, va dedicada mi tesis.

A Carlos, mi más continuo apoyo y fuerza. Gracias por hacer también este proyecto muy tuyo, gracias por querer entender siempre un poco más, por decirme una y mil veces que te volviera a explicar mi tesis. Gracias por creer siempre en mí, y valorarme mucho más de lo que yo lo hago, por hacerme ver que soy importante. Gracias por ser mi principal compañero de vida, y por todo lo que nos queda.

ABSTRACT

Colorrectal cancer (CRC) is the third most diagnosed cancer worldwide with nearly a million of deaths yearly. CRC does not present symptoms until advanced stages, leading to a reduction of the treatment efficacy. Therefore, new biomarkers for early detection need to be assayed. Alterations in different metabolic pathways such as carbohydrate have been broadly analyzed, but new elements of the metabolism have increased its importance in malignant progression, such as lipid metabolism. We first describe a metabolic acyl-CoA synthetase/ stearoyl- CoA desaturase ACSLs/SCD (ACSL1/ACSL4/SCD) signature leading to enhanced invasive and migratory capacities and stimulation of several survival pathways to CRC cells. This mesenchymal phenotype is restored upon reactivation of the master metabolic regulator, AMPK. Regarding the individual contribution of ACSL/SCD network enzymes, ACSL4 is related with increased proliferation and migration and a more glycolytic phenotype; while ACSL1 stimulates the presence of invasion and metastasis markers presenting a lower basal respiratory rate. ACSL1 is also characterized by an acylcarnitines elevation. Polyunsaturated fatty acids (PUFA) lower levels, probable due to a greater utilization, is the main feature for ACSL4 pro-proliferative cells; while monounsaturated fatty acids (MUFA) upregulation characterize the individual overexpression of SCD. The simultaneous overexpression of the network implies upregulated phospholipids and urea cycle derived metabolites showing that the global effect of the network is not performed by the sum of the individual overexpression effects. Besides, ACSL/SCD overexpressed cells present a better overall energetic status showed by lower basal respiration levels and upregulated creatine pathway. Other invasive CRC cell lines present these same features converting ACSL/SCD metabolic network in an example of metabolic adaptations for a more invasive phenotype.

Thus, the development of new therapies targeting this metabolic network may be useful for the cancer progression blockade or as biomarkers of the disease. In this sense, ACSL/SCD overexpression correlates with poorer clinical outcome and increased risk of relapse of stage-II colon cancer patients. Moreover, ACSL/SCD chemical inhibition by a combined specific treatment decreases cancer cell viability without affecting normal colon cells. Post-transcriptional regulation by microRNAs (miRNAs) also represents a therapeutic opportunity for ACSL/SCD axis. We described miR-544a, miR-142 and miR-19b-1 as major overall regulators of the metabolic axis ACSL/SCD. Outstandingly, miR-19b-1 is able to inhibit invasion in several CRC cell lines, and lower miR-19b-1 expression is related with poor survival rate in CRC patients (stages II and III); according to ACSLs/SCD overexpression involvement in patient relapse. This miRNA, therefore, could be used both as therapeutic or prognostic miRNA with a potential noninvasive biomarker role for disease-free survival (DFS) in CRC patients.

CRC-like organoids represent an excellent physiological tool modeling stages I to IV of intestinal tumors. We show that ACSL4 expression augmented with the stages in the organoids while miR-19b-1 diminished its expression. Besides, since Metformin is able to rescue the invasive and migratory phenotype conferred to cancer cells upon ACSL/SCD axis overexpression; we checked the effect of

Metformin treatment in organoids, resulting in a viability decrease in first tumor phases and in a downregulation of the stem cell biomarker LGR5, becoming an appealing chemotherapy drug for intestinal cancers. According to ACSL/SCD metabolic switch, Metformin action in CRC organoids is not related to a Warburg-effect impairment. This research contributes to the current issue of the use of Metformin as an anticancer drug in colorectal cancer (CRC), and reveals organoids as a representative tool platform to assay tumor stage-dependent drugs and a model for specific and personalized treatment.

RESUMEN

El cáncer colorrectal (CCR) es el tercer cáncer más diagnosticado a nivel mundial, con casi un millón de muertes al año. Este tipo de cáncer no presenta síntomas hasta las etapas más avanzadas, lo que conlleva una reducción en la eficacia del tratamiento y, por lo tanto, nuevos biomarcadores para su detección precoz deben ser analizados. Las alteraciones en diferentes vías metabólicas, como los carbohidratos, han sido ampliamente estudiadas. Sin embargo, nuevas rutas del metabolismo han ido aumentado su importancia en la progresión maligna, como es el metabolismo de los lípidos.

En primer lugar, hemos descrito una firma metabólica Acil-CoA sintetasa / Estearoil-CoA desaturasa (ACSLs / SCD (ACSL1 / ACSL4 / SCD)) capaz de aumentar sus capacidades invasivas y migratorias a la vez que estimula varias vías de supervivencia. Este fenotipo mesenquimático se restaura tras la reactivación del principal regulador metabólico, AMPK. Nuestro objetivo es comprender las diferencias funcionales y la contribución individual de la red metabólica de ACSLs/SCD. ACSL4, por su parte, está relacionado con una mayor proliferación y migración; de acuerdo con un fenotipo más glicolítico; mientras que ACSL1 estimula los marcadores de invasión y metástasis que presentan una tasa respiratoria basal más baja. ACSL1 también se caracteriza por un aumento de acilcarnitinas. Los niveles más bajos de ácidos grasos poliinsaturados, probablemente debido a una mayor utilización, es la característica principal de las células pro-proliferativas que sobreexpresan ACSL4; mientras que la sobre regulación de los ácidos grasos monoinsaturados caracteriza la sobreexpresión individual de SCD. La sobreexpresión simultánea de la red implica un aumento de fosfolípidos y metabolitos derivados del ciclo de la urea, lo que demuestra que el efecto global de la red no es la suma de la contribución individual. Además, las células que sobreexpresan ACSL/SCD presentan un mejor estado energético general mostrado por unos niveles de respiración basal más bajos y un aumento de la vía de creatina. Otras líneas celulares de CCR invasivas presentan estas mismas características que convierten a la red metabólica ACSL/SCD en un ejemplo de adaptaciones metabólicas de un fenotipo más invasivo. Por lo tanto, el desarrollo de nuevas terapias dirigidas a esta red metabólica puede ser útil para el bloqueo de la progresión del cáncer así como el estudio de nuevos biomarcadores de la enfermedad. En este sentido, la sobreexpresión de ACSL/SCD se correlaciona con un peor pronóstico clínico y un mayor riesgo de recaída en pacientes con cáncer de colon en estadio II. Desde un punto de vista terapéutico, la inhibición química de ACSL/SCD mediante tratamiento específico combinado disminuye la viabilidad de las células cancerosas sin afectar a las células de colon normales. Los microRNAs (miRNA) emergen como potentes reguladores post-transcripcionales y, por lo tanto, como una oportunidad terapéutica convincente para el eje ACSL/SCD. A partir de una base de datos de treinta y un

supuestos miRNAs comunes que se predice que actúan simultáneamente en la red ACSL/SCD; las validaciones *in vitro* señalan a miR-544a, miR-142 y miR-19b-1 como los principales reguladores globales del eje metabólico. Cabe destacar que una reducción en la expresión del miR-19b-1 está relacionada con una menor tasa de supervivencia en pacientes de CCR (estadios II y III); de acuerdo con los datos de sobreexpresión de ACSL/SCD en la recaída del paciente. Además, el miR-19b-1 es capaz de inhibir la invasión en varias líneas celulares de CCR, de nuevo evidenciando la capacidad del eje ACSL /SCD de conferir propiedades invasivas a dichas células. Este miRNA, por lo tanto, podría usarse como miRNA terapéutico o pronóstico en un posible papel biomarcador no invasivo para la supervivencia libre de enfermedad en pacientes con CCR.

Para un análisis más profundo del eje metabólico, los organoides de tipo CCR implican una herramienta más fisiológica que representa las etapas I a IV del tumor. Se muestra como ACSL4 aumentó mientras que miR-19b-1 disminuyó su expresión, progresivamente a lo largo de la serie de organoides. Además, dado que el eje ACSL/SCD estimula la progresión del cáncer de colon, y la Metformina es capaz de revertir el fenotipo invasivo y migratorio conferido por dicho eje; verificamos el efecto del tratamiento con Metformina en los organoides como modelo para el tratamiento específico y personalizado, convirtiéndose en un fármaco quimioterapéutico plausible en las primeras fases del tumor. La Metformina también es capaz de disminuir la expresión del biomarcador de células madre LGR5 +, reafirmando su uso potencial en los cánceres intestinales. A su vez se muestra que la acción de la Metformina en los organoides tipo CCR no está relacionada con el efecto de Warburg. Esta investigación contribuye a la investigación actual del uso de la Metformina como fármaco anticanceroso en el cáncer colorrectal, así como revela a los organoides como una plataforma ventajosa para analizar fármacos dependientes de la etapa tumoral, acercándonos a una medicina más personalizada.

LIST OF ABBREVIATIONS

AA	Arachidonic acid
ACC	Acetyl-coenzyme A carboxylase / Acetyl-CoA carboxylase
Ac-CoA	Acetyl-coenzyme A or acetyl-CoA
ACLY	ATP citrate lyase
ACSBG	Bubblegum acyl-CoA synthetase
ACSL	Long-chain acyl-CoA synthetase
ACSL1	Long-chain Acyl-CoA synthetase 1
ACSL4	Long-chain Acyl-CoA synthetase
ACSM	Medium-chain acyl-CoA synthetase
ACSS	Small-chain acyl-CoA synthetase
ACSVL	Very long-chain acyl-CoA synthetase
AGPAT	Acylglycerolphosphate acyltransferase
AICAR	5-Aminoimidazole-4-carboxamide ribonucleotide
Akt	Serine/threonine kinase
ALDH1A1	Aldehyde Dehydrogenase 1 Family Member A1
AMPK	AMP-activated protein kinase
APC	Adenomatous polyposis coli gene
ATGL	Triglyceride lipase
ATP	Adenosine triphosphate
CACT	Carnitine-acylcarnitine translocase
cDNA	Complementary DNA
CI	Cell Index
CIC	Citrate carrier
CIN	Chromosomal instability
CMS	Consensus molecular subtypes
COX2	Cyclooxygenase-2
CPTI	Carnitine palmitoyltransferase I
CPTII	Carnitine palmitoyltransferase II
CrAT	Carnitine acetyltransferase
CRC	Colorectal cancer
CSC	Cancer stem cell
Ct	Threshold cycle
CTNNB1	Catenin Beta 1 gene
DAPI	4’,6-diamidino-2-phenylindole
DFS	Disease free survival
DG	Diacylglycerol
DGAT	Diacylglycerol acyltransferase
DNA	Deoxyribonucleic acid
DMEM	Dulbecco Modified Eagle Medium
DMSO	Dimethyl sulfoxide
ECAR	Extracellular Acidification Rate
ECM	Extracellular matrix
EdU	5-ethynyl-2’-deoxyuridine
EMT	Epithelial-mesenchymal transition
EpCAM	Epithelial Cell Adhesion Molecule

ER	Endoplasmic reticulum
Erk	Extracellular-signal-regulated kinase
ETC	Electron transport chain
FA	Fatty acid
FABP	Fatty-acid binding protein
FA-CoA	Fatty acyl-CoA
FADH	Flavin adenine dinucleotide (reduced)
FAO	Fatty acid oxidation
FAP	Familial adenomatous polyposis
FASN	Fatty acid synthase
FBS	Fetal bovine serum
FCCP	Carbonyl cyanide-4 (trifluoromethoxy) phenylhydrazone
FFA	Free-fatty acid
Foxo3	Forkhead Box class O 3
FS	Final Score
GAPDH	Glyceraldehyde-3-phosphate dehydrogenase
GC-MS	Gas Chromatography Mass Spectrometry
GPAT	Glycerol-3-phosphate acyltransferase
GPC	Glycerophosphocholine
GPI	Glycosylphosphatidylinositol
GSH	Glutathione
GSK3β	Glycogen synthase kinase 3 beta
G3P	Glycerol 3-phosphate
HER2	Human epidermal growth factor receptor 2
HCC	Hepatocarcinoma
HNPCC	Hereditary non-polyposis colorectal cancer
HR	Hazard ratio
HSL	Hormone-sensitive lipase
Hyp c	Corrected hypergeometric test
IBD	Inflammatory Bowel disease
IS	Individual score
KRAS	Kirsten rat sarcoma viral oncogene homolog
K18	Keratin 18
LC-MS	Liquid Chromatography Mass Spectrometry
LD	Lipid Droplet
LGR5	Leucine Rich Repeat Containing G Protein-Coupled Receptor 5
LPA	Lysophosphatidic acid
LUAD	Lung adenocarcinoma
MAGL	Monoacylglycerol lipase
MAPK	Mitogen-activated protein kinase
MMR	DNA mismatch repair
MSI	Microsatellite instability
mTOR	Mammalian target of rapamycin
mRNA	Messenger RNA
µM	Micromolar

MiRNAs/ miR	MicroRNAs
MTT	3-(4, 5-dimethylthiazol-2-yl)-2, 5-diphenyltetrazolium bromide
MUFA	Monounsaturated fatty acid
NADH	Nicotinamide adenine dinucleotide
NADPH	Nicotinamide adenine dinucleotide phosphate
OCR	Oxygen consumption rate
ORF	Open reading frame
OA	Oleic acid
OAA	Oxaloacetate
PA	Phosphatidic acid
PAP	Phosphatidic acid phosphohydrolase/ phosphatidic acid phosphatase
PBS	Phosphate buffered saline
PC	Phosphatidylcholine
PCA	Principal component analysis
PE	Phosphatidylethanolamine
PEP	Phosphoenolpyruvate
PFK-1	Phosphofructosekinase-1
PG	Phosphatidylglycerol
PI	Phosphatidylinositol
PI3K	Phosphatidylinositol 3-kinase
PIP3	Phosphatidylinositol (3,4,5)-trisphosphate
PJS	Peutz-Jeghers syndrome
PK	Pyruvate kinase
PLs	Phospholipids
PS	Phosphatidylserine
PTEN	Phosphatase and tensin homolog
PUFA	Polyunsaturated fatty acid
RNA	Ribonucleic acid
ROS	Reactive oxygen species
Rot/AA	Rotenone/Antimycin A
RT-QPCR	Quantitative reverse transcription polymerase chain reaction
SCD	Stearoyl-CoA desaturase
SDS	Sodium dodecyl sulfate
SFA	Saturated fatty acid
SLC25A1	Solute Carrier Family 25 Member 1
SMAD4	SMAD family member 4
SNPs	Single Nucleotide Polymorphisms
SREBP	Sterol regulatory element-binding protein
STK-11	Serine threonine kinase 11
TCA	Tricarboxylic Acid cycle
TG	Triglycerides
TLR	Toll-like receptor
TNBC	Triple-negative breast cancer
TP53 or P53	Tumor protein p53
WB	Western Blot

WT	Wild-type
2D	2-dimensional
2-DG	2-Deoxy-D-glucose
3D	3-dimensional
3’UTR	3´- untranslated region
5-FU	5-fluorouracil

TABLE OF CONTENTS

TABLE OF CONTENTS

INTRODUCTION

1. Colorectal cancer

1.1. Statistics

According to the International Agency for Research on Cancer (IACR), colorectal cancer (CRC) is the third most common cancer in men (746,000 cases, 10% of the total), after lung and prostate cancer, and the second in women (614,000 cases, 9.2% of the total), after breast cancer [1,2].

Latest Spanish statistics from REDECAN (Red Española de Registros de Cáncer)[3], claim that almost 250.000 new patients were diagnosed with invasive cancer: 149,000 in men (60.0%) and 99,000 in women (40. 0 %). In Spain, CRC raises to the second position of the most common cancers both in men (16.6%), after prostate cancer; and in women (16.9%).

Curiously, statistics highlight the stabilization of cancer incidence in men due to a decrease in tobacco-related cancers compensated by the increase in other types of tumors like CRC and prostate cancer. However, in women, the stabilization of breast cancer incidence has been overcome by the escalation of colorectal and tobacco-related cancers incidence.

For the next years, the main efforts will be to intensify smoking control policies and CRC early diagnosis to reduce the incidence of lung cancer and CRC, respectively. For all these facts, CRC has become one of the greatest priorities in worldwide Healthcare Institutions.

1.2. Risk factors

CRC risk factors can be divided into the ones that can be avoided and the ones that cannot be avoided. Generally, CRC rates are found to be higher in developed countries such as in Europe, North America, Japan and Oceania and are increasing rapidly in less developed countries such as Latin America, Asia and Eastern Europe [4], which reflects the influence of western lifestyles implementation and therefore, the existence of avoidable risk factors.

Among these modifiable risk factors, being obese or overweight give a greater chance of developing CRC, especially in men [5]; through plausible biological mechanisms such as insulin resistance, hyperinsulinemia, chronic inflammation, altered levels of growth factors, adipocytokines and steroid hormones [6,7]. Furthermore, diet has been extensively correlated with

cancer; concretely, high red-meat diets (such as beef, pork, lamb, or liver), processed meats (such as bacon, sausages, hot dogs, salami, corned beef, beef jerky and ham) or over-cooked meats (frying, broiling, or grilling), which creates risky chemicals[8–10]. Even though the fats` role it is not completely clear, diets enriched in fibers such as vegetables, fruits or whole-grain foods have been linked to a lower risk of CRC [11].

Physical inactivity has been also related to CRC risk. Albeit mechanisms are not entirely clear, the hypotheses for the benefits of having an active lifestyle are abundant, such as increasing gut motility and reducing gastrointestinal material transit time, enhanced immune function as well as decreasing insulin and insulin-like growth factor levels, decreasing obesity, enhancing free radical scavenger systems and influencing prostaglandin levels [12,13]. Smoking, which is the main risk for developing lung cancer, has been also linked to CRC [14]. Alcohol consumption has been also reported to represent a strong risk; particularly in cancers of the upper aerodigestive tract, CRC, liver and breast cancer through aberrant patterns of DNA methylation [15].

Regarding the CRC risk factors that are not susceptible to be changed, we can find age, with a higher risk above 50; and gender, with a slightly higher risk in man than in woman. Medical histories predisposing to CRC are colorectal polyps and inflammatory bowel disease (IBD), including either ulcerative colitis or Crohn's disease. Finally, genetics is determinant for CRC risk such as having a family history of CRC or adenomatous polyps or having an inherited syndrome like familial adenomatous polyposis (FAP) and Lynch syndrome (hereditary non-polyposis colorectal cancer, or HNPCC) [16–20].

Taking into account the above-mentioned data, changes in diet and lifestyle could prevent the avoidable risk factors improving the quality of life for people. This, together with early diagnosis routines could derive into potent prevention tools for CRC.

1.3. Histopathological characteristics

The intestinal wall includes three layers: mucosa (which includes epithelial cells, basement membrane, lamina propria [connective tissue] and muscularis mucosae), submucosa (with three levels of depth) and muscularis propria (the muscle layer) (Figure 1).

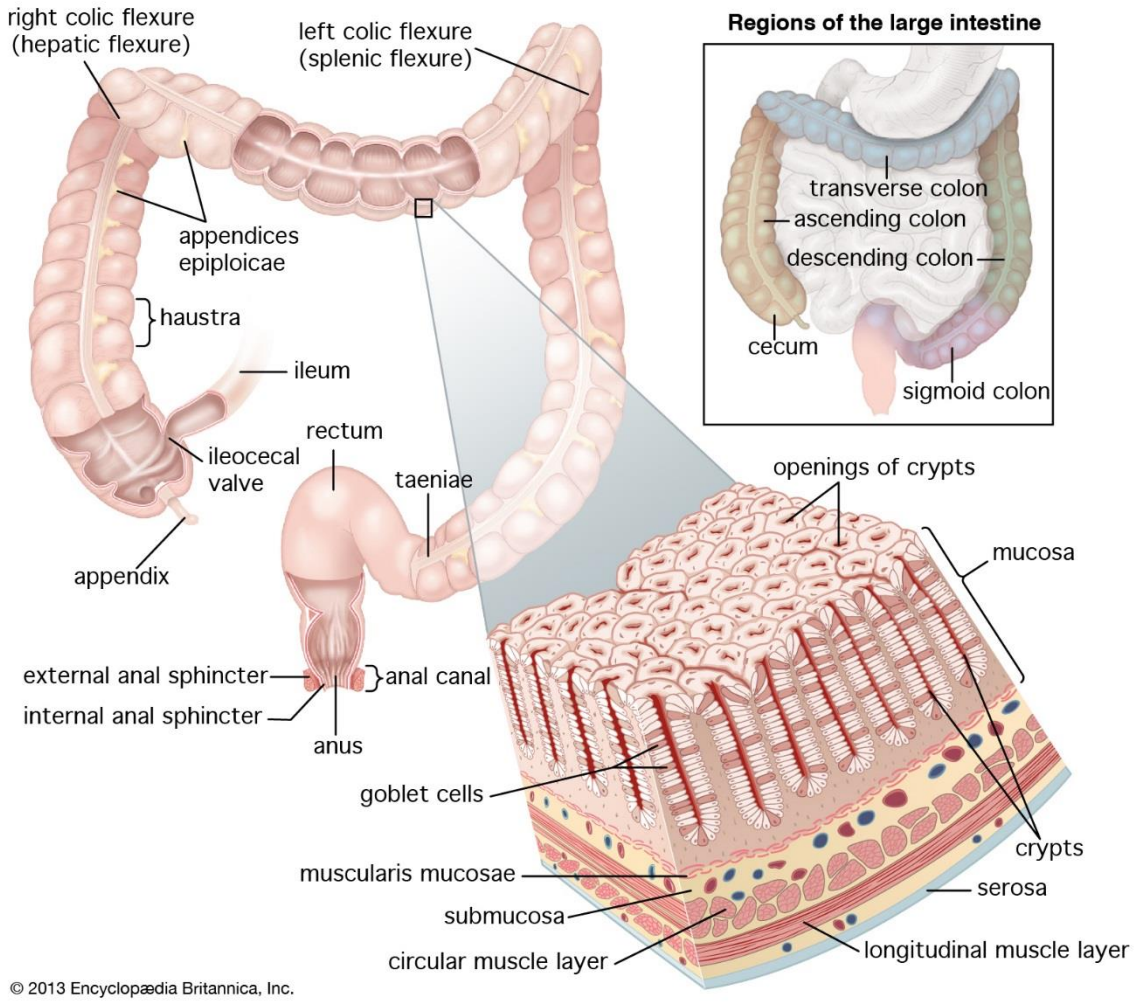

Figure 1: Human large intestine division. (Source: Encyclopædia Britannica, Inc. [21])

The intestinal epithelium is in constant flux of cell renewal to maintain homeostasis processes [22]. The epithelial cells keep attached to the basement membrane, which is part of the extracellular matrix. The assembly is performed by different proteins secreted by both epithelial and stromal cells, mainly fibroblast which lie below the membrane. Other cell types in this stromal cell layer include endothelial cells, which form the walls of capillaries, lymphatic vessels and immune cells.

Beneath this layer, there is a thick layer of smooth muscles responsible for intestinal peristalsis through periodic contractions.

The earliest phases of colorectal tumorigenesis initiate in the normal mucosa, in the epithelial layer; which could undergo a generalized disorder of cell replication with the appearance of clusters of enlarged crypts (aberrant crypts) showing proliferative, biochemical and biomolecular abnormalities. It is possible to observe a variety of tissue states with different degrees of abnormality, to mildly divergent tissues and high malignancy state, and finally into multiple metastatic growths. The majority of colorectal malignancies develop from adenomatous polyps. These can be defined as well determined masses of epithelial dysplasia, with uncontrolled crypt cell division. All these forms are considered benign until neoplastic cells pass through the muscularis mucosae and infiltrate the submucosa [23] (Figure 2).

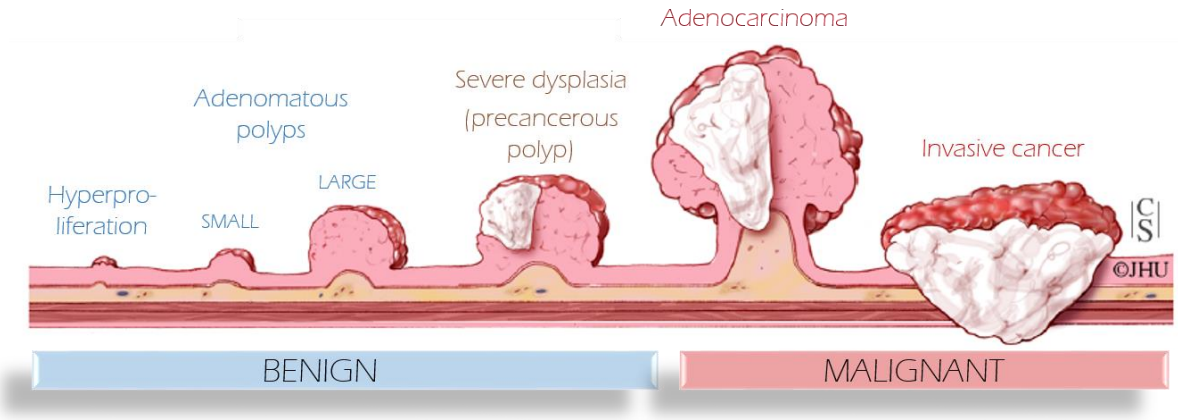

Figure 2: Colorectal cancer development from lesions in the colon and polyps. (Source: Adapted from Johns Hopkins Colon Cancer Center [24]).

Among colorectal carcinomas, more than 90% are adenocarcinomas, originated from epithelial cells of the colorectal mucosa. Other rare types of colorectal carcinomas include neuroendocrine, squamous cell, adenosquamous, spindle cell and undifferentiated carcinomas. The glandular formation is the main characteristic of adenocarcinoma, which is also the basis for histologic tumor grading. Besides, in well-differentiated adenocarcinoma, more than 95% of the tumor is gland forming [25].

The reasons why the incidence of CRC is so high could be determined by the histopathological characteristics of the tissue. Large intestine owns a high rate of cell division required to maintain

the rapid turnover of cells within the intestinal epithelia, which causes a high incidence of DNA replication errors and therefore the accumulation of DNA mutations in these cells. Also, the direct exposure of intestinal cells to potential carcinogens via ingested food further increases the mutation rate.

1.4. Staging

Since 1959, The American Joint Committee on Cancer (AJCC) established a universal staging model named Tumor-Node-Metastasis (TNM), which has been developed and improved over the years.

The TNM (Tumor, Nodes, and Metastasis) system is based on tumor infiltration degree and divides it regarding the intestinal wall layer in which it has spread. Thus, it codes the extent of the primary tumor (T), whether it arrives at regional lymph nodes (N), or invades other organs causing distant metastases (M) [26,27].

Tis represents the carcinoma in situ or intramucosal carcinoma (involvement of lamina propria with no extension through muscularis mucosae). When the tumor invades submucosa it is entitled T1. If the tumor moves through the muscularis propria it is called T2. In T3, the tumor is able to invade the pericolorectal tissues. Finally, in T4a, the tumor invades through the visceral peritoneum, and in T4b, the tumor directly invades or adheres to other adjacent organs or structures. Lymph node detection is also remarkably important to predict the outcome of patients. To this aim, the number of regional lymph nodes must be examined. The N0 classification means lymph nodes are metastases free. When 1-3 lymph nodes are detected it changes to N1. In N2, metastases in 4 or more regional lymph nodes can be counted. The M0 and M1 values for cancer patients, indicates the presence or absence of metastases respectively. The TNM categories are combined in stage groups, ranging from 0 (in situ tumor) to IV (distant metastasis). The higher the stage is, the less the probability of survival. In fact, the survival rate at 5 years of people with stage I colon cancer is about 92%, while stage IV colon cancer patients have a 5-year relative survival rate of about 11% [28–30].

Table 1: TNM staging. (Source: Based on American Joint Committee on Cancer data (AJCC))

Stage 0:	Tis	N0	M0
Stage I:	T1 - T2	N0	M0
Stage IIA:	T3	N0	M0
Stage IIB:	T4a	N0	M0
Stage IIC:	T4b	N0	M0
Stage IIIA:	T1 - T2	N1 / N1c	M0
	T1	N2a	M0
Stage IIIB:	T3 - T4a	N1 / N1c	M0
	T2 - T3	N2a	M0
	T1 - T2	N2b	M0
Stage IIIC:	T4a	N2a	M0
	T3 - T4a	N2b	M0
	T4b	N1 - N2	M0
Stage IVA:	any T	any N	M1a
Stage IVB:	any T	any N	M1b
Stage IVC:	any T	any N	M1c

1.5. Genetics

In recent times it has been demonstrated with increasing evidence the heterogeneity of CRC and that these molecular or genetic differences in the tumor, determine the prognosis and response to treatment [31].

Traditionally, CRC has been divided as following described. Most of the CRC cases are sporadic (70-80%), which consists of the acquisition of somatic mutations and in which there is no family history or genetic predisposition. The remaining cases (20-30%) are divided into: inherited (less than 10%), in which germline mutations are present and can be transmitted between generations, and familial (or non-syndromic), among close-degree relatives [32]. They have a higher risk of developing CRC in comparison with the general population, although not as high as in the inherited syndromes [33]. A small subgroup of around 1–2 % of CRC cases is the consequence of IBD [34].

Among the CRCs which present a hereditary origin (inherited), we can mention the two most common types: Familial adenomatous polyposis (FAP) and the Hereditary Non-Polyposis CRC (HNPCC, also named Lynch syndrome).

As it is above mentioned, CRC occurs sporadically in the majority of cases, mainly in patients who have a median age of 70–75 years, and approximately 70% of these tumors develop in the distal colon. Genetically, their development is due to the accumulation of abnormalities in tumor suppressor genes and oncogenes [35]. Sporadic CRC follows different genetic pathways such as: chromosomal instability (CIN) (70% of sporadic CRC) [36], microsatellite instability (MSI) pathway caused by dysfunction of DNA MMR genes, mostly *MLH1* [37] and CpG island methylation [38].

Previous research postulated the adenoma-carcinoma transition theory proposed by Fearon and Vogelstein [39] in which specific somatic mutations promoting tumorigenesis were acquired. Their multistep cancer progression model is popularly called the Vogelgram and suggests that the adenoma to carcinoma sequence is initiated by alterations in the *APC* gene, followed by mutations in *KRAS* or *BRAF* genes, *PI3KCA* or *PTEN*, mutations or loss of *TTP53* gene and of SMAD family member 4 (*SMAD4*) (Figure 3). The Vogelgram is based on the CIN pathway for sporadic CRC.

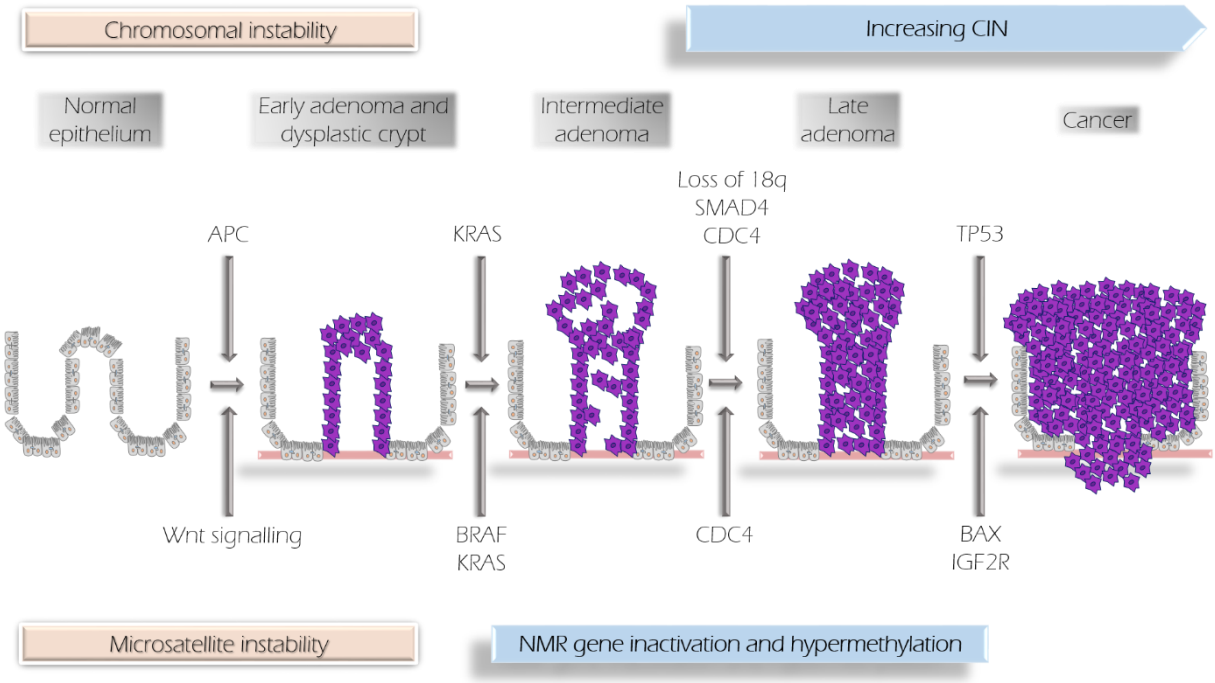

Figure 3 Adenoma–carcinoma sequence model for chromosomal instability in colorectal cancer (Source: Adapted from Walther, A. *et al.* [40])

1.5.1 The Molecular Consensus Subtypes of CRC

Although different efforts have been made to stratify CRC through gene expression profiling in different groups [41–45],no one of them lead to a useful, consistent and universal classification system making traditional classifications sometimes insufficient to determine the scope of the prognosis and the accuracy to treatment [31].

The Cancer Genome Atlas (TCGA) is an ambitious project which applies high-throughput genome analysis techniques together with bioinformatics to catalogue genetic mutations in different types of cancer [46]. CRC results were released in 2012 [47]. To date, though, the most compelling CRC classification was performed by an international expert consortium [48] that describes four consensus molecular subtypes (CMS) after analysis of 18 different CRC gene expression datasets, including data from TCGA in conjunction with molecular data on mutations and somatic copy number alterations (SCNA) for a subset of samples (Figure 4).

This CMS classification has been suggested as the basis for upcoming clinical stratification in terms of subtype-based targeted interventions, although further research is needed to fully complete this classification [32]. The first subtype is CMS1 (microsatellite instability-immune) or MSI-like. It represents the 14 % of CRC and is characterized by a hypermutated status due to defective DNA mismatch repair. This group, evidence a strong immune activation and poor survival rates. The CMS2 subtype (canonical, 37 %) shows epithelial features and are activated by the Wnt-β-catenin pathway. CMS2 patients have a better survival rate after relapse compared with the other subtypes. The CMS3 (metabolic, 13 %) subtype, more hypermutated/MSI than CMS2 and CMS4, still, presents fewer SCNA. It is frequently KRAS mutated, displays epithelial markers and present a general metabolic dysregulation. The CMS4 subtype (mesenchymal, 23 %) shows epithelial-mesenchymal transition (EMT) genes expression increased, TGF-β over activation, and overexpression of genes involved in angiogenesis, matrix remodeling and stromal invasion. CMS4 patients have the poorest overall and relapse-free survival among all the subtypes. The final 13% is grouped in a mixed subtype which represents a transition phenotype or intratumor heterogeneity [48].

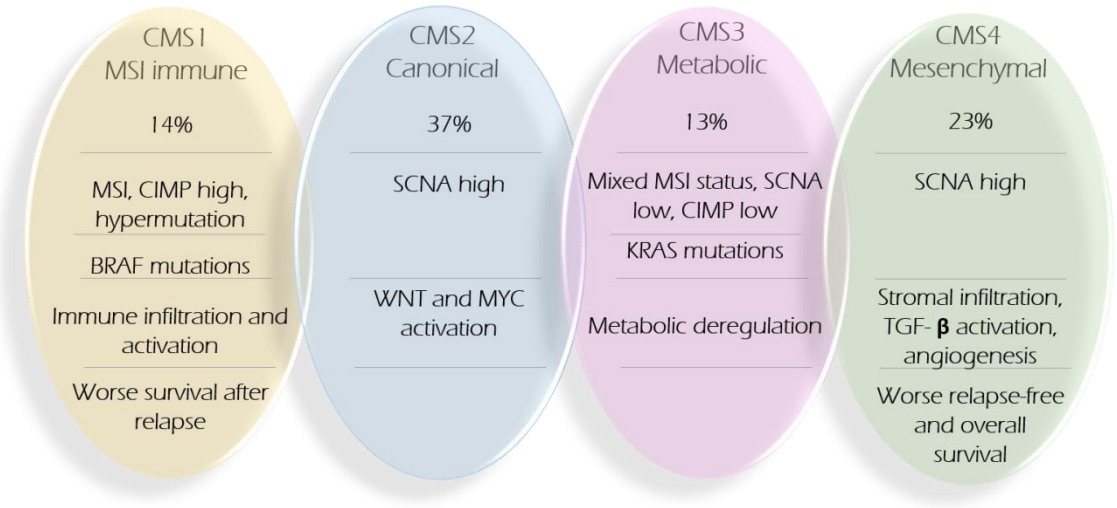

Figure 4: Consensus Molecular Subtypes classification (Source: Adapted from Guinney, J. *et al.* [48])

2. Metabolic abnormalities in cancer

2.1. Metabolic reprogramming as a hallmark of cancer

In a landmark article [49] the development of a human tumor is characterized by six different biological capabilities comprising sustaining proliferative signaling, evading growth suppressors, resisting cell death, enabling replicative immortality, inducing angiogenesis, and activating invasion and metastasis. Genome instability and inflammation were not initially incorporated but both of them underlie these hallmarks. Over the last decade, the understanding of the dimension and complexity of a tumor lead to the incorporation of the two last hallmarks [50]: reprogramming of energy metabolism and evading immune destruction (Figure 5).

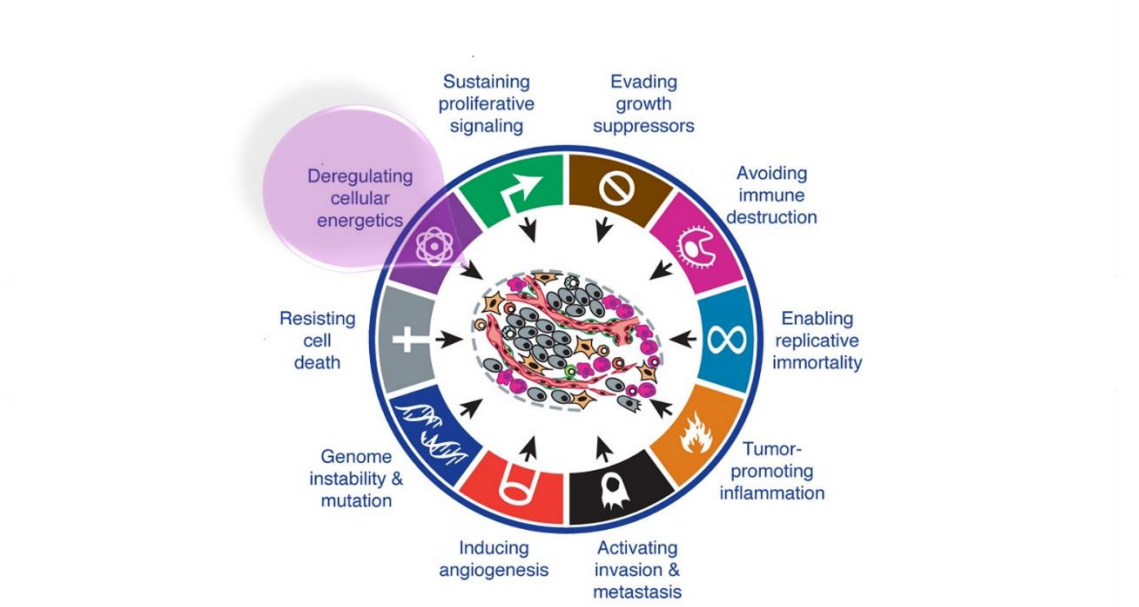

Figure 5: The Hallmarks of cancer. The next generation (Source: Adapted from Hanahan, D. & Weinberg, R. A.[50])

Over the last decade, the interest in metabolic research with respect to cancer has been expansively increased. Since 1990 the scientific production linking cancer and metabolism has increased more than 10-fold (Table 2).

Table 2: Number of publications since 1990 regarding cancer and metabolism- (Source: Based on Web of Science, Clarivate statistics content)

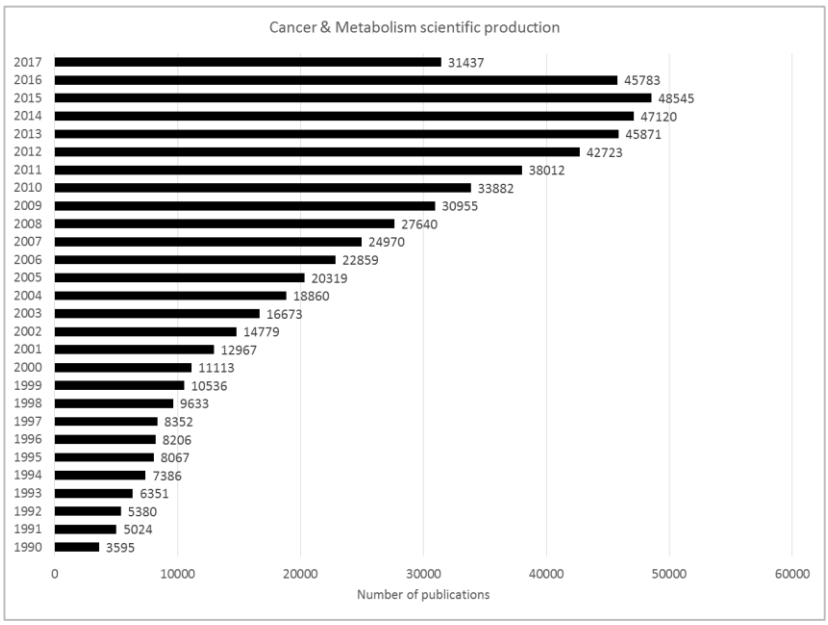

2.2. Glucose and glutamine abnormalities in cancer development.

Cancer is mainly considered a cell growth and proliferation disorder. Cellular building blocks, such as nucleic acids, proteins, carbohydrates and lipids are required to this effect [51]. Tumor cells alter their metabolism to accumulate intermediates as sources of these building blocks; which will efficiently generate energy and biomass components for their expansion and later dissemination. Despite the high diversity in type and etiology, cancer cells frequently share this metabolic reprogramming feature.

The first and most characterized tumor metabolism event to be described is an exacerbated glucose uptake and glycolysis utilization leading to increased lactate production, so that carbohydrates from glucose even in normoxic condition are not used for maximal ATP generation via mitochondrial respiration, but to make up other molecules instead of oxidizing them to carbon dioxide [51]. This phenomenon is often denoted as the "Warburg effect" due to Dr. Otto Warburg discovery between 1930 and 1956 [52], which could be understood as an energetically wasteful alteration.

Another metabolic alteration in which cancer cells depend on is the glutamine consumption. Glutamine serves as an important source of reduced nitrogen and carbon for amino-acids, nucleotides and lipids biosynthesis [53]. Glutamine is the major substrate to produce α-ketoglutarate, which enters in the Krebs cycle and it is responsible also for the production of pyruvate [54]. Glutamine metabolism also leads by reversal enzymes reactions to citrate, essential for the production of acetyl-groups for fatty acid synthesis (FAS) [55].

Even though lipid- and cholesterol-associated pathways are functionally dependent on glucose and glutamine catabolic pathways, these metabolic pathways are now recognized as relevant metabolic features with a key role in tumorigenesis (Figure 6).

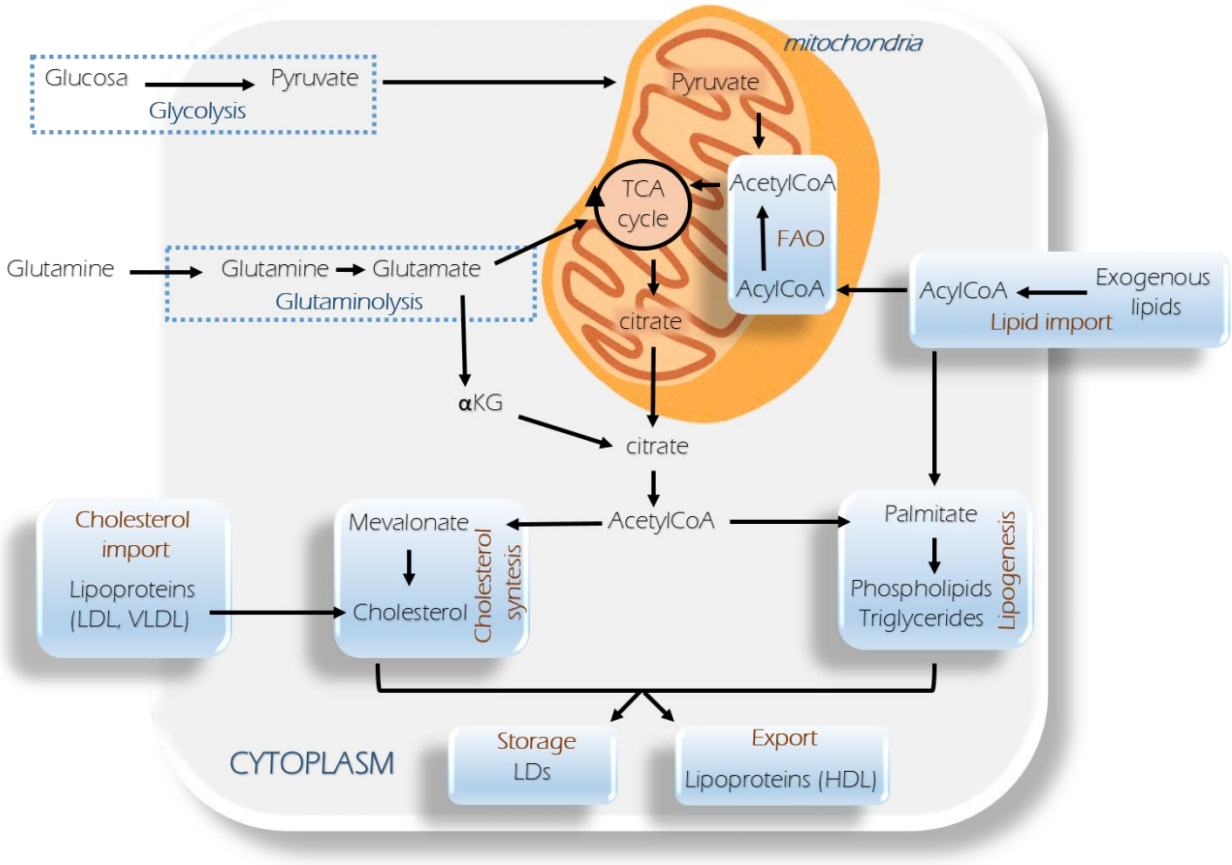

Figure 6: Main metabolic pathways in cancer cells.

2.3. Lipid metabolism alterations during cancer development: FA metabolism significance

Lipids comprehend a vast group of molecules in terms of their chemical structure**:** fatty acids (FA) chain length, position and number of double bonds and backbone structure (glycerol and sphingoid bases). Lipids perform multiple biochemical functions during cancer development including cell membrane composition (phosphatidylcholine (PC) and phosphatidylethanolamine (PE), sterols, sphingolipids, and lyso-phospholipids (lyso-PLs)), lipid rafts formation for signaling, protein recruitment and thus protein-protein interactions leading to signal transduction involved in cell survival, angiogenesis, and metastatic processes; as well as energy sources [51,56,57].

The majority of these lipids contain FA in their backbones. FA are made up of a terminal carboxyl group and a hydrocarbon chain that can be either saturated or unsaturated. As a lipid category, FA are also essential for energy storage, membrane biogenesis, and the creation of signaling molecules. FA as building block could be provided by both, exogenous sources or being

synthesized *de novo*. As the main source of lipids, proliferating tumor cells prefer to synthesize FA *de novo*, rather than utilizing exogenous sources like the majority of non-transformed human cells [58,59]. The point of departure for *de novo* FA synthesis is acetyl-CoA which connects this route with major core metabolic pathways.

Lipid metabolism abnormalities have recently become a remarkable feature of cancer metabolism. Despite initially not been paid too much attention, FA metabolism abnormalities in cancer progression have been increasingly recognized over the last years, in fact, there has been a 10-fold increment in the scientific production on the topic (Table 3) in the last years. One of these first reports, in 1950, suggested the tumor cells rewiring in the glucose and lipid metabolism scenario to sustain their growth and survival [58,60]. Since then, several reports claimed the importance of FA availability in the progression of cancer [51], devoting special attention to the reprogramming of FA metabolism that suggests novel therapeutic approaches to fight cancer [51,61–64]. Of importance are the recent reports of FA metabolism in cancer stem cells [65,66].

Table 3: Number of publications since 1990 regarding cancer and lipid metabolism - (Source: Based on Web of Science, Clarivate statistics content).

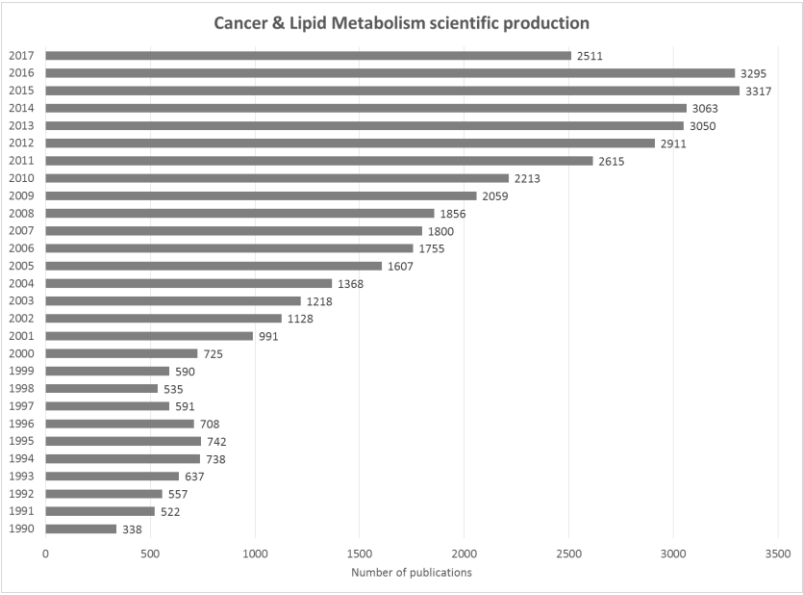

2.3.1. Restricting fatty acid availability

Nowadays, there is plenty of evidence suggesting that enzymes involved in lipid synthesis pathways, and especially in FA synthesis and availability, could be appealing therapeutic targets in cancer. To this aim, five ways to target FA availability can be considered (Cruz-Gil et al, "review submitted for publication"), such as targeting lipid storage formation, their hydrolysis, FA synthesis, FA oxidation, and finally, avoiding FA activation.

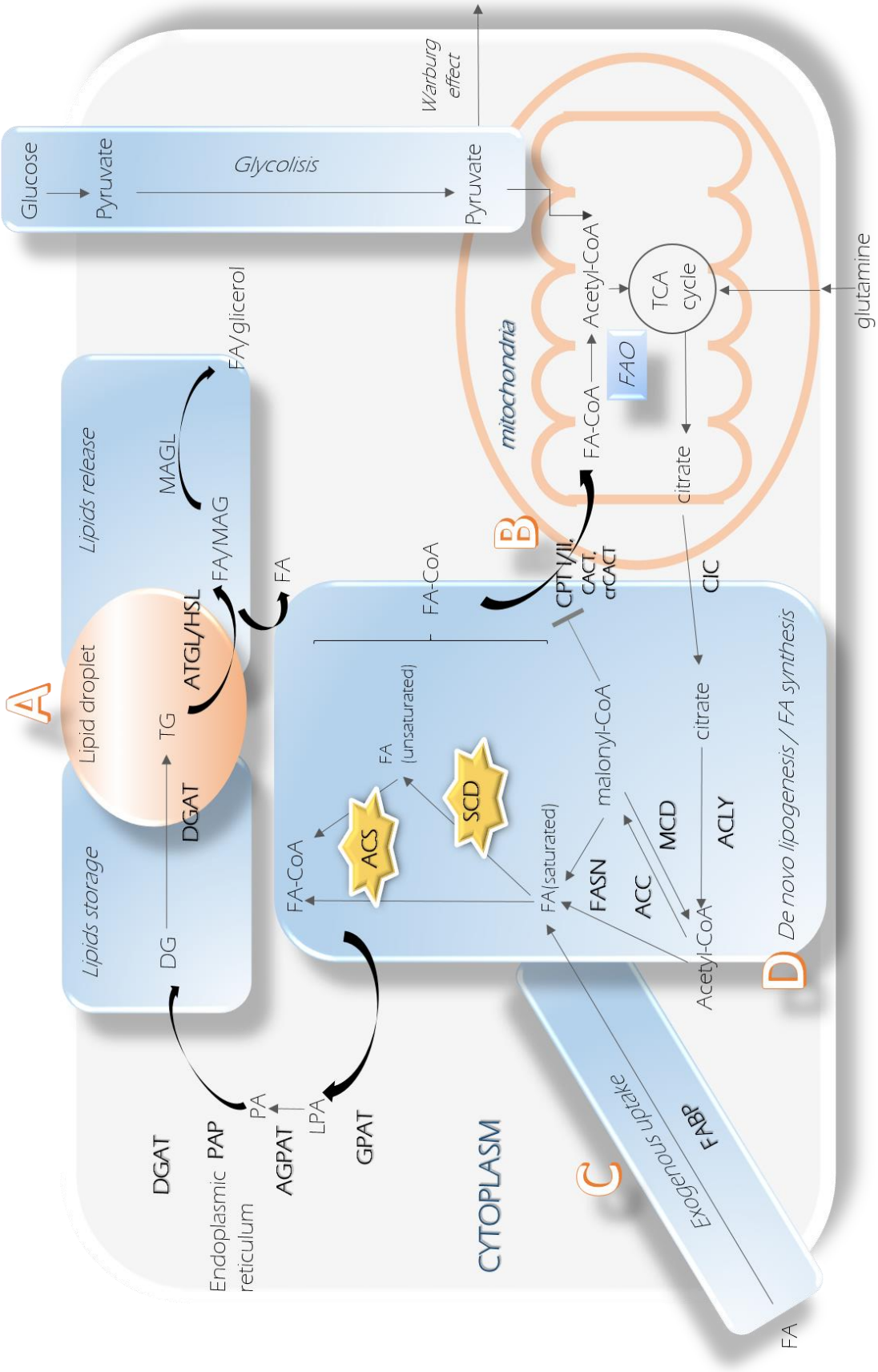

Figure 7: Fatty acid pathways involvement in cancer progression (Source: Cruz-Gil, et al., submitted for publication)

2.3.1.1. Increasing lipids storage

Lipid droplets (LD) represent the main site of energy storage [67] in nearly every eukaryotic cell [68]. Tumor cells prefer endogenous sources, accumulating these LD [69] and being considered as hallmarks of cancer aggressiveness [70,71]. The goal could probably be to avoid lipotoxicity of lipids in the cytoplasm or to have a readily available source of them [69]. Glycerol-3-phosphate acyltransferase (GPAT), acylglycerolphosphate acyltransferase (AGPAT), phosphatidic acid phosphohydrolase (Lipin or PAP), and diacylglycerol acyltransferase (DGAT) are part of this route converting FA-CoA into diacylglyceride (DG) (Figure 7, A, lipids storage). The pathway intermediates could lead to the synthesis of biological membranes components, or act as lipid signaling molecules for cancer progression [72]. Hence, these enzymes overexpression, except for the last one, lead to cancer events [51,73–76], suggesting that efforts should be focused on their blockade [77]. Increasing storage through DGAT activation could be a potential strategy for cancer prevention [78,79], since endogenous FA availability represents also an oncogenic stimulus *per se* that could lead to tumor malignant progression [80]. This strategy should be accompanied by lipids hydrolysis obstruction. All in all, LDs storage role in cancer cells is still not well understood [81] and need further study to be considered as a potential target for cancer treatment.

2.3.1.2. Avoiding lipid droplets hydrolysis

During LD hydrolysis and release of their molecules (Figure 7, A, lipids release), the triglyceride (TG) molecule is hydrolyzed consequentially by three enzymes**: triglyceride lipase (ATGL), hormone-sensitive lipase (HSL), and monoacylglycerol lipase (MAGL)**. Preventing the release of FAs from TG can be a strategy to reduce their availability.

ATGL is the rate-limiting enzyme hydrolyzing TG into DG and FA. Elevated ATGL (and HSL to an extent) activity may be a general feature of many cancer types as a strategy to obtain an extra FAs input [82]. However, other studies report the downregulation of ATGL linked with several malignant tumors [83–85]. In these cases, though, the overexpression of ATGL or HSL could be detrimental for the patient due to its association with cachexia [86]. Upregulated expression of MAGL was observed in several human cancers and primary tumors [87,88]. In conclusion, there are again scarce data concerning lipids storage and release role in cancer progression. Moreover, certain enzymes display dual roles dependent on the tumor type as well as lipids droplets that show a controversial role in cancer. Further analysis is needed before considering them as potential targets for therapeutic strategies, claiming that other routes could be more suitable when confronting cancer.

2.3.1.3. Unraveling fatty acid oxidation

Fatty acid oxidation (FAO) is mainly a repeated cycling for FA shortening producing in each cycle NADH, FADH, and acetyl-CoA. NADH and FADH besides representing redox power, could enter the electron transport chain (ETC), therefore producing ATP [56]. It has long been thought that cancer cells prevail in the utilization of metabolic intermediates for anabolic processes which aim is to construct cell building blocks. Therefore, enhancing catabolic routes such as FAs β-oxidation to limit their concentration levels could, in theory, be beneficial. Nevertheless, data from experiments testing this idea are contradictory. Cancer cells could require increased ATP production in different situations. In fact, greater evidence has been reported in the last years linking elevated levels of different enzymes related to oxidation processes in cancer [56].

For FAO it is essential the carnitine palmitoyltransferase system that is in charge of transporting FA, previously activated as FA-CoA, from the cytoplasm into the mitochondria to enter the β-oxidation route (Figure 7, B). This transport system is composed by **carnitine palmitoyltransferase I** (**CPTI)**, the **carnitine-acylcarnitine translocase** (**CACT**), **carnitine palmitoyltransferase II** (**CPTII)** and the **carnitine acetyltransferase (CrAT),** which closes the carnitine cycle. The connection of this transport system with cancer has been extensively described by Melone *et al*. [89].

The reported overexpression of the previous enzymes in different cancer types [89] suggests that FA could serve as energy sources and metabolic fuel for tumor growth and proliferation through the mitochondrial oxidation pathway. But controversial results exist, especially for CPTII [90,91], which difficult the establishment of therapeutic strategies based on these enzymes. Nevertheless, further studies over the entire system could open a new avenue of cancer therapies.

2.3.1.4. Avoiding extra fatty acids input

Fatty-acid-binding proteins (FABPs) are a small intracellular lipid transporters family with an affinity for long-chain free fatty acids and other ligands. These enzymes transfer FA from extracellular compartments besides being involved in intracellular transport [92]. Despite FABPs do not take part in *de novo* FA synthesis pathways (Figure 7, C), this family blockade needs to be taken into consideration since some tumors gather lipids from their surroundings to potentiate *de novo* FA synthesis for their own benefit [61]. Though distinct isoforms of these enzymes have been found upregulated in several tumors [93,94], controversial results are also found, such as those indicating a negative correlation between FABP4 overexpression and cancer progression in

(HER2)-positive breast tumors [95]. It is noteworthy that these enzymes perform not only intracellular but also extracellular actions. New studies point out their critical role as mediators of metabolic and inflammatory processes [96,97]; and some specific isoforms are also involved in hormone control [98]. Hence, these enzymes arise as interesting candidates for the development of therapeutic strategies, which justify further and deeper studies.

2.3.1. 5. Blocking Fatty Acid Synthesis enzymes

Finally, the main and most effective way to reduce FA availability is to inhibit the enzymes responsible for their synthesis (Figure 7, D). The linking point between glucose metabolism and *de novo* lipogenesis is the citrate. The citrate enters the Krebs cycle when is located in mitochondria, but its translocation to the cytoplasm by mitochondrial **citrate carrier (CIC)** or SLC25A1, feeds *de novo* FA synthesis [99]. Limiting this translocation by inhibiting this carrier has been performed resulting in anti-tumor activity [100]. However, CIC inhibition could lead to citrate accumulation inside the mitochondria, feeding the TCA cycle and therefore exacerbating the Warburg effect, which could represent a handicap for its potential use as a therapy.

Blocking the next enzyme in the route, **ATP citrate lyase (ACLY, ACL, or ATPCL)**, has stronger effects than CIC [101]. ACLY converts citrate to acetyl CoA and its levels have been found to be fairly increased in tumors compared to normal cells, including CRC, broadly reviewed by Khwairakpam *et al*. [102]. Nevertheless, inhibiting this enzyme would affect other pathways since its product acetyl-CoA is a core central molecule not only to FA synthesis but also to glucose, glutamine and mevalonate pathways [103], as well as to protein acetylation reactions, controlling major cellular processes such as autophagy, energy metabolism, mitosis, etc. [104,105].

Acetyl-CoA carboxylase (ACC) is a rate-limiting enzyme in *de novo* fatty acid synthesis converting acetyl-CoA in Malonyl-CoA. Malonyl-CoA synthesized by ACC isoform 1 (ACC1) is the substrate for FA synthesis, but if synthesized by ACC2 is a CPT inhibitor, thus preventing FA degradation via β-oxidation [106]. ACC has been extensively documented in cancer development and progression [106,107]. In the majority of studies, the overexpression of FA synthesis enzymes such as ACC along with its immediate downstream group of enzymes known as FASN, indicates tumor progression and cell malignancy [106,108,109].

Fatty acid synthase (FASN) is possibly the most studied enzyme related to FA metabolism and cancer. FASN catalyzes consecutive condensation reactions to form long-chain fatty acids from a molecule of acetyl-CoA and malonyl-CoA, mostly generating 16-carbon palmitate. FASN is associated with poor clinical outcomes, presents a universal upregulation and is involved in the progression, maintenance and enhancement of the malignant phenotype in most human cancers [110–115]. Despite the more than proved evidence for FASN involvement in tumor metabolic reprogramming, the clinical scenario has remained uncompleted with first generation inhibitors, though it is getting improved with next-generation FASN inhibitors [116].

Finally, it is worthy to briefly mention the role of **sterol regulatory element-binding protein (SREBP)** in cancer metabolism, able to modify metabolic genes expression. SREBP is conceived as the master transcriptional regulator of FA synthesis [117], and represents gene expression control of the main lipid metabolism enzymes. In non-transformed cells it maintains lipid homeostasis [118], regulating genes from the routes previously mentioned (ACLY, ACC, FAS, as well as SCD-1, and GPAT). In addition, a growing number of reports suggest SREBP implication in uncontrolled cancer cells proliferation such in prostate cancer patients [119] or breast cancer patients [120]. Hence, SREBP inhibition in cancer cells leading to FA synthesis genes downregulation could represent a therapeutic window to prevent cancer cell proliferation.

2.3.1.6. Fatty acid activation: strategic core in metabolism obstruction

Acyl-CoA Synthetases

Before a FA enters any metabolic pathway it needs to be activated by the addition of a molecule of coenzyme A (CoA). These free FA are converted to acyl-CoA (FA-CoA) by **acyl coenzyme A synthetase (ACS)** (Figure 7, E) in an ATP-dependent manner in the presence of CoA and Mg^{2+} [121]. This allows the FA to enter multiple physiological and metabolic routes such as TG synthesis and cholesterol esters, retinal esters and phospholipids, β-oxidation (peroxisomes, mitochondria), ω-oxidation (ER), elongation and/or desaturation, signaling molecules and protein acylation among others [122]. The largest family of mammalian ACS is the long-chain acyl-CoA synthetases (ACSL) family, which catalyze the formation of acyl-CoA from FA with 12-20 carbon atoms chain lengths [123]. To date, five isoforms of the ACSL mammalian family have been identified: ACSL1, -3, -4, -5 and -6, which present different preferences regarding the chain length of their FAs substrates.

The expression of ACSL family members varies in different tissues and also in its subcellular location [122].

ACSL1 is expressed in multiple subcellular locations such as mitochondria, peroxisomes, plasma membrane, ER and lipid droplets nucleus; but also in GLUT4 vesicles, reviewed by Grevengoed *et al*. [122]. It has been associated with the elevated levels of the unsaturated FA oleate and linoleate [124,125]. ACSL3 is abundantly expressed in lipid droplets and ER and is mainly required for FA uptake. Importantly, its N-terminus is able to translocate FAs from the ER to LD [126]. ACSL4 is most commonly located in the ER, mitochondrial-associated membrane, and peroxisomes [127] and has a clear substrate preference for arachidonate with respect to linoleic acid [128]. ACSL4 has also been reported to increase the conversion of free arachidonic acid (AA) into prostaglandins and into PE, PI and TG [129,130]. ACSL5 is also located on mitochondria, supporting FA synthesis and β-oxidation [131] with a marked preference for palmitic acid, palmitoleic acid, oleic acid and linoleic acid [132]. Finally, ACSL6 is found in the plasma membrane and has a clear preference for C16-C20 saturated and polyunsaturated FAs [133,134]. Together with ACSL3, it is predominant in the brain [135].

Acyl-CoA Synthetases and cancer

Previous reports associated patients with inflammatory bowel disease (IBD) with the over-expression of ACSL1 and ACSL5 in the terminal ileum and colon [136]. IBD represents a risk feature for developing CRC [137], suggesting the possible role of these isoforms in CRC initiation. A systematic analysis of the ACSL family members gene expression in various kinds of cancers has also been made [132] . This analysis concluded that ACSL1 was upregulated in CRC but diminished in lung and breast cancer as well as in the brain, cervical, esophageal, head and neck, leukemia, liver, and sarcoma cancers. Chen *et al*. also analyzed the prognostic value of ACSL1 in cancer progression, relating breast cancer and CRC patients' poorer survival rates with increased ACSL1 expression.

ACSL3 has been reported to be overexpressed in lung cancer [138] and melanoma [132], but in contrast lower levels were found in prostate cancer tissues [139] or ovarian cancer [132]. Besides, from the systematic analysis previously mentioned, ACSL3 was overexpressed in head-neck and liver cancer, but it was under expressed in CRC.

ACSL4 was previously associated with the colon carcinogenesis [132,140,141]; with tumor cell growth in liver cancer [142], and described as an independent prognostic factor in patient tissue analysis [143]. Similarly, it has been implicated in cell growth, invasion and hormonal resistance in prostate

cancer cell lines [144], positively correlated with a specific subtype of breast cancer and frequently downregulated in gastric cancer tissues [145]. ACSL4 was downregulated in tumor bladder, brain, leukemia, and lung cancer [132].

On the contrary, ACSL5 lower expression was observed in the CRC tissue, leading to longer disease free-survival (DFS) [146]. High expression of ACSL5 predicted good prognosis in glioma [147], breast, ovarian, and lung tumors, predicting good prognosis [137].

ACSL6 was decreased in most forms of cancers, except for CRC; according to Chen Oncomine analysis [132]. In addition, the expression of ACSL6 was downregulated in leukemia with good prognosis, emerging as a potential tumor suppressor gene in leukemia [132].

Stearoyl-CoA desaturase 1

Stearoyl-CoA desaturase (SCD) is a rapidly-degraded ER membrane protein which catalyzes the first desaturation in delta 9-cis carbon of acyl-CoA (Figure 7, E), downstream ACSLs action. It presents a clear preference for palmitoyl-CoA (C16:0) and stearoyl-CoA (C18:0) producing palmitoleoyl-CoA (C16:1) and oleoyl-CoA (C18:0), respectively. The products of SCD desaturation also act as substrates for the synthesis of different lipids such as phospholipids, diacylglycerols, triglycerides, cholesterol and wax esters. There are two isoforms of SCD in human cells (SCD1 and SCD5). SCD1 gene is ubiquitously expressed while SCD5 expression is limited in certain adult human tissues [148–150].

Stearoyl-CoA desaturase 1 and cancer

SCD represents the biosynthetic source of components for a plethora of lipids, such as the precursors oleic and palmitoleic acids, the most abundant MUFAs with central roles in tumor progression allowing cellular membrane biogenesis, energy storage and cell signaling [151].

The ratio between saturated versus unsaturated fatty acids (SFA / MUFA) is crucial for cancer cells since its alterations affect fluidity and protein dynamics. Several studies point to elevated MUFAs in blood cancer patients causing an increase of cancer episodes, poorer prognosis and higher death rate in patients [152,153] (for review see [154]). Likewise, along the years SCD has been reported to have a determinant role in various types of tumor including lung, breast, prostate, colon, kidney, thyroid and lymphoma, and its inhibition has shown effectiveness for suppressing different tumor aspects (reviewed in [151,154]). For instance, SCD regulates apoptosis in

hepatocarcinoma [155] and prostate cells [156], increases hepatoma cells proliferation [157], and its inhibition reduces tumor cells survival in breast and prostate cancer [158].

Regarding CRC, SCD is able to promote tumor cell proliferation and apoptosis inhibition [159], besides augmenting metastasis through MUFA increased production [160]. In addition, SCD is involved in several gene signatures, evidencing that *de novo* fatty acid synthesis is increased in these tumors [161,162].

SCD1 is key in the control of the overall scenario of lipid synthesis in cancer cells [154] by mainly three processes. Firstly, SCD1 channels FA to the different lipid metabolic routes, on one hand by augmenting MUFA ratio for the biosynthesis of phospholipids needed for the membrane biogenesis process in rapidly replicating cells; and on the other hand by reducing the toxic accumulation of extra SFA in cell membranes, which generates ER stress, lipid-mediated cytotoxicity and, eventually, cell death [163,164]. Secondly, SCD is able to modulate the catalytic activity of ACC through the saturated acyl-CoA molecules which act as allosteric inhibitors of ACC [165,166]. Finally, SCD1 could enhance the lipogenesis induced by SREBP [154] . Additional SCD1 overexpression known effects in cancer include increased cell proliferation, survival, cell cycle progression, colony formation and invasiveness, which leads to tumor formation and metastasis [154].

3. Posttranscriptional regulation: miRNAs

Post-transcriptional regulatory mechanisms might represent new therapeutic opportunities for cancer treatment. Among them, microRNAs (miRNAs), have emerged as potent epigenetic modulators [167].

miRNAs are endogenous non-coding small RNAs which were first discovered in 1993 in the nematode *C.elegans* [168]. MiRNAs play key roles in the regulation of gene expression at the post-transcriptional level, fine-tuning the expression of almost 30% of all mammalian protein-encoding genes. A mature microRNA is constituted by approximately 18-22 nucleotides in length in single-stranded RNA molecules [169]. To date, over 38500 miRNAs have been identified and cataloged in the public database miRbase (www.mirbase.org). MiRNAs have been identified in animals, plants and viruses [170].

3.1. MicroRNAs transcription, processing and gene expression regulation

Genes encoding for microRNAs are transcribed by RNA polymerase II as long primary transcripts (pri-microRNA). Also in the nucleus, a pri-microRNA is processed by a protein complex containing the RNase III enzyme Drosha, to form a hairpin-like of approximately 70 nucleotide precursor microRNA (pre-microRNA). This precursor is subsequently exported to the cytoplasm by Exportin 5 where it is processed again by a second RNase III enzyme, DICER, producing the mature microRNA. The mature microRNA is then incorporated into a ribonuclear particle to form the RNA-induced silencing complex, RISC, which mediates gene silencing, bind to complementary regions within messenger RNAs to promote their degradation through precisely complementary pairing and/or to inhibit translation through non-precisely complementary pairing [167,169,171,172]. Gene silencing is usually performed upon the binding of the miRNA to the 3'UTR of the targeted mRNA, leading to the suppression of the protein synthesis and/or by initiating mRNA degradation (Figure 8).

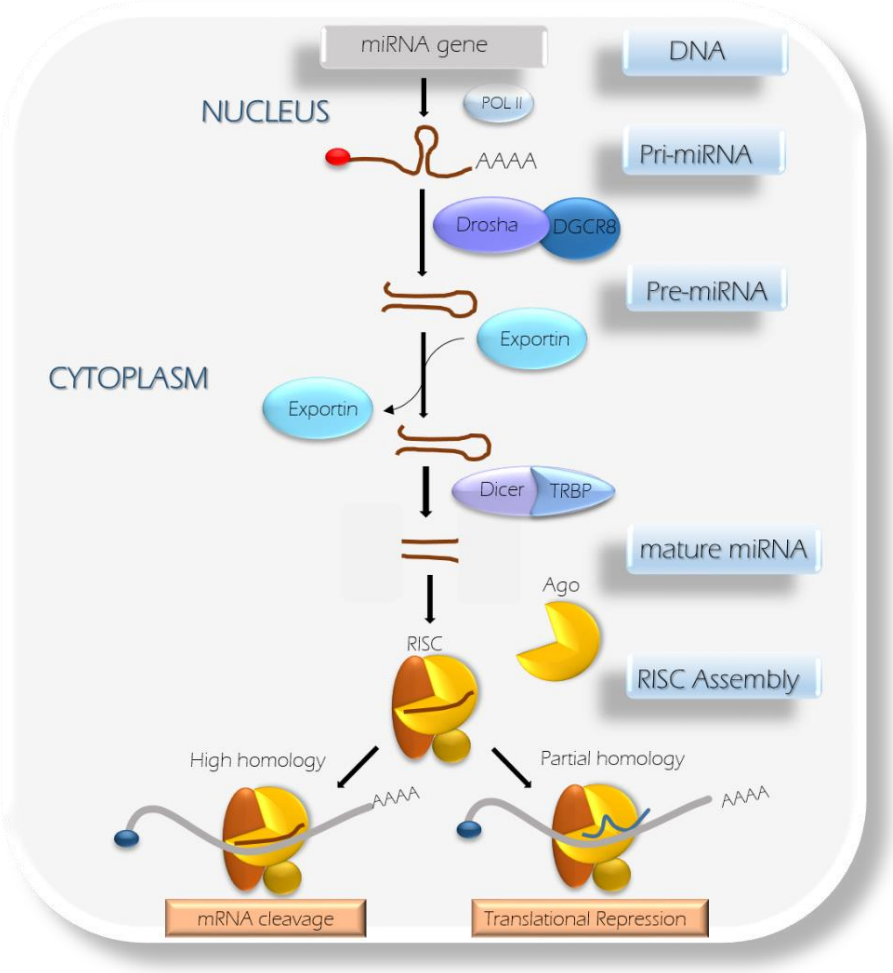

Figure 8: Canonical pathway of microRNA synthesis.

3.2. MicroRNAs biological functions

MicroRNAs have been reported in a wide range of biological processes. They are involved in the development and physiology of animals and plants. Regarding animals, miRNAs are key regulatory elements in cell differentiation and development. Still, viruses take advantage of miRNAs to take control of their host cell; as well as host cells use miRNAs to target vital viral functions for example in HIV-1 or hepatitis C virus (HCV) replication [173,174].

They are involved in neurogenesis and also in the maintenance of the survival of mature neurons and their function. Several miRNAs regulate the maturation and function in synaptic plasticity [175] or midbrain dopaminergic neurons [176].

miRNAs have also emerged as critical regulatory features in the mammalian immune system, which controls the generation and activation of granulocytes [177], and their deregulation is related to psoriasis-affected skin, contributing to the dysfunction of the cross-talk between resident and infiltrating cells [178], among others.

Furthermore, they also take part in developmental angiogenesis, blood stem cell formation, and plays a role in the pathology of vascular disease [179]. Among other processes of miRNAs regulatory role we can find cardiac [180] and skeletal muscle development [181], in the response to stress, insulin secretion, cholesterol metabolism, aging ,cell proliferation and apoptosis [182,183].

3.3. MicroRNAs in cancer development and other diseases

Since miRNAs contribute in most aspects of cellular differentiation and homeostasis, they subsequently play key roles in many pathologies, including cancer. More than 50% of miRNA genes are located in cancer-associated genomic regions forming central nodal points in cancer progression [184], where they can act as both oncogenes (oncomiRs) or tumor suppressors (TS) depending on their targets. Previous studies point to different miRNAs roles involving cancer development and maintenance [185], stemness [186,187], metastasis, EMT or angiogenesis [188,189], and drug resistance [187].

In the majority of the tumors, it has been reported the dysregulation of miRNA expression profiles depicting any of the abovementioned functions [190,191]. Though, it is a challenge to make an accurate miRNA classification as oncomiRs or TS since they differ from specific tissues and differentiation stages [192–194]. Another complication is that a single mature miRNA can be

implicated in multiple targets [195]. This together with tissue-specific expression could implicate a miRNA as a TS in one context and as an oncogene in another. Yet it is also necessary to clarify whether these altered expression patterns are the cause of cancer progression or it is an indirect effect of previous phenotypic changes [169].

Several oncomiRs have been observed in a wide range of tumor cell lines (miR-21 in breast, colon, lung liver; miR-155 in Lymphoma, leukemia, breast, colon, lung; miR-222 in osteosarcoma, glioma, breast cancer,, miR-378 in breast carcinoma, etc.) as well as the expression of TS miRs were reported diminished in many cancer cell lines (miR-1 in prostate cancer, head and neck, miR-7 in breast, ovarian cancer and miR-18a in CRC, miR-34a in breast, lung, colon, kidney, prostate, bladder, etc.), examples synthesized in [196].

At times, miRNAs are situated in polycistronic miRNA "clusters", where a single primary transcript generates multiple miRNA genes. The miR-17-92 miRNA cluster is the most complex and is highly conserved among all vertebrates. Among humans, the cluster is composed of six mature miRNAs (miR-17, miR-18a, miR-19a, miR-19b-1, miR-20a and miR-92-1). [197,198]. Although the mainstream supports miR-17-92 as an oncogene there is strong evidence that it also acts as a TS. In the following thesis, miR-19b-1, a miRNA of this cluster, will be discussed as a TS miRNA.

Some other emerging roles of miRNAs in disease include type 2 diabetes [199] and several diseases of the central nervous system including Alzheimer's, Parkinson's disease, Huntington's disease, schizophrenia and autism [200].

3.4. MicroRNAs as biomarkers or therapeutic targets

Different strategies in order to change the expression of a particular cancer-associated miRNA have been reported. The inhibition of tumor-promoting miRNA activity can be achieved by different miRNA inhibitors and oligomers, among others. On the contrary, to keep and augment TS miRNA expression it can be achieved by miRNA mimetics [196]. All these therapies development endorse that miRNAs may be used as therapeutic targets and tools in cancer treatment.

As well, miRNAs could also be used as potential biomarkers. Specific miRNA expression signatures have been identified in different cancer pathologies [201,202] to predict clinical outcomes, and also among different cancer stages during its development. Besides, the

possibility to detect miRNAs in body fluids such as serum plasma, saliva or urine makes them ideal tools for an early cancer detection, significantly contributing to the treatment success [203].

4. ORGANOIDS: 3D cultures

For a better understanding of CRC progression; more personalized and physiological tools are needed since most of the available data rely on traditional studies using cancer cell lines cultures. In this way, the organoid culture system opens a new methodological door for *ex vivo* studies.

4.1. Intestinal anatomy and function: The birth of organoids

Adult tissue-derived epithelial organoids, also called "miniguts" [204] are stereotypic tissue-like structures derived from digestive healthy tissues or tumors which mimics *in vitro* the tissue composition and morphology of their *in vivo* counterparts [205]. This methodology was first established in long-term primary culture from mouse small intestinal crypts to generate epithelial organoids with crypt- and villus-like epithelial domains representing both progenitor and differentiated cells [206].

The epithelium of the adult small intestine forms a contiguous two-dimensional sheet: crypts and villus. New cells are added in the crypts and removed by apoptosis upon reaching the villus tips a few days later. Stem cells and Paneth cells at the crypt bottom escape this flow

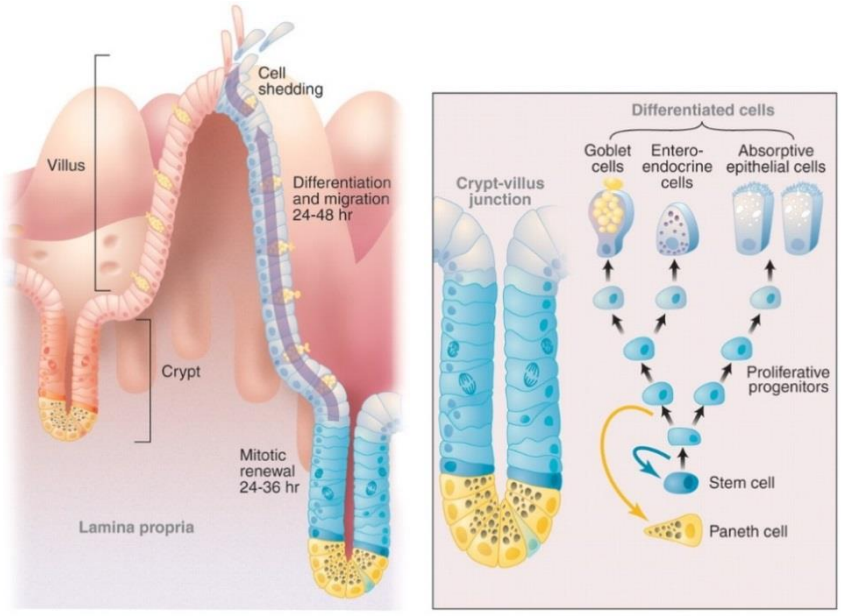

Figure 9: The anatomy of the small intestinal epithelium (Source: Radtke, F. & Clevers, H.[207])

The organoids technology takes advantage of the intestinal epithelium self-renewing capacity. Organoids starts from Lgr5+ gut or duct epithelial stem cells forming symmetric cyst structures, which finally will form budding structures resembling intestinal crypts (Figure 10). These budding structures are formed by these Lgr5+ stem cells flanked by differentiated daughter cells [204]. In small intestinal organoids, Lgr5+ stem cells receive niche signals from the neighboring differentiated Paneth cells for their self-renewal [208]. This process takes from 7-10 days; later splitting of organoids leads to single cells dissociation and the formation of new organoids that could be indefinitely propagated through such passaging.

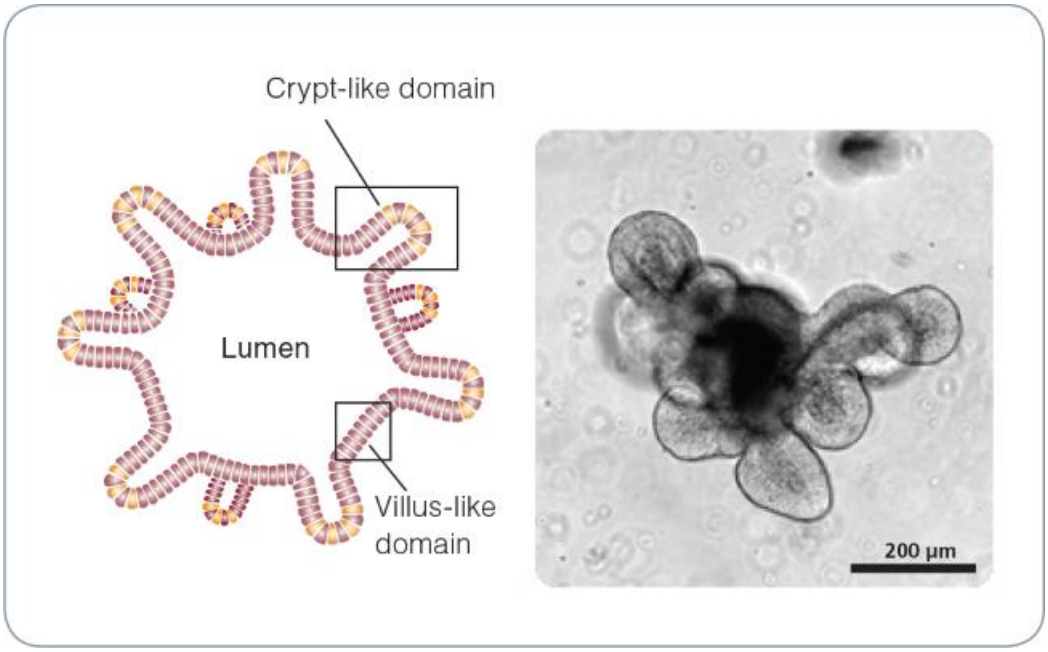

Figure 10: Intestinal organoid morphology. (Source: STEM CELL Technology [209])

One of the critical steps of organoids is their culture conditions, which should recapitulate each tissue stem cell microenvironments from where they come. Organoids can also be employed for *in vitro* generation of digestive tissue from embryonic, pluripotent and induced pluripotent stem cells [205], to phenocopy diseases such as cystic fibrosis [210] and can be easily manipulated by genetic engineering tools such as transfection, viral transduction and CRISPR/Cas9 technique [211–214]. Along with small intestinal organoids, similar epithelial organoids culture conditions for other mouse and human digestive epithelial tissues were also adapted [208,215–217] including tumor-derived organoids from cancer patients. Importantly, organoids grow as pure epithelial cultures without any contamination of vessels, immune cells or non-transformed mesenchymal which leads to an accurate sequencing or expression profiling [205]

4.2. Organoids uses and benefits of the 3D system

Modeling cancer by the organoids 3D culture has raised to an undisputedly and invaluable research tool. The fact that organoids own all the epithelial cell type hierarchy provides a functionally, physiologically relevant and similar model to *in vivo* response than conventional 2D culture methods. Human CRC organoids present varied requirements in terms of niche factors dependent on the pathways mutated, making them harder to culture. Besides, CRC is one of the most heterogeneous cancers, mostly in its last stages. However, murine organoids allow an accurate monitoring of the mutations and the cancer stage, together with the ease of manipulation, exploiting new lines of research using CRISPR and siRNA techniques.

In the past five-year period, translational research in regards to organoids has experimented a great growth with the establishment of human organoid biobanks [218] or by the possibility to correct mutations in *ex vivo* tumors using gene-editing techniques and further implantation of the genetically engineered organoids [213]. Organoids models suppose this "missing gap" among *in vivo* and *in vitro* studies, which in precise situations would allow continuing the research with the ethical advantage of reducing the animals suffering and for the obvious economic reasons. In summary, the utility of 3D organoid culture as a model for personalized medicine is in great expansion.

HYPOTHESIS & OBJECTIVES

HYPOTHESIS

Metabolic reprogramming is essential for tumor aggressiveness, and more precisely, lipid metabolism becomes crucial for energy supplies and a building blocks source for the tumor progression. Nonetheless, deeper analysis of lipid metabolism enzymes role in cancer is still necessary. We postulate that the metabolic enzyme family, ACSL, which represents a key point in the departure of FAs into different catabolic or anabolic routes, together with the immediately downstream enzyme, SCD, also key in the partition of desaturated active FAs, would be essential in cancer progression. Therefore, targeting these enzymes would also inhibit the progression of the tumor. Since some metabolic drugs such as Metformin have demonstrated a therapeutic role in cancer, knowing the status of this pathway in CRC patients could be relevant for the potential targeted use of these metabolic drugs in CRC patients.

OBJECTIVES

1. To unravel the role of the lipid metabolic enzymes ACSL and SCD on CRC tumor progression.

1.1. *In vitro* analysis of the metabolic enzymes, individually and in combination, using CRC-derived cell lines.

1.2. Analysis of the specific metabolomic profiles associated to the enzymes dysregulation.

2. To describe the possible association of the enzymes with clinical prognosis in CRC to be used as therapeutic targets and biomarkers of the progression of the disease.

2.1. Analysis of the expression of ACSL and SCD genes in CRC patient's cohorts to be used as a biomarker in the clinics.

2.2. *In vitro* analysis of the pharmacological specific inhibition effect over ACSL and SCD enzymes.

2.3. Identification and analysis of the best regulatory microRNAs for ACSL and SCD enzymes, searching their possible use as noninvasive biomarkers.

3. To develop a model of intestinal organoids to validate the relevance of this pathway as an *in vitro* approach for personalized medicine.

RESULTS

OVERALL RESULTS SUMMARY

This Doctoral Thesis aims to describe the reprogramming metabolic pathways involved in FA activation that a colorectal cell could suffer for its malignant transformation to CRC. ACSL represent a key point in the departure of FAs into different catabolic or anabolic routes, and we postulated that this family is essential in tumor progression, together with the immediately downstream enzyme, SCD, also key in the desaturation of active FAs. Both enzymes where previously described in CRC progression independently, and previous studies from the group highlighted their overexpression in a genetic fingerprint involved in CRC patients prognosis [162]. Thus, we first aimed **to unravel the role of these enzymes in tumor progression (Objective 1).**

To that end, we first followed an *in vitro* approach in which we overexpressed ACSL and SCD metabolic enzymes in human CRC cell lines individually and in combination (**Objective 1.1**.). This work suggested that there was a synergistic effect in tumor progression when ACSL and SCD were expressed together. Results demonstrated that the simultaneous overexpression of two isoforms of the ACSL family, ACSL1 and ACSL4 plus the desaturase SCD, promoted the adquisition of mesenchymal characteristics, conferring cancer stem cells properties to cells, increasing cellular migration and invasion and stimulating several survival pathways, (PUBLICATION I, Oncotarget 2015).

To further verify these results, we analyzed the metabolomic profile of the individual contribution of these enzymes in comparison to their simultaneous overexpression (**Objective 1.2**.). As it is shown in PUBLICATION II (Scientific reports 2017), acylcarnitines upregulation, polyunsaturated or monounsaturated FA dysregulation characterizes the individual overexpression of ACSL1, ACSL4 OR SCD, respectively. However, higher phospholipid levels, urea cycle upregulation and upregulated creatine pathway characterize the complete ACSL/SCD network metabolic action evidencing that the complete axis phenotype is not the sum of individual enzymes effects. Indeed, only the complete ACSL/SCD network -driven cells present metabolic features that also characterize other invasive and metastatic cells.

Once determined the ACSL/SCD network importance in CRC progression, new therapeutic opportunities for CRC treatment might be considered. We aimed **to describe the potential role of these enzymes as therapeutic targets and biomarkers of the progression of the disease (Objective 2).** To clarify the prognostic value of the axis to be used as a biomarker in the clinics, cohorts of CRC patients were analyzed for gene expression (**Objective 2.1**.). Results showed that patients with simultaneous overexpression of ACSL1, ACLS4 and SCD, displayed significant increased risk of relapse than other patients within the same clinicopathological stage

(PUBLICATION I, Oncotarget 2015). Once established the potential relevance of this pathway as a biomarker of the disease, its role as a therapeutic target was also analyzed. Through *in vitro* analyses, the combination of low doses of pharmacological inhibitors targeting specifically ACSL and SCD were used (**Objective 2.2**.), and we observed a dramatic inhibition of cell viability in a synergistic manner without having any effect in normal colonocytes, representing a new therapeutic possibility and concluding with the objective (reported in PUBLICATION I, Oncotarget 2015).

Regarding the inhibition of these enzymes expression, the reported existence of the epigenetic modulators such as miRNAs with great impact on metabolic homeostasis could represent a source for regulating these metabolic enzymes as well as being used as clinical biomarkers due to its capacity to be detectable in body fluids such as urine or plasma. Thus, the possibility to detect miRNAs in body fluids as noninvasive biomarkers, together with their potential regulating role of this pathway, made us to focus on finding regulatory miRNAs of the axis (**Objective 2.3**.). A screen of miRNAs simultaneously targeting ACSL1, ACSL4 and SCD evidences three miRNAs as regulators of the ACSL/SCD protumorigenic network. Importantly, one of these candidate miRNAs, miR-19b-1, correlates with a better prognosis in CRC patients, designating it as a promising noninvasive biomarker in CRC, fulfilling the objective 2.3. (PUBLICATION III, JLR 2017)

Finally, when referring to targeted and personalized approaches for cancer patients, new approaches would be necessary to explore the potential use of a specific therapeutic approach in a concrete patient. To date, platforms such as ex vivo explants cultures to test drugs were currently used. However, they do not allow an accurate analysis of the molecular characteristics of the tumor, and therefore they are still susceptible for improvement. In this sense, organoids technology embodies a more physiological tool to check the status of ACSL/SCD axis as well as its regulatory miRNAs. Thus, our last objective has been **to establish organoids models of intestinal tumors to evaluate their potential as a more adequate tool to analyze the effect of ACSL/SCD pathway in CRC (Objective 3).** In this way, as a first approach to develop human organoids, a model of murine CRC-like organoids following the different stages of the disease were established. As it is shown in PUBLICATION IV (Submitted for publication), ACSL4 is progressively overexpressed throughout the CRC-like organoids stages; while miR-19b-1 expression behaves in an opposite fashion. In the search of new drugs targeting the axis, we demonstrate that organoids also represent a great tool to study stage-dependent drugs. In this way, Metformin arises as an efficient treatment in CRC organoids first stages, completing the third block of objectives and extensively explained in PUBLICATION IV.

Table 4: Articles association to the Thesis objectives

	OBJECTIVE	ARTICLE ASSOCIATED
1.1	*In vitro* analysis of the metabolic enzymes, individually and in combination, using CRC cell lines.	Ruth Sánchez-Martínez, Silvia Cruz-Gil et al. **Oncotarget 2015**
1.2	Analysis of the specific metabolomic profiles associated to the enzymes dysregulation.	Ruth Sánchez-Martínez, Silvia Cruz-Gil et al. **Scientific Reports 2017**
2.1	Analysis of the expression of ACSL and SCD genes in CRC patient's cohorts to be used as a biomarker in the clinics.	Ruth Sánchez-Martínez, Silvia Cruz-Gil et al. **Oncotarget 2015**
2.2	*In vitro* analysis of the pharmacological specific inhibition effect over ACSL and SCD enzymes.	Ruth Sánchez-Martínez, Silvia Cruz-Gil et al. **Oncotarget 2015**
2.3	Identification and analysis of the best regulatory microRNAs for ACSL and SCD enzymes, searching their possible use as noninvasive biomarkers.	Silvia Cruz-Gil et al. **Journal of Lipid Research 2017**
3	To develop a model of intestinal organoids to validate the relevance of this pathway as an "in vitro" approach for personalized medicine.	Silvia Cruz-Gil et al. **Journal of Lipid Research (submitted for publication)**

PUBLICATION I

A link between lipid metabolism and epithelial-mesenchymal transition provides a target for colon cancer therapy.

Ruth Sánchez-Martínez, Silvia Cruz-Gil, Marta Gómez de Cedrón, Mónica Álvarez-Fernández, Teodoro Vargas, Susana Molina, Belén García, Jesús Herranz, Juan Moreno-Rubio, Guillermo Reglero, Mirna Pérez-Moreno, Jaime Feliu, Marcos Malumbres, Ana Ramírez de Molina

Doi: 10.18632/oncotarget.5340.

PUBLICATION I SUMMARY

A link between lipid metabolism and epithelial-mesenchymal transition provides a target for colon cancer therapy

The unusual metabolic reprogramming in a cell is considered a critical hallmark of cancer. In addition to the well-studied tumor carbohydrate metabolism, other metabolic pathways involved in malignant progression, such as lipid metabolism, demand further attention. Throughout this publication, we set up the basis of the present Doctoral Thesis. Here we described a metabolic ACSL/SCD network, capable of triggering invasive and mesenchymal features in CRC cells. The enzymes at issue were two members of the long-chain acyl-CoA synthetases (ACSL) family, isoform 1 and 4. ACSL family activates FAs from free FAs to fatty acyl-CoA (FA-CoA). This bioactive pool of FA-CoA can henceforth enter multiple physiological and metabolic routes. The third enzyme is the Stearoyl-CoA desaturase (SCD) which catalyzes the desaturation of FA-CoA. The products of SCD desaturation also serve as substrates for the synthesis of different complex lipids.

We performed the ACSL1, ACSL4 and SCD simultaneous overexpression (x3 cells) through specific lentiviruses in CRC cell lines (DLD-1) and we observed a phenotypic change characterized by a spindle-like shape and a scattered distribution, consistent with an EMT phenotype. To confirm this EMT phenotype, characterized also by cell-to-cell adhesion lost, E-cadherin marker was measured by immunofluorescence technique, confirming that it was mislocalized in x3 cells. Besides, β-catenin, a transcriptional coactivator, switched from the membrane to the nucleus. Furthermore, GSK3β inhibitory phosphorylation was shown highly increased in x3 cells by western blot technique (WB), allowing β-Catenin nuclear translocation to promote the transcription of mesenchymal-promoting genes. Different markers were also checked by qPCR, in x3 cells, whereas different mesenchymal markers were found overexpressed, the epithelial ones appeared downregulated. Since EMT processes are known to present cancer stem cells features, we measured CRC stem cells markers where we found x3 cells positively enriched on these proteins. In accordance, x3 cells were able to form tridimensional colonies in a “grape-like” or even “stellate” shape highlighting the mesenchymal behavior of these cells and suggesting invasive capacities.

Using wound-healing assays, we confirmed the migratory enhanced capacities of x3 cells. Moreover, we observed the gain of invasiveness upon the three enzymes overexpression in the poorly invasive DLD-1 cells, using Matrigel chambers experiments. Even though some enzymes individually promoted those effects, none of these effects was as prominent as the three

enzymes simultaneous overexpression effect. Colony formation experiments, used to analyze long-term growth and survival, showed x3 cells with a more than twice efficiency in colony formation compared to control cells. To accurately assay proliferation, we performed EdU assays with no substantial differences in proliferation in any of the cell lines. We next analyzed Erk and Akt activation, two well-known pathways for cell survival involved in mesenchymal features induction mainly through GSK3β regulation, finding a significant activation of both cascades in x3 cells. Again, we observed partial effects in single overexpression cases, such as SCD overexpressing cells, but far from the three enzymes overexpression full effect. Hence, ACSL1, ACSL4 and SCD act as a network specifically promoting invasion and survival but not proliferation, unlike Warburg driven tumors. In agreement with that, x3 cells did not show increased glycolytic activity analyzed by L-lactate measurements when compared with DLD-1 control cells. Furthermore, we proved the implication of the master metabolic regulator, AMPK, upon treatment with three different AMPK activators; Metformin, phenformin and AICAR that resulted in the DLD-1 epithelial phenotype rescue. As well, ACC, an AMPK downstream target, turns inactive by phosphorylation when induced by AMPK activators in x3 cells. Furthermore, Metformin treatment stimulated the expression of epithelial markers and decreased mesenchymal gene expression levels. AMPK is considered a tumor suppressor, inhibiting tumor metabolism through Akt-MDM2-Foxo3 signaling axis. This is in agreement with the increased Akt signaling observed in x3 cells. However, Akt inhibitor IV does not revert EMT suggesting additional pathways affected by AMPK signaling that are also needed for a complete rescue.

We further analyzed 77 samples from stage-II CRC patient's series and a further 119 stage-II CRC patients validation series, finding that the combined overexpression of ACSL1, ACSL4 and SCD in patients results in a poorer outcome and higher risk of relapse compared with the upregulation of each of the genes alone. This suggests an increased aggressiveness of tumors overexpressing ACSL/SCD network.

We wanted to assay the therapeutic potential of targeting the ACSL/SCD axis using chemical inhibitors. For this, we assayed the combination of Triacsin C, an ACSL inhibitor, and A939572 an SCD inhibitor. This combination synergistically reduces CRC cells viability without affecting normal colon cells. Importantly, this combination was also operative in CRC cells resistant to current chemotherapy (5-FU) and able to reverse the mesenchymal phenotype of x3 cells to the initial situation resembling control cells. Together with these results, we observed an increase in epithelial markers expression and a reduced expression of mesenchymal-promoting -genes in treated x3 cells. Hence, the pharmacological inhibition of ACSL/SCD network is able to

counteract the x3 cells invasive features and may designate the ACSL/SCD axis interference as a promising opportunity for cancer therapy development.

PUBLICATION I CONCLUSIONS

- A cooperative metabolic network comprising ACSL1, ACSL4 and SCD is involved in colorectal cancer progression.
- Simultaneous overexpression of ACSL1, ACSL4 and SCD induces mesenchymal features, confers the cells cancer stem cells properties, increases cellular migration and invasion and stimulates several survival pathways.
- The combination of low doses of pharmacological inhibitors targeting both ACSL and SCD dramatically affects cancer cell viability in a synergistic manner without having any effect in normal colonocytes.
- CRC patients with tumors displaying simultaneous overexpression of ACSL1, ACLS4 and SCD show an increased risk of relapse than other patients within the same clinicopathological stage.
- **ACSL/SCD network might be relevant for colon cancer progression through conferring increased energetic capacity and invasive and migratory properties to cancer cells and might represent a new therapeutic opportunity for colon cancer treatment**

My concrete contribution to this part of the research was first learning and improve the techniques above-mentioned. The principal author, Ruth Sanchez and I worked together on the whole project.

A link between lipid metabolism and epithelial-mesenchymal transition provides a target for colon cancer therapy

Ruth Sánchez-Martínez[1], Silvia Cruz-Gil[1,*], Marta Gómez de Cedrón[1,*], Mónica Álvarez-Fernández[2], Teodoro Vargas[1], Susana Molina[1], Belén García[1], Jesús Herranz[3], Juan Moreno-Rubio[4,5], Guillermo Reglero[1], Mirna Pérez-Moreno[6], Jaime Feliu[4], Marcos Malumbres[2], Ana Ramírez de Molina[1]

[1]Molecular Oncology and Nutritional Genomics of Cancer Group, IMDEA Food Institute, CEI UAM + CSIC, Madrid, Spain

[2]Cell Division and Cancer Group, Spanish National Cancer Research Centre (CNIO), Madrid, Spain

[3]Biostatistics Unit, IMDEA Food Institute, CEI UAM+CSIC, Madrid, Spain

[4]Medical Oncology, La Paz University Hospital (IdiPAZ-UAM), Madrid, Spain

[5]Precision Oncology Laboratory (POL), Infanta Sofía University Hospital, Madrid, Spain

[6]Epithelial Cell Biology Group, Spanish National Cancer Research Centre (CNIO), Madrid, Spain

[*]These authors have contributed equally to this work

Correspondence to:
Ana Ramírez de Molina, **e-mail:** ana.ramirez@imdea.org

Keywords: colorectal cancer, lipid metabolism, acyl-CoA synthetases, stearoyl-CoA desaturase, epithelial-mesenchymal transition

Received: June 08, 2015 Accepted: September 24, 2015 Published: October 05, 2015

ABSTRACT

The alterations in carbohydrate metabolism that fuel tumor growth have been extensively studied. However, other metabolic pathways involved in malignant progression, demand further understanding. Here we describe a metabolic acyl-CoA synthetase/ stearoyl-CoA desaturase ACSL/SCD network causing an epithelial-mesenchymal transition (EMT) program that promotes migration and invasion of colon cancer cells. The mesenchymal phenotype produced upon overexpression of these enzymes is reverted through reactivation of AMPK signaling. Furthermore, this network expression correlates with poorer clinical outcome of stage-II colon cancer patients. Finally, combined treatment with chemical inhibitors of ACSL/SCD selectively decreases cancer cell viability without reducing normal cells viability. Thus, ACSL/SCD network stimulates colon cancer progression through conferring increased energetic capacity and invasive and migratory properties to cancer cells, and might represent a new therapeutic opportunity for colon cancer treatment.

INTRODUCTION

Colorectal cancer (CRC) is one of the most deathly tumors worldwide. In addition to genetic modifications, factors causing metabolic alterations such as obesity, sedentarism and westernized diet, are risk factors for the disease [1]. Metabolic reprogramming is a distinguished cancer hallmark [2]. It is well known the Warburg effect by which cancer cells preferentially drive glucose metabolism to lactate production under aerobic conditions [3]. In addition to carbohydrate metabolism, other metabolic pathways have been found to be altered in cancer [4]. Lipid metabolism, represents an extremely relevant source of energy and structural and biosynthetic resources [5, 6].

De novo fatty acid synthesis is required for membrane production, essential for cell growth and proliferation. In addition, an appropriate ratio between saturated and monounsaturated fatty acids (SFA and MUFA, respectively) is needed for proper membrane fluidity and cell function. An increased content of MUFA has been observed in several cancers [7] and it has been proposed as a predictive marker [8]. The rate-limiting enzyme converting SFA into MUFA is steraroyl-CoA desaturase-1 (SCD), which introduces a double bound into palmitic acid and stearic acid giving rise to palmitoleic and oleic acid, respectively [9]. SCD have been described upregulated in several types of human tumors and its expression has been correlated with malignant transformation, proliferation and survival [10–14].

Acyl-CoA synthetases (ACSL) catalyze the conversion of long chain fatty acids to acyl-CoA, which is critical for phospholipid and triglyceride synthesis,

lipid modification of proteins as well as for fatty acid β-oxidation [15]. These enzymes have been related to carcinogenesis [16, 17]. Although involved in the same reaction, enzymes of ACSL family differ in substrate specificity, subcellular localization, and tissue distribution. In fact, these enzymes use saturated and unsaturated fatty acids of 8–22 carbons as substrates with the exception of ACSL4 that shows a clear preference for arachidonic acid as a substrate [6]. ACSL4 increases proliferation, tumor growth and survival in breast, prostate, colon and liver malignancies [18–21]. Remarkably, ACSL4 overexpression channels fatty acids preferentially towards phosphatidylinositol, an effect not observed for ACSL1 [22]. ACSL1 has been recently involved in lipid metabolism alterations in cancer [23], including in a screening in colon cancer of lipid metabolism-related genes recently conducted in our research group [24, 25].

Epithelial-mesenchymal transition (EMT) is a conserved morphogenetic program characterized by the loss of epithelial phenotype and the gain of mesenchymal features [26]. Epithelial cells discard their cell polarity and cell-cell adhesion and acquire a mesenchymal morphology with migration and invasion capability. These properties promote metastasis and the development of several neoplasias [27]. Loss of E-Cadherin and nuclear translocation of β-Catenin constitute known EMT biomarkers. β-Catenin translocation to the nucleus leads to invasion genes transcription [28]. This requires avoiding β-Catenin rapid cytosolic degradation by the proteasome, achieved upon GSK3β phosphorylation [29]. An implication of carbohydrates metabolism in the EMT phenotype acquisition and maintenance has been reported [30, 31] although no connection has been yet described with fatty acid metabolism.

Here we identify a cooperative metabolic network comprising ACSL1, ACSL4 and SCD, involved in CRC progression. The simultaneous overexpression of ACSL1, ACSL4 and SCD induces EMT, increases cellular migration and invasion and stimulates several survival pathways. Besides, the combination of low doses of pharmacological inhibitors for ACSL and SCD, dramatically decreases cancer cell viability in a synergistic manner. Moreover, such combination also reduces cell viability of chemotherapy resistant colon cancer cells without having any effect in normal colonocytes. Finally, the clinical relevance of these findings is underscored in CRC patients with tumors displaying ACSL1/ACSL4/SCD simultaneous overexpression that show an increased risk of relapse compared to other patients within the same clinicopathological stage.

RESULTS

Lipid metabolism enzymes overexpression confers EMT properties to colon cancer cells

The aim of this study was to perform a comparative analysis of the potential involvement of ACSL1 and ACSL4 in CRC, in addition to analyzing whether their combination with the related enzyme SCD might increase tumorigenesis due to the probable role of SCD in preventing lipotoxic effects that could result from ACSL overexpression. For this purpose we generated human colon cancer stable cell lines overexpressing either ACSL1, ACSL4 or SCD (ACSL1 cells, ACSL4 cells, and SCD cells, respectively) or the three genes simultaneously (x3 cells), transducing the DLD-1 CRC cell line with specific lentiviruses. An equivalent control vector which does not express any ORF was also used to generate the No ORF cell line. Transcript levels of ACSL1, ACSL4 and SCD were measured to ensure that stable expression of the constructs was achieved (Figure 1A), which was further confirmed by Western Blot analysis of the proteins levels (Figure 1B).

Unlike No ORF controls, nor any of the cell lines overexpressing any of these genes individually, x3 cells displayed a more spindle-like shape with a more scattered distribution, resembling mesenchymal or fibroblast-like phenotype (Figure 1C). Since this morphological change resembled an EMT phenotype characterized by loss of cell-cell adhesion, we next analyzed the expression of the epithelial marker E-Cadherin. As shown in Figure 1D, the membrane-associated pattern of expression of E-Cadherin was disrupted upon ACSL1, ACSL4 and SCD simultaneous overexpression. Mislocalization of E-cadherin was more evident in the areas where the more fusiform and rounded x3 cells were present (Figure 1D, bottom panel, arrow). Moreover, loss of β-Catenin from the membrane and a clear increase in nuclear localization was also found in x3 cells when compared with No ORF control cells (Figure 1E). This is also in agreement with a loss of epithelial characteristics and gain of an EMT phenotype, since its translocation to the nucleus would lead to the transcription of invasion genes [28]. Figure 1F shows how GSK3β inhibitory phosphorylation is highly increased in x3 cells, allowing β-Catenin nuclear translocation. β-Catenin acts as a transcriptional coactivator at the nucleus promoting the transcription of EMT genes [32]. Accordingly, together with a decrease in the expression of the epithelial markers *E-Cadherin, K18* and *Na^+/K^+ATPase β1*, x3 cells increased the expression levels of EMT associated genes *N-cadherin, Slug* and *Vimentin* (Figure 1G) which are normally not expressed in the markedly epithelial DLD-1 cells.

Accordingly with the lack of any morphological change, no mislocalization of E-cadherin nor changes in epithelial markers were observed in cell lines singly overexpressing any of these genes (Supplementary Figure S1A–S1B). Interestingly, an increase in GSK3β phosphorylation was also observed in SCD cells (Supplementary Figure S1C). In contrast, only cells overexpressing ACSL1, but not ACSL4 or SCD (data not shown) displayed an up-regulation of *N-cadherin* and *Slug* expression (Supplementary Figure S1D). These results suggest that each gene might be contributing in different aspects of EMT, though the cooperation of the three genes is needed to trigger the EMT program.

Cells undergoing EMT have been described to present cancer stem cells features [33]. Accordingly, x3 cells were significantly enriched in the well-established markers of CRC stem cells *CD44, LGR5, ALDH1A1, EpCAM* and *CD29* when compared with No ORF cells (Figure 1H). Moreover, x3 cells form tridimensional colonies with differential morphologies when grown in matrigel. While No ORF cells displayed the normal DLD-1 spheroid round morphology termed as "mass" [34, 35] (Figure 1I, left panel), x3 cells whether presented "grape-like" spheroids with loose cell-cell contacts (Figure 1I, central panel) or even "stellate" colonies with invasive projections able to bridge several cell colonies (Figure 1I, right panel). This again highlights the more mesenchymal behavior of x3 cells and suggests an invasive capacity for these cells.

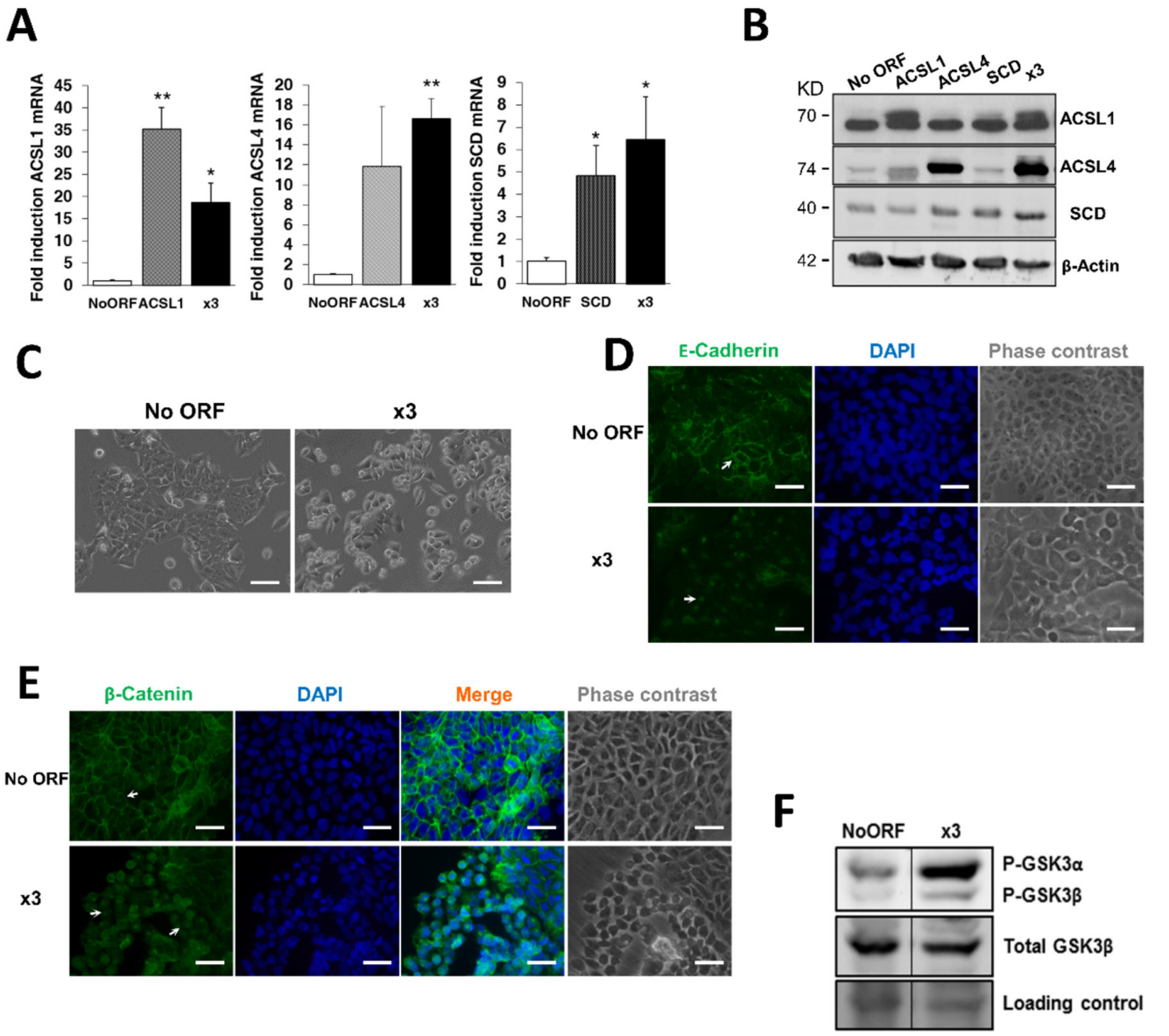

Figure 1: ACSL1, ACSL4 and SCD overexpression induces EMT in CRC cells. A. Stable cell lines overexpressing ACSL1, ACSL4 and SCD, alone or in combination (x3) were generated using lentiviral transduction and expression levels of every gene were measured by RT-QPCR. **B.** Protein expression levels of ACSL1(upper band), ACSL4 and SCD for each cell line were detected by Western Blot with specific antibodies. β-Actin detection was used as a loading control. **C.** Representative phase contrast images showing atypical morphology of x3 cells compared to control No ORF cells. Scale bars, 100 μm. **D–E.** Representative immunofluorescence images of E-Cadherin (green) (D) or β-Catenin (green) (E) cellular distribution of No ORF and x3 cells. Arrows indicate the different expression patterns in the cellular distribution of E-Cadherin (D) or β-Catenin (E) in both types of cells. Nuclei were stained with DAPI (blue) and equivalent phase contrast images were taken. Scale bars, 50 μm. **F.** Levels of GSK3 phosphorylation detected by Western Blot using a phospho-specific antibody (Ser21/9). Total GSK3β levels detection and Ponceau-stained band served as loading controls. Bottom panel: Quantification of bands intensity showing the ratio of phosphorylated to total protein. (*Continued*)

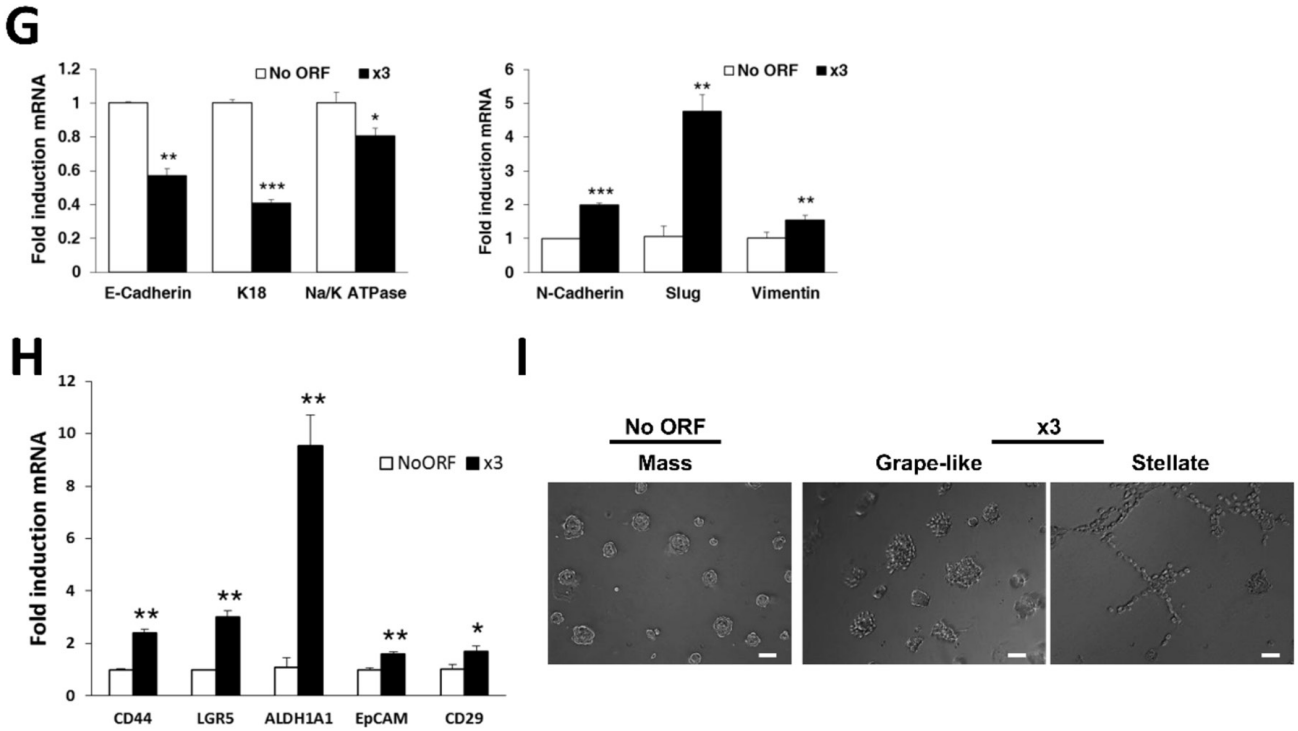

Figure 1: (*Continued*) ACSL1, ACSL4 and SCD overexpression induces EMT in CRC cells. G. RT-QPCR analysis of epithelial (*E-Cadherin, K18* and *Na+/K+ATPase β1*) and mesenchymal genes (*N-Cadherin, Slug* and *Vimentin*) for x3 cells compared to levels in No ORF control cells. **H.** The expression levels of the colon cancer stem cell markers *CD44, Lgr5, ALDH1A1, EpCAM* and *CD29* were measured by RT-QPCR in x3 cells and compared to the levels in No ORF control cells. **I.** Phase contrast pictures showing the different morphology of spheroids formed by No ORF and x3 cells cultured under 3D on-top assay conditions. Scale bars, 100 μm. Experiments in A, G and H were performed in triplicates ($n = 3$). Results represent the mean ±SD ($n = 3$). *, $p < 0.05$, **, $p < 0.01$, ***, $p < 0.001$.

ACSL/SCD metabolic network fuels migration, invasion and cell survival

The acquisition of migratory and invasive properties is a general feature of cells undergoing EMT, crucial for metastasis formation and cancer progression. In order to check if the combination of ACSL and SCD overexpression could confer cancer cells a gain of migratory capacity, we performed wound healing assays. Figure 2A shows how x3 cells present an increased migration ability compared to No ORF cells. As illustrated in the magnification, x3 cells close the wound upon random migration, characteristic of a mesenchymal behavior. In contrast, No ORF control cells, ACSL1, SCD, and more markedly ACSL4, display the collective unidirectional migration of cohesive epithelial sheets. Furthermore, poorly invasive DLD-1 cells gain the ability to invade through Matrigel (Figure 2B) upon ACSL1, ACSL4 and SCD simultaneous overexpression (x3). The invasion capacity was also increased upon individual overexpression, especially in the case of ACSL1 cells. However, any of these individual effects was less prominent that the one observed in x3 cells. These results highlight the cooperative effect in promoting migration and invasion achieved when these three metabolic genes act in a combined manner.

Cancer cells often use metabolic strategies to promote cell survival and proliferation. To analyze whether an increased lipid metabolism caused by ACSL1, ACSL4 and SCD overexpression could be implicated in these processes, we first performed clonogenic assays to monitor long-term growth and survival. Figure 2C shows that x3 cells present more than twice efficiency in colony formation compared to control cells. In contrast, none of the individual overexpression caused this increase in the number of colonies formed indicating again that it is the combination of the three genes that confers the cells the more aggressive characteristics.

To directly assay cell proliferation we analyzed the incorporation of EdU as a measure of DNA synthesis rate. No significant changes in proliferation were found in any of the stable cell lines (Figure 2D). Since colony formation needs cell proliferation, we also performed those EdU assays in conditions of confluence to make these assays more comparable to the growth conditions in the colonies produced during clonogenic assays. Again, we do not find substantial differences in proliferation in any of the cell lines (Supplementary Figure S2). A number of EMT regulators have been reported not to increase proliferation, and invasive cells associated to decreased cell cycle progression [36, 37]. We next analyzed Erk and Akt activation, two well-known

pathways for cell survival involved in EMT induction mainly through GSK3β regulation [38]. We found a significant activation of both cascades in x3 cells (Figure 2E). Besides, a clear increase in Erk and Akt phosphorylation was found in SCD cells, as well as in ACSL4 cells in the case of Akt phosphorylation. These partial activations per se may be insufficient but may contribute to the full effect and phenotype observed in x3 cells.

All these data suggest that unlike other tumor metabolic pathways such as the Warburg effect, the ACSL/SCD network acts specifically promoting invasive and pro-survival properties without major effects on cell proliferation. In agreement with that, x3 cells did not show increased glycolytic activity when compared with No ORF control cells (Figure 2F). This reveals that EMT promotion might require particular metabolic advantages other than pro-proliferative aerobic glycolysis.

AMPK signaling counteracts the EMT phenotype triggered by the ACSL/SCD signaling network

In addition to classical oncogenic pathways [38], nutrient sensing and inflammation regulators have been more recently added to the list of EMT-inducers [39, 40]. Since ACSL/SCD overexpression may represent

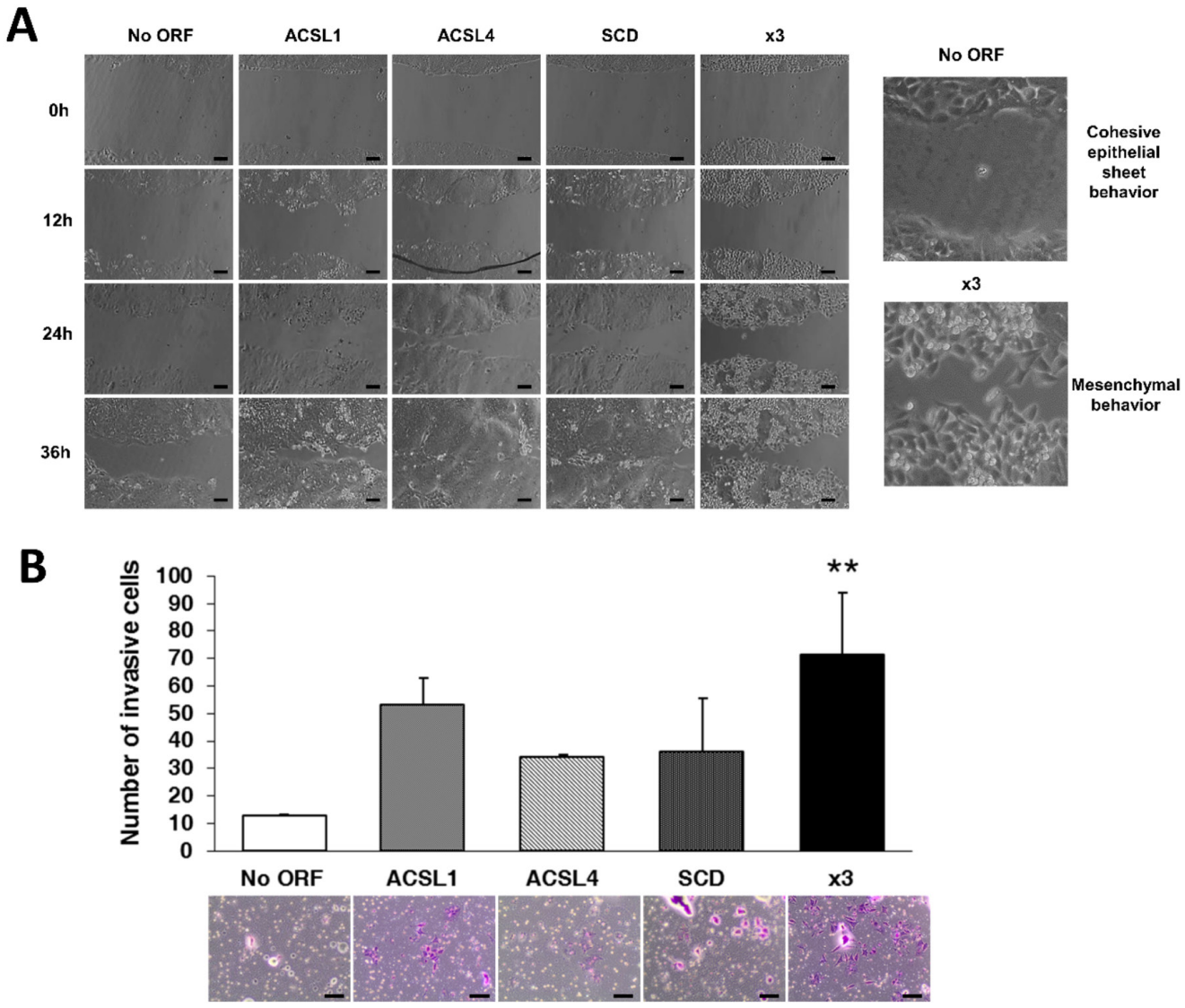

Figure 2: Combination of ACSL with SCD overexpression stimulates migration, invasion and colony formation without major effects on proliferation. A. Phase contrast pictures of wound healing assay comparing migratory capacities of No ORF, ACSL1, ACSL4, SCD and x3 cells. Magnification (right panels) shows the different behavior of control and x3 cells at 36 hours of wound closure. Scale bars, 100 μm. **B.** Boyden chamber transwell assay of invasion through Matrigel. After 48 hours, cells were fixed and stained with crystal violet (bottom panels) and counted under an optical microscope. Migratory cells were quantified as the average number of cells found in five random microscope fields in three independent inserts. Scale bars, 50 μm. (*Continued*)

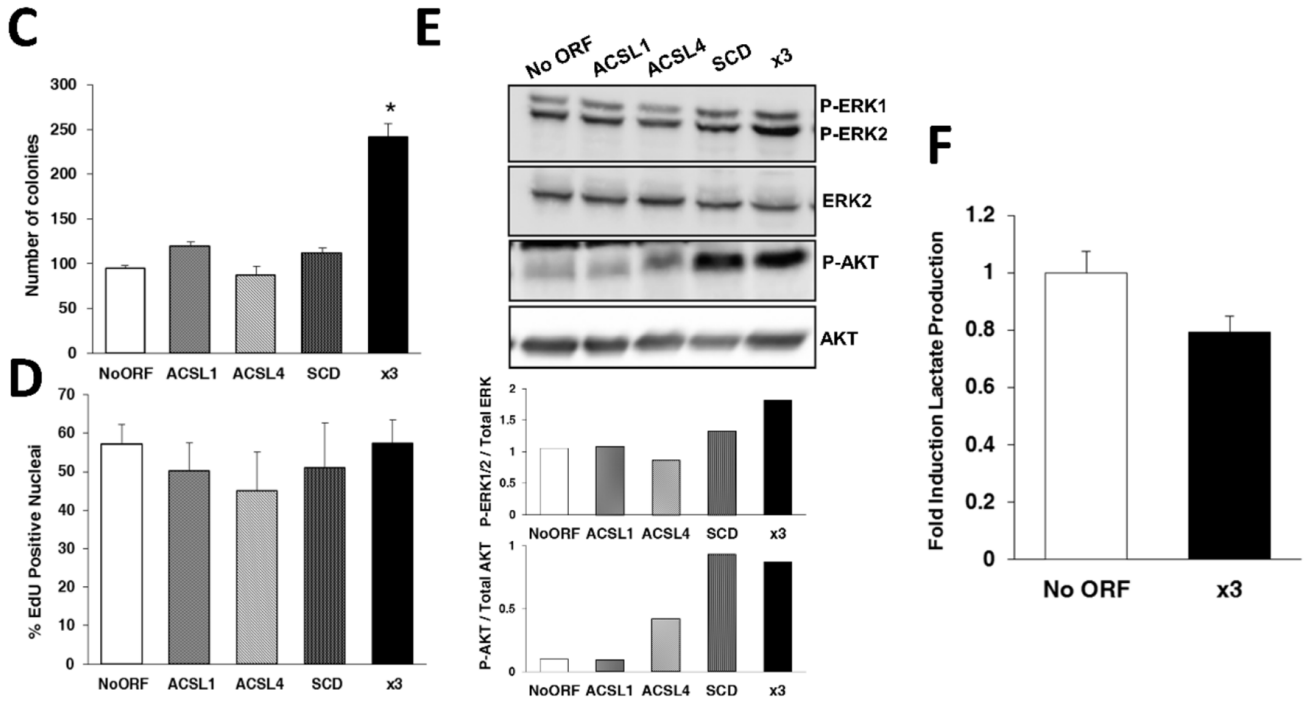

Figure 2: (*Continued*) Combination of ACSL with SCD overexpression stimulates migration, invasion and colony formation without major effects on proliferation. C. Clonogenic assay quantification. Individual cells were plated and colonies formed were grown during 2 weeks. Data are presented as the average number of colonies resultant for each cell line. **D.** Quantification using fluorescence microscopy of EdU incorporation as a measure of cell proliferation. **E.** Erk1/2 and Akt phosphorylation were detected by Western Blot with phospho-specific antibodies (Tyr204 Erk and Thr308 Akt). Total Erk and Akt were used as their respective controls. Bottom panels: Quantification of bands intensity showing the ratio of phosphorylated to total protein. **F.** Quantification of extracellular L- Lactate produced by No ORF and x3 cells. Experiments in B, C, D and F were performed in triplicates ($n = 3$). Results represent the mean ±SD ($n = 3$). *, $p < 0.05$, **, $p < 0.01$.

an energetic advantage, we wondered if the master regulator of energy balance, AMPK, was involved. This kinase, considered to act as a tumor suppressor by inhibiting tumor metabolism and associated cell growth signaling pathways [41] has been described to suppress EMT by regulating the Akt-MDM2-Foxo3 signaling axis [42]. Accordingly, treatment with three different AMPK activators; metformin, phenformin and AICAR, was able to rescue the DLD-1 epithelial phenotype (Figure 3A).

Besides sharing arachidonic acid as a substrate, ACSL4 regulates COX-2 expression and thus prostaglandin production [19], also implicated in cell malignancy and EMT promotion [43]. Since x3 cells, but not any of individually overexpressing cell lines, show increased levels of COX-2 expression (Figure 3B); we surmised that x3 EMT might be mediated by a COX-2 dependent mechanism. Conversely, treatment with the COX-2 inhibitor NS-398 had no effect on the x3 cells phenotype reversion (Figure 3C, central panel). Moreover, despite the strong Akt activation in x3 cells (Figure 2E), the treatment with Akt inhibitor IV (Figure 3C, right panel) was also inefficient to revert x3 mesenchymal features. This drug only inhibited cell viability of both cell lines without altering their morphological features. These data pointed towards AMPK signaling as key for maintaining the DLD-1 cells epithelial phenotype. This was further demonstrated by analysis of the downstream AMPK target, Acetyl-CoA Carboxylase (ACC), which is inactivated upon phosphorylation at Ser79 (P-ACC). The ACC inhibitory phosphorylation was induced upon metformin or phenformin treatment in x3 cells (Figure 3D). Furthermore, metformin treatment stimulated the expression of the epithelial markers *E-Cadherin, K18* and *Na^+/K^+ATPase β1* and decreased the expression levels of the EMT-induced genes *N-Cadherin* and *Slug* in x3 cells without increasing those levels in control No ORF cells (Figure 3E).

Stage-II CRC patients with simultaneous overexpression of ACSL1, ACSL4 and SCD have worse clinical outcome

In order to determine the clinical relevance of ACSL/SCD network activation in CRC, we analyzed the putative association between the simultaneous overexpression of ACSL1, ACLS4 and SCD with clinical outcome in a set of 77 samples from stage-II CRC patients. Towards this aim we have recently developed a global analysis of lipid metabolism-related genes [25]. Median follow-up of these patients was 71.5 months. The 3-year disease

free survival (DFS) was 72.3%, 22 patients (28.57%) relapsed. Clinico-histopathological characteristics of these patients are detailed in Supplementary Table S1. An initial screening performed showed that 16 out of 70 lipid metabolism-related genes analyzed, including ACSL1, ACLS4 and SCD, might have a putative association with tumor aggressiveness [25]. Thus, we performed a comparative analysis of the relationship between the individual expression of these genes and their combined overexpression in these patients. As expected from the screening, Kaplan-Meier plots for disease free-survival of ACLS1, ACSL4 or SCD showed an association between high expression of each of these genes and poorer clinical outcome (Figure 4A, 4B and 4C). Moreover, the multivariable model x3 (combined expression of ACSL1, ACSL4 and SCD) showed that the simultaneous overexpression of the ACSL/SCD network resulted in a stronger and more potent association with patient relapse (Figure 4D and Table 1), confirming the acquisition of increased aggressive properties of CRC tumors with these characteristics.

We validated these results in an independent and bigger cohort of 119 stage II CRC patients with a median follow-up of 43 months and 3-year DFS of 86.1% respectively, from which 18 patients relapsed (15.3%) (Clinico-pathological characteristics summarized in Supplementary Table S1). The univariate cox regression analysis in this validation group also showed a statistical association between overexpression of each gene and clinical outcome (Figure 4, Table 1). The multivariate analysis in this validation group further demonstrated that the combined overexpression of these genes was associated with a higher increased risk of relapse of stage-II CRC patients, with higher power and statistical strengthening than any of these genes individually (x3: HR (95% CI) = 8.68 (1.9–39.66); p = 6e-04), which is more than 2-fold higher than any of these genes separately, results that were confirmed after adjusting for clinical confusing factors (Table 1).

These results, not only show the clinical relevance of the overexpression of these genes in CRC, but also demonstrate that their combination is associated with an

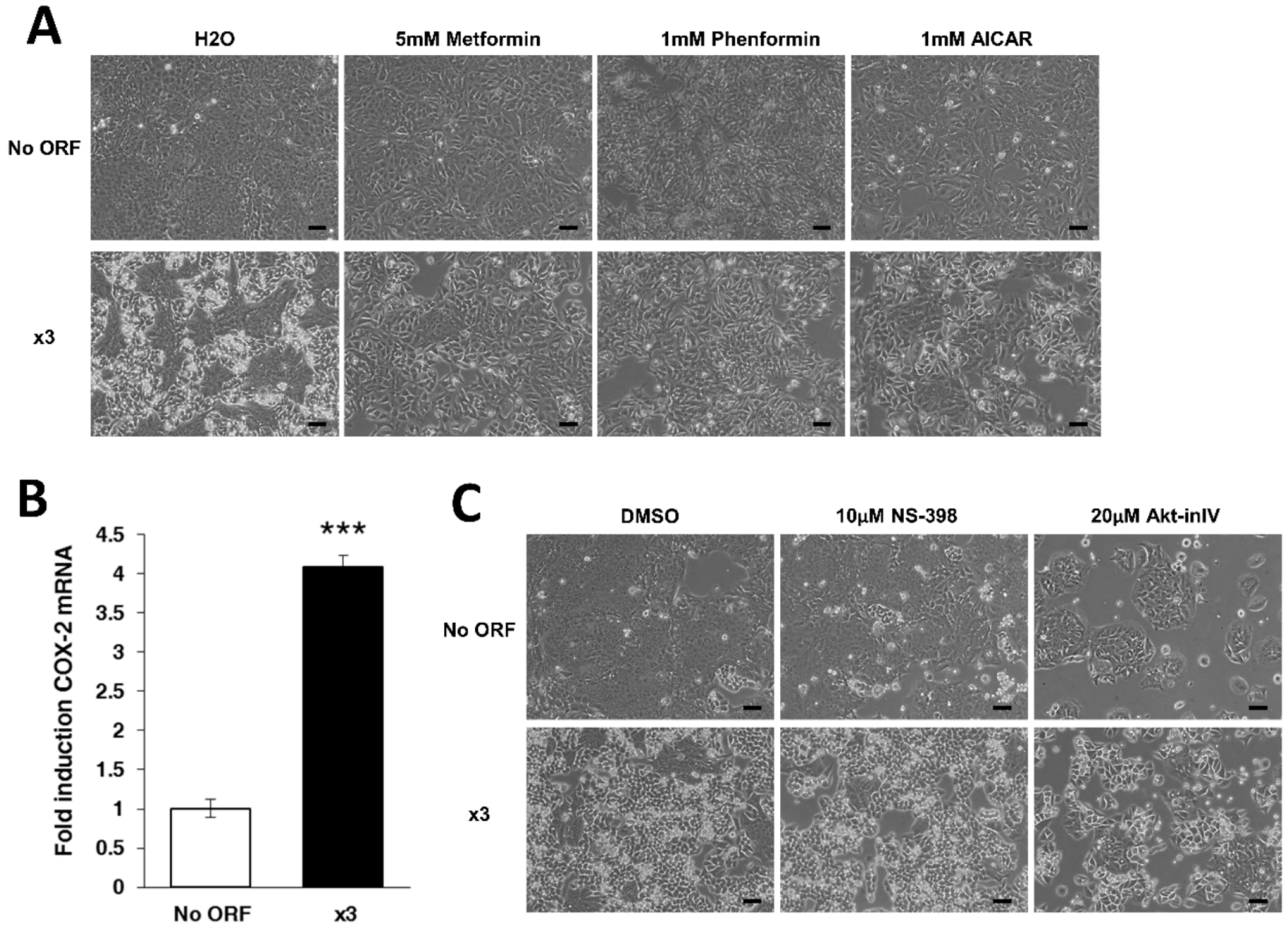

Figure 3: AMPK activation rescues normal DLD-1 epithelial phenotype. A. Representative phase contrast pictures of No ORF and x3 cells treated either with 5 mM metformin, 1 mM phenformin, 1 mM AICAR or vehicle (water) for 48 hours. Scale bars, 100 µm. **B.** COX-2 expression levels of x3 cells compared to control No ORF cells, measured by RT-QPCR. **C.** Pictures represent cells treated for 48 hours either with the COX-2 inhibitor NS-398 (10 µM), the Akt inhibitor IV (Akt-inIV, 2 µM), or with an equivalent amount of DMSO as control. Scale bars, 100 µm. (*Continued*)

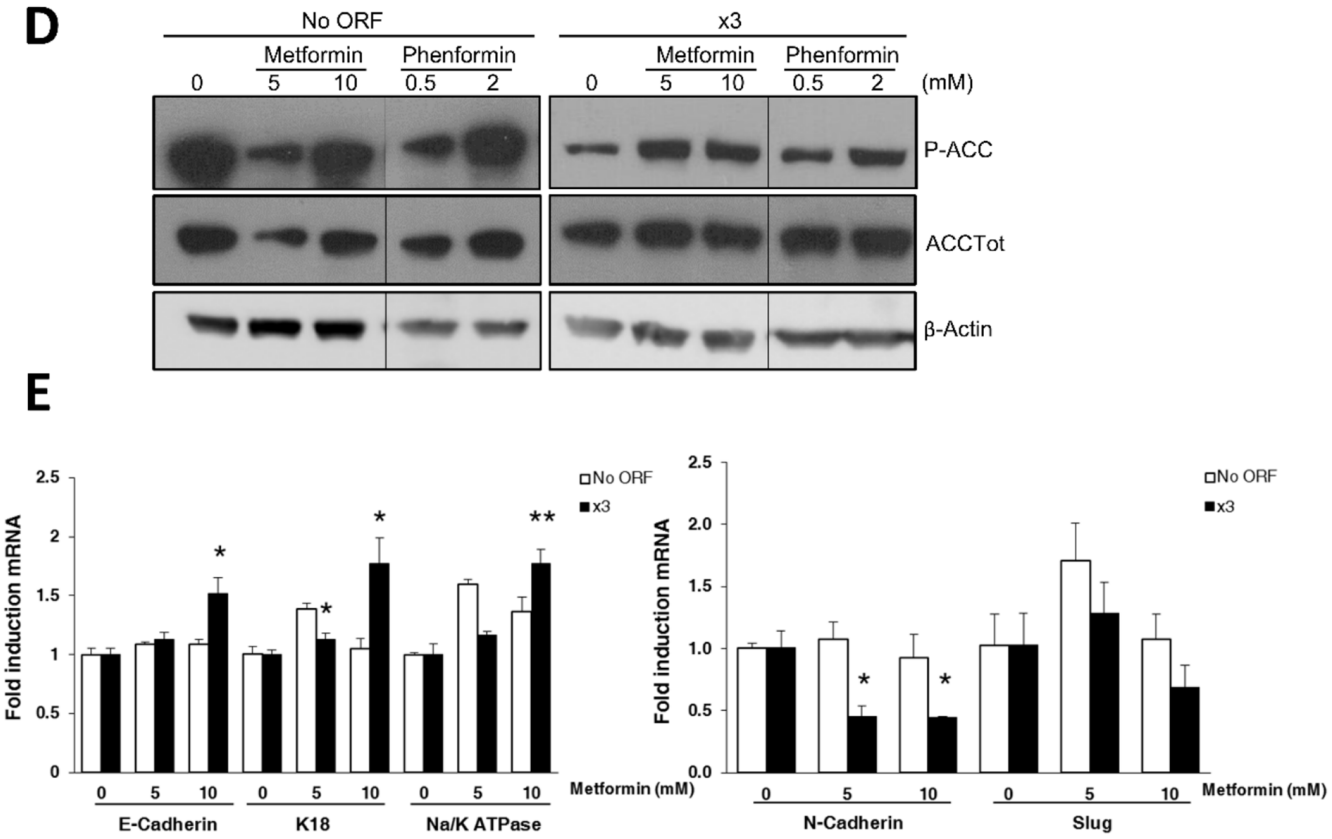

Figure 3: (*Continued*) AMPK activation rescues normal DLD-1 epithelial phenotype. D. Western blotting of ACC phosphorylation upon 48 hours of metformin (5 and 10 mM) or phenformin (0.5 and 2 mM) treatment in No ORF and x3 cells. Total protein extracts were blotted using a phospho-specific antibody (Ser79) and a total ACC antibody. β-Actin detection was used as a loading control. **E.** RT-QPCR analysis shows mRNA levels of epithelial markers (*E-Cadherin, K18* and *Na+/K+ATPase β1*) upon 48 hours of metformin treatment (5 and 10 mM) in No ORF and x3 cells (left panel). Similarly, right panel presents the levels of the mesenchymal markers *N-Cadherin* and *Slug* in these cell lines under similar treatments. The values for every gene are presented as fold change referenced to their respective control (0 mM metformin) within each cell line. Results in C and E were performed in triplicates, and represent the mean ±SD. *, $p < 0.05$, **, $p < 0.01$, ***, $p < 0.001$.

increased aggressiveness of CRC tumors in a clinical setting. Collectively, these results imply that ACSL1, ACSL4 and SCD increased expression might act as a marker of poor prognosis which contributes to reduced disease free survival of colon cancer patients. Very likely, the EMT program triggered by the ACSL1/ACSL4/SCD axis would be implicated in facilitating the spread of the disease.

Combined pharmacological inhibition of the ACSL/SCD network synergy to selectively inhibit cancer cells viability and mesenchymal features

The robust protumor action of ACSL1/ACSL4/SCD network, together with the fact that all three of them are lipid metabolism enzymes, makes these druggable proteins attractive targets for cancer therapy. For this reason, we evaluated the combined effect on colon cancer cell viability of Triacsin C, a specific inhibitor of ACSL, and the SCD inhibitor A939572, both previously reported to reduce tumor growth both *in vitro* and *in vivo* [14, 17]. Triacsin C was able to decrease cell viability in DLD-1 and SW620 cell lines in a dose-dependent manner (Figure 5A). A similar effect was achieved upon treatment with A939572 (Figure 5B). Since the use of high concentrations of pharmacological inhibitors may cause side effects and act on other pathways, the combination of the two compounds might inhibit ACSL/SCD network and exert a similar action using much lower concentrations of both compounds .

Lower concentrations of Triacsin C and A939572 alone or in combination were used in a panel of colon cancer cell lines (Figure 5C). As expected, treatment with 1 μM Triacsin C or with 0.5 μM A939572 moderately decreased DLD-1 and SW620 cells viability, but importantly, the combined action of both inhibitors caused a strong cancer cell viability reduction. Furthermore, Triacsin C and A939572 individually had no effect on the viability of the more resistant HT-29 and LS174T cells; however, a potent inhibition was observed when those low doses of both compounds were used (Figure 5C).

In addition, to analyze the effect of these compounds on CRC cells resistant to conventional chemotherapy, we used a subclone of SW620 cells previously described [44],

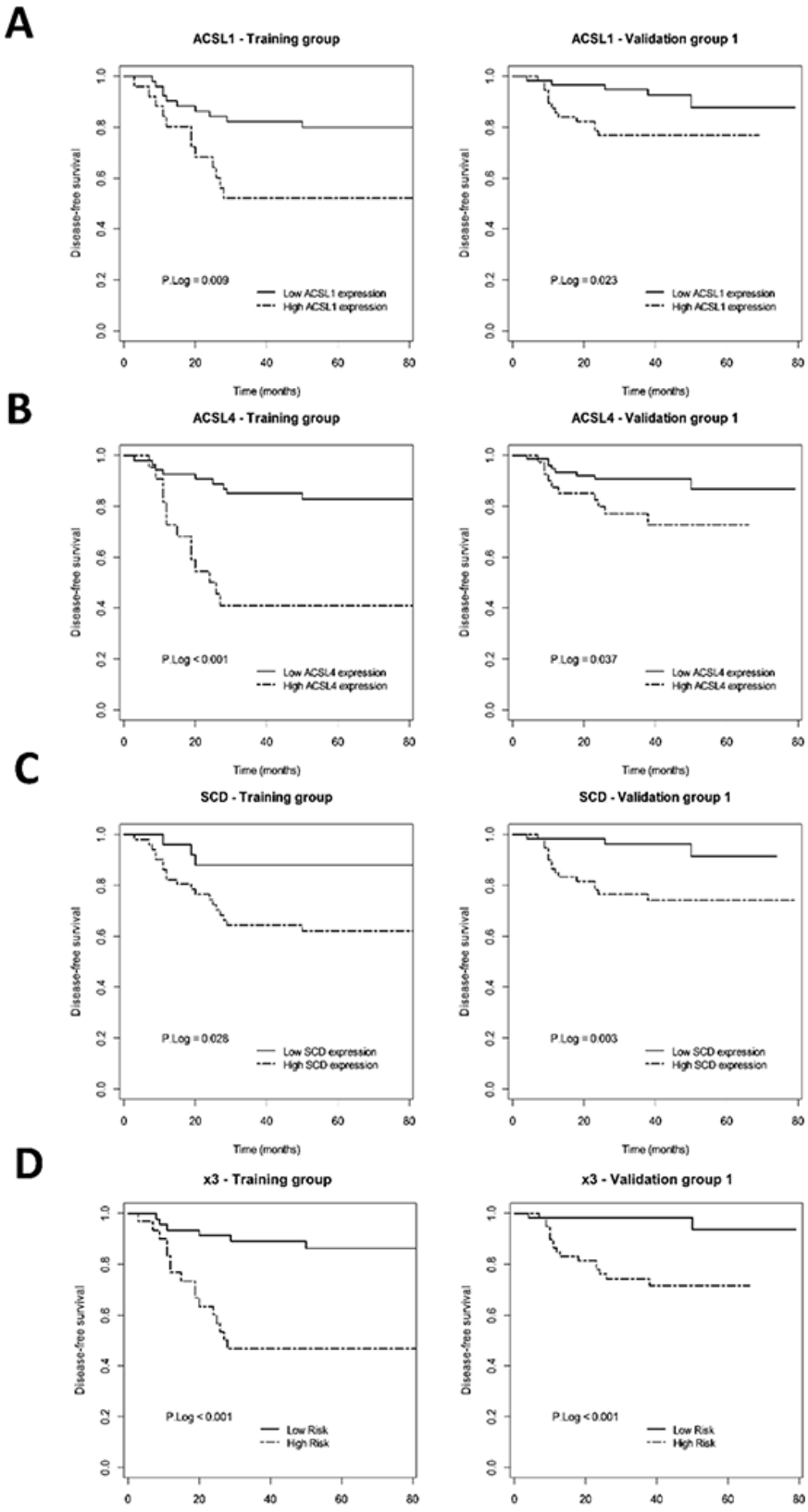

Figure 4: Prognostic value of ACSL1/ACSL4/SCD individual or simultaneous (x3) overexpression in early-stage CRC patients. Kaplan-Meier plots representing DFS for ACSL1 **A.** ACSL4 **B.** SCD **C.** and x3 **D.** overexpressing early-stage CRC patients and p Log Rank value in the training and validation groups are shown.

Table 1: Univariate and Multivariate Cox regression analyses for Disease-free survival of the ACSL1, ACSL4 and SCD genes, the multivariable model x3 (combined expression of ACSL1, ACSL4 and SCD) in stage II CRC samples from the training group and the validation group

Variable	Training group (n = 77)								Validation group (n = 119)							
	Low Risk		High Risk		Unadjusted		Adjusted#		Low Risk		High Risk		Unadjusted		Adjusted#	
	R	N	R	N	HR (95% CI)	*P*	HR (95% CI)	*P*	R	N	R	N	HR (95% CI)	*P*	HR (95% CI)	*P*
ACSL1	10	51	12	26	2.93 (1.26–6.81)	0.013	2.34 (0.91–6.02)	0.082	5	61	13	58	3.12 (1.11–8.76)	0.021	3.86 (1.16–12.79)	0.017
ACSL4	9	54	13	23	4.92 (2.09–11.62)	0	5.6 (2.19–14.32)	0	8	78	10	41	2.59 (1.02–6.57)	0.045	2.31 (0.85–6.27)	0.1
SCD	3	26	19	51	3.57 (1.06–12.08)	0.018	3.13 (0.9–10.93)	0.046	3	57	15	62	5.32 (1.54–18.38)	0.002	4.08 (1.12–14.9)	0.017
x3	6	46	16	31	5.36 (2.09–13.74)	0.000	4.99 (1.81–13.77)	0.001	2	58	16	61	9 (2.07–39.21)	0.0002	8.68 (1.9–39.66)	6E-04

Abbreviations: HR (95% CI), hazard ratio and corresponding 95% confidence interval from adjusted or unadjusted Cox regression analyses; P, *p* value from adjusted or unadjusted Cox regression analyses; N, N° of patients in each risk group; R, N° of patients with relapse.

#Cox regression analyses were adjusted for T stage, Vascular invassion, Perineural invassion, Bowel Obstruction/ Perforation and Age > 70.

which is resistant to 5-Fluorouracil. The drugs had little (Triacsin C), or no effect (A939572) on SW620–5FU-R when applied separately. Nonetheless, a strong cooperative effect was found upon simultaneous treatment with ACSL and SCD inhibitors (Figure 5D).

Since the EMT program observed in x3 cells is triggered by the combined action of ACSL with SCD, we wanted to assay the effect on EMT of their inhibitors. Combined treatment with low doses of these drugs was able to reverse the mesenchymal phenotype of x3 cells to a situation resembling No ORF cells (Figure 5E). Furthermore, this was accompanied by an increase in the expression of epithelial markers and a reduced expression of EMT-genes in x3 cells (Figure 5F). Hence, the pharmacological inhibition of ACSL/SCD network is able to counteract the x3 cells EMT features.

Finally, the ability of a compound to discriminate cancer cells from their normal counterparts is the basis for successful cancer treatment. For this reason, we assayed the effect of Triacsin C and A939572 on the viability of normal colonocytes. Very importantly, the same inhibitors concentrations that caused a massive loss of viability of colon cancer cell lines (Figure 5C and 5D) were completely ineffective when applied to normal colonocytes CCD18Co (Figure 5G). This was further confirmed using another normal colon cell line, CCD841 (Figure 5H) resulting in a similar behavior. Thus, the inhibition of ACSL1/ACSL4/ SCD axis by means of the selective effect of these drugs on cancer cells arises as a promising therapeutic strategy.

DISCUSSION

We show for the first time how the overexpression of lipid metabolism genes can lead to EMT induction and increased migratory and invasive properties. ACSL1/ ACSL4/SCD overexpression in CRC cells causes a phenotypic switch to a mesenchymal-like condition characterized by rounded cell morphology and E-Cadherin and β-Catenin mislocalization (Figure 1D and 1E). This phenotypic change, which leads to an increased migration and invasion (Figure 2) is only achieved upon overexpression of the three proteins, presumably having each of them more partial but differential functions. ACSL1 may be an initiator of the process since its overexpression stimulates EMT genes expression (Supplementary Figure S1D). ACSL1 seems also to be fundamental for invasive abilities (Figure 2B) which could be caused by an increased expression of invasive genes such as matrix degrading enzymes. For its part, SCD overexpression strongly increases inhibitory phosphorylation of GSK3β (Supplementary Figure S1C). This may be a consequence of SCD overexpression-induced Akt activation (Figure 2E) which phosphorylates and inactivates GSK3β [38, 45, 46], avoiding β-catenin degradation and allowing further EMT signaling . Indeed, SCD knock-down impairs β-catenin signaling and inhibits EMT-like behavior of metastatic breast cancer cells [47]. SCD may maintain the network signaling through Erk and Akt stimulation (Figure 2E)

which are key for EMT programs [48]. In fact, oleic acid, the main product of SCD, activates Akt pathway while palmitic acid has the opposite effect [49]. Very likely, SCD maintenance of the cancer preferred MUFA/SFA ratio, is the driving force of Erk and Akt signaling as observed in lung and prostate cancers [10, 50]. Hence, the SCD-induced increase in MUFA content seems crucial to maintain EMT and tumor dissemination. We found no evidence highlighting any specific role of ACSL4 overexpression in EMT onset. However, due to its substrate preference for arachidonic acid, and the reported crosstalk with COX-2 [18, 19], ACSL4 could favor prostaglandin production and other inflammatory mediators of EMT [40, 43]. Conversely, ACSL4-overexpressing cells display a more epithelial-like behavior in wound healing assays (Figure 2A). It could be possible that upon feeding EMT, ACSL4 could provide the necessary plasticity to revert to the epithelial phenotype through a mesenchymal–epithelial transition (MET) [26], crucial for the growth and establishment of metastasis.

Even though Warburg-like metabolism seems to be present in most malignancies, alternative energy sources can be used depending on the tumor context

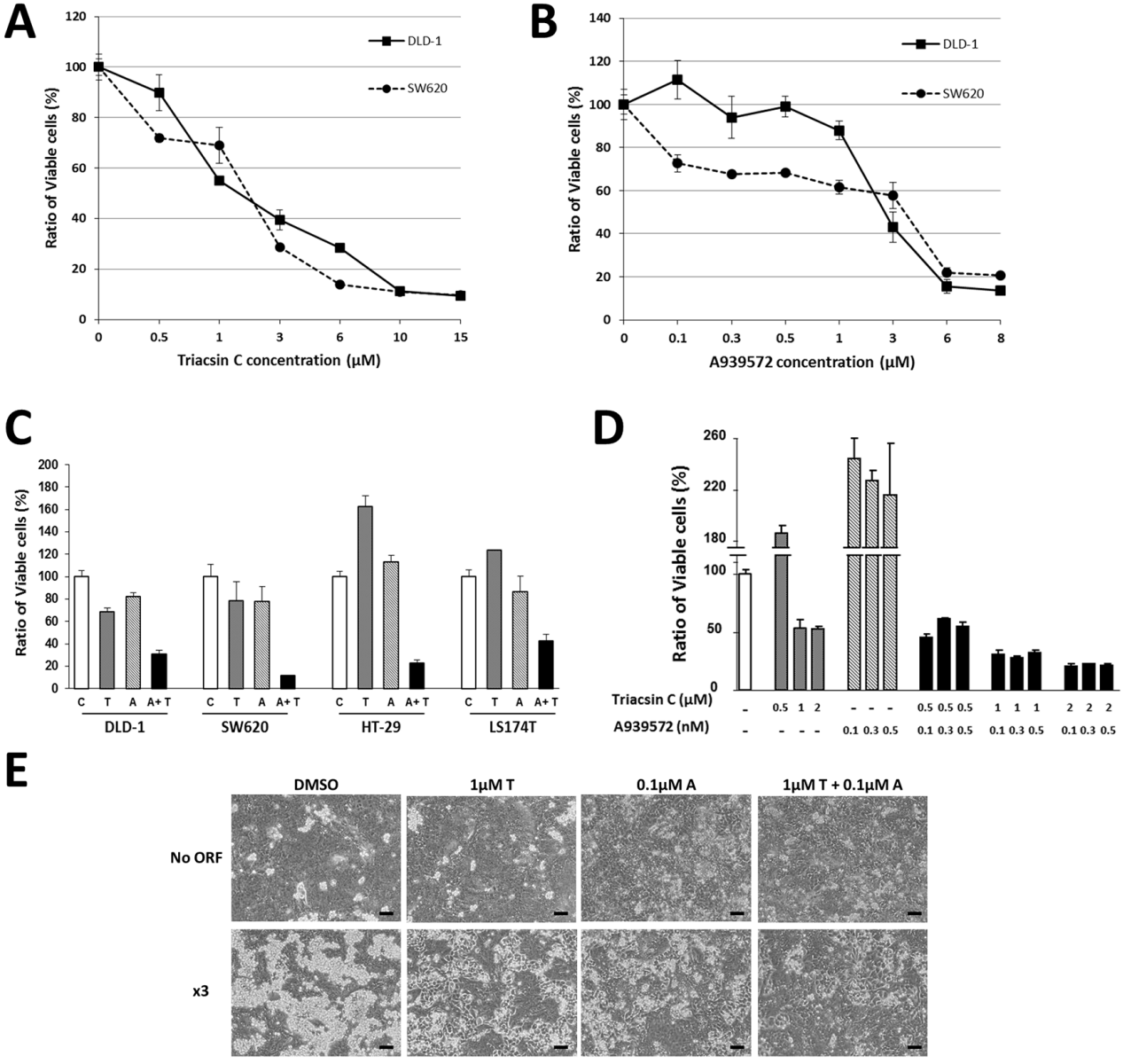

Figure 5: Synergistic effect of ACSL and SCD inhibitors on CRC cells. A–B. Dose–response curves of the MTT cell viability assays after 48 hours treatment of SW620 and DLD-1 colon cancer cells with increasing concentrations of ACSL inhibitor Triacsin C (A) or SCD inhibitor A939572 (B). **C.** MTT cell viability assays in DLD-1, SW620, HT-29 and LS174T colon cancer cell lines show synergistic action on cell viability of low doses of Triacsin C (1 μM) and A939572 (0.5 μM) upon 48 hours treatment. **D.** Response of SW620–5FU-R cells in MTT assays to the 48 hours treatment with different concentrations of Triacsin C and/or A939572. **E.** Representative phase contrast pictures of No ORF and x3 cells treated with vehicle (DMSO), Triacsin C (1 μM) and/or A939572 (0.1 μM) for 48 hours. Scale bars, 100 μm. (*Continued*)

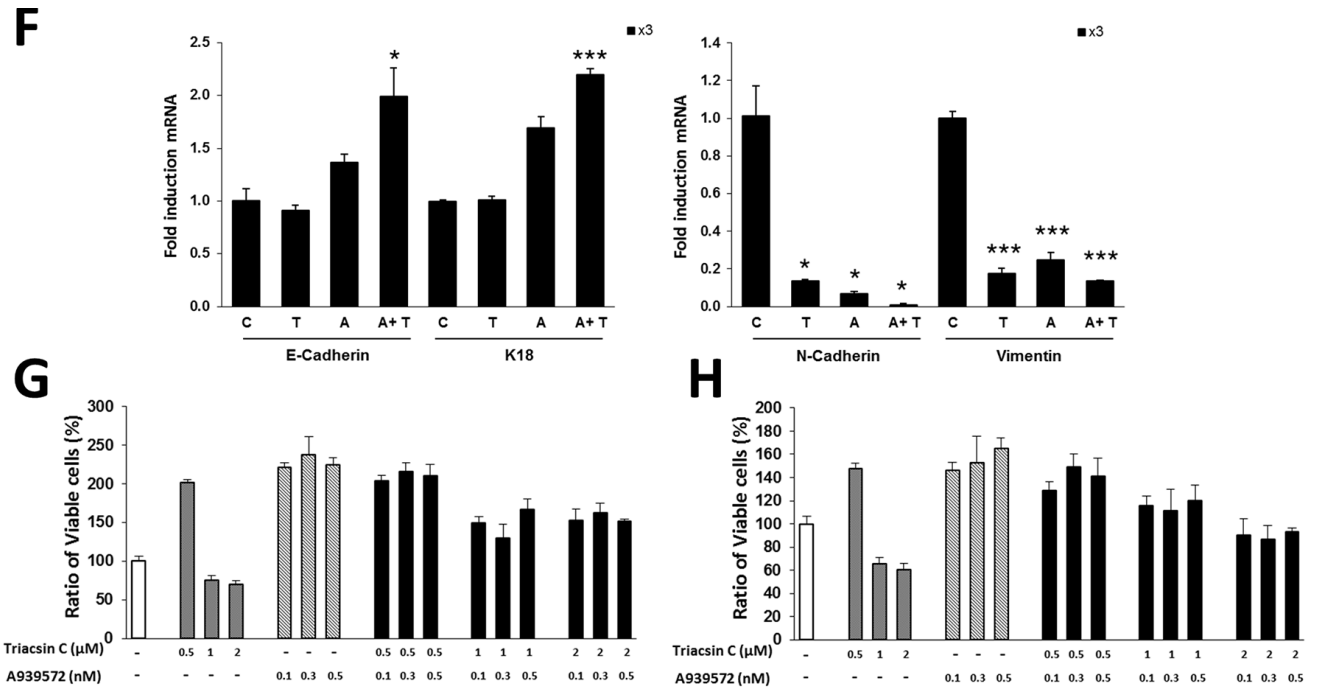

Figure 5: (*Continued*) Synergistic effect of ACSL and SCD inhibitors on CRC cells. F. RT-QPCR analysis showing the x3 cells mRNA levels of the epithelial markers *E-Cadherin, K18* and *Na+/K+ATPase β1* and the mesenchymal markers *N-Cadherin* and *Slug* upon 48 hours of treatment with Triacsin C (1 μM) and/or A939572 (0.1 μM). **G–H.** MTT cell viability assays in normal colonocytes. CCD18Co (G), or CCD841 cells (H), were treated for 48 hours with different concentrations of Triacsin C and/or A939572. Data are represented as the mean ±SD ($n = 3$) in all the plots. C = Vehicle, T = Triacsin C, A = A939572, A+T = A939572+Triacsin C. *, $p < 0.05$, ***, $p < 0.001$.

[4], suggesting an intrinsic metabolic flexibility for cancer cells. ACSL/SCD network promotes migration and invasion without main effects on cell proliferation (Figure 2). Hence, it is reasonable to think that an enhanced lipid metabolism has more implications other than support proliferation like pro-proliferative aerobic glycolysis. In fact, x3 cells show no increase, but a slight decrease in lactate production (Figure 2F). Altered lipid metabolism may be more directed to provide EMT and invasion. Interestingly, it has been reported a monoacylglycerol lipase-governed fatty acid network which drives invasion and cancer pathogenesis [51]. This could be initially driven by an EMT mechanism as the one generated by the ACSL1/ACSL4/SCD axis. On the other hand, lipids are important signaling molecules triggering a number of protumor pathways. SCD inhibition decreases the synthesis of PIP_3, crucial for Pi3K/Akt signaling [10]. Furthermore, arachidonic acid, the main ACSL4 substrate, is one of the most common fatty acids of PIP_3. ACSL, especially ACSL4, also stimulate fatty acid entry into β-oxidation [15] which generates not only ATP but also redox power necessary to counteract tumor oxidative stress [5]. Lipid anabolism and catabolism alterations have been proposed to coexist in tumor cells [52]. Therefore, an increased fatty acid catabolism caused by ACSL overexpression, along with increased de novo fatty acid synthesis and advantageous MUFA content upon SCD upregulation could generate an array of protumorigenic signals capable of supporting malignancies through an initial EMT program.

The abnormal metabolism of x3 cells provides an energetic advantage crucial to EMT promotion and invasiveness. Such is the case, that if energy homeostasis is disrupted either upon AMPK signaling reactivation (Figure 3) or upon simultaneous chemical inhibition of ACSL and SCD (Figure 5E and 5F), epithelial features are rescued. Defective AMPK signaling seems to be the main mechanism to drive EMT by the ACSL/SCD network since interference with other pathways already described to cause EMT such as Pi3K/Akt or COX-2 [43, 48] had no effect on the original phenotype recovery (Figure 3C). AMPK could be suppressing EMT through the regulation of the Akt-MDM2-Foxo3 signaling axis as recently proposed [42]. This is in agreement with the increased Akt signaling observed in x3 cells (Figure 2E). However, Akt inhibitor IV fails to revert EMT suggesting additional pathways affected by AMPK signaling that are also needed for a complete rescue. On the other hand, SCD downregulation activates AMPK [10, 53] but no link has been established between AMPK and ACSL. Since free fatty acids are able to activate AMPK [54] ACSL overexpression could prevent this activation through the conversion of fatty acids into Acyl-CoAs.

ACSL1 implication in triglyceride synthesis [55] together with the function of ACSL4 in phospholipids channeling [22] suggests an increased lipid synthesis upon

ACSL overexpression. Its associated lipotoxicity would be counteracted by SCD overexpression. Accordingly, x3 cells have 20% less fat content than No ORF cells (data not shown). Thus, either a more efficient energetic use of lipids or an abnormally increased metabolism allows malignant features of x3 cells. Their advantage does not rely on exogenous lipid supply as no variations were found when experiments were performed upon serum lipid depletion or serum content reduction (data not shown). Besides, there was no increase in lipid incorporation neither of oleic acid nor palmitic acid into lipid vesicles upon ACSL1, ACSL4 or SCD overexpression (data not shown). In agreement with that, the described monoacylglycerol-lipase invasive signature also shows independence from extrinsic fatty acids supply [51].

The combined overexpression of ACSL1/ACSL4/SCD shows a poorer outcome and higher risk of relapse when compared to the upregulation of each of the genes separately in stage II-CRC patients (Figure 4 and Table 1). This suggests an increased aggressiveness of tumors overexpressing ACSL/SCD network. This fatty acid metabolism switch that acts through an EMT program is thus an example of how different types of metabolic reprogramming can be used by tumors to increase their malignity depending on the needs and the environment (Figure 6). The combination of ACSL/SCD inhibitors synergistically reduces cancer cells viability without decreasing normal cells viability (Figure 5C, 5G and 5H). Furthermore, this is also effective in CRC cells resistant to conventional chemotherapy (Figure 5D). Therefore, this sort of "synthetic lethality" caused by the combined action of ACSL and SCD inhibitors represents a new way of addressing tumor metabolism and may designate the ACSL/SCD axis interference as a promising opportunity for cancer treatment.

MATERIALS AND METHODS

Cell culture

Colon cancer cell lines, normal colon cell lines, and HEK-293T cells, were obtained from American Type Culture Collection (ATCC, Manassas, VA, USA), cultured in DMEM supplemented with 10% FBS and maintained under standard conditions. SW620–5FU-R cells were generated by exposing parental cells to increasing concentrations of the drug for 15 months as previously described [44]. All cell lines were authenticated by microsatellite genotyping. The 3D on top assays were performed as previously described [56]. Cells were plated in Matrigel (BD Biosciences, Franklin Lakes, NJ. USA) at a density of 10000 cells per well in 24-well plates and cultured for up to a week. Images were captured using a Leica DM IL microscope (Leica Microsystems, Wetzlar, Germany), with a 10X Plan Fluotar objective and registered using Leica Application Suite (LAS, Leica).

Reagents

Commercial antibodies used are listed in Supplementary Table S2. Antibody against SCD-1 [57] was a kind gift from Dr. Jean-Baptiste Demoulin, Université Catholique de Louvain, Brussels, Belgium. Anti-human ACSL4 was generously provided by Dr. Stephen Prescott, University of Utah, Salt Lake, USA and Dr. Diana Stafforini, Huntsman Cancer Institute, University of Utah, USA, and used as indicated in [58]. Triacsin C was purchased from Santa Cruz (Santa Cruz, CA, USA); A939572 was from Biofine International (Biofine International Inc, Vancouver, Canada); Metformin, Phenformin, AICAR, NS-398 and Akt Inhibitor IV were from Sigma-Aldrich, (Sigma-Aldrich, St. Louis, MO, USA).

Lentivirus-mediated stable overexpression of ACSL1, ACSL4 and SCD

HEK 293T cells were transfected using Lipofectamine 2000 (Life Technologies, Carlsbad CA, USA) with lentiviral vectors expressing ACSL1, ACSL4, SCD or No ORF empty vector (DNA 2.0, Menlo Park CA, USA) along with a set of packaging plasmids (Addgene, Cambridge MA, USA). DLD-1 cells were infected with supernatant produced upon 48 hours transfection in HEK293T cells and 4 μg/μl polybrene (Millipore) as coadjutant. Selection was performed during 1 week by adding 2 μg/ml puromycin, 3 μg/ml blasticidin, and 150 μg/ml hygromycin, (Sigma) for SCD, ACSL4, and ACSL1 constructs respectively.

Western blot

Cells were lysed in Laemmli buffer, proteins were separated by SDS–polyacrylamide gel electrophoresis and transferred onto a nitrocellulose membrane (Bio-Rad Laboratories, Hercules, CA, USA). The membranes were blocked using 5% nonfat dry milk in TBS 0.05% Tween-20. Primary antibodies were incubated overnight at 4°C and upon 1 hour incubation with secondary antibodies signal detection was performed using the Clarity Western ECL Substrate (Bio-Rad). β-actin determination or Ponceau stain were used as loading controls.

Cell viability assay

Cell viability was determined by seeding 25000 cells per well in 24-well plates and treated with the corresponding compounds for 48 hours. Upon treatment, cells were incubated 3 hours with 3-(4,5-dimethyl-thyazol-2-yl)-2,5-diphenyl-tetrazolium (MTT, Sigma). The resultant formazan was dissolved in DMSO and its quantity determined by measuring absorbance at 560 nm. Data were expressed as the ratio of viable cells (%) which represents the percentage of viable cells upon treatment compared with the non-treated cells (100% ratio of viable cells).

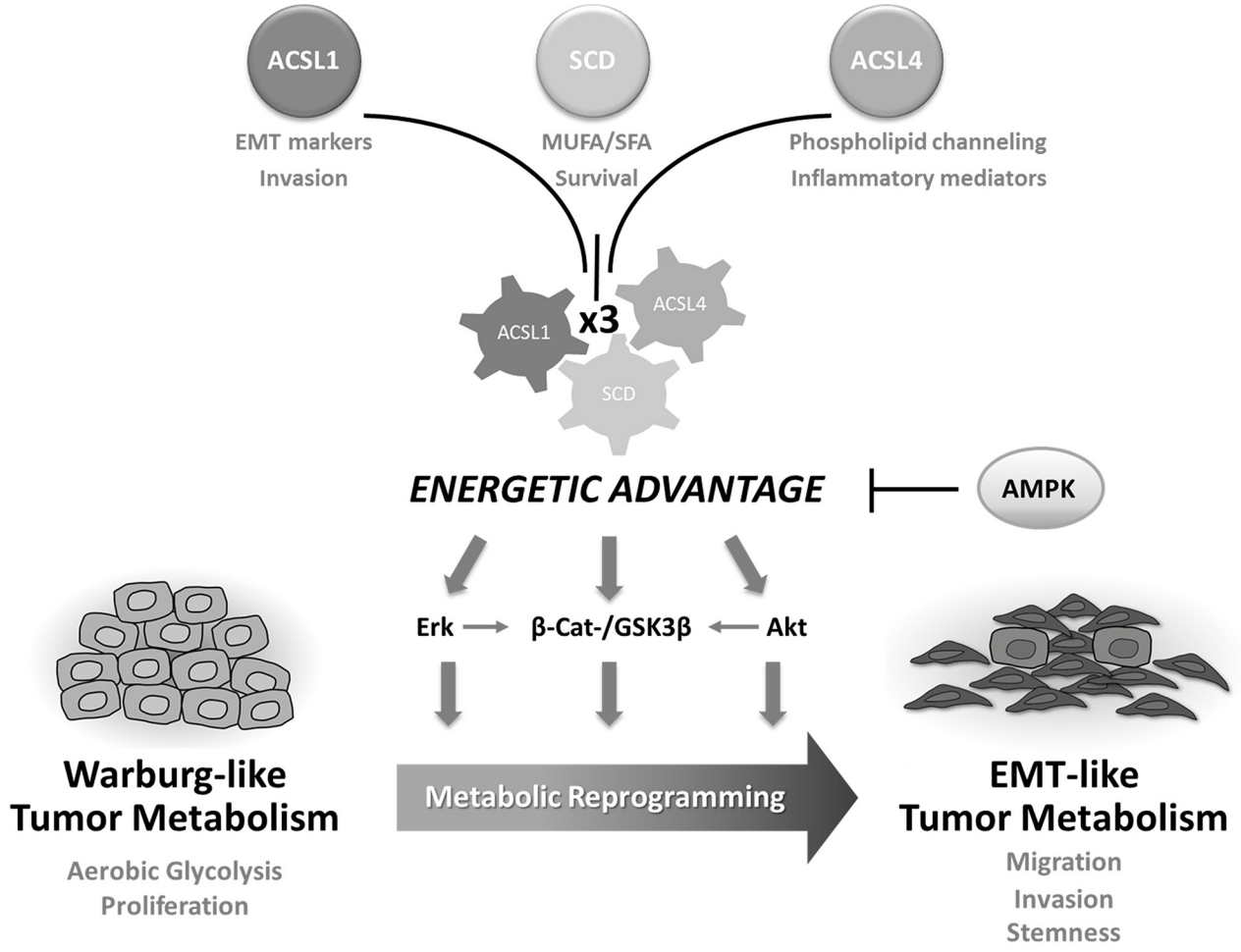

Figure 6: ACSL/SCD-mediated tumor metabolic reprogramming. The combined action of ACSL1, ACSL4 and SCD confers an energetic advantage to tumor cells that stimulates several EMT-promoting and survival pathways. Lipid metabolism switches Warburg-like tumor metabolism into EMT-like tumor metabolism leading to a gain of mesenchymal and stem cell properties as well as migratory and invasive capabilities. This process can be reversed upon re-activation of AMPK signaling.

L-Lactate quantification

Cells were seeded at a density of 5000 cells per well in a 96-well plate. At 12 hours, medium was changed to 2% FBS and kept for 24 hours at 37°C before quantification. Using Cayman's Glycolysis cell-based assay (Cayman, Ann Arbor, MI, USA, 600450) extracellular L-Lactate was measured by determining absorbance at 490 nm.

Quantitative real-time PCR

Total RNA was extracted using Tri Reagent (Sigma). 400 ng of RNA were reverse-transcribed using the High Capacity RNA-to-cDNA Master Mix system (Life Technologies). qPCR was performed in the 7900HT Real-Time PCR System (Life Technologies) using VeriQuest SYBR Green qPCR Master Mix (Affymetrix, Santa Clara, CA, USA) and gene specific primers listed in Supplementary Table S3. Values were corrected by *GAPDH* expression. The $2^{-\Delta\Delta Ct}$ method was applied to calculate the relative gene expression.

Immunofluorescence

Cells were fixed with 4% paraformaldehyde for 10 minutes at room temperature, then permeabilized 20 minutes with 0.5% triton X-100, and stained with the primary antibody (1:100) followed with incubation with Alexa 488-conjugated anti-mouse secondary antibody (1:1000) and/or with DAPI (Prolong Gold antifade, Life Technologies) to visualize nuclei. Images were captured using a Leica DM IL microscope, with a 20X Plan Fluotar objective and registered using Leica Application Suite (LAS).

EdU incorporation assay

Cells were plated on coverslips and incubated 24 hours before treatment with 10 μM EdU for 3 hours. In the case of the EdU assays in confluent conditions, EdU treatment was added once cells reached confluence. Cells were fixed with paraformaldehyde (4%) for 8 minutes and incorporation of EdU was

assayed using Click-iT® EdU Alexa Fluor® 488 Imaging Kit (Life Technologies). Coverslips were mounted on slides and nuclear DNA stained with DAPI. Images were captured using a Leica DM IL microscope, with a 40X Plan Fluotar objective and registered using LAS software.

Invasion assays

A density of 50000 cells was seeded into the inserts of a BD Matrigel™ invasion chamber (BD Biosciences) in serum-free DMEM. Medium containing 10% FBS was placed in the lower chamber as a chemoattractant. After 48 hours, inserts were fixed and stained with crystal violet, non-migrated cells removed using cotton swabs and images captured using an Olympus CKX41 microscope (Olympus, Tokyo, Japan), with a 20X LCAch objective and registered using analysis getIT software (Olympus)

Clonogenic assay

Single cell suspensions were seeded in 6-well plates at a density of 300 cells per well in 10% FBS DMEM. After 2 weeks, colonies were fixed and stained with crystal violet. Wells were photographed and colonies counted.

Wound healing assays

Cell migration was assayed using 24-well plates with IBIDI Culture-Inserts (IBIDI GmbH, München, Germany), where no cell damage occurs. 40000 cells were seeded into the two reservoirs of the same culture insert and incubated until confluence was reached. Inserts were removed and migration was monitored by taking pictures every 12 hours using a Leica DM IL microscope, with a 10X Plan Fluotar objective.

Patients and samples

80 patients as training and 120 as validation set of stage II CRC patients undergoing surgery between 2000–2004 and 2004–2008 respectively in La Paz University Hospital, were enrolled in the study. Formalin-Fixed, Paraffin-Embedded (FFPE) samples were obtained with the patient's authorization and with the approval of the human research Ethics review Committee of La Paz University Hospital (HULP-PI-1452). Inclusion criteria: Age ≥18, completely resected rectal cancer or colon adenocarcinoma located at ≥15 cm of the anal verge as determined by endoscopy or above the peritoneal reflection in the surgical resection, confirmed Stage II AJCC/UICC primary CRC and follow-up of at least 36 months. Exclusion criteria: death within 30 days after surgery, other cancers in previous 5 years and inflammatory bowel disease or specific gene-related cancer.

Statistical analysis

Significance between groups was determined by *t*-test analyses. Data with $P < 0.05$ were considered statistically significant (*, $P < 0.05$; **, $P < 0.01$; ***, $P < 0.001$). Disease free survival (DFS) was estimated using Kaplan-Meier method. Log-rank test and Univariate Cox regression analysis was performed to test the association between DFS and gene expression. Hazard ratios (HR) and 95% CI were calculated from the Cox regression model, adjusted for potential confounding factors. All reported *p* values were two-sided. Statistical significance was defined as $p < 0.05$. The statistical analyses were performed using the R statistical software version 2.15 (http://www.r-project.org).

ACKNOWLEDGMENTS AND FUNDING

We thank Dr. Jean-Baptiste Demoulin for the anti-SCD1 antibody and Dr. Stephen Prescott and Dr. Diana Stafforini for anti-ACSL4 antibody.

CONFLICTS OF INTEREST

Authors declare no potential conflict of interest

GRANT SUPPORT

This work has been supported by Ministerio de Economía y Competitividad del Gobierno de España (MINECO, Plan Nacional I+D+i AGL2013-48943-C2), Gobierno regional de la Comunidad de Madrid (P2013/ABI-2728, ALIBIRD-CM) and EU Structural Funds.

REFERENCES

1. Esposito K, Chiodini P, Capuano A, Bellastella G, Maiorino MI, Rafaniello C, Panagiotakos DB, Giugliano D. Colorectal cancer association with metabolic syndrome and its components: a systematic review with meta-analysis. Endocrine. 2013; 44:634–647.
2. Hanahan D, Weinberg RA. Hallmarks of cancer: the next generation. Cell. 2011; 144:646–674.
3. Hsu PP, Sabatini DM. Cancer Cell Metabolism: Warburg and Beyond. Cell. 2008; 134:703–707.
4. Cairns RA, Harris IS, Mak TW. Regulation of cancer cell metabolism. Nat Rev Cancer. 2011; 11:85–95.
5. Carracedo A, Cantley LC, Pandolfi PP. Cancer metabolism: fatty acid oxidation in the limelight. Nat Rev Cancer. 2013; 13:227–232.
6. Mashima T, Seimiya H, Tsuruo T. De novo fatty-acid synthesis and related pathways as molecular targets for cancer therapy. Br J Cancer. 2009; 100:1369–1372.

7. Patra SK. Dissecting lipid raft facilitated cell signaling pathways in cancer. Biochim Biophys Acta. 2008; 1785:182–206.
8. Chajès V, Thiébaut ACM, Rotival M, Gauthier E, Maillard V, Boutron-Ruault M-C, Joulin V, Lenoir GM, Clavel-Chapelon F. Association between Serum trans-Monounsaturated Fatty Acids and Breast Cancer Risk in the E3N-EPIC Study. Am J Epidemiol. 2008; 167:1312–1320.
9. Enoch HG, Catalá A, Strittmatter P. Mechanism of rat liver microsomal stearyl-CoA desaturase. Studies of the substrate specificity, enzyme-substrate interactions, and the function of lipid. J Biol Chem. 1976; 251:5095–5103.
10. Fritz V, Benfodda Z, Rodier G, Henriquet C, Iborra F, Avancès C, Allory Y, de la Taille A, Culine S, Blancou H, Cristol JP, Michel F, et al. Abrogation of de novo lipogenesis by stearoyl-CoA desaturase 1 inhibition interferes with oncogenic signaling and blocks prostate cancer progression in mice. Mol Cancer Ther. 2010; 9:1740–1754.
11. Igal RA. Stearoyl-CoA desaturase-1: a novel key player in the mechanisms of cell proliferation, programmed cell death and transformation to cancer. Carcinogenesis. 2010; 31:1509–1515.
12. Mason P, Liang B, Li L, Fremgen T, Murphy E, Quinn A, Madden SL, Biemann H-P, Wang B, Cohen A, Komarnitsky S, Jancsics K, et al. SCD1 inhibition causes cancer cell death by depleting mono-unsaturated fatty acids. PloS One. 2012; 7:e33823.
13. Roemeling CA von, Marlow LA, Wei JJ, Cooper SJ, Caulfield TR, Wu K, Tan WW, Tun HW, Copland JA. Stearoyl-CoA Desaturase 1 Is a Novel Molecular Therapeutic Target for Clear Cell Renal Cell Carcinoma. Clin Cancer Res. 2013; 19:2368–2380.
14. Roongta UV, Pabalan JG, Wang X, Ryseck R-P, Fargnoli J, Henley BJ, Yang W-P, Zhu J, Madireddi MT, Lawrence RM, Wong TW, Rupnow BA. Cancer cell dependence on unsaturated fatty acids implicates stearoyl-CoA desaturase as a target for cancer therapy. Mol Cancer Res MCR. 2011; 9:1551–1561.
15. Coleman RA, Lewin TM, Horn CGV, Gonzalez-Baró MR. Do Long-Chain Acyl-CoA Synthetases Regulate Fatty Acid Entry into Synthetic Versus Degradative Pathways? J Nutr. 2002; 132:2123–2126.
16. Gaisa NT, Reinartz A, Schneider U, Klaus C, Heidenreich A, Jakse G, Kaemmerer E, Klinkhammer BM, Knuechel R, Gassler N. Levels of acyl-coenzyme A synthetase 5 in urothelial cells and corresponding neoplasias reflect cellular differentiation. Histol Histopathol. 2013; 28:353–364.
17. Mashima T, Oh-hara T, Sato S, Mochizuki M, Sugimoto Y, Yamazaki K, Hamada J, Tada M, Moriuchi T, Ishikawa Y, Kato Y, Tomoda H, et al. p53-defective tumors with a functional apoptosome-mediated pathway: a new therapeutic target. J Natl Cancer Inst. 2005; 97:765–777.
18. Cao Y, Pearman AT, Zimmerman GA, McIntyre TM, Prescott SM. Intracellular unesterified arachidonic acid signals apoptosis. Proc Natl Acad Sci U S A. 2000; 97:11280–11285.
19. Maloberti PM, Duarte AB, Orlando UD, Pasqualini ME, Solano AR, López-Otín C, Podestá EJ. Functional interaction between acyl-CoA synthetase 4, lipooxygenases and cyclooxygenase-2 in the aggressive phenotype of breast cancer cells. PloS One. 2010; 5:e15540.
20. Monaco ME, Creighton CJ, Lee P, Zou X, Topham MK, Stafforini DM. Expression of Long-chain Fatty Acyl-CoA Synthetase 4 in Breast and Prostate Cancers Is Associated with Sex Steroid Hormone Receptor Negativity. Transl Oncol. 2010; 3:91–98.
21. Sung YK, Hwang SY, Park MK, Bae HI, Kim WH, Kim J-C, Kim M. Fatty acid-CoA ligase 4 is overexpressed in human hepatocellular carcinoma. Cancer Sci. 2003; 94:421–424.
22. Küch E-M, Vellaramkalayil R, Zhang I, Lehnen D, Brügger B, Sreemmel W, Ehehalt R, Poppelreuther M, Füllekrug J. Differentially localized acyl-CoA synthetase 4 isoenzymes mediate the metabolic channeling of fatty acids towards phosphatidylinositol. Biochim Biophys Acta. 2014; 1841:227–239.
23. Cui M, Wang Y, Sun B, Xiao Z, Ye L, Zhang X. MiR-205 modulates abnormal lipid metabolism of hepatoma cells via targeting acyl-CoA synthetase long-chain family member 1 (ACSL1) mRNA. Biochem Biophys Res Commun. 2014; 444:270–275.
24. Vargas T, Moreno-Rubio J, Herranz J, Cejas P, Molina S, González-Vallinas M, Ramos R, Burgos E, Aguayo C, Custodio AB, Reglero G, Feliu J, et al. Genes associated with metabolic syndrome predict disease-free survival in stage II colorectal cancer patients. A novel link between metabolic dysregulation and colorectal cancer. Mol Oncol. 2014.
25. Vargas T, Moreno-Rubio J, Herranz J, Cejas P, Molina S, González-Vallinas M, Mendiola M, Ramírez de Molina A. ColoLipidGene: signature of lipid metabolism-related genes to predict prognosis in stage-II colon cancer patients. Oncotarget. Oncotarget. 2015; 6:7348–7363.
26. Nieto MA, Cano A. The epithelial-mesenchymal transition under control: global programs to regulate epithelial plasticity. Semin Cancer Biol. 2012; 22:361–368.
27. Gupta GP, Massagué J. Cancer metastasis: building a framework. Cell. 2006; 127:679–695.
28. Korinek V, Barker N, Morin PJ, van Wichen D, de Weger R, Kinzler KW, Vogelstein B, Clevers H. Constitutive transcriptional activation by a beta-catenin-Tcf complex in APC-/- colon carcinoma. Science. 1997; 275:1784–1787.
29. Clevers H. Wnt/beta-catenin signaling in development and disease. Cell. 2006; 127:469–480.
30. Dong C, Yuan T, Wu Y, Wang Y, Fan TWM, Miriyala S, Lin Y, Yao J, Shi J, Kang T, Lorkiewicz P, St Clair D, et al. Loss of FBP1 by Snail-mediated repression provides metabolic advantages in basal-like breast cancer. Cancer Cell. 2013; 23:316–331.

31. Lin C-C, Cheng T-L, Tsai W-H, Tsai H-J, Hu K-H, Chang H-C, Yeh C-W, Chen Y-C, Liao C-C, Chang W-T. Loss of the respiratory enzyme citrate synthase directly links the Warburg effect to tumor malignancy. Sci Rep. 2012; 2:785.
32. Gilles C, Polette M, Mestdagt M, Nawrocki-Raby B, Ruggeri P, Birembaut P, Foidart J-M. Transactivation of Vimentin by β-Catenin in Human Breast Cancer Cells. Cancer Res. 2003; 63:2658–2664.
33. Mani SA, Guo W, Liao M-J, Eaton EN, Ayyanan A, Zhou AY, Brooks M, Reinhard F, Zhang CC, Shipitsin M, Campbell LL, Polyak K, et al. The epithelial-mesenchymal transition generates cells with properties of stem cells. Cell. 2008; 133:704–715.
34. Luca AC, Mersch S, Deenen R, Schmidt S, Messner I, Schäfer K-L, Baldus SE, Huckenbeck W, Piekorz RP, Knoefel WT, Krieg A, Stoecklein NH. Impact of the 3D Microenvironment on Phenotype, Gene Expression, and EGFR Inhibition of Colorectal Cancer Cell Lines. PLoS ONE. 2013; 8:e59689.
35. Kenny PA, Lee GY, Myers CA, Neve RM, Semeiks JR, Spellman PT, Lorenz K, Lee EH, Barcellos-Hoff MH, Petersen OW, Gray JW, Bissell MJ. The morphologies of breast cancer cell lines in three-dimensional assays correlate with their profiles of gene expression. Mol Oncol. 2007; 1:84–96.
36. Browne G, Sayan AE, Tulchinsky E. ZEB proteins link cell motility with cell cycle control and cell survival in cancer. Cell Cycle Georget Tex. 2010; 9:886–891.
37. Evdokimova V, Tognon C, Ng T, Ruzanov P, Melnyk N, Fink D, Sorokin A, Ovchinnikov LP, Davicioni E, Triche TJ, Sorensen PHB. Translational activation of snail1 and other developmentally regulated transcription factors by YB-1 promotes an epithelial-mesenchymal transition. Cancer Cell. 2009; 15:402–415.
38. Lamouille S, Xu J, Derynck R. Molecular mechanisms of epithelial-mesenchymal transition. Nat Rev Mol Cell Biol. 2014; 15:178–196.
39. Gulhati P, Bowen KA, Liu J, Stevens PD, Rychahou PG, Chen M, Lee EY, Weiss HL, O'Connor KL, Gao T, Evers BM. mTORC1 and mTORC2 regulate EMT, motility, and metastasis of colorectal cancer via RhoA and Rac1 signaling pathways. Cancer Res. 2011; 71:3246–3256.
40. Wang H, Wang H-S, Zhou B-H, Li C-L, Zhang F, Wang X-F, Zhang G, Bu X-Z, Cai S-H, Du J. Epithelial-Mesenchymal Transition (EMT) Induced by TNF-α Requires AKT/GSK-3β-Mediated Stabilization of Snail in Colorectal Cancer. PLoS ONE. 2013; 8:e56664.
41. Shackelford DB, Shaw RJ. The LKB1-AMPK pathway: metabolism and growth control in tumour suppression. Nat Rev Cancer. 2009; 9:563–575.
42. Chou C-C, Lee K-H, Lai I-L, Wang D, Mo X, Kulp SK, Shapiro CL, Chen C-S. AMPK Reverses the Mesenchymal Phenotype of Cancer Cells by Targeting the Akt-MDM2-Foxo3a Signaling Axis. Cancer Res. 2014. canres.0135.2014.
43. Neil JR, Johnson KM, Nemenoff RA, Schiemann WP. Cox-2 inactivates Smad signaling and enhances EMT stimulated by TGF-beta through a PGE2-dependent mechanisms. Carcinogenesis. 2008; 29:2227–2235.
44. González-Vallinas M, Molina S, Vicente G, de la Cueva A, Vargas T, Santoyo S, García-Risco MR, Fornari T, Reglero G, Ramírez de Molina A. Antitumor effect of 5-fluorouracil is enhanced by rosemary extract in both drug sensitive and resistant colon cancer cells. Pharmacol Res Off J Ital Pharmacol Soc. 2013; 72:61–68.
45. Behrens J, Jerchow BA, Würtele M, Grimm J, Asbrand C, Wirtz R, Kühl M, Wedlich D, Birchmeier W. Functional interaction of an axin homolog, conductin, with beta-catenin, APC, and GSK3beta. Science. 1998; 280:596–599.
46. Kim K, Lu Z, Hay ED. Direct evidence for a role of beta-catenin/LEF-1 signaling pathway in induction of EMT. Cell Biol Int. 2002; 26:463–476.
47. Mauvoisin D, Charfi C, Lounis AM, Rassart E, Mounier C. Decreasing stearoyl-CoA desaturase-1 expression inhibits β-catenin signaling in breast cancer cells. Cancer Sci. 2013; 104:36–42.
48. Ha G-H, Park J-S, Breuer E-KY. TACC3 promotes epithelial-mesenchymal transition (EMT) through the activation of PI3K/Akt and ERK signaling pathways. Cancer Lett. 2013; 332:63–73.
49. Hardy S, Langelier Y, Prentki M. Oleate activates phosphatidylinositol 3-kinase and promotes proliferation and reduces apoptosis of MDA-MB-231 breast cancer cells, whereas palmitate has opposite effects. Cancer Res. 2000; 60:6353–6358.
50. Scaglia N, Igal RA. Inhibition of Stearoyl-CoA Desaturase 1 expression in human lung adenocarcinoma cells impairs tumorigenesis. Int J Oncol. 2008; 33:839–850.
51. Nomura DK, Long JZ, Niessen S, Hoover HS, Ng S-W, Cravatt BF. Monoacylglycerol lipase regulates a fatty acid network that promotes cancer pathogenesis. Cell. 2010; 140:49–61.
52. Feizi A, Bordel S. Metabolic and protein interaction subnetworks controlling the proliferation rate of cancer cells and their impact on patient survival. Sci Rep. 2013; 3.
53. Scaglia N, Chisholm JW, Igal RA. Inhibition of stearoylCoA desaturase-1 inactivates acetyl-CoA carboxylase and impairs proliferation in cancer cells: role of AMPK. PloS One. 2009; 4:e6812.
54. Za'tara G, Bar-Tana J, Kalderon B, Suter M, Morad E, Samovski D, Neumann D, Hertz R. AMPK activation by long chain fatty acyl analogs. Biochem Pharmacol. 2008; 76:1263–1275.
55. Li LO, Ellis JM, Paich HA, Wang S, Gong N, Altshuller G, Thresher RJ, Koves TR, Watkins SM, Muoio DM, Cline GW, Shulman GI, et al. Liver-specific loss of long chain acyl-CoA synthetase-1 decreases triacylglycerol synthesis and beta-oxidation and alters phospholipid fatty acid composition. J Biol Chem. 2009; 284:27816–27826.

56. Lee GY, Kenny PA, Lee EH, Bissell MJ. Three-dimensional culture models of normal and malignant breast epithelial cells. Nat Methods. 2007; 4:359–365.

57. Demoulin J-B, Ericsson J, Kallin A, Rorsman C, Rönnstrand L, Heldin C-H. Platelet-derived growth factor stimulates membrane lipid synthesis through activation of phosphatidylinositol 3-kinase and sterol regulatory element-binding proteins. J Biol Chem. 2004; 279:35392–35402.

58. Cao Y, Murphy KJ, McIntyre TM, Zimmerman GA, Prescott SM. Expression of fatty acid-CoA ligase 4 during development and in brain. FEBS Lett. 2000; 467:263–267.

SUPPLEMENTARY FIGURES AND TABLES

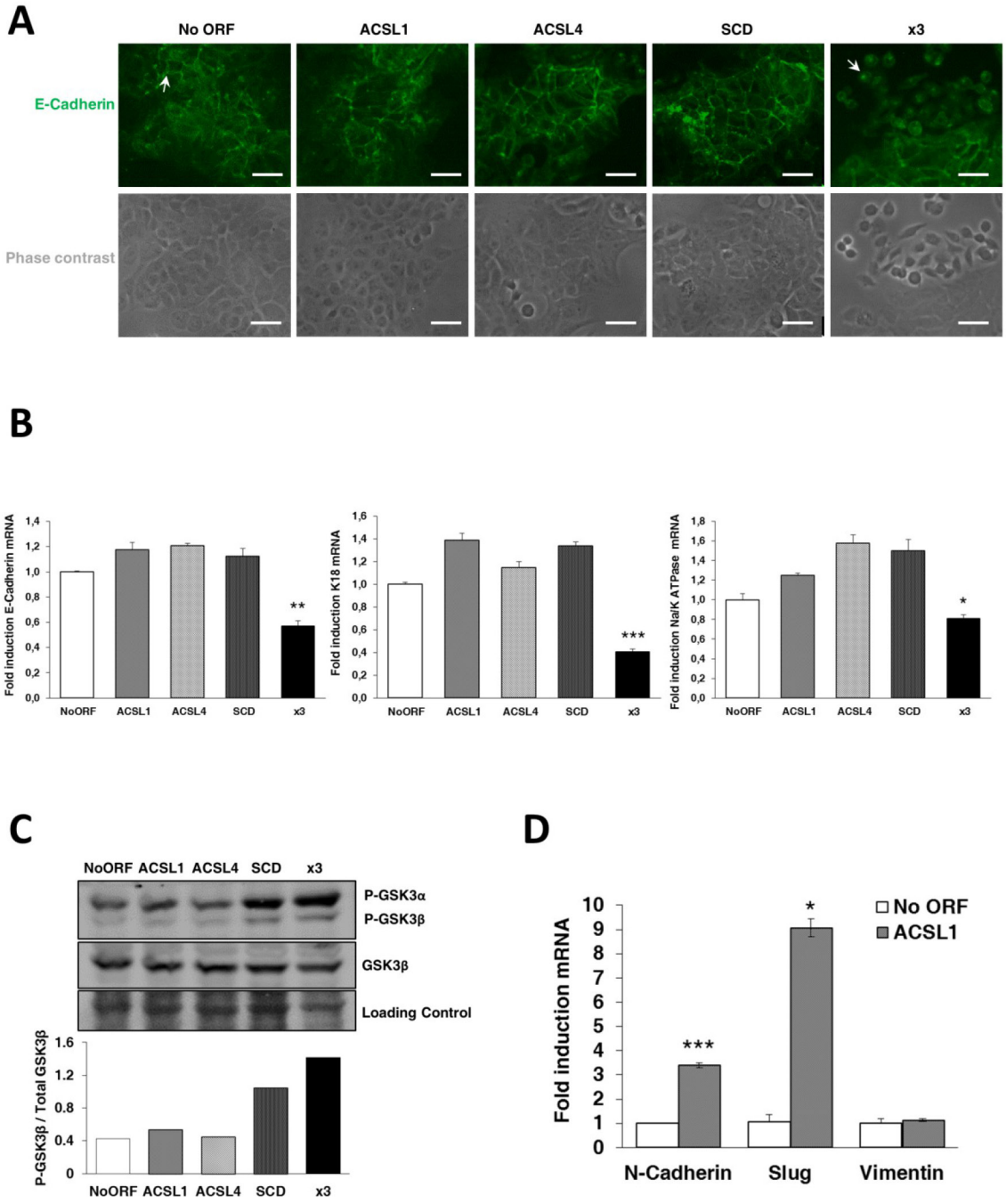

Supplementary Figure S1: Individual overexpression of ACSL1, ACSL4 and SCD is not sufficient to promote complete EMT morphological program. A. Fluorescence microscopy showing normal distribution of E-Cadherin (green) in No ORF, ACSL1, ACSL4, SCD and x3 cells. Arrows indicate the differential cellular distribution of E-Cadherin in control and x3 cells. No morphological changes are observed in phase contrast images (bottom panels) except for x3 cells. Scale bars, 50 µm. **B.** RT-QPCR analysis of epithelial genes *E-Cadherin* (left panel), *Keratin 18* (central panel) an *Na+/K+ATPase β1* (right panel). A decrease in mRNA levels is only found in the case of x3 cells compared to control No ORF and ACSL1, ACSL4 and SCD cells. **C.** Levels of GSK3 phosphorylation detected by Western Blot using a phospho-specific antibody (Ser21/9). Total GSK3β levels detection and Ponceau-stained band served as loading controls. Bottom panel: Quantification of bands intensity showing the ratio of phosphorylated to total protein. **D.** ACSL1 stable overexpression alone increases EMT genes expression levels but this is insufficient to drive a complete phenotypical change. Mesenchymal genes (*N-Cadherin, Slug* and *Vimentin*) expression levels were measured by RT-QPCR. Experiments in B and D were performed in triplicates ($n = 3$). Results represent the mean ±SD ($n = 3$). *, $p < 0.05$, **, $p < 0.01$, ***, $p < 0.001$.

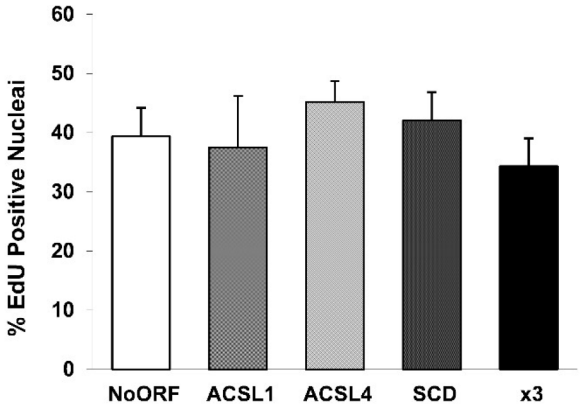

Supplementary Figure S2: Absence of major changes in proliferation upon ACSL1, ACSL4 and SCD overexpression in confluent conditions. Quantification using fluorescence microscopy of EdU incorporation in confluent cells as a measure of cell proliferation. Experiment was performed in triplicates ($n = 3$). Results represent the mean ±SD ($n = 3$).

Supplementary Table S1: Clinical and histopathological characteristics of patients

Characteristics	Stage II CRC					
	Training group			Validation group		
		n° of Patients	(%)		*n*° of Patients	(%)
Total sample size (*n*)		77	(100)		119	(100)
Age at Diagnosis (years)						
Mean	68.22			66.08		
Median	69			66		
Age Range	32–86			26–91		
<70		42	(54.55)		73	(61.34)
≥70		35	(45.45)		46	(38.66)
Gender						
Female		33	(42.86)		54	(45.38)
Male		44	(57.14)		65	(54.62)
Stage						
IIA (T3 N0 M0)		56	(72.73)		70	(58.82)
IIB (T4 N0 M0)		21	(27.27)		49	(41.18)
Total Lymph Nodes Resected						
Mean Lymph nodes resected	12.09			14.20		
Range of Lymph nodes examined	1–29			0–43		
≤12		46	(59.7)		54	(45.4)
>12		30	-39		62	(52.1)
Unknown		1	(1.3)		3	(2.5)

Characteristics	Stage II CRC					
	Training group			Validation group		
		n° of Patients	(%)		*n*° of Patients	(%)
Location of Primary						
Cecum and Ileocecal Valve		2	(2.6)		13	(10.92)
Acending colon and Hepatic flexure		29	(37.66)		29	(24.37)
Transverse colon		6	(7.79)		6	(5.04)
Splenic flexure and Descending colon		5	(6.49)		17	(14.29)
Sigmoid colon and rectosigmoid junction		34	(44.16)		54	(45.38)
Rectum		1	(1.3)		0	
Grade/Differentiation						
Well		5	(6.49)		10	(8.4)
Moderately		66	(85.71)		95	(79.8)
Poor		5	(6.49)		10	(8.4)
Unknown		1	(1.3)		4	(3.4)
Bowel Obstruction/Perforation						
Yes		10	(12.99)		45	(37.82)
No		67	(87.01)		74	(62.18)
Other Histological Features						
Perineural invasion		12	(15.58)		25	(21)
Vascular invasion		22	(28.57)		31	(26.05)
Adjuvant treatment						
Yes		47	(61.04)		76	(63.87)
No		30	(38.96)		43	(36.13)
Disease-free survival						
Patients with recurrence		22	(28.57)		18	(15.13)
Overall survival						
n° of Exitus		13	(16.88)		11	(9.24)

Supplementary Table S2: Commercial antibodies used in this study

Name	Company	Cat No
Anti-E Cadherin antibody [HECD-1]	Abcam	ab1416
Purified Mouse Anti-β-Catenin	BD Transduction	610154
ACSL1 Rabbit Polyclonal Antibody	Cell Signaling	4047
Phospho-Acetyl-CoA Carboxylase (Ser79) Antibody	Cell Signaling	3661
Acetyl-CoA Carboxylase (C83B10) Rabbit mAb	Cell Signaling	3676
Phospho-Akt (Ser473) Polyclonal Antibody	Cell Signaling	9271
Akt (pan) (C67E7) Rabbit mAb	Cell Signaling	4691
Phospho-GSK-3α/β (Ser21/9) Rabbit Polyclonal Antibody	Cell Signaling	9331
GSK-3β (27C10) Rabbit mAb	Cell Signaling	9315
p-ERK (E4) Mouse mAb	Santa Cruz	sc-7383
ERK2 (C-24) Rabbit Polyclonal Antibody	Santa Cruz	sc-154
Monoclonal Anti-β-Actin, mouse antibody	Sigma	A1978
Horseradish peroxidase conjugated antibody anti-mouse	Millipore	AP308P
Horseradish peroxidase conjugated antibody anti-rabbit	Millipore	AP307P
Alexa 488-conjugated anti-mouse antibody	Invitrogen	A-11001

Supplementary Table S3: Primers used for quantitative real-time PCR

Gene name	forward primer	reverse primer
ACSL1	ACATTATGTTCCTGGGCCCA	AGTCAGAAGGCCATTGTCGA
ACSL4	GGCACAACAGAAAGGGGTAG	GGTTCCTCAGCTCCTTCCTT
SCD-1	TGCCCACCACAAGTTTTCAG	CATCAGCAAGCCAGGTTTGT
E-CADHERIN (CDH1)	GAACGCATTGCCACATACAC	GAATTCGGGCTTGTTGTCAT
KERATIN 18 (KRT18)	GAGTATGAGGCCCTGCTGAA	CAGACACCACTTTGCCATCC
NA+/K+ATPASE B1(ATP1B1)	GCCTCCCAAGAATGAGTCCT	ATTTGGGCTGCAGGAGTTTG
N-CADHERIN (CDH2)	CGGTTTCATTTGAGGGCACA	TTGGAGCCTGAGACACGATT
SLUG (SNAI2)	CGTTTTCCAGACCCTGGTT	CTGCAGATGAGCCCTCAGA
VIMENTIN	GAGTCCACTGAGTACCGGAG	ACGAGCCATTTCCTCCTTCA
COX-2	ATCACAGGCTTCCATTGACC	CAGGATACAGCTCCACAGCA
CD44	AGCAGCGGCTCCTCCAGTGA	CCCACTGGGGTGGAATGTGTCT
LGR5	TCCAACCTCAGCGTCTTCAC	CGCAAGACGTAACTCCTCCA
ALDH1A1	TGTTAGCTGATGCCGACTTG	TTCTTAGCCCGCTCAACACT
EPCAM	CGCAGCTCAGGAAGAATGTG	TGAAGTACACTGGCATTGACG
CD29(ITGB1)	CATCTGCGAGTGTGGTGTCT	GGGGTAATTTGTCCCGACTT
GAPDH	TGGTATCGTGGAAGGACTCATGAC	ATGCCAGTGAGCTTCCCGTTCAGC

PUBLICATION II

Complementary ACSL isoforms contribute to a non-Warburg advantageous energetic status characterizing invasive colon cancer cells.

Ruth Sánchez-Martínez, Silvia Cruz-Gil, María Soledad García-Álvarez, Guillermo Reglero, Ana Ramírez de Molina.

Doi: 10.1038/s41598-017-11612-3

PUBLICATION II SUMMARY

Complementary ACSL isoforms contribute to a non-Warburg advantageous energetic status characterizing invasive colon cancer cells

In this work we aimed to clarify the individual contribution and functional differences of the participating enzymes in the context of the whole network action. Here we show how deregulation of metabolic enzymes leads to global metabolic editing to fuel tumour transformation associated with the invasive features of cancer cells. Using the XCelligence technology to assay real-time cell proliferation in DLD-1 CRC cells stably overexpressing either ACSL1, ACSL4 or SCD, a clear increase in proliferation was only found upon ACSL4 overexpression when compared to control cells. However, proliferation rates were similar to the control in the case of ACSL1 cells and reversed in SCD proliferating cells. In addition, wound healing assays showed that ACSL4 cells presented a faster unidirectional migration of cohesive epithelial sheets that could be related to proliferation stimulation. Conversely, significantly more ACSL1 cells were able to invade through matrigel when compared to ACSL4 or control cells. ACSL1 overexpression, but not ACSL4, stimulated N-cadherin or Slug expression, well-known mesenchymal markers related to invasion and metastasis.

Through the extracellular acidification rate (ECAR) analysis using a Seahorse bioanalyzer, we observed that ACSL4 cells displayed the highest glycolytic function; according to their proliferative potential. In turn, ACSL4 presented an oxygen consumption rate (OCR) similar to control cells, indicating no altered performance of the mitochondria; while ACSL1 basal OCR was significantly lower, reflecting the mitochondria diminished workflow and probably an enhanced energetic status. All these data highlighted the different contributions to cancer cell features of each isoform with distinctive tumorigenic features in cancer cells. To gain insight into individual metabolic differences the axis enzymes, we performed metabolomics analysis using the Metabolon ® platform. ACSL1 overexpressing cells were mostly characterized by an increase in acylcarnitine levels that could be due to fatty acid oxidation reduction in mitochondria corresponding with the lower OCR previously found for ACSL1 cells. However, polyunsaturated fatty acids (PUFA) were the most remarkable feature of ACSL4 cells, probably reflecting the greatest utilization for membrane biogenesis. In SCD cells, mono-unsaturated fatty acids (MUFA), SCD natural products were elevated in a predictable fashion. The most outstanding results were obtained in x3 cells (494 differential biochemicals) where we found increased phospholipids levels of different classes; basic components of cell membranes, cell proliferation and cancer signaling [51,56,57]. Furthermore, x3 cells showed an elevation of some urea cycle

derived metabolites, such as polyamines, extensively related to cell proliferation and growth [219,220]. Creatine and creatine phosphate, also found elevated, were in line with a more favourable energy status. Curiously, this altered metabolism in x3 cells is not associated with an increased proliferation, as demonstrated by real-time cell proliferation assays. Thus, x3 cells altered metabolic profile should be fuelling malignant characteristics other than proliferation, as invasiveness or a more favoured energetic balance. Creatine levels in x3 cells was also assayed, as well as in several CRC invasive/metastatic cell lines. These cell lines presented increased creatine levels compared with less invasive and primary tumor-derived cells, suggesting that the creatine levels can be a common feature of CRC cells invasiveness and metastatic capacity. On the other hand, OCR analysis was performed in x3 cells and their control counterpart as well as in the well-known metastatic CRC cell line sw620 and its control primary tumor-derived cell line SW480. Invasive/Metastatic cell lines, x3 and SW620, presented a decreased basal rate of mitochondria oxidation when compared with their corresponding control non-invasive cells without major changes in glycolysis (ECAR). This reduced basal oxidative metabolism was in accordance with less oxidative stress in x3 cells, as was revealed by increased reduced glutathione (GSH) levels in x3 and sw620 cells.

PUBLICATION II CONCLUSIONS

- ACSL isoforms show functional and metabolic differences. ACSL4 fuels proliferation and migration accompanied by a more glycolytic phenotype. ACSL1 stimulates invasion displaying a lower basal respiration.
- The elevation of acylcarnitines, lower levels of PUFA, and the upregulation of MUFA are the most remarkable metabolic features of the individual overexpression of ACSL1, ACSL4 and SCD.
- Higher phospholipid levels and urea cycle upregulation characterize ACSL/SCD action as a network, a differential phenotype that cannot be explained by additive functions of each enzyme separately.
- ACSL/SCD network produce more energetically efficient cells which present lower basal respiration levels and upregulated creatine pathway. These features also characterize other invasive and metastatic cells.
- **ACSL/SCD network exemplifies specific metabolic adaptations for invasive cancer cells.**

I contributed to the whole experimental part, with special emphasis in Metabolon analysis and in Seahorse experiments. I also contributed to the manuscript elaboration and response to reviewers.

SCIENTIFIC REPORTS

OPEN

Complementary ACSL isoforms contribute to a non-Warburg advantageous energetic status characterizing invasive colon cancer cells

Received: 30 June 2017
Accepted: 25 August 2017
Published online: 11 September 2017

Ruth Sánchez-Martínez, Silvia Cruz-Gil, María Soledad García-Álvarez, Guillermo Reglero & Ana Ramírez de Molina

Metabolic reprogramming is one of cancer hallmarks. Here, we focus on functional differences and individual contribution of acyl coA synthetases (ACSL) isoforms to the previously described ACSL/stearoyl-CoA desaturase (ACSL1/ACSL4/SCD) metabolic network causing invasion and poor prognosis in colorectal cancer (CRC). ACSL4 fuels proliferation and migration accompanied by a more glycolytic phenotype. Conversely, ACSL1 stimulates invasion displaying a lower basal respiratory rate. Acylcarnitines elevation, polyunsaturated fatty acids (PUFA) lower levels, and monounsaturated fatty acids (MUFA) upregulation characterize the individual overexpression of ACSL1, ACSL4 and SCD, respectively. However, the three enzymes simultaneous overexpression results in upregulated phospholipids and urea cycle derived metabolites. Thus, the metabolic effects caused by the network are far from being caused by the individual contributions of each enzyme. Furthermore, ACSL/SCD network produces more energetically efficient cells with lower basal respiration levels and upregulated creatine pathway. These features characterize other invasive CRC cells, thus, ACSL/SCD network exemplifies specific metabolic adaptations for invasive cancer cells.

Cancer energy relies on metabolic editing to fuel malignant transformation[1]. A great deal of effort has been done to characterize tumours metabolic phenotypes and new oncometabolites are constantly being described as markers of the disease[2]. Besides well-known carbohydrate metabolism alterations, it is becoming clear that there is an increasing range of metabolic adaptations that tumours can use to sustain their growth[3–9].

Metabolic changes in cancer cells are often linked to growth and survival pathways driving different aspects of tumorigenesis. For instance, glycolytic behaviour associates with Akt and Erk pathways[10–13], while *Myc* oncogene could govern glutamine addiction[14]. Alterations in lipid metabolism, both catabolic and anabolic, are part of the metabolic reprogramming that occurs in tumour cells in response to gene mutations, loss of tumour suppressors and epigenetic modifications[15,16]. Fatty acid (FA) metabolism enzymes have been found to be essential for neoplastic growth[17–20] as well as lipid signalling triggers key tumorigenic pathways[21–23].

Interconnection of metabolic pathways allows that metabolic enzymes deregulation in cancer exert unexpected effects on non-directly related routes[24]. Besides, cross-talk with tumorigenic pathways can cause activation of further metabolic routes triggered by core cancer signalling. This way, metabolic enzymes deregulation not only affect the proportion of their expected substrates and products as well as their immediate pathways. In some cases, substantial changes in unexpected parallel metabolic routes can be observed, allowing the connection with cell cycle regulation, redox management and other changes favouring different tumour cells characteristics[25,26].

We have previously described a lipid network able to trigger epithelial-mesenchymal transition (EMT) and invasion, which is overexpressed in colorectal cancer (CRC) patients with poorer outcomes[19]. This network comprises ACSL1 and ACSL4, members of the fatty acid activating enzymes acyl coA synthetases (ACSL), critical for

Molecular Oncology and Nutritional Genomics of Cancer Group, IMDEA Food Institute, CEI UAM+CSIC, E28049, Madrid, Spain. Correspondence and requests for materials should be addressed to R.S.-M. (email: ruth.sanchez@imdea.org) or A.R.M. (email: ana.ramirez@imdea.org)

lipid synthesis, modification and β-oxidation[27]; and the stearoyl-CoA desaturase (SCD), the main enzyme controlling the rate of saturated (SFA) vs unsaturated fatty acids (MUFA)[28], crucial for cancer cells[29]. These enzymes have been related to the prognosis and progression of several malignancies[30–36]. Despite ACSL isoforms can catalyse the same reaction, to bind a molecule of Acetyl–CoA to a fatty acid giving rise to an Acyl-CoA, there is increasing evidence for a specialization in the substrates, functions and cellular localizations. ACSL1 has been reported to be more inclined to triglyceride synthesis[37,38]. In contrast, ACSL4, that prefers longer polyunsaturated fatty acids (PUFA) as substrates such as arachidonic acid, has been proposed to channel FA towards phospholipids[39]. Here we further analyse the individual contributions of each enzyme to the ACSL/SCD network and the metabolic characteristics accompanying ACSL/SCD invasive cells. We present an example on how deregulation of metabolic enzymes gives rise to global metabolic changes that derive into specific ways of tumour fuelling associated with the invasive features of cancer cells.

Results

Metabolic differences correspond to diverse protumorigenic features conferred by ACSL1 and ACSL4 isoforms. In an earlier report, we described an ACSL1/ACSL4/SCD network causing EMT and invasion in CRC cells[19]. To address more in detail the individual contributions of each enzyme integrating the ACSL/SCD axis we started investigating the differences among ACSL1 and ACSL4 isoforms. First, using DLD-1 CRC cells stably overexpressing ACSL1 or ACSL4 proteins (ACSL1 or ACSL4 cells)[19] we assayed cell proliferation. We used XCelligence technology to monitor real-time cell proliferation of these cell lines. ACSL4 overexpression caused the highest increase in proliferation when compared to control No ORF cells (Fig. 1A). Accordingly, the use of shRNAs against ACSLs (Supplementary Figure 1) caused the opposite effect, being again ACSL4 the isoform whose depletion caused the strongest effect on proliferation (Fig. 1B). The same tendency was observed in ACSL1 overexpressing or depleted cells, however, the effect was less marked. Specially, ACSL1 cells almost proliferated at a similar rate to the No ORF control cells. Curiously, SCD caused a reverse effect, decreasing proliferation rate upon overexpression (SCD cells[19]) and a proliferation increase in the case of shSCD cells (Fig. 1A,B and Supplementary Figure 1). Wound healing assays are normally performed to assay migratory capacity. However, wounds can be closed by unidirectional migration of cohesive epithelial sheets that can be related to proliferation abilities. Would healing assays show that ACSL4 cells were able to close the wound faster than the ones overexpressing ACSL1 (Fig. 1C), displaying this collective unidirectional migration of cohesive epithelial sheets that could be related to the stimulatory effect of ACSL4 on proliferation (Fig. 1A). Conversely, significantly more ACSL1 cells were able to invade through matrigel when compared to ACSL4 or poorly invasive DLD-1 No ORF control cells (Fig. 1D). Correspondingly, ACSL1 overexpression but not ACSL4 stimulated *N-cadherin* or *Slug* expression (Fig. 1E), well-known EMT markers involved in cancer invasion and metastasis[40,41]. This mesenchymal tendency of ACSL1 cells could lead them to close the wound more efficiently than No ORF control cells as can be inferred from the wound closure morphology (Fig. 1C). Taken together, these results highlight the different contributions to cancer cell features of both isoforms.

It is well know the relation between metabolic alterations fuelling different malignant aspects of tumour cells, such as the pro-proliferative Warburg effect[42]. For this reason, we wanted to check the glycolytic potential, as the aerobic glycolysis is one of the most remarkable features of proliferative cancer cells. Extracellular acidification rate was measured to assay glycolytic function of ACSL1, ACSL4 and No ORF control DLD-1 cells. In accordance with their proliferative potential, the highest basal glycolysis, glycolytic capacity and reserve was found for ACSL4 cells when compared to No ORF cells, finding an intermediate glycolytic phenotype for ACSL1 cells (Fig. 2A,B). We further wanted to check the oxidative metabolism reflecting the mitochondrial activity of these cell lines (Fig. 2C). Differently, ACSL4 presented both, a basal and maximal oxygen consumption rate (OCR) similar to No ORF cells, however, ACSL1 basal OCR was significantly lower than the other cell clones, highlighting again the metabolic differences among ACSL isoforms. Consequently, knocking down of ACSLs by shRNA means presented the opposite effect. In this case, shACSL1 cells presented the highest basal and maximal OCR, and again, ACSL4 and control (shCtrl) cells presented a parallel behaviour (Fig. 2D). All these data suggest that different metabolic performances are associated with distinctive tumorigenic features in cancer cells.

Metabolic profiling segregates ACSL isoforms and malignant features of CRC cells. To gain further insight into the functional differences between ACSL1 and ACSL4, and to elucidate the metabolic features corresponding to the ACSL/SCD network enzymes, we performed metabolomics analysis using ACSL1 and ACSL4 cells together with the corresponding DLD-1 cells overexpressing SCD (SCD cells) and the three enzymes at the same time (x3 cells)[19]. A total of 494 differential biochemicals were identified. Figure 3A shows a summary of the numbers of metabolites that achieved statistical significance ($p \leq 0.05$), as well as those with approaching significance ($0.05 < p < 0.10$). A principal component analysis, (PCA), was done to visualize how samples, within a group, cluster with respect to their data-compressed "principle components". Figure 3B shows how all sample groups were well segregated from each other based on differences in their overall metabolic signature. According to this analysis, ACSL1 samples were the ones that were less separated from No ORF control ones, and, thus, more similar regarding their metabolic profiles. In contrast, the combination of overexpressed enzymes (x3) generated an overall metabolite profile most significantly diverged from the control.

Regarding the individual metabolic characteristics for each enzyme overexpression, ACSL1 cells were mostly characterized by an increase in acylcarnitine levels (Fig. 3C, Supplementary File 1). While ACSL4 and SCD cells also displayed some increases in acylcarnitines relative to control, ACSL1 was consistently the highest. Acylcarnitines are generated through the transfer of carnitine for CoA on acyl-CoA derivatives of long-chain FA by carnitine palmityoltransferase (CPT), to transport them through the mitochondrial membrane. Thus, elevated acylcarnitine levels can be due to increased CPT activity resulting from an increase in the cytoplasmic acyl-CoA substrate levels, such as the ACSL1 products.

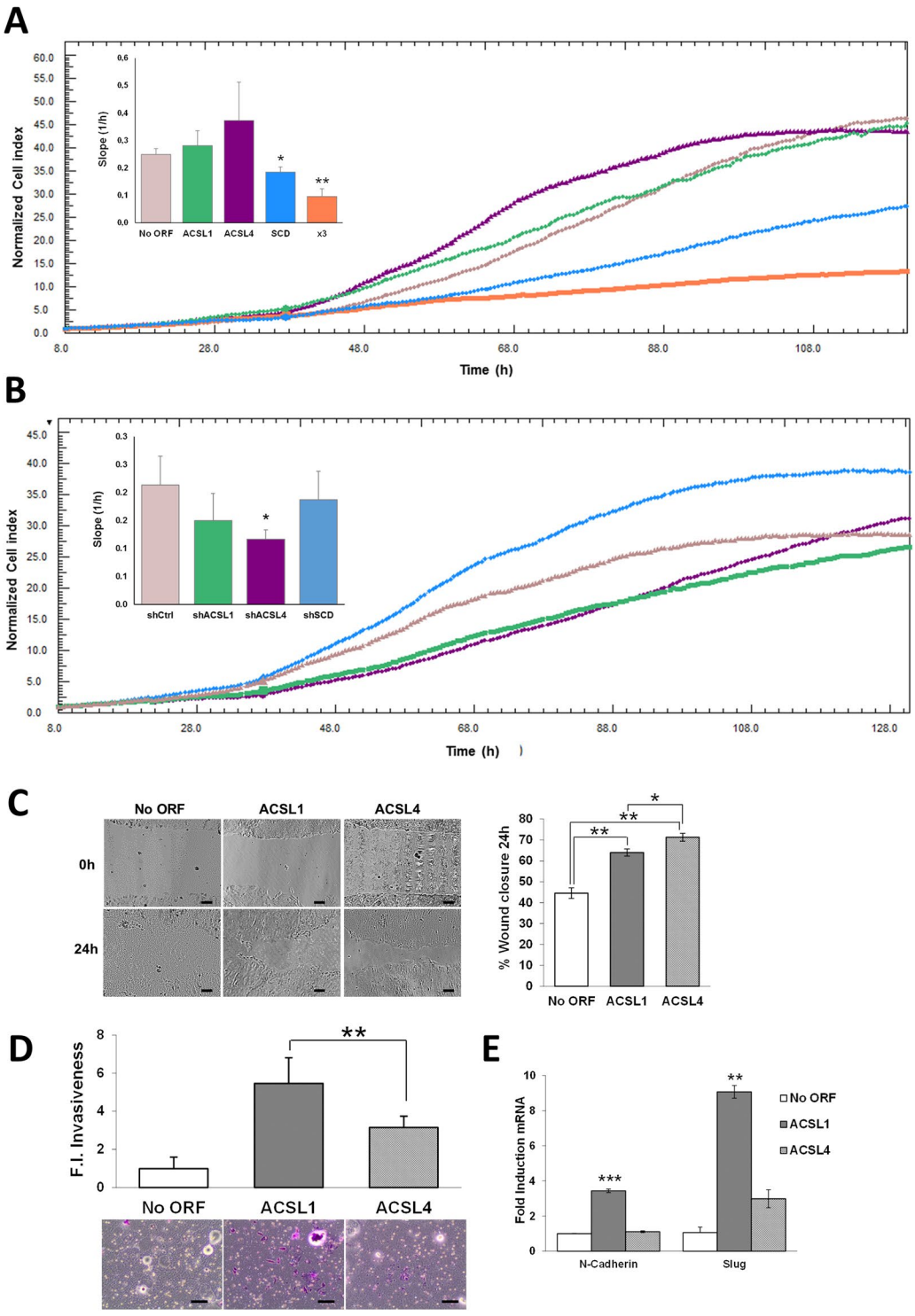

Figure 1. Comparison of protumorigenic capabilities conferred by ACSL isoforms to CRC cells. (**A**) Real-time monitoring of cell proliferation for cells overexpressing ACSL1, ACSL4, SCD, both individually or simultaneously (x3). (**B**) Real-time monitoring of cell proliferation for cells stably expressing shRNAs for ACSL1 (shACSL1), ACSL4 (shACSL4), SCD (shSCD) or scramble (shCtrl). Representative experiments are shown. Bar chart indicates the curves slope (proliferation rate) as the average of 3 independent experiments (n = 3). (**C**) Phase contrast pictures of wound healing assay comparing migratory capacities of No ORF, ACSL1 and ACSL4 cells. Quantification (right panel) shows the different behaviour of control, ACSL1 and ACSL4 cells at 24 hours of wound closure. Scale bars, 100 μm. (**D**) Boyden chamber transwell assay of 48 hours of invasion through Matrigel. Migratory cells were quantified as the average number of cells found in five random microscope fields in three independent inserts. Scale bars, 50 μm. (**E**) RT-QPCR analysis of mesenchymal genes (*N-Cadherin* and *Slug*) for ACSL1 and ACSL4 cells compared to levels in No ORF control cells. Experiments were performed in triplicates (n = 3). Results represent the mean ± SD (n = 3). *$p < 0.05$, **$p < 0.01$, ***$p < 0.001$.

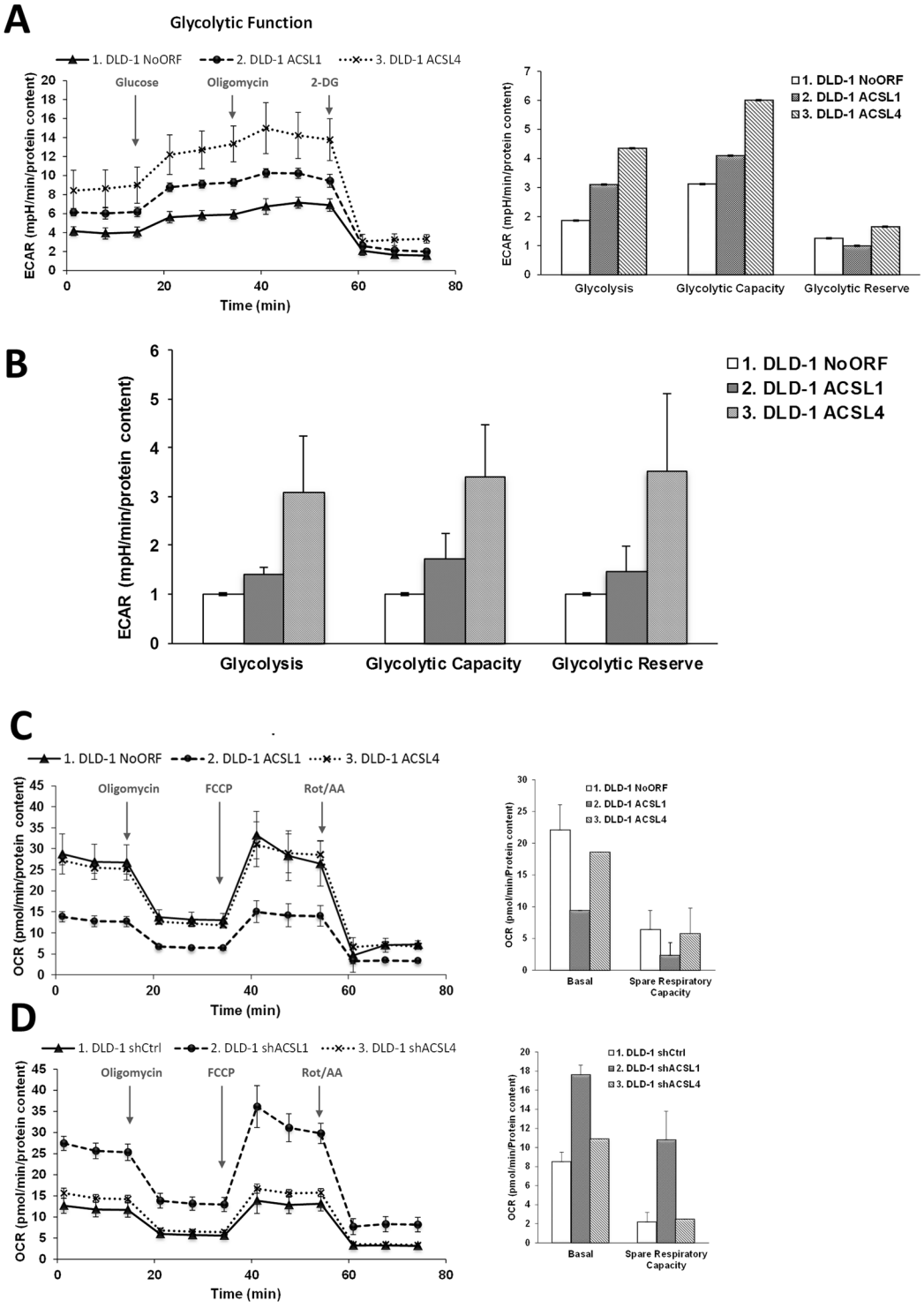

Figure 2. Bioenergetic characterization of ACSL1 and ACSL4 isoforms. (**A**) Glycolytic profile of No ORF, ACSL1 and ACSL4 cells. Cells were starved 1 h and a half and Extracellular Acidification Rate (ECAR) levels were measured using a Seahorse extracellular flux analyser. Addition of 10 µM glucose was used for the measurement of glycolysis rate. Maximal ECAR was measured upon 0.5 µM Oligomycin treatment. 50 mM 2-DG inhibits all glycolysis showing non-glycolytic acidification. Right panel shows the quantification of Glycolysis (measurement of glycolytic process rate), Glycolytic Capacity (Maximum response to glycolytic demand from stress) and Glycolytic Reserve (Reserve capacity available to utilize glycolysis beyond the basal rate). (**B**) Average quantification of glycolytic parameters in 3 independent experiments (n = 3) with 12 replicates each. (**C**) Oxygen consumption rate (OCR) of No ORF, ACSL1 and ACSL4 cells. Bioenergetics parameters were obtained by adding 2 µM Oligomycin to block ATP-linked OCR, 0.2 µM FCCP to uncouple mitochondria for maximal OCR and 0.5 µM Rotenone/Antimycin A (Rot/AA) to shut down mitochondrial respiration. Right panel reflects the quantification of basal respiration (oxygen consumption used to meet

cellular ATP demand, calculated by subtracting non-mitochondrial OCR obtained upon Rot/AA addition) and spare respiratory capacity (capability to respond to an energetic demand, calculated as the difference between maximal and basal OCR). (**D**) OCR measurements over time for cells stably expressing shRNAs for ACSL1 (shACSL1), ACSL4 (shACSL4) or scramble (shCtrl) and respiratory parameters quantification (right panel). **A**, **C** and **D** show representative experiments of 3 or 4 experiments (n = 3).

In spite of belonging to the same family that ACSL1 and the possibility to perform equivalent reactions, lower levels of polyunsaturated fatty acids (PUFA) were the most remarkable feature of ACSL4 cells (Fig. 3D, Supplementary File 1). Not surprisingly, among the significantly downregulated PUFA we can find all preferred ACSL4 substrates, such as arachidonate, docohexanoate and eicosapentaenoate. ACSL1 cells presented downregulated PUFA levels as well, even though it was not so marked as in ACSL4 cells, suggesting certain function overlapping.

As expected, several monounsaturated fatty acids (MUFA) were elevated relative to control in the SCD overexpressing cells, while their corresponding saturated substrate fatty acids were not (Fig. 3E, Supplementary File 1). Palmitoleate, one of the main products of SCD was clearly upregulated in these cells. Even though we did not find an elevation of the enzyme main product, oleate (18:1n9), this can be explained by conversion into eicosenoate (20:1n9) and erucate (22:1n9) upon elongase action.

The most striking results were found for the x3 cells. Figure 4 shows the main metabolic pathways enriched upon ACSL1, ACSL4 and SCD simultaneous overexpression, mainly involved in fatty acid, carbohydrate, nucleotides and energy metabolism. As a first distinctive feature, x3 cells showed higher levels of many phospholipids in the phosphatidylcholine, phosphatidylethanolamine and phosphatidylinositol classes (Fig. 5A, Supplementary File 1). Phospholipids make up the largest lipid component of cell membranes, crucial for cell proliferation and cancer signalling. x3 cells also displayed elevated choline and choline phosphate levels (Fig. 5A) that could be a result of phospholipid degradation, but lysolipids are generally down in the SCD and x3 cells, consistent with a decrease in phospholipid turnover (Supplementary File 1). In addition, many monoacylglycerols were up in x3 as well as in SCD relative to No ORF cells (Fig. 5A, Supplementary File 1). Other lipids varied in an opposite sense, such as sphinganine whose levels drop precipitously in x3 cells while, accordingly, products downstream of sphinganine were elevated, such as phosphoethanolamine, the ceramide N-palmitoyl-sphingosine and sphingomyelin (Supplementary Figure 2 and Supplementary File 1).

The second distinctive feature of ACSL/SCD axis was the elevation of some urea cycle derived metabolites (Fig. 5B). The highly-elevated polyamines spermine and spermidine derive from the urea cycle metabolite ornithine and other urea cycle metabolites such as arginine, ornithine and urea were also elevated (Fig. 5C). Elevated polyamine levels have been associated with increased cell proliferation and other malignant features[43,44]. Moreover, creatine and creatine phosphate were also elevated in x3 cells, potentially indicating a more favourable energy status in those cells relative to the other clones (Fig. 5C).

The glycolysis pathway was also altered in x3 cells. The intermediates dihydroxyacetone phosphate, 3-phosphoglycerate and phosphoenolpyruvate (PEP) were strongly elevated in x3 cells (Supplementary Figure 3 and Supplementary File 1). PEP levels elevation could be due to a decline in pyruvate kinase (PK), or an increase in phosphofructosekinase-1 (PFK-1) activities. Despite the much higher PEP levels, pyruvate levels were not significantly changed. PK activity can be down-regulated by increases in Acetyl-CoA levels, coincident with higher Acetyl-CoA in x3 cells. PFK-1 increased activity is also supported by decreased levels of the PFK-1 substrate, fructose-6-phosphate and elevation of its product, fructose 1,6-bisphosphate, up in x3 cells (Supplementary Figure 3 and Supplementary File 1).

Increases in the amount of phospholipids, sphingomyelins and ceramides and polyamines, have been reported to stimulate proliferation[23,44]. Thus, the more aggressive characteristics of x3 cells could be due to an increased cell proliferation. We have previously reported that the simultaneous overexpression of ACSL/SCD was not accompanied of increased proliferation[19]. Figure 1A shows how ACSL1/ACSL4/SCD simultaneous overexpression (x3 cells) not only does not increase cell proliferation but also causes the opposite effect, presenting the lowest proliferation rate among all the cell lines. Thus, x3 cells altered metabolic profile should be fuelling malignant characteristics other than proliferation, as invasiveness or a favoured energetic balance. In this sense, more invasive and metastatic CRC cell lines presented increased creatine levels compared with less invasive and primary tumour derived cells (Fig. 6). Hence, upregulated creatine pathway (Figs 4, 5C and 6) could reflect a more favourable energy status that could be crucial for processes other than cell proliferation such as cell invasion.

ACSL/SCD overexpression phenocopies metabolic features of metastatic cells. This improved energetic status was further studied by analysing OCR in x3 cells. This invasive cell line presented a decreased basal OCR when compared with non-invasive No ORF cells (Fig. 7A), that, consequently, derived in a decreased OCR consumption under stressed conditions (FCCP addition). However, differences were not so patent when glycolysis was assayed, since extracellular acidification rate (ECAR) was mostly similar (or slightly less) to control cells (Fig. 7B). When both parameters of cell metabolism were analysed in a combined way, without main differences in glycolysis, the core dissimilarity was a lesser basal rely of oxidative metabolism in mitochondria (Fig. 7C). This attenuated basal oxidative metabolism is in accordance with less oxidative stress in x3 cells, as is reflected by increased reduced glutathione (GSH) levels in x3 cells (Fig. 7D) and upregulated general glutathione metabolism (Fig. 4 and Supplementary File 1).

We wondered if these metabolic differences identified in ACSL/SCD overexpressing cells were a common feature of other invasive cells. For this purpose, we comparatively studied metabolic differences among primary tumour SW480 cells and SW620 cells, derived from a metastasis of the same patient. Interestingly, the metastatic

A

Statistical Comparisons Welch's Two-Sample t-Test					
Significantly Altered Biochemicals		Total biochemicals $p \leq 0.05$	Biochemicals (↑|↓)	Total biochemicals $0.05 < p < 0.10$	Biochemicals (↑|↓)
Comparisons to Control	*ACSL1* / *No ORF*	32	14|18	27	8|19
	ACSL4 / *No ORF*	31	15|16	31	16|15
	SCD / *No ORF*	95	61|34	61	34|27
	x3 / *No ORF*	167	124|43	50	34|16

B

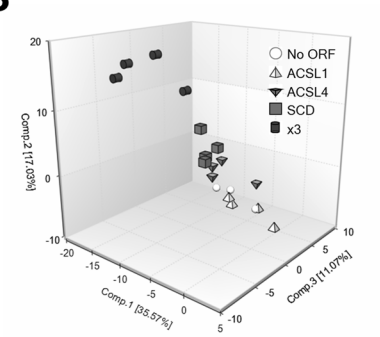

C

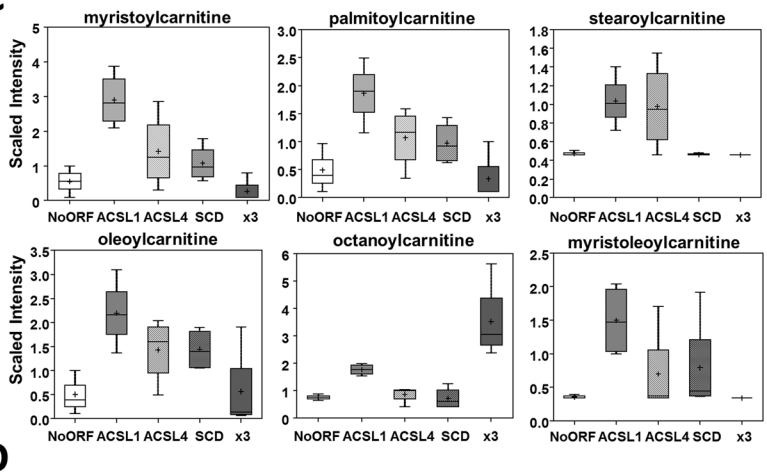

D

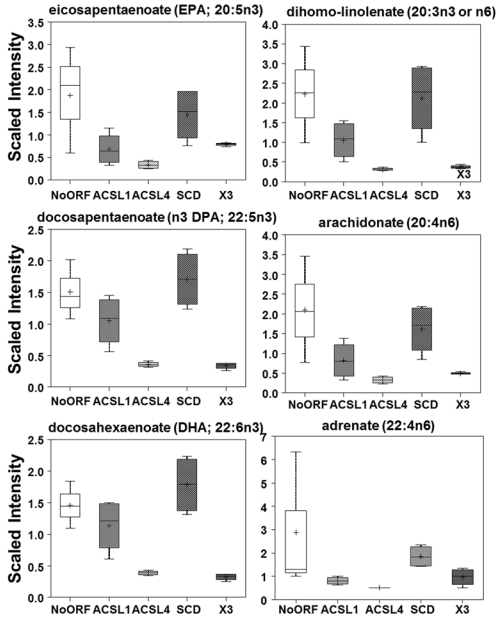

E

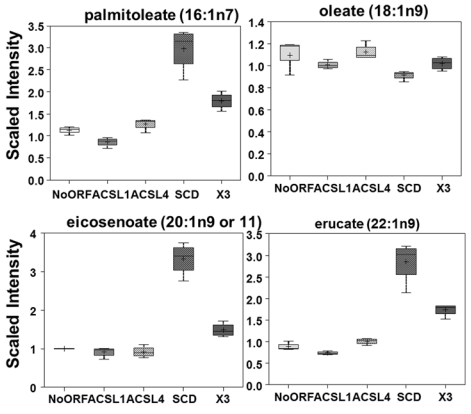

Figure 3. Individual overexpression of ACSL1, ACSL4 or SCD associates to changes in specific sets of metabolites. (**A**) Metabolomic analysis statistical summary of colon cancer cells overexpressing ACSL1, ACSL4 and SCD. Table indicates the number of biochemicals with statistical significance ($p \leq 0.05$) or with approaching significance ($0.05 < p < 0.10$) from dataset analysis with a total 494 named biochemicals detected. Black numbers indicate upregulated metabolites as grey colour indicates the downregulated ones. Welch's two-sample t-test was used to identify biochemicals that differed significantly between experimental groups. (**B**) Principal component analysis (PCA) segregation of DLD-1 expression-subtypes based on differences in metabolic signature. (**C**) Acylcarnitines are elevated most dramatically in DLD-1 cells expressing ACSL1. Box plots show the scaled intensity (Y axis) for each chemical. Mean, median and maximum and minimum values of the distribution are represented in the plots. (**D**) DLD-1 cells expressing ACSL4 present lower PUFA levels. Box plots for the levels of representative polyunsaturated fatty acids are shown. (**E**) Monounsaturated fatty acids are elevated in DLD-1 cells expressing SCD. Levels of the unsaturated fatty acids palmitoleate, oleate, eicosenoate and erucate are represented.

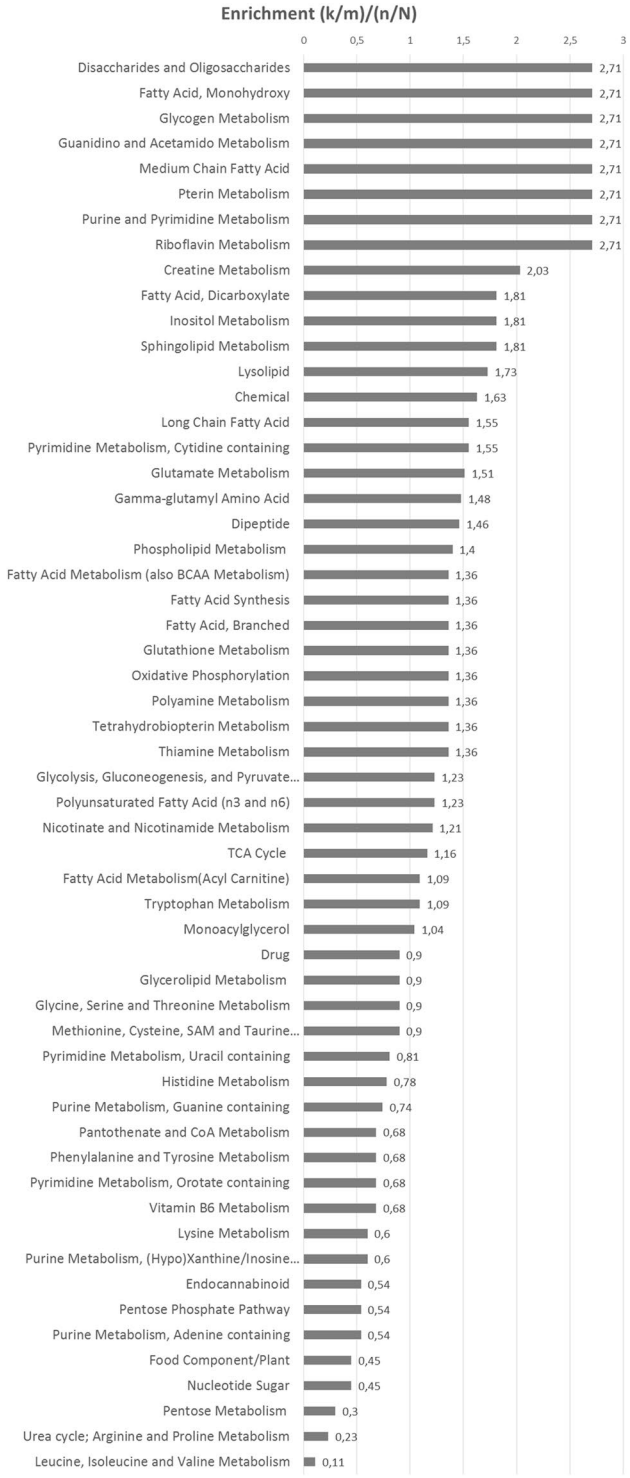

Figure 4. Pathway enrichment of cells simultaneously overexpressing ACSL1, ACSL4 and SCD. Plot shows the main metabolic pathways differentially regulated upon ACSL1, ACSL4 and SCD overexpression (x3).

cell line presented a lower basal respiration (Fig. 7E) compared to the parental SW480 cell line, equivalent to the difference found among respiratory behaviour of x3 cells when compared with their non-invasive control No ORF cells. Similarly, there were no substantial differences in glycolytic performance between SW480 and SW620 cells (Fig. 7F), and again, we can conclude that the major difference among primary tumour and metastatic CRC cells was that they can maintain their energetic homeostasis with a lower basal rate of mitochondrial oxidation without glycolytic changes (Fig. 7G). Likewise, increased levels of GSH were also found for metastatic SW620 cells, very likely indicating a lower oxidative stress (Fig. 7H).

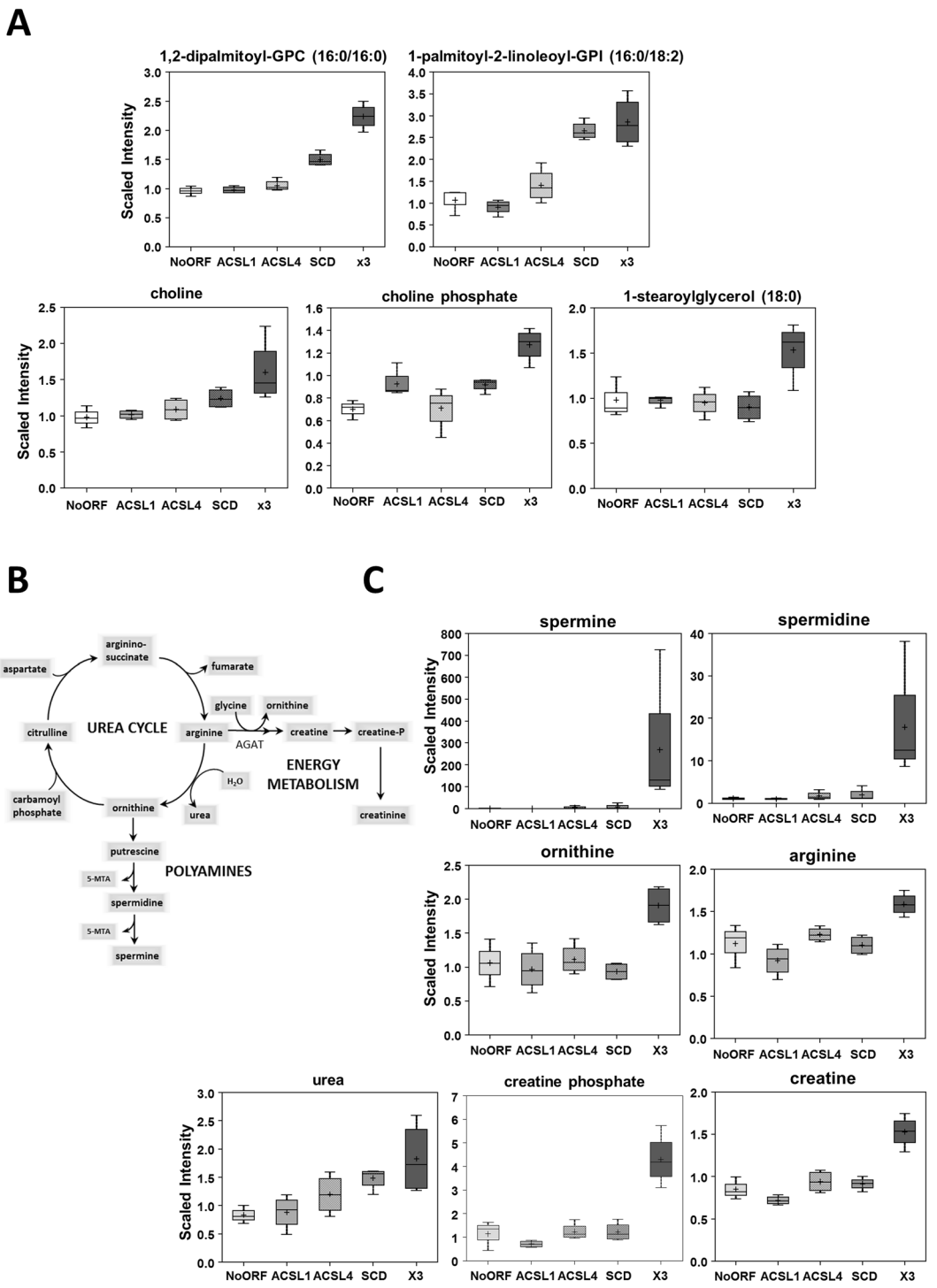

Figure 5. Increased phospholipids levels and urea cycle metabolites characterize x3 cells. (**A**) Higher phospholipid levels in DLD-1 cells expressing ACSL1, ACSL4 and SCD along with increased levels of choline, choline phosphate and monoacylglycerols. GPC = Glycerophosphocholine, GPI = glycosylphosphatidylinositol. (**B**) Schematic view of urea cycle and derived routes. (**C**) Urea Cycle-derived metabolites are highly elevated in x3 cells. The upregulated levels in x3 cells of the polyamines spermine and spermidine, the urea cycle intermediates ornithine and arginine, as well as the ones for creatine and creatine phosphate are presented. Box plots show the scaled intensity (Y axis) for each metabolite. Mean, median, and maximum and minimum values of the distribution are represented.

Discussion

In this work, we have analysed the metabolic characteristics defining ACSL/SCD action on CRC cells and their connection with the protumorigenic features intrinsic to each enzyme network integrant, highlighting

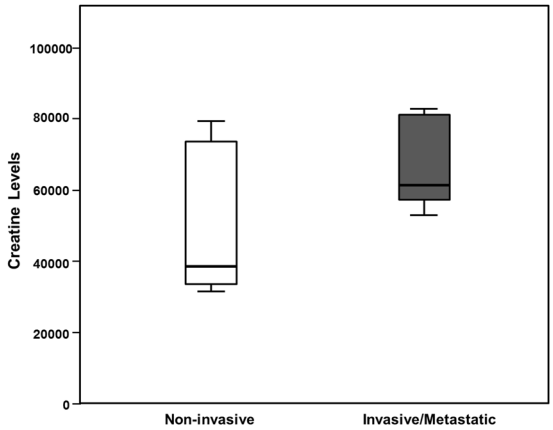

Figure 6. The more invasive and metastatic CRC cells display increased creatine levels. Correlation of Creatine levels with invasiveness in different CRC cell lines. Non-invasive cell lines: DLD-1 NoORF, HCT116, HT29, CaCo2, LS174T and SW480. Invasive or metastatic cell lines: DLD-1 x3, SW620, Colo205, LoVo and T84.

the functional dissimilarities among the ACSL members that demanded further attention. ACSL1 and ACSL4 showed an association between high expression of each isoform and poorer clinical outcome of stage-II CRC patients that resulted in a stronger and more potent association with patient relapse in the context of the ACSL/SCD network[19]. Besides, systematic analysis of ACSLs expression and clinical outcomes in several human cancers points towards ACSL1 upregulation in CRC and breast cancer and downregulation in lung cancer. Similarly, ACSL4 has been found upregulated in CRC, but in contrast predicted better prognosis in breast, brain and lung tumours. Therefore, ACSLs member's role in the development of different types of tumours can be diverse, finding even ACSLs with a tumour suppressor profile such as ACSL5 and ACSL6[45].

Our results show that ACSL4 preferentially stimulates proliferation in CRC cells (Fig. 1A) and this is associated to a more glycolytic phenotype compared to control or ACSL1 cells, without major changes in mitochondrial performance (Fig. 2A, 2B and 2C). In contrast, ACSL1 is characterized by minor effects in proliferation or glycolytic performance (Figs 1A and 2A), though presents an inclination to invasive capabilities accompanied by a decreased basal OCR (Figs 1D,E and 2C) as found for the invasive x3 cells. This was further validated when opposite results were found upon the use of specific shRNAs (Figs 1B and 2D). In similar fashion, metabolic profiles were substantially different for both ACSL isoforms, highlighting the functional differences among them.

ACSL1 overexpression was mostly characterized by the elevation of acylcarnitines probably owed to increased CPT activity upon augmented acyl-CoA levels caused by ACSL1 overexpression (Fig. 3C). For instance, elevated oleoylcarnitine agrees with the fact that oleate is one of the ACSL1 preferred substrates. Upregulated acylcarnitines could be also associated with a fatty acid oxidation (FAO) reduction in the mitochondria that should be accompanied by decreased Acetyl-CoA, down slightly in ACSL1, but up significantly in x3 cells (Supplementary Figure 3). This could be connected to the lower basal OCR registered for ACSL1 cells (Fig. 2C) but not for the lower basal OCR in x3 (Fig. 7A). Nevertheless, acylcarnitines might be mediating invasive capabilities important for cancer progression since these FAO intermediates levels have been found dramatically upregulated in several malignancies[46–49].

Lower PUFA were the defining feature of **ACSL4** cells. This may reflect greater PUFA utilization to synthesize complex lipids, such as the phospholipids required for membrane biogenesis, crucial for cancer cells. Though elevated phospholipids were not characteristic of ACSL4 cells (Supplementary File 1), this could be the key contribution of ACSL4 to the ACSL/SCD network phenotype as demonstrated by elevated phospholipids levels in x3 cells (Fig. 5A). In line with this, it has been described in other cell contexts ACSL4-mediated PUFA incorporation into complex lipids[50,51]. Not surprisingly, **SCD** desaturase overexpression was accompanied by a clear MUFA upregulation, its natural products. Curiously, most of these MUFAs were lower in x3, which may again reflect greater incorporation into complex lipids. In general, SCD cells metabolic profile is the most similar to x3 cells and they present similar proliferation tendencies as ACSL/SCD cells though with a mild effect (Fig. 1A,B and Supplementary File 1). This is in agreement with previous findings in which SCD overexpression induced Erk and Akt activation, as was also the case with x3 cells[19]. Nonetheless, a complete EMT and invasive phenotype is only found in the case of the full ACSL/SCD axis overexpression, though it has been described a SCD knock-down impairment of EMT-like behaviour in other tumours[52]. Together with ACSL1 fuelling the mitochondria and its pro-invasive actions, and ACSL4 PUFA managing for complex lipid formation, SCD could help providing an appropriate MUFA/PUFA ratio that could stimulate further invasive signalling mediated by increased levels of phospholipids and ceramides in ACSL/SCD cells. In this sense, unsaturated fatty acids seem to be crucial for ACSL/SCD phenotype.

Interestingly, x3 cells metabolic landscape cannot be explained as the sum of ACSL1, ACSL4 and SCD individual profiles. Unexpectedly, x3 cells displayed upregulated complex lipids such as phospholipids and sphinganine-derived ceramides and sphingolypids (Figs 4 and 5A and Supplementary Figure 2) which through lipid signalling may alter key regulatory pathways[21–23] such as Akt, activated in x3 cells[19]. Furthermore, affected pathways not directly associated with lipid metabolism, such as urea cycle and glycolysis were found (Fig. 5B,C

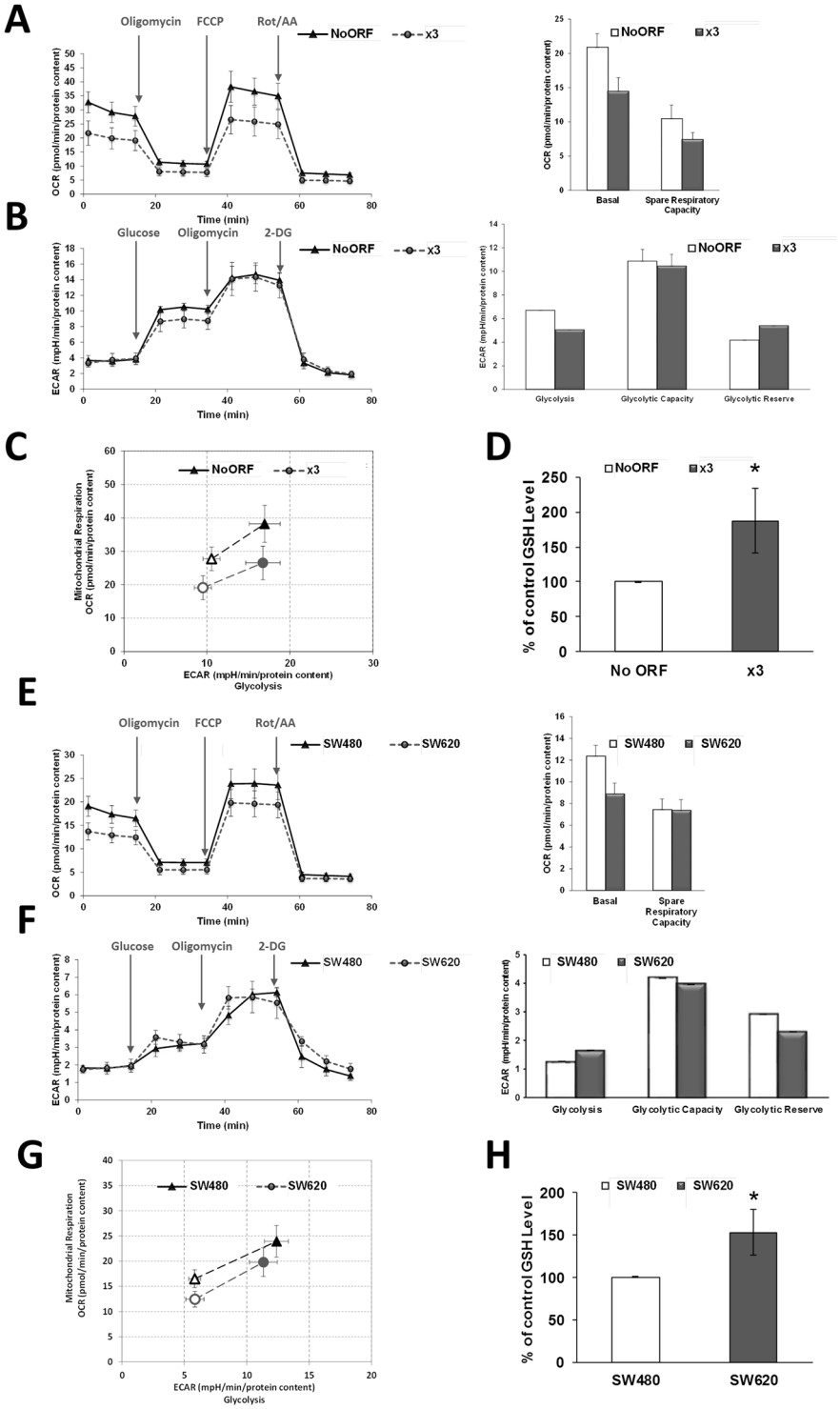

Figure 7. Bioenergetic profile of cells overexpressing ACSL1, ACSL4 and SCD resembles those from metastatic cells. (**A**) Seahorse assay of oxygen consumption rate for No ORF and x3 cells before and after 1 μM Oligomycin, 0.2 μM FCCP and 0.5 μM Rotenone/Antimycin A (Rot/AA) addition. Basal respiration and spare respiratory capacity quantification (right panel). (**B**) No ORF and x3 cells glycolytic profile. Cells were starved 1 h and a half and ECAR levels were measured before and after addition of 10 μM glucose, 0.5 μM Oligomycin and 50 mM 2-DG. Right panel shows the quantification of Glycolysis, Glycolytic Capacity and Glycolytic Reserve for each DLD-1 clone. (**C**) Metabolic phenotype plot depicting the relative metabolic state of cells under baseline and stressed conditions. Baseline Phenotype: OCR and ECAR of cells at starting assay conditions (empty circle and empty triangle). Stressed Phenotype: OCR and ECAR of cells under an induced energy demand, here achieved upon FCCP treatment (full circle and full triangle). (**D**) Levels of reduced glutathione for DLD-1 No ORF and x3 cells. (**E**) Seahorse assay of oxygen consumption rate for SW480 and SW620 cells before and after 1 μM Oligomycin, 0.6 μM FCCP and 0.5 μM Rot/AA addition. Quantification of basal respiration and spare

respiratory capacity (right panel). (**F**) Glycolytic profile of SW480 and SW620 cells. Cells were starved 1 h and a half and ECAR levels were measured before and after addition of 10 µM glucose, 0.5 µM Oligomycin and 50 mM 2-DG. Right panel shows the quantification of Glycolysis, Glycolytic Capacity and Glycolytic Reserve for each cell type. (**G**) Metabolic phenotype plot depicting the relative metabolic state of cells under baseline and stressed conditions. Baseline Phenotype: OCR and ECAR of cells at starting assay conditions (empty circle and empty triangle). Stressed Phenotype: OCR and ECAR of cells under an induced energy demand, such as FCCP treatment (full circle and full triangle). (**H**) Levels of reduced glutathione for SW480 and metastatic SW620 cells. (**A**,**B**,**C**,**E**,**F** and **G**) show representative experiments of 3 or more experiments (n = 3). Results in (**D** and **H**) represent the mean ± SD of 3 experiments (n = 3). *$p < 0.05$.

and Supplementary Figure 3). The urea cycle stimulation could be derived from the increased Acetyl-CoA levels that x3 cells present (Supplementary Figure 3). Polyamines have been extensively related to cell proliferation and growth[43,44]. Recently, they have been involved as crucial for protein translation, key to cancer invasion and metastasis[53,54]. Inhibition of polyamine synthesis also decreased the amount of metastasis in several cancer models[44]. Polyamines could be distinctive oncometabolites of metastatic cells, since metastatic SW620 cell present higher levels of polyamines than their corresponding primary tumour cells, SW480 as well as higher activity of the key regulatory enzymes of polyamine biosynthesis[55]. Creatine and phosphocreatine were also clearly upregulated in x3 cells (Figs 4 and 5C) indicating a more advantageous energetic status that could be essential for invasive features development. In this sense, phosphocreatine, has been reported to directly fuel tumour growth and liver metastasis in CRC[56], and both creatine and creatinine downregulate toll-like receptors (TLRs) expression in macrophages[57], which could be used by tumour cells as an immunosuppressive strategy to favour metastasis. This is in accordance with our results showing increased creatine levels in the more invasive and metastatic CRC cells (Fig. 6). Regarding glycolytic perturbations (Supplementary Figure 3), increased PEP levels and normal pyruvate could be a reflect of less demand of TCA feeding from pyruvate (from carbohydrates) explaining lower basal OCR consumption since a more energetic status is achieved through other alternative supplies, such as FAO, that could be fed by ACSL1 overexpression. Nevertheless, FAO inhibitor etomoxir is not sufficient to revert the EMT phenotype of ACSL/SCD cells that, conversely, can be achieved upon a more drastic energetic restriction caused by AMPK signalling reactivation upon metformin treatment[19] (Supplementary Figure 4). Thus, it seems that x3 cells present a better overall energetic status that even though it is not due to observable differences in ATP content (data not shown), is reflected by lower basal OCR and elevated creatine pathway that could be partly fed by ACSL1-drived increased FAO and sustained through other levels dependent on further phospholipid signalling supported by ACSL4 and SCD increased activities as PUFA and MUFA suppliers, respectively.

Importantly, x3 cells metabolic capacities were reproduced in a model of primary and metastatic CRC cell lines, SW480 and SW620. More invasive or metastatic cells, performed mitochondrial oxidation at a lower rate without glycolytic changes, pointing to an overall energetic advantage in invasive cells that could derive from increased energetic efficiency or from an augmented utilization of alternative fuels. Furthermore, both invasive x3 and metastatic SW620 cells presented increased GSH compared to their corresponding non-invasive control cells (Fig. 7D,H). This lower oxidative stress is further supported by increased gammaglutamyl-aminoacids in x3 cells (Supplementary File 1), as markers of glutathione regeneration and decreased levels of NADPH (Supplementary File 1), which could be explained by greater use for GSH generation, since pentose phosphate pathway presented no downregulation (Supplementary File 1). Furthermore, the other core reducing agent, NADH presented upregulated levels in x3 cells. Although oxidative stress role in tumour progression has been controversial, new studies indicate that cancer cells must increase their capacity to withstand oxidative stress to produce distant metastasis[58–60].

Methods

Cell culture, stable cell lines generation and reagents. Cell lines, obtained from ATCC (ATCC, Manassas, VA, USA) were cultured in DMEM 10% FBS and maintained under standard conditions. Etomoxir and Metformin were purchased form Sigma-Aldrich (Sigma-Aldrich, St. Louis, MO, USA). Images were captured using a Leica DM IL microscope (Leica Microsystems, Wetzlar, Germany), with a 10X Plan Fluotar objective and registered using Leica Application Suite (LAS). DLD-1 cells stably overexpressing ACSL1, ACSL4, SCD and ACSL1/ACSL4/SCD (x3) were generated with specific lentivirus or an equivalent control vector which does not express any ORF (No ORF cell line) as described[19]. For shACSL1, shACSL4 and shSCD cells generation, HEK 293T cells were transfected with Mission specific lentiviral vectors (TRCN0000045518, TRCN0000045541, TRCN0000312672) or a shControl pLKO.1 empty vector (Sigma-Aldrich, St. Louis, MO, USA) along with packaging plasmids (Addgene, Cambridge MA, USA). Supernatant produced upon 48 h transfection in HEK293T cells was used to infect DLD-1 cells followed by puromycin selection (2 µg/ml) during 1 week.

Quantitative real-time PCR. RNA (400 ng) was reverse-transcribed using the High Capacity RNA-to-cDNA Master Mix system (Life Technologies, Carlsbad CA, USA). qPCR was performed using VeriQuest SYBR Green qPCR Master Mix (Affymetrix, Santa Clara, CA, USA) in the 7900HT Real-Time PCR System (Life Technologies). Gene specific primers for *ACSL1* (Fw: 5′-ACATTATGTTCCTGGGCCCA-3′ and Rv: 5′-AGTCAGAAGGCCATTGTCGA-3′), *ACSL4* (Fw: 5′-GGCACAACAGAAAGGGGTAG-3′ and Rv: 5′-GGTTCCTCAGCTCCTTCCTT-3′), *SCD* (Fw: 5′-TGCCCACCACAAGTTTTCAG-3′ and Rv: 5′-CATCAGCAAGCCAGGTTTGT-3′), *CDH2* (N-cadherin) (Fw: 5′-CGGTTTCATTTGAGGGCACA-3′ and Rv: 5′-TTGGAGCCTGAGACACGATT-3′) and SNAI2 (Slug) (Fw: 5′-CGTTTTCCAGACCCTGGTT-3′ and Rv: 5′-CTGCAGATGAGCCCTCAGA-3′) were used and *GAPDH* expression (Fw:

5′-TGGTATCGTGGAAGGACTCATGAC-3′ and Rv: 5′-ATGCCAGTGAGCTTCCCGTTCAGC-3′) used for normalization. Relative gene expression was calculated using the $2-\Delta\Delta Ct$ method.

Western Blot and antibodies. Cells were lysed in Laemmli buffer and boiled at 95 °C for 10 min. Proteins were separated by SDS–polyacrylamide gel electrophoresis and transferred onto a nitrocellulose membrane (Bio-Rad Laboratories, Hercules, CA, USA). The membranes were blocked using 5% non-fat dry milk in TBS 0.05% Tween-20, and incubated with primary antibodies overnight at 4 °C. After incubation with secondary antibodies, Clarity Western ECL Substrate (Bio-Rad Laboratories) was used for signal detection and Vinculin determination or unspecific band were used as loading controls. Anti-human ACSL4 was generously provided by Dr. Stephen Prescott, University of Utah, Salt Lake, USA and Dr. Diana Stafforini, Huntsman Cancer Institute, University of Utah, USA, and used as indicated[61]. Antibody against SCD[62] was a kind gift from Dr. Jean-Baptiste Demoulin, Université Catholique de Louvain, Brussels, Belgium. anti ACSL1 (4047) was obtained from Cell Signaling (Cell Signaling Technology Inc., Beverly, MA, USA) and anti-Vinculin (V9131) and β-Actin (A1978) were from Sigma.

Proliferation assays. Proliferation was analysed in real-time using the xCELLigence™ system (ACEA Biosciences, San Diego, CA). Real-time monitoring of cell proliferation, xCELLigence™ system measurements were performed by spreading 10000 cells over a FN-coated gold electrode sensor plate. Cellular impedance recordings converted to a cell index (CI) allow for the assessment of attached cells. Real-time monitoring of proliferation was performed for 8 days in 15 min intervals.

Wound healing. A density of 40000 cells per reservoir was plated using IBIDI-Inserts (IBIDI GmbH, München, Germany) and incubated until confluence was reached. Upon inserts removal, migration was monitored and registered every 12 h using a 10X Plan Fluotar objective (Leica).

Invasion assays. BD Matrigel™ invasion chambers (BD Biosciences) were seeded with 50000 cells in serum-free DMEM. After 48 h, using DMEM 10% FBS as a chemoattractant, inserts were fixed and stained with crystal violet. Once non-migrated cells were removed with cotton swaps, pictures were taken using an Olympus CKX41 microscope (Olympus, Tokyo, Japan), with a 20X LCAch objective and registered using analysis getIT software (Olympus).

Oxygen consumption rate (OCR) and extracellular acidification rate (ECAR). OCR and ECAR were monitored as indicators of mitochondrial respiration and glycolytic function study with an XF96 Extracellular Flux Analyzer using XF Cell Mito Stress Test kit and XF Glycolysis Stress kit according to manufacturer instructions (Seahorse Biosciences, North Billerica, MA, USA). Cell seeding number was optimized (50000 cells/well for DLD-1 and SW480 cells and 90000 cells/well for SW620 cells. For mitochondrial stress test, cells were plated into XF96 plates and regular culture media was replaced at 24 hours with 2 mM pyruvate, 2 mM glutamine and 10mMglucose supplemented Base media (Seahorse Bioscience) upon several washes. Cells were placed in a non-CO_2 37 °C incubator for 1 hour, prior to assay. Upon basal rate measurements were taken, mitochondrial respiratory chain drugs were added, following Mito Stress kit specifications. 2 µM Oligomycin was used to block ATP-linked oxygen consumption, 0.2 µM FCCP (0.6 µM for SW480 and SW620 cells) as an uncoupling agent to obtain maximal respiration and 0.5 µM Rotenone/Antimycin A to inhibit complex I and III, stopping all mitochondrial respiration. For glycolysis analysis, 2 mM pyruvate and 2 mM glutamine supplemented Base media was used and cells were incubated without CO_2 for 1 hour and a half. Following Glycolysis Stress kit specifications, 10 µM glucose was injected to stimulate glycolysis, 0.5 µM Oligomycin to obtain maximal glycolytic capacity upon oxygen consumption inhibition and 50 mM 2-Deoxy-D-glucose (2-DG) to shut down all glycolysis. OCR and ECAR were measured 3 times following injection of each drug, and normalized to protein content. At least 6 replicates per condition were done for each experiment.

Statistical analysis. Significance between groups was determined by t-test. All reported p values were two-sided. Statistical significance was defined as $p < 0.05$. The statistical analyses were performed using the R statistical software version 3.1.1 (www.r-project.org).

Global metabolomic profiling. Eleven million of cells from each DLD-1 cell clone were collected, rinsed with PBS, and the snap-frozen cell pellets were submitted to Metabolon Inc for global metabolomic analysis. Each condition included four replicates. A combination of GC-MS and LC-MS methods were used, and each metabolite amount was normalized to total protein amount of the individual cell pellets. Briefly, proteins were precipitated with methanol under vigorous shaking for 2 min (Glen Mills GenoGrinder 2000) followed by centrifugation to recover chemically diverse metabolites. The UPLC-MS/MS portion was based on a Waters ACQUITY ultra-performance liquid chromatography (UPLC) and a Thermo Scientific Q-Exactive high resolution/accurate mass spectrometer interfaced with a heated electrospray ionization (HESI-II) source and Orbitrap mass analyser operated at 35,000 mass resolution. The sample extract was dried then reconstituted in acidic or basic LC-compatible solvents, each of which contained 8 or more injection standards at fixed concentrations to ensure injection and chromatographic consistency. One aliquot was analysed using acidic positive ion optimized conditions and the other using basic negative ion optimized conditions in two independent injections using separate dedicated columns (Waters UPLC BEH C18–2.1 × 100 mm, 1.7 µm). Extracts reconstituted in acidic conditions were gradient eluted from a C18 column using water and methanol containing 0.1% formic acid. The basic extracts were similarly eluted from C18 using methanol and water, however with 6.5 mM Ammonium Bicarbonate. The third aliquot was analysed via negative ionization following elution from a HILIC

column (Waters UPLC BEH Amide 2.1 × 150 mm, 1.7 µm) using a gradient consisting of water and acetonitrile with 10 mM Ammonium Formate. The MS analysis alternated between MS and data-dependent MS2 scans using dynamic exclusion, and the scan range was from 80–1000 m/z. The samples destined for analysis by GC-MS were dried under vacuum for a minimum of 18 h prior to being derivatized under dried nitrogen using bistrimethyl-silyltrifluoroacetamide. Derivatized samples were separated on a 5% diphenyl / 95% dimethyl polysiloxane fused silica column (20 m × 0.18 mm ID; 0.18 um film thickness) with helium as carrier gas and a temperature ramp from 60° to 340 °C in a 17.5 min period. Samples were analysed on a Thermo-Finnigan Trace DSQ fast-scanning single-quadrupole mass spectrometer using electron impact ionization (EI) and operated at unit mass resolving power. The scan range was from 50–750 m/z. Raw data was extracted, peak-identified and QC processed using Metabolon's hardware and software. Compounds were identified by comparison to library entries of purified standards or recurrent unknown entities.

Principal Components Analysis (PCA). Principal components analysis is an unsupervised analysis that reduces the dimension of the data. Each principal component is a linear combination of every metabolite and the principal components are uncorrelated. The number of principal components is equal to the number of observations. The first principal component is computed by determining the coefficients of the metabolites that maximizes the variance of the linear combination. The second component finds the coefficients that maximize the variance with the condition that the second component is orthogonal to the first. The third component is orthogonal to the first two components and so on. The total variance is defined as the sum of the variances of the predicted values of each component (the variance is the square of the standard deviation), and for each component, the proportion of the total variance is computed.

Creatine determination. CRC cells were seeded into 6-well plates in appropriate growth medium. Upon subconfluence, cells were collected, homogenized and proteins removed using 10 kDa MWCO spin filters. Relative creatine content was assayed using Creatine Assay Kit (Sigma) according to the manufacturer's instructions and fluorescence intensity measured with a GloMax®-Multi Detection System (Promega, Madison, WI, USA). Values were normalized to total protein content.

Reduced glutathione measurement. Cells were seeded at a density of 20000 cells per well (30000 in the case of SW620 cells) in a 96-well plate. At 24 hours, medium was removed, cells lysed, and the relative levels of reduced glutathione (GSH) were determined using GSH-GSSG-Glo™ Glutathione Assay (Promega). Luminescence intensity of the samples was measured with a GloMax®-Multi Detection System (Promega).

Data availability. All data generated or analysed during this study are included in this published article (and its Supplementary Information files).

References

1. Hanahan, D. & Weinberg, R. A. Hallmarks of cancer: the next generation. *Cell* **144**, 646–674 (2011).
2. Nowicki, S. & Gottlieb, E. Oncometabolites: tailoring our genes. *FEBS J.* **282**, 2796–2805 (2015).
3. Boroughs, L. K. & DeBerardinis, R. J. Metabolic pathways promoting cancer cell survival and growth. *Nat. Cell Biol.* **17**, 351–359 (2015).
4. Frezza, C. *et al*. Haem oxygenase is synthetically lethal with the tumour suppressor fumarate hydratase. *Nature* **477**, 225–228 (2011).
5. Jain, M. *et al*. Metabolite profiling identifies a key role for glycine in rapid cancer cell proliferation. *Science* **336**, 1040–1044 (2012).
6. Metallo, C. M. *et al*. Reductive glutamine metabolism by IDH1 mediates lipogenesis under hypoxia. *Nature* **481**, 380–384 (2012).
7. Possemato, R. *et al*. Functional genomics reveal that the serine synthesis pathway is essential in breast cancer. *Nature* **476**, 346–350 (2011).
8. Schug, Z. T. *et al*. Acetyl-CoA synthetase 2 promotes acetate utilization and maintains cancer cell growth under metabolic stress. *Cancer Cell* **27**, 57–71 (2015).
9. Shaul, Y. D. *et al*. Dihydropyrimidine accumulation is required for the epithelial-mesenchymal transition. *Cell* **158**, 1094–1109 (2014).
10. Buzzai, M. *et al*. The glucose dependence of Akt-transformed cells can be reversed by pharmacologic activation of fatty acid β-oxidation. *Oncogene* **24**, 4165–4173 (2005).
11. Elstrom, R. L. *et al*. Akt Stimulates Aerobic Glycolysis in Cancer Cells. *Cancer Res.* **64**, 3892–3899 (2004).
12. Gough, D. J. *et al*. Mitochondrial STAT3 supports Ras-dependent oncogenic transformation. *Science* **324**, 1713–1716 (2009).
13. Yang, W. *et al*. ERK1/2-dependent phosphorylation and nuclear translocation of PKM2 promotes the Warburg effect. *Nat. Cell Biol.* **14**, 1295–1304 (2012).
14. Wise, D. R. *et al*. Myc regulates a transcriptional program that stimulates mitochondrial glutaminolysis and leads to glutamine addiction. *Proc. Natl. Acad. Sci. USA* **105**, 18782–18787 (2008).
15. Carracedo, A., Cantley, L. C. & Pandolfi, P. P. Cancer metabolism: fatty acid oxidation in the limelight. *Nat. Rev. Cancer* **13**, 227–232 (2013).
16. Currie, E., Schulze, A., Zechner, R., Walther, T. C. & Farese, R. V. Cellular Fatty Acid Metabolism and Cancer. *Cell Metab.* **18**, 153–161 (2013).
17. Mashima, T. *et al*. Acyl-CoA synthetase as a cancer survival factor: its inhibition enhances the efficacy of etoposide. *Cancer Sci.* **100**, 1556–1562 (2009).
18. Menendez, J. A. & Lupu, R. Fatty acid synthase and the lipogenic phenotype in cancer pathogenesis. *Nat. Rev. Cancer* **7**, 763–777 (2007).
19. Sánchez-Martínez, R. *et al*. A link between lipid metabolism and epithelial-mesenchymal transition provides a target for colon cancer therapy. *Oncotarget* (2015).
20. Zaidi, N. *et al*. Lipogenesis and lipolysis: the pathways exploited by the cancer cells to acquire fatty acids. *Prog. Lipid Res.* **52**, 585–589 (2013).
21. Bunney, T. D. & Katan, M. Phosphoinositide signalling in cancer: beyond PI3K and PTEN. *Nat. Rev. Cancer* **10**, 342–352 (2010).
22. Hannun, Y. A. & Obeid, L. M. Principles of bioactive lipid signalling: lessons from sphingolipids. *Nat. Rev. Mol. Cell Biol.* **9**, 139–150 (2008).
23. Wymann, M. P. & Schneiter, R. Lipid signalling in disease. *Nat. Rev. Mol. Cell Biol.* **9**, 162–176 (2008).
24. Folger, O. *et al*. Predicting selective drug targets in cancer through metabolic networks. *Mol. Syst. Biol.* **7**, 501 (2011).

25. Ou, J. *et al.* Loss of abhd5 promotes colorectal tumor development and progression by inducing aerobic glycolysis and epithelial-mesenchymal transition. *Cell Rep.* **9**, 1798–1811 (2014).
26. Sellers, K. *et al.* Pyruvate carboxylase is critical for non-small-cell lung cancer proliferation. *J. Clin. Invest.* **125**, 687–698 (2015).
27. Coleman, R. A., Lewin, T. M., Horn, C. G. V. & Gonzalez-Baró, M. R. Do Long-Chain Acyl-CoA Synthetases Regulate Fatty Acid Entry into Synthetic Versus Degradative Pathways? *J. Nutr.* **132**, 2123–2126 (2002).
28. Enoch, H. G., Catalá, A. & Strittmatter, P. Mechanism of rat liver microsomal stearyl-CoA desaturase. Studies of the substrate specificity, enzyme-substrate interactions, and the function of lipid. *J. Biol. Chem.* **251**, 5095–5103 (1976).
29. Patra, S. K. Dissecting lipid raft facilitated cell signaling pathways in cancer. *Biochim. Biophys. Acta* **1785**, 182–206 (2008).
30. Cao, Y., Pearman, A. T., Zimmerman, G. A., McIntyre, T. M. & Prescott, S. M. Intracellular unesterified arachidonic acid signals apoptosis. *Proc. Natl. Acad. Sci. USA* **97**, 11280–11285 (2000).
31. Maloberti, P. M. *et al.* Functional interaction between acyl-CoA synthetase 4, lipooxygenases and cyclooxygenase-2 in the aggressive phenotype of breast cancer cells. *PloS One* **5**, e15540 (2010).
32. Mashima, T. *et al.* p53-defective tumors with a functional apoptosome-mediated pathway: a new therapeutic target. *J. Natl. Cancer Inst.* **97**, 765–777 (2005).
33. Noto, A. *et al.* Stearoyl-CoA desaturase-1 is a key factor for lung cancer-initiating cells. *Cell Death Dis.* **4**, e947 (2013).
34. Roongta, U. V. *et al.* Cancer cell dependence on unsaturated fatty acids implicates stearoyl-CoA desaturase as a target for cancer therapy. *Mol. Cancer Res. MCR* **9**, 1551–1561 (2011).
35. Vargas, T. *et al.* ColoLipidGene: signature of lipid metabolism-related genes to predict prognosis in stage-II colon cancer patients. *Oncotarget* (2015).
36. Wu, X. *et al.* ACSL4 promotes prostate cancer growth, invasion and hormonal resistance. *Oncotarget* **6**, 44849–44863 (2015).
37. Cui, M. *et al.* MiR-205 modulates abnormal lipid metabolism of hepatoma cells via targeting acyl-CoA synthetase long-chain family member 1 (ACSL1) mRNA. *Biochem. Biophys. Res. Commun.* **444**, 270–275 (2014).
38. Li, L. O. *et al.* Liver-specific loss of long chain acyl-CoA synthetase-1 decreases triacylglycerol synthesis and beta-oxidation and alters phospholipid fatty acid composition. *J. Biol. Chem.* **284**, 27816–27826 (2009).
39. Küch, E.-M. *et al.* Differentially localized acyl-CoA synthetase 4 isoenzymes mediate the metabolic channeling of fatty acids towards phosphatidylinositol. *Biochim. Biophys. Acta* **1841**, 227–239 (2014).
40. Gupta, G. P. & Massagué, J. Cancer metastasis: building a framework. *Cell* **127**, 679–695 (2006).
41. Nieto, M. A. & Cano, A. The epithelial-mesenchymal transition under control: global programs to regulate epithelial plasticity. *Semin. Cancer Biol.* **22**, 361–368 (2012).
42. Hsu, P. P. & Sabatini, D. M. Cancer Cell Metabolism: Warburg and Beyond. *Cell* **134**, 703–707 (2008).
43. Russell, D. & Snyder, S. H. Amine synthesis in rapidly growing tissues: ornithine decarboxylase activity in regenerating rat liver, chick embryo, and various tumors. *Proc. Natl. Acad. Sci. USA* **60**, 1420–1427 (1968).
44. Soda, K. The mechanisms by which polyamines accelerate tumor spread. *J. Exp. Clin. Cancer Res.* **30**, 95 (2011).
45. Chen, W.-C. *et al.* Systematic Analysis of Gene Expression Alterations and Clinical Outcomes for Long-Chain Acyl-Coenzyme A Synthetase Family in Cancer. *PloS One* **11**, e0155660 (2016).
46. Camarda, R. *et al.* Inhibition of fatty acid oxidation as a therapy for MYC-overexpressing triple-negative breast cancer. *Nat. Med.* **22**, 427–432 (2016).
47. Chughtai, K., Jiang, L., Greenwood, T. R., Glunde, K. & Heeren, R. M. A. Mass spectrometry images acylcarnitines, phosphatidylcholines, and sphingomyelin in MDA-MB-231 breast tumor models. *J. Lipid Res.* **54**, 333–344 (2013).
48. Ganti, S. *et al.* Urinary acylcarnitines are altered in human kidney cancer. *Int. J. Cancer* **130**, 2791–2800 (2012).
49. Wettersten, H. I. *et al.* Grade-Dependent Metabolic Reprogramming in Kidney Cancer Revealed by Combined Proteomics and Metabolomics Analysis. *Cancer Res.* **75**, 2541–2552 (2015).
50. Klett, E. L. *et al.* Diminished acyl-CoA synthetase isoform 4 activity in INS 832/13 cells reduces cellular epoxyeicosatrienoic acid levels and results in impaired glucose-stimulated insulin secretion. *J. Biol. Chem.* **288**, 21618–21629 (2013).
51. Tuohetahuntila, M. *et al.* Role of long-chain acyl-CoA synthetase 4 in formation of polyunsaturated lipid species in hepatic stellate cells. *Biochim. Biophys. Acta* **1851**, 220–230 (2015).
52. Mauvoisin, D., Charfi, C., Lounis, A. M., Rassart, E. & Mounier, C. Decreasing stearoyl-CoA desaturase-1 expression inhibits β-catenin signaling in breast cancer cells. *Cancer Sci.* **104**, 36–42 (2013).
53. Bhat, M. *et al.* Targeting the translation machinery in cancer. *Nat. Rev. Drug Discov.* **14**, 261–278 (2015).
54. Mandal, S., Mandal, A., Johansson, H. E., Orjalo, A. V. & Park, M. H. Depletion of cellular polyamines, spermidine and spermine, causes a total arrest in translation and growth in mammalian cells. *Proc. Natl. Acad. Sci.* **110**, 2169–2174 (2013).
55. Duranton, B. *et al.* Polyamine metabolism in primary human colon adenocarcinoma cells (SW480) and their lymph node metastatic derivatives (SW620). *Amino Acids* **24**, 63–72 (2003).
56. Loo, J. M. *et al.* Extracellular Metabolic Energetics Can Promote Cancer Progression. *Cell* **160**, 393–406 (2015).
57. Leland, K. M., McDonald, T. L. & Drescher, K. M. Effect of creatine, creatinine, and creatine ethyl ester on TLR expression in macrophages. *Int. Immunopharmacol.* **11**, 1341–1347 (2011).
58. Herraiz, C. *et al.* Reactivation of p53 by a Cytoskeletal Sensor to Control the Balance Between DNA Damage and Tumor Dissemination. *J. Natl. Cancer Inst.* **108** (2016).
59. Le Gal, K. *et al.* Antioxidants can increase melanoma metastasis in mice. *Sci. Transl. Med.* **7**, 308re8 (2015).
60. Piskounova, E. *et al.* Oxidative stress inhibits distant metastasis by human melanoma cells. *Nature* **527**, 186–191 (2015).
61. Cao, Y., Murphy, K. J., McIntyre, T. M., Zimmerman, G. A. & Prescott, S. M. Expression of fatty acid-CoA ligase 4 during development and in brain. *FEBS Lett.* **467**, 263–267 (2000).
62. Demoulin, J.-B. *et al.* Platelet-derived growth factor stimulates membrane lipid synthesis through activation of phosphatidylinositol 3-kinase and sterol regulatory element-binding proteins. *J. Biol. Chem.* **279**, 35392–35402 (2004).

Acknowledgements

This work was supported by MINECO (Plan Nacional I + D + i AGL2013-48943-C2 and AGL2016-76736-C3), CAM (P2013/ABI-2728, ALIBIRD-CM) and EU Structural Funds. We thank Susana Molina and Lara P. Fernández (Molecular Oncology and Nutritional Genomics of Cancer Group, IMDEA Food Institute) for their assistance during figures preparison.

Author Contributions

All experiments were planned by R.S.-M. and A.R.-M., and experimental procedures conducted by R.S.-M., S.C.-G. and M.S.-G.-A. The manuscript was prepared by R.S.-M. and A.R.-M. Financial support was obtained by G.R. and A.R.-M., and G.R. critically revised the manuscript.

Additional Information

Supplementary information accompanies this paper at doi:10.1038/s41598-017-11612-3

Competing Interests: The authors declare that they have no competing interests.

Publisher's note: Springer Nature remains neutral with regard to jurisdictional claims in published maps and institutional affiliations.

Supplementary Figures

Complementary ACSL isoforms contribute to a non-Warburg advantageous energetic status characterizing invasive colon cancer cells

Ruth Sánchez-Martínez[1*], Silvia Cruz-Gil[1], María Soledad García-Álvarez[1], Guillermo Reglero[1], Ana Ramírez de Molina[1*]

[1]Molecular Oncology and Nutritional Genomics of Cancer Group, IMDEA Food Institute, CEI UAM + CSIC, E28049, Madrid, Spain. *Corresponding Author

Figure S1

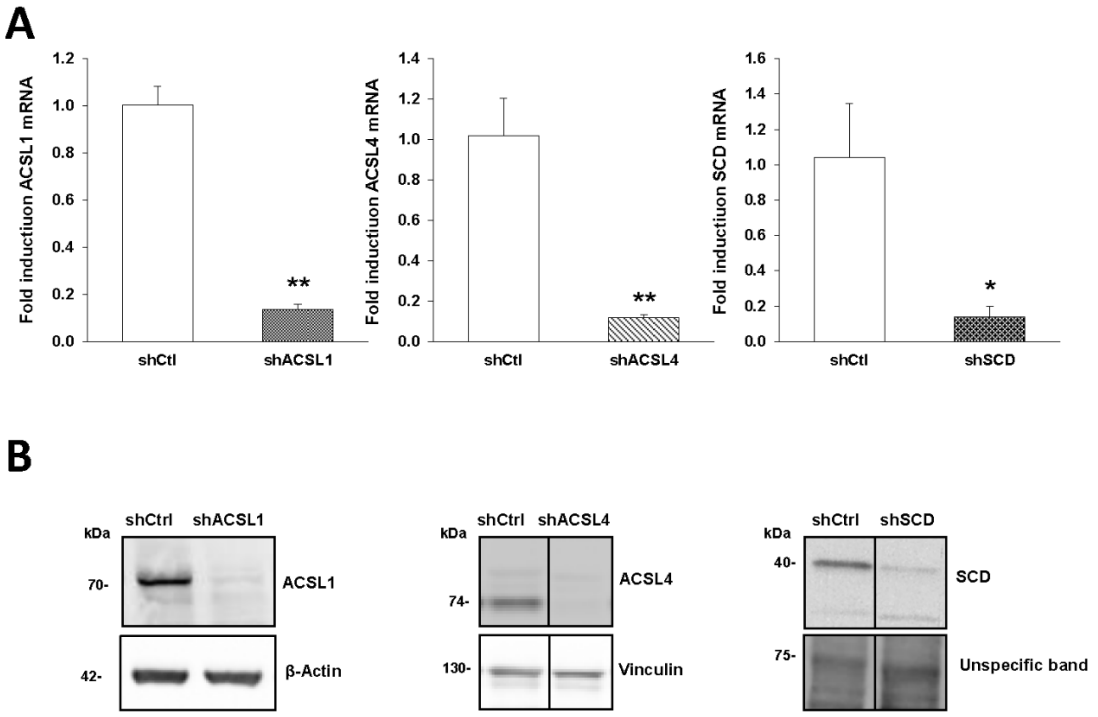

Figure S1. ACSL1, ACSL4 and SCD knock-down by shRNA means. Related to Figure 1,2 and 6.

A. Cell lines stably expressing shRNAs for ACSL1 (shACSL1), ACSL4 (shACSL4), SCD (shSCD) or scramble (shCtrl) were generated using lentiviral transduction and knock-down of every gene was measured by RT-QPCR. B. Protein expression levels of ACSL1 (upper band), ACSL4 and SCD for each cell line were detected by Western Blot with specific antibodies. Vinculin or an unspecific band detection were used as a loading control. Experiments in B were performed in triplicates (n = 3). Results represent the mean ±SD (n = 3). *, $p < 0.05$, **, $p < 0.01$, ***, $p < 0.001$.

Figure S2

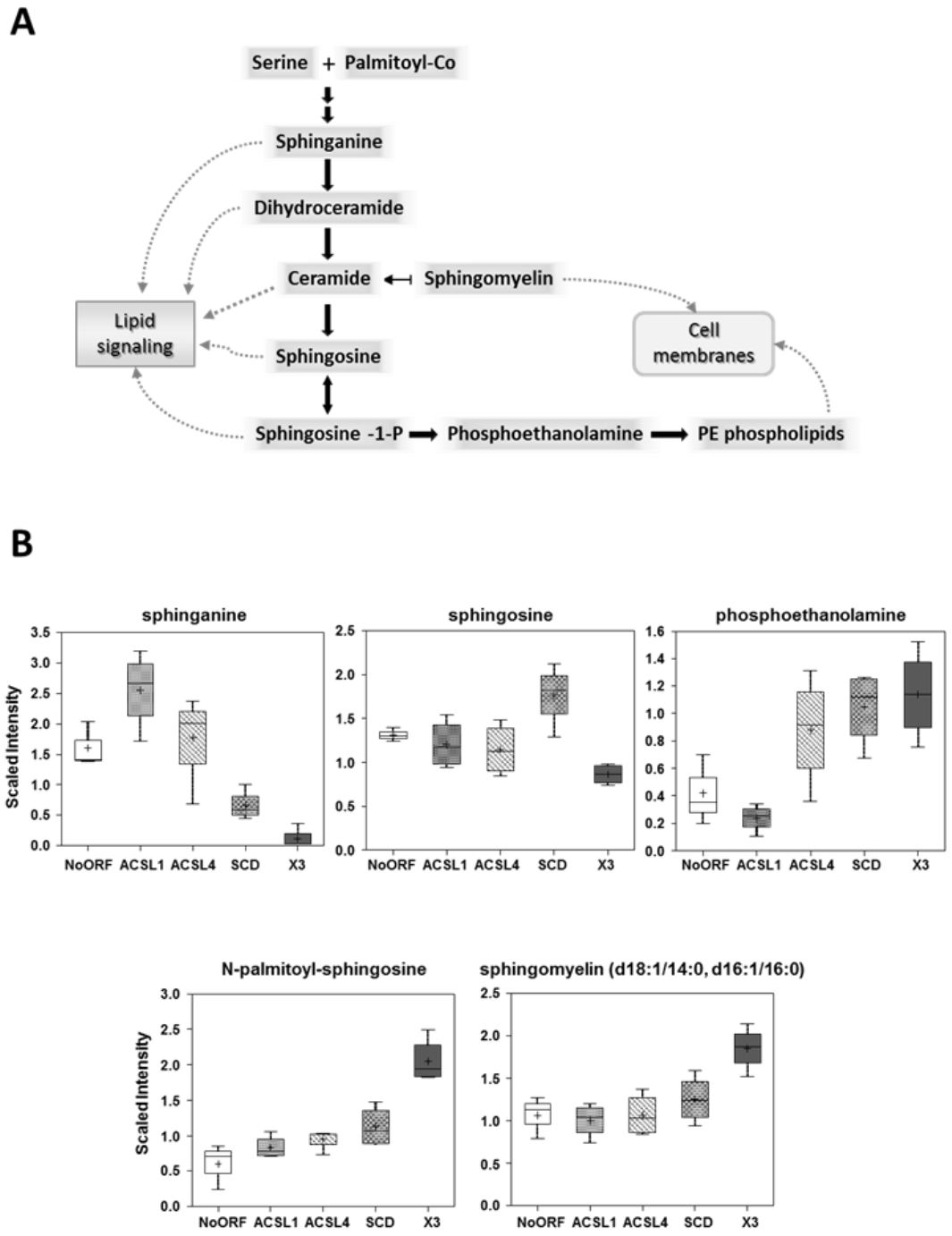

Figure S2. Sphinganine levels are strongly reduced in x3 cells. Related to Figure 5.

A. Schematic representation of sphinganine metabolism. B. Sphinganine and sphingosine levels are reduced in DLD-1 cells expressing ACSL1, ACSL4 and SCD. Accordingly, derived complex lipids such as phosphoethanolamine, the ceramide N-palmitoyl-sphingosine and sphingomyelin are augmented. Box plots show the scaled intensity (Y axis) for each metabolite. Mean, median and maximum and minimum values of the distribution are represented.

Figure S3

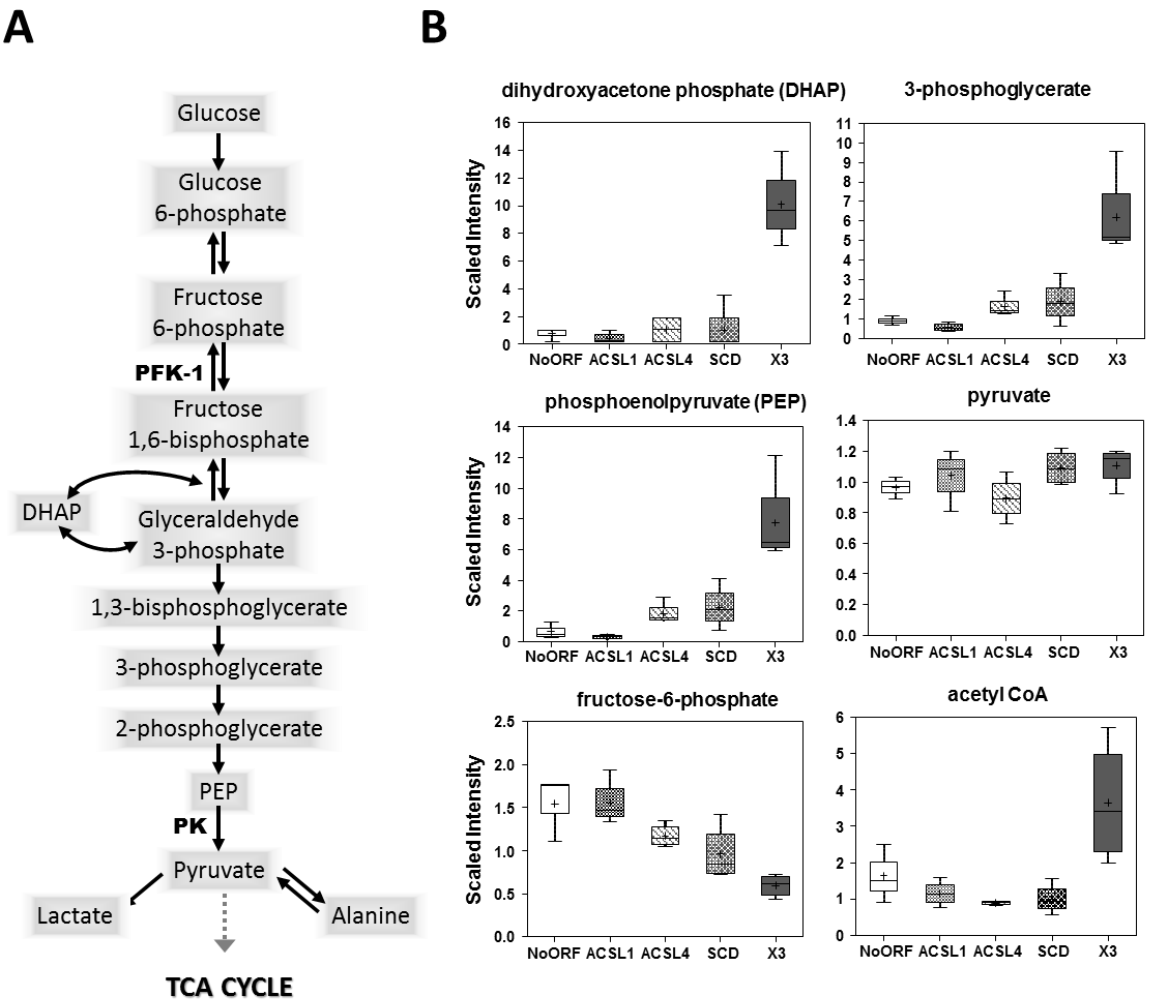

Figure S3. Perturbations in glycolysis pathway in X3 cells. Related to Figure 4 and 5.

A. Schematic representation of glycolysis (DHAP: dihydroxyacetone phosphate; PEP: phosphoenolpyruvate; PFK-1: phosphofructokinase 1; PK: pyruvate kinase). B. Box plots show the scaled intensity (Y axis) for several glycolytic metabolites in the different DLD-1 expression-subtypes. Mean, median and maximum and minimum values of the distribution are represented in the plots.

Figure S4

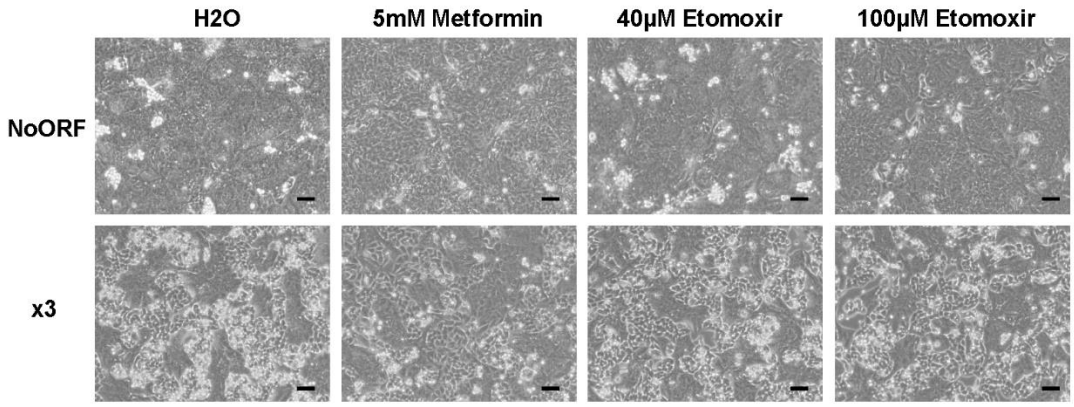

Figure S4. Etomoxir treatment is not able to reverse x3 cells EMT phenotype while metformin treatment rescues normal DLD-1 epithelial phenotype. Related to Discussion.

Representative phase contrast pictures of No ORF and x3 cells treated either with 5 mM metformin, 40mM Etomoxir, 100mM Etomoxir or vehicle (water) for 48 hours. Scale bars, 100 μm.

PUBLICATION III

Targeting the lipid metabolic axis ACSL/SCD in colorectal cancer progression by therapeutic miRNAs: miR-19b-1 role

Silvia Cruz-Gil, Ruth Sánchez-Martínez, Marta Gómez de Cedrón, Roberto Martín-Hernández, Teodoro Vargas, Susana Molina, Jesús Herranz, Alberto Dávalos and Ana Ramírez de Molina.

DOI:10.1194/jlr.M076752

PUBLICATION III SUMMARY

Targeting the lipid metabolic axis ACSL/SCD in colorectal cancer progression by therapeutic miRNAs: miR-19b-1 role

In this work we aimed to analyze the role of miRNAs as regulators of the ACSL/SCD axis. miRNAs are potent epigenetic modulators of several cell processes including tumorigenesis and may represent a therapeutic opportunity for targeting the network.

We first performed a bioinformatics prediction of common miRNAs regulating ACSL1/ACSL4/SCD pro-tumorigenic axis obtaining 31 putative miRNAs. We developed an interaction scoring method based on RT-QPCR data able to reflect the potency of the miRNA candidates in targeting the axis components mRNAs, to select stronger miRNA-ACSL/SCD axis genes interactions. The lower the scores are, the higher the targets depletion is, which selected miR-544a, miR-142 and miR-19b-1 as the most promising candidates for axis negative regulators. Then, confirmation of miRNAs action on their targets (ACSL1, ACSL4 and SCD) was analyzed by WB. Furthermore, dual-luciferase assays were performed to show the direct interaction of candidate miRNAs to their targets reflected by their binding on the corresponding 3' UTRs.

In order to confirm these miRNAs prognosis value, their expression levels were evaluated in CRC patients (CRC stage II patients n=80; 17,50% of recurrence; CRC stage III patients n=46; 39.13% of recurrence) showing a clear correlation between disease-free survival (DFS) in stage II patients and the expression levels of miR19b-1-5p or miR19-b-3p (mature isoforms). Furthermore, miR-19b-3p prognostic value was also observed in stage III CRC patients. Finally, to evaluate whether miR-19b-1 isoforms might constitute independent prognostic classifiers, clinical and histopathological data were included in both univariate and multivariate Cox regression analyses revealing that both miR-19b-1 forms were DFS independent prognostic biomarkers in stage II CRC patients. Again, only miR-19b-3p constituted a DFS independent prognostic biomarker in stage III CRC patients. Hence, miR-19b-1 can be considered as a potential miRNA involved in the inhibition of the ACSL/SCD network, with a predictive value of good prognosis in CRC patients.

We performed an *in silico* functional analysis, elucidating putative miRNA biological effects by Genecodis 3 and TarBase database. MiR-19b-1 was putatively involved in focal adhesions and actin cytoskeleton regulation, both related to invasion and migration. In line with this, Matrigel-based invasion assays showed a clear decrease in the number of invasive cells when miR-19b-1 was electroporated in CRC cell lines. Hence, mir-19b-1 blocks CRC cells invasion, in agreement

with the opposite effect exerted by its targets ACSL1, ACSL4 and SCD, reported in publication I. We finally analyzed miR-19b-1 link to lipid metabolism accordingly to the condition of lipid metabolism enzymes of its targets. By TG and neutral lipids intracellular content analysis we showed the minus accumulation of lipid droplets upon miR-19b-1 transfection; corresponding to ACSLs/SCD targeting and therefore the inhibition of the previous steps to TG synthesis. Besides, by respiratory analysis using Seahorse bioanalyzer we observed that upon miR-19b-1 transfection, the respiratory capacity of cells was compromised, leading to an even a more dramatic effect upon FA oxidation inhibition.

PUBLICATION III CONCLUSIONS

- A screen of miRNAs simultaneously targeting ACSL1, ACSL4 and SCD evidences miR-142, miR-544a and miR-19b-1 as regulators of the *ACSL/SCD* protumorigenic network involved in invasiveness and poor prognosis of CRC.
- miR-19b-1 expression correlates with a better prognosis in stage II and III CRC patients, arising as a promising therapeutic miRNA in CRC.
- mir-19b-1 inhibits cancer cells invasion, counteracting the opposite effect exerted by its targets from the *ACSL/SCD* axis.
- The possibility to detect miRNAs in body fluids designates miR-19b-1 as a potential noninvasive biomarker in CRC.

My personal contribution to these results was to conduct the design of the experiments and their experimental development, as well as the manuscript preparation and revision. My supervisors raised this project and guide me during the whole process.

This article was selected by the American Society for Biochemistry and Molecular Biology (ASBMB) to make a review on its informative magazine entitled “miRNAs take the wrecking ball to colorectal cancer” (ASBMB Today, Vol.17, No.3, March 2018).

Targeting the lipid metabolic axis *ACSL/SCD* in colorectal cancer progression by therapeutic miRNAs: miR-19b-1 role

Silvia Cruz-Gil[1], Ruth Sanchez-Martinez[1,*], Marta Gomez de Cedron[1], Roberto Martin-Hernandez[2], Teodoro Vargas, Susana Molina[1], Jesús Herranz[3], Alberto Davalos[4], Guillermo Reglero[1] and Ana Ramirez de Molina[1, *].

[1]Molecular Oncology and Nutritional Genomics of Cancer Group/ IMDEA Food Institute, CEI UAM + CSIC, Madrid, Spain.

[2]Bioinformatics Unit, IMDEA Food Institute, CEI UAM+CSIC, Madrid, Spain.

[3]Biostatistics Unit, IMDEA Food Institute, CEI UAM+CSIC, Madrid, Spain.

[4]Disorders of Lipid Metabolism and Molecular Nutrition group/ IMDEA Food Institute, CEI UAM + CSIC, Madrid, Spain.

[*]Correspondence to: Dr. Ana Ramirez de Molina. (E-mail: ana.ramirez@imdea.org); and Dr. Ruth Sanchez Martinez (E-mail: ruth.sanchez@imdea.org).

Molecular Oncology and Nutritional Genomics of Cancer Group/IMDEA Food Institute, CEI UAM + CSIC. Ctra. De Cantoblanco, 8 E-28049 Madrid. Spain. Phone +34672134921.

Running title

ACSL/SCD regulatory miRNAs involved in CRC progression

Abbreviations

Colorectal cancer (CRC); acyl-CoA synthetase (ACSL) stearoyl-CoA desaturase (*SCD*); miRNAs (miRNAs/miR); disease-free survival (DFS); epithelial-mesenchymal transition (EMT);

individual score (IS); final Score (FS); Quantitative reverse transcription polymerase chain reaction (RT-QPCR); Hazard ratios (HR); corrected hypergeometric test (Hyp c).

Abstract

Abnormal acyl-CoA synthetase/ stearoyl-CoA desaturase (ACSL/SCD) lipid network fuels colon cancer progression endowing cells with invasive and migratory properties. Therapies against this metabolic network may be useful to improve clinical outcomes. Since miRNAs (miRNAs/miR) are important epigenetic regulators, we investigated novel miRNAs targeting this pro-tumorigenic axis; and hence to be used both as therapeutic or prognostic miRNAs. Thirty one putative common miRNAs were predicted to target simultaneously the three enzymes comprising *ACSL/SCD* network. Target validation by RT-QPCR, Western blotting and luciferase assays showed miR-544a, miR-142 and miR-19b-1 as major regulators of the metabolic axis *ACSL/SCD*. Importantly, lower miR-19b-1 expression associates with a decreased survival rate in CRC patients, accordingly with *ACSL/SCD* involvement in patient relapse. Finally, miR-19b-1 regulates the pro-tumorigenic axis *ACSL/SCD* being able to inhibit invasion in colon cancer cells. Since its expression correlates with an increased survival rate in CRC patients, we propose miR-19b-1 as a potential noninvasive biomarker of disease-free survival (DFS) and a promising therapeutic miRNA in CRC.

JOURNAL OF LIPID RESEARCH

Graphical abstract

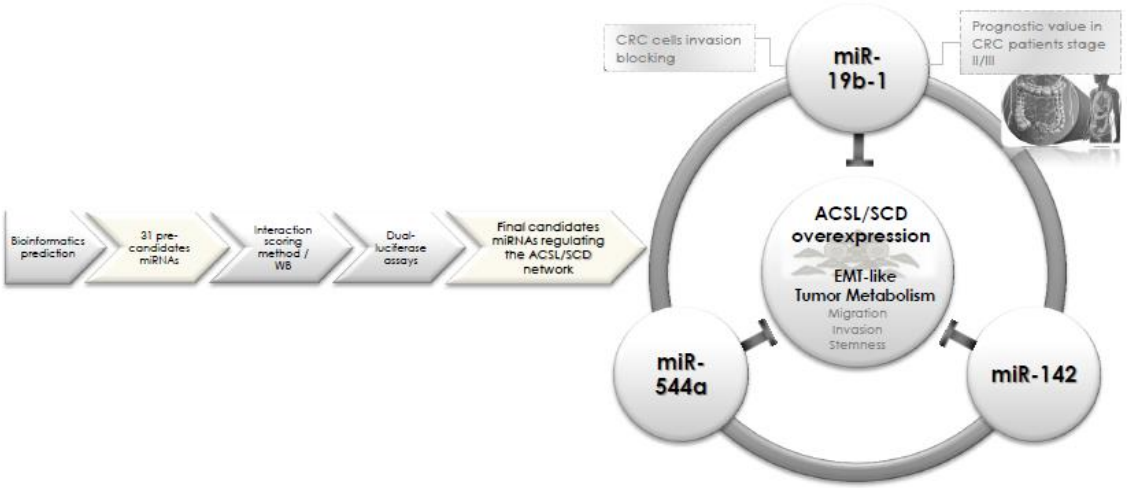

Keywords: microRNA, Colorectal tumors, Patient relapse, Invasiveness, Cancer, Molecular biology, Lipid and lipoprotein metabolism, Fatty Acid/Metabolism, Clinical Studies.

1. Introduction

CRC, one of the most commonly diagnosed cancers, has one of the highest prevalence and mortality rates among malignant tumors (1). Energetic metabolism reprogramming is one of the emerging hallmarks of cancer. Adjustments of energy metabolism are triggered to fuel the uncontrolled growth of cancer cells. Lipid metabolism is altered in cancer, among other metabolic pathways (2, 3), and it represents an important source of energy and structural and biosynthetic resources fundamental for carcinogenic processes (3, 4).

Our group identified a cooperative lipid metabolism related genes involved in CRC (5): two members of the acyl-CoA synthetase (ACSL) family: *ACSL1* and *ACSL4*; and the stearoyl desaturase (*SCD*). ACSL1 and ACSL4 catalyze the conversion of long chain fatty acids to acyl-CoA (6) and have been related to carcinogenesis (4, 7). SCD, the rate-limiting enzyme converting saturated into monounsaturated fatty acids, is also related to malignant transformation, proliferation or survival (8–10). ACSL/SCD lipid network fuels migratory and invasive properties through EMT induction and it is associated with an increased risk of relapse in CRC patients (5).

miRNAs are endogenous non-coding small RNAs that have recently emerged as potent epigenetic modulators, which specifically bind to complementary regions within messenger RNAs to promote their degradation and/or to inhibit translation (11, 12). miRNAs regulate cellular homeostasis and development and also several processes involved in tumorigenesis (12–14). The reported crosstalk between miRNAs and several lipid metabolism processes like lipogenesis, lipolysis or lipophagy (13) could contribute to their action as tumor suppressors or as oncomiRNAs.

Here, we characterize novel regulators of the whole *ASCL/SCD* network through miRNAs screening. Firstly, using bioinformatics approaches, then testing the effect of the strongest miRNAs candidates on *ACSL/SCD* axis and validating their specificity through the action on their

3'UTR. Finally, we evaluated the expression of the most remarkable regulator in stage II and III CRC patients.

2. Materials and methods

2.1. Cell culture and reagents

SW620, DLD-1, LoVo and HEK-293T cell lines were obtained from ATCC, maintained under standard conditions, *Mycoplasma* tested every two weeks and 3-4 passages (2-3 weeks) for each cell line were used for experiments between collection and thawing. Commercial antibodies used are listed in Supplementary Table 3. Antibody against SCD (15) was a gentle contribution from Dr. Jean-Baptiste Demoulin, Université Catholique de Louvain, Brussels, Belgium. Anti-human ACSL4 was generously granted by Dr. Stephen Prescott, University of Utah, Salt Lake, USA and Dr. Diana Stafforini, Huntsman Cancer Institute, University of Utah, USA, and used as indicated (16).

2.2. Bioinformatics tools

Four different algorithms were used simultaneously in order to identify miRNA-genes interactions: miRanda, PITA, TargetScan and PicTar5. miRanda (17) and TargetScan (18) use the degree of sequence complementarity as primary key parameters to identify miRNA-mRNA interactions. PITA (19) utilize thermodynamics as the main criterion and miRanda has also included this feature. PicTar5 (20) or the mirSVR scoring model (21) collect different types of features derived from the latest in vivo and in-vitro assays and utilize machine learning techniques to find the feature patterns shared by true miRNA-target interactions. A prediction was considered valid whenever co-occurs in at least 2 algorithms. For miRNAs functional analysis, Genecodis 3 (22) determined overrepresented biological processes from gene Ontology or overrepresented pathways from Panther database.

To provide a miRNA-mRNA interaction scoring schema we used the miRanda / mirSVR scoring schema. miRanda algorithm provides alignment, thermodynamic, and conservation scores and mirSVR algorithm uses the machine-learning based score (http://www.microrna.org/). Alignment and conservation scores reflect level of complementarity between sequences and conservation of the target site among vertebrates, respectively. The seed category represents the number of nucleotides interacting at the seed level. An 8 seed-category or 8mer site (8 monomer site), means an interaction between all nucleotides from 2-9, and 7mer site from 2-8, and an 6mer site between all nucleotides from 2-7. However, 0 represents a mismatch somewhere along the nucleotides 2-7 within the seed, so 5 or fewer nucleotides interact**.** mirSVR score (21) detects experimentally verified non-canonical miRNA-mRNA interactions. The higher the probability of downregulation, the lower the mirSVR score is. Cutoff was set at -0.5, since 15% of all the predicted targets have a score lower than 0.5, and at such score the expected probability of observing a minimal log expression change of -0.1 is approximately 50%.

2.3. Quantitative real-time PCR and interaction score method generation

Mimic miRNAs (30 nM) were transfected into HEK-293T cells (Lipofectamine® 2000, Thermo Fisher Scientific). Total RNA was extracted 48 hours post transfection using Tri Reagent (Sigma) and reverse-transcribed using the High Capacity RNA-to-cDNA Master Mix system (Life Technologies). RT-QPCR was performed using VeriQuest SYBR Green qPCR Master Mix (Affymetrix, Santa Clara, CA, USA) and gene specific primers listed in Supplementary Table 1. miRNAs expression in patients was monitored using TaqMan® MicroRNA Reverse Transcription Kit (ThermoFisher Scientific), and Taq-man miRNA probes for RT-QPCR (Supplementary Table 2). The $2^{-\Delta\Delta Ct}$ method was applied to calculate the relative gene or miRNA expression.

Regarding the interaction scoring method, individual score (IS) was obtained by subtracting the replicas mean (2-ΔΔCt) for each miRNA-gene interaction by the global mean (2-ΔΔCt average

among the 31 miRNAs for each gene). In this way, we select only the best interactions for each gene. Consequently, final Score (FS) represents the average of the 3 individual scores of each miRNA for the 3 target genes *ACSL1, ACSL4* and *SCD*. FS gets lower as the probability of downregulation increases. Individual $2^{-\Delta\Delta Ct}$ data (fold change), replicas mean, global mean and IS and FS are listed in Supplementary Table 5 for each miRNA-gene interaction.

2.4. Western Blot

Mimic miRNAs (60 nM) were transfected into HEK-293T cells (Lipofectamine® 2000, Thermo Fisher Scientific). Cell lysates were separated on SDS-PAGE, transferred onto nitrocellulose membranes, blocked with 5 % nonfat dry milk and probed with the antibodies listed in Supplementary Table 3. Signal detection was performed using the Clarity Western ECL Substrate (Bio-Rad). Vinculin determination was used as loading control.

2.5. Dual-luciferase assays (cloning and co-transfection)

Sequences for *ACSL1 (ENST00000281455)*, *ACSL4* (*ENST00000348502)* and *SCD* (*ENST00000370355)* were cloned into psiCheck2 by DNA 2.0. 50.000 HEK-293T cells were transfected using Lipofectamine2000 (Invitrogen) according to the manufacturer's recommendations. Each co-transfection reaction contained 100 ng of either psiCheck2-3´-UTR-*ACSL1*, psiCheck2-3´UTR-*ACSL4* or psiCheck2-3´-UTR-*SCD*, and 30 nM of each mimic miRNA. The relative luciferase activity (Renilla luminescence/ firefly luminescence) was determined after transfection using the Dual-Luciferase Reporter Assay System (Promega) representing the translational repression of *ACSL1, ACSL4* and *SCD* upon binding to their 3′UTR of candidate miRNAs.

2.6. Patients and samples

80 CRC stage II and 46 CRC stage III patients from La Paz University Hospital were enrolled in the study. Formalin-Fixed, Paraffin-Embedded (FFPE) samples were obtained with the patient's authorization and with the approval of the human research Ethics review Committee of La Paz University Hospital (HULP-PI-1452). Clinico-histopathological data of patients were prospectively collected on clinical history and were confirmed by oncologists of the hospitals implicated in this study (Supplementary Table 4).

2.7. Invasion assays

SW620 or LoVo cells were nucleotransfected (Neon® Transfection System, ThermoFisher) with 30 nM mimic miR-19b-1 (miR-19b-1) or a control miRNA (miR-Ctrl). For rescue experiments miRNAs were co-transfected with 300 ng of vectors expressing the coding sequence of ACSL1, ACSL4, SCD (DNA 2.0, Menlo Park CA, USA). Cells were seeded in 0.1% FBS- DMEM using Matrigel Invasion Chambers (Corning). DMEM 10% FBS is used as chemoattractant. After fixation and staining, images were captured (Olympus CKX41) and registered (getIT software, Olympus).

2.8. Neutral lipid content distribution

DLD-1 cells were transfected with Lipofectamine2000 with mimic miRNAs (30 nM) for 48h. Oleic acid conjugated with BSA (0,5mM) was added the day before the analysis to increase the lipid content. Fatty acid free BSA was used as vehicle for the control group.

Triglycerides (TG) analysis: Cell lipids were extracted with chloroform-methanol (23) and analyzed enzymatically using commercial kits (from Spinreact, Sant Esteve de Bas, Spain). Lipids were expressed as µg TG/mg of protein.

Bodipy staining for microscopy: Cells were treated with 2 µM BODIPY staining solution (BODIPY™ 493/503, Invitrogen) in PBS for 15 min at 37 °C and fixed with 4%

paraformaldehyde. Images were captured using a Leica DM IL microscope, with a 40X Plan Fluotar objective and registered using Leica Application Suite (LAS).

2.9. Oxygen consumption rate (OCR)

OCR was monitored as an indicator of mitochondrial respiration with an XF96 Extracellular Flux Analyzer using XF Cell Mito Stress Test kit according to manufacturer instructions (Seahorse Biosciences, North Billerica, MA, USA). Cells were seeded into XF96 plates with DMEM 10% FBS at a density of 90000 cells/well for SW620 cells, as described in (24), and transfected the following day with mimic miRNAs (30 nM) using Lipofectamine2000. Upon several washes, media was replaced for 1 hour prior to assay with Krebs Henseleit Buffer (KHB; 111mM NaCl, 4.7mM KCl, 1.25mM CaCl2, 2mM MgSO4, 1.2mM NaH2PO4) supplemented with 2.5mM Glucose, 0.5mM Carnitine and 5mM Hepes, as FAO (fatty acid oxidation) media. Etomoxir (Sigma), a CPT-1 (carnitine palmitoyl transferase-1) inhibitor and therefore a fatty acid oxidation inhibitor, was added to the media 15 min prior to assay. Once basal rate measurements were taken, mitochondrial respiratory chain drugs were added, following Mito Stress kit specifications. 2 µM Oligomycin was used to block ATP-linked oxygen consumption, 0.6 µM FCCP as an uncoupling agent to obtain maximal respiration and 0.5 µM Rotenone/Antimycin A to inhibit complex I and III, stopping all mitochondrial respiration. OCR was measured 3 times following injection of each drug, and normalized to total protein content. At least 6 replicates per condition were done for each experiment.

2.10. Statistical analysis

Time to relapse was obtained for the analysis of 3-year DFS, defined from the time of surgical procedure. The Kaplan-Meier method was used to estimate DFS. Log-rank test for Univariate Cox regression analysis was performed to test association between DFS and individual miRNA expression. Hazard ratios (HR) and 95% CI were calculated from the adjusted Cox regression model (vascular invasion, lymphatic invasion, perineural invasion, together with age > 70). All

reported *P-values* were two-sided. Statistical significance was defined as p<0·05. Statistical analyses were done by R statistical software v3.1 (www.r-project.org).

3. Results

3.1. Bioinformatics prediction of common miRNAs regulating *ACSL1/ACSL4/SCD* pro-tumorigenic axis

MiRanda, PITA, TargetScan and PICTAR5 were run in order to identify miRNA-genes interactions. Considering a valid prediction whenever it co-occurred in at least 2 algorithms, we identified 31 putative miRNAs (Figure 1.A) capable to target simultaneously *ACSL1*, *ACSL4* and *SCD*. A more restrictive prediction based on the co-occurrence of at least 3 algorithms was also performed. Venn diagram shows the intersection of predictions for 28 common miRNAs of *ACSL1/ACSL4/SCD* (Figure 1.B). Since the number did not vary significantly, we thus considered the initial 31 candidate miRNAs for further *in vitro* validation.

3.2. Screening of the predicted miRNAs evidences miR-544a, miR-142 and miR-19b-1 as regulators of the ACSL1/ACSL4/SCD network

Since *in vitro* screening and validation are essential to avoid false predictions, HEK-293T cells were transfected with miRNA mimics and measured the ACSL1/ACSL4/SCD protein expression levels. We next developed an interaction scoring method based on RT-QPCR data to select stronger miRNA-gene interactions based on better mRNA depletions. Table (Figure 2.A) shows individual scores (IS) and final scores (FS) from miRNA-gene interactions. The lower the scores are, the higher the targets depletion is. We defined a FS cutoff of -0.35 which selects miR-544a (FS= -0.474), miR-142 (FS= -0.416) and miR-19b-1 (FS= -0.354) as best candidates.

We further confirmed their action on their targets by WB (Figure 2.B). The FS (-0.474) for miR-544a is in accordance with a reduction of the targets protein expression (52%, 80% and 26% of protein downregulation of ACSL1, ACSL4 and SCD, respectively). miR-142 obtained a FS of -0.416 (-0.421/-0.25/-0.577 as IS for ACSL1/ACSL4/SCD, respectively), which is in agreement with a 70%, 57% and 49% of protein downregulation of ACSL1, ACSL4 and SCD, respectively. Finally, miR-19b-1 (FS=-0.354) showed 38%, 89% and 77% of protein downregulation of ACSL1, ACSL4 and SCD, respectively; also in agreement with previous IS (-0.298/-0.295/-0.468 for ACSL1/ACSL4/SCD, respectively). Additionally, two miRNAs not pre-selected, miR-578 and miR-199b, with higher FS and therefore less predicted capacity to downregulate the targets, were also able to downregulate the three target proteins in the case of miR-199b (44%, 54% and 75% of protein downregulation of ACSL1, ACSL4 and SCD, respectively); and ACSL4 and SCD proteins in the case of miR-578 (0%, 48% and 33% of protein downregulation of ACSL1, ACSL4 and SCD, respectively). We also analyzed miR-205, whose prognostic value in CRC has been described (14) and miR-106, characterized as a biomarker in CRC (25, 26). Although miR-205 and miR-106-a were good candidates globally (FS –0.205 and -0.282, respectively), only miR-205 presented significant protein downregulations (45%, 92% and 67% of ACSL1, ACSL4 and SCD protein downregulation, respectively).

Even though miR-205 and miR-199b presented significant downregulation capacity at the protein level; we decided to further continue studying miR-544a, miR-142 and miR-19b-1, as the most robust candidates downregulating both RNA and protein levels of the ACSL/SCD pro-tumorigenic axis.

To complement WB results, those mRNA-miRNA interactions were quantified based on the miRanda/mirSVR scoring schema. Regarding *ACSL1* (Figure 2.C upper table), selected miRNAs alignment scores were quite low, since 120 is the minimum score for a target to be considered as valid. It is remarkable that 4 out of 5 interactions were canonical at the seed level. MirSVR scores, which get lower as downregulation probability increases, were better for 7mer sites. Curiously,

miR-544a had a high probability to downregulate *ACSL1*, stated by a mirSVR score of -1.0027, demonstrating this score ability to detect non-canonical miRNA-mRNA interactions. Thus, miR-142-3p, which has a canonical 7mer interaction site together with good alignment, energy and conservation scores, and miR-544a, which it is not a canonical interaction but presents a significantly low mirSVR score, may be among the best candidates. Regarding miR-19b-1 mature forms: miR-19b-1-5p (MIMAT0004491) and miR-19b-3p (MIMAT0000074); further *in vitro* assessment is needed since they present the minimal alignment score to be considered as valid candidates and the mirSVR does not reflect a high downregulation probability. In the case of *ACSL4* (Figure 2.C middle table), the highest alignment scores correspond to 7mer canonical sites, which in addition have acceptable mirSVR scores based on our cutoff. The miR-19b-1-5p interaction does not account for a canonical site type, and the mirSVR score does not reflect a potential non-canonical interaction. Regarding *SCD* (Figure 2.C lower table), the alignment and energy scores were strong and all the interaction sites were canonical with a 7 nucleotides interaction along the seed with the exception of miR-19b-1-5p whose interaction is not potent enough to overcome the detection threshold. This was also the case for the *ACSL4*-miR-142-5p interaction. Considering the above-mentioned results, we reaffirm the decision to consider miR-544a, miR-142, and miR-19b-1 as the best candidates to regulate the *ACSL1*/*ACSL4*/*SCD* pro-tumorigenic axis for more detailed analysis.

3.3. MiR-142, miR-544a and miR-19b-1 target the 3´UTR of *ACSL1*, *ACSL4* and *SCD*

To validate the direct interaction of these miRNAs to their targets we performed dual-luciferase assays (Figure 2D). In agreement with previous results, miR-544a, miR-142 and miR-19b-1 downregulated the activity of the three reporter constructions reflecting their binding on the corresponding 3' UTRs. Hence, we assumed miR-544a, miR-142, and miR-19b-1 as validated miRNAs regulating the *ACSL*/*SCD* pro-tumorigenic axis.

3.4. Low expression of miR-19b-1 correlates with a poorer prognosis in CRC stage II and stage III patients

In order to confirm these miRNAs potency as regulators of *ACSL*/*SCD* axis involved in CRC prognosis, their expression levels were evaluated in CRC patients. For both mature forms of miR-142 [miR-142-3p (MIMAT0000434); miR-142-5p (MIMAT0000433)] and for miR-544a, significant correlation with DFS was not found (data not shown). However, both miR-19b mature forms significantly predict DFS in CRC stage II patients. MiR-19b-5p displayed a HR (95% CI):0.27(0.09-0.78), log-rank p=0.0097 (Figure 3A) and miR-19b-3p a HR (95% CI):0.27 (0.09-0.77), log-rank p=0.0087 (Figure 3B). Furthermore, miR-19b-3p prognostic value was also observed in III CRC patients DFS [HR (95% CI):0.37(0.14-0.97), log-rank p=0.034] (Figure 3C and D). Finally, to evaluate whether miR-19b-1 might constitute independent prognostic classifiers, clinical and histopathological data were included in both univariate and multivariate Cox regression analyses (Figure 3E) revealing that both miR-19b-1 forms were DFS independent prognostic biomarkers in stage II CRC patients: miR-19b-1-5p: HR(95% CI):0.22(0.07-0.74), p=0.0111; and miR-19b-3p: HR(95% CI):0.25(0.08-0.78), p=0.0173 (Figure 3E). Again, only miR-19b-3p [HR (95% CI):0.37(0.14-0.98), p= 0.041] constituted a DFS independent prognostic biomarkers in stage III CRC patients (Figure 3E). Hence, miR-19b-1 could be considered as a potential miRNA with predictive value related with good prognosis in CRC patients through the inhibition of the *ACSL*/*SCD* network activation.

3.5. MiR-19b-1 blocks cell invasion and regulates lipid metabolism in CRC cells

To further validate miR-19b-1 interference with CRC cell invasiveness mediated by ACSL/SCD axis, we performed an *in silico* functional analysis, elucidating putative miRNA biological effects. Figure 4A shows biological processes ordered according to the increasing number of genes

involved in each statistically significant process (Hyp_c < 0,05); while in Figure 4B are ordered by corrected hypergeometric test (Hyp c). Interestingly, focal adhesions (Hyp_c =0,001) and actin cytoskeleton regulation (Hyp_c =0,011), both related with invasion and migration (27, 28) are putatively elicited by miR-19b-1; in accordance with the reported ACSL/SCD effect promoting invasion and migration (5). To confirm the miR-19b-1 implication in these processes we performed a matrigel-based invasion assay in two well-known invasive CRC cell lines: SW620 and LoVo (Figure 4C). Remarkably, in both cases, a clear decrease in the number of invasive cells was observed upon miR-19b-1 electroporation. Therefore, miR-19b-1 blocks CRC cells invasion, which is in agreement with the opposite effect exerted by its targets *ACSL1*, *ACSL4* and *SCD* (5). To demonstrate whether the effect of miR-19b-1 in CRC cells invasion is regulated directly by the suppression of ACSL1, ACSL4 and SCD we performed rescue experiments by reintroducing ACSL1, ACSL4 and SCD in miR-19b-1 transfected cells. As shown in Figure 4D, the invasive phenotype of CRC cells is significantly recovered when miR-19b-1 transfection is combined with ACSL/SCD expression vectors lacking the 3' UTR and thus not affected by miR-19b-1 regulation. This demonstrates that re-expression of the ACSL/SCD axis is able to recover the lost invasion upon miR-19b-1 treatment of SW620 cells, and therefore, it evidences the specific role of miR-19b-1/ACSL/SCD regulatory axis in controlling CRC invasion.

To further assess the impact of our miRNA candidate in lipid metabolism we measured the triglyceride levels in miR-19b-1 transfected cells, as shown in Figure 4E. Since CRC cells are not normally storing substantial amounts of neutral lipids, cells were exposed to oleic acid (OA) to favor lipids storage. Under these conditions, cells transfected with miR-19b-1 presented a clear reduction in the cellular triglyceride (TG) content indicating that miR-19b-1 diminishes neutral lipids accumulation in the cells. As a complementary analysis, we also used the Bodipy fluorophore, a specific dye for cellular neutral lipid droplets. Figure 4F shows again that cells transfected with miR-19b-1 are less prone to neutral lipid droplets accumulation upon oleic acid supplementation (OA-BSA), compared to the vehicle control alone (BSA).

To get further insight into miR-19b-1 metabolic role on CRC cells, we performed bioenergetics experiments using the *Seahorse* XF bioanalyzer. Figure 4G shows that miR-19b-1 does not only trigger an overall effect on lipid droplets maintenance or mobilization; but also at the bioenergetic level. Upon treatment with a β-oxidation inhibitor (Etomoxir), which inhibits FA transport to mitochondria and therefore respiration dependent on FA, miR-19b-1 transfected cells present a lower maximal oxygen consumption rate compared to miR control cells. As a consequence of this, the spare capacity (measured as the difference between maximal respiration and the correspondent basal respiration) is null in cells transfected with miR-19b-1, differently from cell transfected with miR control. This spare respiratory capacity indicates the presence of a reserve that is accessible for the cells in case of a bioenergetic demand or a stressful situation. These results suggest that miR-19b-1 compromises respiratory capacity of cells, leading to even a more dramatic effect upon FA oxidation inhibition, eliminating the spare respiratory capacity of cells.

4. Discussion

ACSL/SCD network is a clear example of how cancer cells reprogram their metabolism to promote cell invasion and poorer disease prognosis (5). Hence, it is crucial to unveil this network regulating mechanisms in order to design effective cancer therapies. In this sense, regulatory miRNAs emerge as promising therapeutic tools and non-invasive biomarkers since they can be detected in body fluids.

Combined bioinformatics tools led us to a 31 candidates miRNAs library (Figure 1), that were screened by analyzing their effect on their targets *ACSL1*/*ACSL4*/*SCD* expression using a novel interaction scoring method (Figure 2A). WB, miRanda/mirSVR scoring schema and dual-luciferase assays (Figure 2) validated miR-544a, miR-142, and miR-19b-1 as *ACSL/SCD* regulators. Importantly, miR-19b-1 lower expression correlates with a poorer prognosis in stage II and III CRC patients (Figure 3) suggesting a protective role for this miRNA in CRC, very likely through its involvement in cell invasion and lipid metabolism regulation (Figure 4).

Here we have used novel scoring approaches for a more convenient managing and screening of bioinformatics data. For instance, the interaction scoring method enables us to select the best miRNA candidates for a combination of targets. Furthermore, the combination of two important bioinformatic tools in the defined miRanda/mirSVR scoring schema allow us to detect canonical and non-canonical interaction sites which are often filtered out during the prediction process by most algorithms such as miRanda, making hard to detect experimentally verified non-canonical interactions. This was the case for miR-544a-*ACSL1* interaction, whose mirSVR score of -1.0027 represented a high downregulation probability, which was further validated despite not having a canonical interaction (17).

miR-19b-1, is a member of the miR-17-92 cluster frequently recognized as an oncomiR (29). This cluster has been associated to CRC (30) among other cancers (31). However, recent studies

describe miR-19 to be decreased in gastric cancer (32, 33) suggesting that miR-17-92 cluster role needs to be further investigated. Probably these miRNAs roles and expression may be tissue and tumor stage dependent (34). This study opens a new avenue for miR-17-92 cluster involvement in CRC regulation; particularly, miR-19b-1, since its potential role as a tumor suppressor is here described.

An important finding is miR-19b-1 ability to inhibit CRC cells invasion. *In silico* analysis indicates this miRNA implication in processes like focal adhesions and regulation of actin cytoskeleton. Focal adhesions, which regulate cellular behaviors such as cell proliferation, migration, and invasion (35), also connect ECM and thus, tumor microenvironment to actin cytoskeleton also involved in cancer cell migration and invasion (28). The fact that miR-19b-1 may be able to inhibit these processes is in agreement with previous findings describing *ACSL*/*SCD* metabolic signature to promote invasion and migration (5).

In this vein, miR-19b-1 implication on lipid metabolism agrees with the condition of lipid metabolism enzymes of its targets ACSL1, ACSL4 and SCD. The use of two different tracers of lipid trafficking points towards the role of this miRNA in the maintenance of lipid droplets, either causing a decreased intake, an impaired incorporation of the fatty acids into neutral lipids, or an increased mobilization. miR-19b-1 could act by inhibiting *de novo* lipogenesis by targeting fatty acid (FA) activating enzymes (ACSLs and SCD), and therefore the previous steps to TG synthesis, leading to less accumulation of lipid droplets. Furthermore, Seahorse analysis suggest that miR-19b-1 compromises the respiratory capacity of cells potentiating the effect of the β-oxidation inhibitor Etomoxir. Again, by inhibiting ACSL-mediated FA activation, miR-19b-1 would lead to a diminished β-oxidation, and to a limited maximal mitochondrial respiration and impaired spare capacity. Nevertheless, further studies will help to elucidate the mechanisms underlying the miRNAs fine-tuning control of lipid metabolism fueling cancer energy.

Considering miR-19b-1 interacting together with the other selected candidates, miR-142 and miR-544a, a Panther analysis designates Wnt route as the most represented biological pathway

common to these 3 miRNAs (Supplementary Figure 1). Wnt activation requires avoiding β-Catenin degradation upon GSK3β inhibitory phosphorylation leading to invasion genes transcription (36). ACSL/SCD increases GSK3β phosphorylation, activating Wnt signaling and EMT (5), therefore the downregulation elicited by these miRNAs over this network suggests a role for them in Wnt regulation. Although with an opposite role, miR-544a has been involved in Wnt pathway actions in gastric and lung cancer (37, 38). MiR-142-3p has been reported to target cancer stem cell markers such as the Wnt target LGR5 in CRC cells (39), in agreement with its action on ACSL/SCD network; also involved in cancer stem cell features generation (5). Furthermore, reported miR-142-3p downregulation in CRC patients (40) supports our bioinformatics analysis. All this data come up with the idea of miRNA networks controlling functional gene interactions such as *ACSL/SCD*.

Finally, we propose miR-19b-1 as a potential noninvasive biomarker given its strong association with a better prognosis in CRC patients and as promising therapeutic miRNA inhibiting CRC cells invasion. miR-19b-1 could be used as a biomarker of CRC prognosis, which could be done either by directly evaluating its expression in biopsy tissues as described here, or its circulating levels in serum as previously described for other types of cancer (33). From a therapeutic point of view, miRNA replacement therapy could be an alternative to increase the expression of this particular miRNA in colorectal tissue, as exemplified by the use of miR-34 for other types of human neoplasias (41). Other alternatives such as dietary modulation of the miRNA could also be possible, since it has been recently showed miR-19b-1 induction by low protein diet in piglets (42). However, more in vivo research to test efficacy and safety issues is needed before we could benefit from therapeutic approaches to increase miRNA levels in humans.

Acknowledgements

We thank Dr. Jean-Baptiste Demoulin for the anti-SCD1 antibody and Dr. Stephen Prescott and Dr. Diana Stafforini for anti-ACSL4 antibody.

Conflict of Interest

Authors declare no potential conflict of interest.

Grant Support

This work was supported by Ministerio de Economía y Competitividad del Gobierno de España (MINECO, Plan Nacional I+D+i AGL2013-48943-C2 and AGL2016-76736-C3), Gobierno regional de la Comunidad de Madrid (P2013/ABI-2728, ALIBIRD-CM) and EU Structural Funds.

References

1. Siegel, R. L., K. D. Miller, and A. Jemal. 2016. Cancer statistics, 2016. CA. Cancer J. Clin. 66: 7–30.

2. Cairns, R. A., I. S. Harris, and T. W. Mak. 2011. Regulation of cancer cell metabolism. Nat. Rev. Cancer. 11: 85–95.

3. Carracedo, A., L. C. Cantley, and P. P. Pandolfi. 2013. Cancer metabolism: fatty acid oxidation in the limelight. Nat. Rev. Cancer. 13: 227–232.

4. Mashima, T., H. Seimiya, and T. Tsuruo. 2009. De novo fatty-acid synthesis and related pathways as molecular targets for cancer therapy. Br. J. Cancer. 100: 1369–1372.

5. Sánchez-Martínez, R., S. Cruz-Gil, M. Gómez de Cedrón, M. Álvarez-Fernández, T. Vargas, S. Molina, B. García, J. Herranz, J. Moreno-Rubio, G. Reglero, M. Pérez-Moreno, J. Feliu, M. Malumbres, and A. Ramírez de Molina. 2015. A link between lipid metabolism and epithelial-mesenchymal transition provides a target for colon cancer therapy. Oncotarget. 6: 38719–38736.

6. Coleman, R. A., T. M. Lewin, C. G. Van Horn, and M. R. Gonzalez-Baró. 2002. Do long-chain acyl-CoA synthetases regulate fatty acid entry into synthetic versus degradative pathways? J. Nutr. 132: 2123–2126.

7. Gaisa, N. T., A. Reinartz, U. Schneider, C. Klaus, A. Heidenreich, G. Jakse, E. Kaemmerer, B. M. Klinkhammer, R. Knuechel, and N. Gassler. 2013. Levels of acyl-coenzyme A synthetase 5 in urothelial cells and corresponding neoplasias reflect cellular differentiation. Histol. Histopathol. 28: 353–364.

8. Mason, P., B. Liang, L. Li, T. Fremgen, E. Murphy, A. Quinn, S. L. Madden, H.-P. Biemann, B. Wang, A. Cohen, S. Komarnitsky, K. Jancsics, B. Hirth, C. G. F. Cooper, E. Lee, S. Wilson, R. Krumbholz, S. Schmid, Y. Xiang, M. Booker, J. Lillie, and K. Carter. 2012. SCD1 inhibition causes cancer cell death by depleting mono-unsaturated fatty acids. PloS One. 7: e33823.

9. Roongta, U. V., J. G. Pabalan, X. Wang, R.-P. Ryseck, J. Fargnoli, B. J. Henley, W.-P. Yang, J. Zhu, M. T. Madireddi, R. M. Lawrence, T. W. Wong, and B. A. Rupnow. 2011. Cancer cell dependence on unsaturated fatty acids implicates stearoyl-CoA desaturase as a target for cancer therapy. Mol. Cancer Res. MCR. 9: 1551–1561.

10. von Roemeling, C. A., L. A. Marlow, J. J. Wei, S. J. Cooper, T. R. Caulfield, K. Wu, W. W. Tan, H. W. Tun, and J. A. Copland. 2013. Stearoyl-CoA desaturase 1 is a novel molecular therapeutic target for clear cell renal cell carcinoma. Clin. Cancer Res. Off. J. Am. Assoc. Cancer Res. 19: 2368–2380.

11. Ahmad, N., S. Haider, S. Jagannathan, E. Anaissie, and J. J. Driscoll. 2014. MicroRNA theragnostics for the clinical management of multiple myeloma. Leukemia. 28: 732–738.

12. Bartel, D. P. 2004. MicroRNAs: Genomics, Biogenesis, Mechanism, and Function. Cell. 116: 281–297.

13. Gómez de Cedrón, M., and A. Ramírez de Molina. 2016. Microtargeting cancer metabolism: opening new therapeutic windows based on lipid metabolism. J. Lipid Res. 57: 193–206.

14. Orang, A. V., R. Safaralizadeh, M. A. Hosseinpour Feizi, and M. H. Somi. 2014. Diagnostic and prognostic value of miR-205 in colorectal cancer. Asian Pac. J. Cancer Prev. APJCP. 15: 4033–4037.

15. Demoulin, J.-B., J. Ericsson, A. Kallin, C. Rorsman, L. Rönnstrand, and C.-H. Heldin. 2004. Platelet-derived growth factor stimulates membrane lipid synthesis through activation of phosphatidylinositol 3-kinase and sterol regulatory element-binding proteins. J. Biol. Chem. 279: 35392–35402.

16. Cao, Y., K. J. Murphy, T. M. McIntyre, G. A. Zimmerman, and S. M. Prescott. 2000. Expression of fatty acid-CoA ligase 4 during development and in brain. FEBS Lett. 467: 263–267.

17. John, B., A. J. Enright, A. Aravin, T. Tuschl, C. Sander, and D. S. Marks. 2004. Human MicroRNA targets. PLoS Biol. 2: e363.

18. Friedman, R. C., K. K.-H. Farh, C. B. Burge, and D. P. Bartel. 2009. Most mammalian mRNAs are conserved targets of microRNAs. Genome Res. 19: 92–105.

19. Kertesz, M., N. Iovino, U. Unnerstall, U. Gaul, and E. Segal. 2007. The role of site accessibility in microRNA target recognition. Nat. Genet. 39: 1278–1284.

20. Krek, A., D. Grün, M. N. Poy, R. Wolf, L. Rosenberg, E. J. Epstein, P. MacMenamin, I. da Piedade, K. C. Gunsalus, M. Stoffel, and N. Rajewsky. 2005. Combinatorial microRNA target predictions. Nat. Genet. 37: 495–500.

21. Betel, D., A. Koppal, P. Agius, C. Sander, and C. Leslie. 2010. Comprehensive modeling of microRNA targets predicts functional non-conserved and non-canonical sites. Genome Biol. 11: R90.

22. Tabas-Madrid, D., R. Nogales-Cadenas, and A. Pascual-Montano. 2012. GeneCodis3: a non-redundant and modular enrichment analysis tool for functional genomics. Nucleic Acids Res. 40: W478-483.

23. Folch, J., M. Lees, and G. H. Sloane Stanley. 1957. A simple method for the isolation and purification of total lipides from animal tissues. J. Biol. Chem. 226: 497–509.

24. Sánchez-Martínez, R., S. Cruz-Gil, M. S. García-Álvarez, G. Reglero, and A. R. Molina. 2017. Complementary ACSL isoforms contribute to a non-Warburg advantageous energetic status characterizing invasive colon cancer cells. Sci. Rep. 7: 11143.

25. Chen, W.-Y., X.-J. Zhao, Z.-F. Yu, F.-L. Hu, Y.-P. Liu, B.-B. Cui, X.-S. Dong, and Y.-S. Zhao. 2015. The potential of plasma miRNAs for diagnosis and risk estimation of colorectal cancer. Int. J. Clin. Exp. Pathol. 8: 7092–7101.

26. Zhang, L., L. Meng, Z. Fan, B. Liu, Y. Pei, and Z. Zhao. 2014. [Expression of plasma miR-106a in colorectal cancer and its clinical significance]. Nan Fang Yi Ke Da Xue Xue Bao. 34: 354–357.

27. Nagano, M., D. Hoshino, N. Koshikawa, T. Akizawa, and M. Seiki. 2012. Turnover of Focal Adhesions and Cancer Cell Migration. Int. J. Cell Biol. [online] https://www.hindawi.com/journals/ijcb/2012/310616/ (Accessed October 2, 2017).

28. Yamaguchi, H., and J. Condeelis. 2007. Regulation of the actin cytoskeleton in cancer cell migration and invasion. Biochim. Biophys. Acta. 1773: 642–652.

29. Mo, M.-H., L. Chen, Y. Fu, W. Wang, and S. W. Fu. 2012. Cell-free Circulating miRNA Biomarkers in Cancer. J. Cancer. 3: 432–448.

30. Diosdado, B., M. A. van de Wiel, J. S. Terhaar Sive Droste, S. Mongera, C. Postma, W. J. H. J. Meijerink, B. Carvalho, and G. A. Meijer. 2009. MiR-17-92 cluster is associated with 13q gain and c-myc expression during colorectal adenoma to adenocarcinoma progression. Br. J. Cancer. 101: 707–714.

31. Kandalam, M. M., M. Beta, U. K. Maheswari, S. Swaminathan, and S. Krishnakumar. 2012. Oncogenic microRNA 17-92 cluster is regulated by epithelial cell adhesion molecule and could be a potential therapeutic target in retinoblastoma. Mol. Vis. 18: 2279–2287.

32. YANG, O., J. HUANG, and S. LIN. 2014. Regulatory effects of miRNA on gastric cancer cells. Oncol. Lett. 8: 651–656.

33. Zhang, J., Y. Song, C. Zhang, X. Zhi, H. Fu, Y. Ma, Y. Chen, F. Pan, K. Wang, J. Ni, W. Jin, X. He, H. Su, and D. Cui. 2015. Circulating MiR-16-5p and MiR-19b-3p as Two Novel Potential Biomarkers to Indicate Progression of Gastric Cancer. Theranostics. 5: 733–745.

34. Reid, G., M. B. Kirschner, and N. van Zandwijk. 2011. Circulating microRNAs: Association with disease and potential use as biomarkers. Crit. Rev. Oncol. Hematol. 80: 193–208.

35. Wozniak, M. A., K. Modzelewska, L. Kwong, and P. J. Keely. 2004. Focal adhesion regulation of cell behavior. Biochim. Biophys. Acta BBA - Mol. Cell Res. 1692: 103–119.

36. Clevers, H. 2006. Wnt/beta-catenin signaling in development and disease. Cell. 127: 469–480.

37. Yanaka, Y., T. Muramatsu, H. Uetake, K. Kozaki, and J. Inazawa. 2015. miR-544a induces epithelial-mesenchymal transition through the activation of WNT signaling pathway in gastric cancer. Carcinogenesis. 36: 1363–1371.

38. Mo, X.-M., H.-H. Li, M. Liu, and Y.-T. Li. 2014. Downregulation of GSK3β by miR-544a to maintain self-renewal ability of lung caner stem cells. Oncol. Lett. 8: 1731–1734.

39. Shen, W.-W., Z. Zeng, W.-X. Zhu, and G.-H. Fu. 2013. MiR-142-3p functions as a tumor suppressor by targeting CD133, ABCG2, and Lgr5 in colon cancer cells. J. Mol. Med. Berl. Ger. 91: 989–1000.

40. Ghanbari, R., N. Mosakhani, J. Asadi, N. Nouraee, S. J. Mowla, Y. Yazdani, A. Mohamadkhani, H. Poustchi, S. Knuutila, and R. Malekzadeh. 2015. Downregulation of Plasma MiR-142-3p and MiR-26a-5p in Patients With Colorectal Carcinoma. Iran. J. Cancer Prev. 8: e2329.

41. Beg, M. S., A. J. Brenner, J. Sachdev, M. Borad, Y.-K. Kang, J. Stoudemire, S. Smith, A. G. Bader, S. Kim, and D. S. Hong. 2017. Phase I study of MRX34, a liposomal miR-34a mimic, administered twice weekly in patients with advanced solid tumors. Invest. New Drugs. 35: 180–188.

42. Sun, R.-P., Q.-Y. Xi, J.-J. Sun, X. Cheng, Y.-L. Zhu, D.-Z. Ye, T. Chen, L.-M. Wei, R.-S. Ye, Q.-Y. Jiang, and Y.-L. Zhang. 2016. In low protein diets, microRNA-19b regulates urea synthesis by targeting SIRT5. Sci. Rep. 6: srep33291.

A

miRNA	miRBase ID
hsa-miR-544-a	MI0003515
hsa-miR-142	MI0000458
hsa-miR-19b-1	MI0000074
hsa-miR-224	MI0000301
hsa-miR-106a	MI0000113
hsa-miR-31	MI0000089
hsa-miR-20b	MI0001519
hsa-miR-20a	MI0000076
hsa-miR-342	MI0000805
hsa-miR-205	MI0000285
hsa-miR-449b	MI0003673
hsa-miR-26b	MI0000084
hsa-miR-548b	MI0003596
hsa-miR-199b	MI0000282
hsa-miR-106b	MI0000734
hsa-miR-548a-3	MI0003612
hsa-miR-515-1	MI0003144
hsa-miR-519d	MI0003162
hsa-miR-19a	MI0000073
hsa-miR-195	MI0000489
hsa-miR-556	MI0003562
hsa-miR-186	MI0000483
hsa-miR-369	MI0000777
hsa-miR-17	MI0000071
hsa-miR-578	MI0003585
hsa-miR-34c	MI0000743
hsa-miR-93	MI0000095
hsa-miR-875	MI0005541
hsa-miR-548c	MI0003630
hsa-miR-940	MI0005762
hsa-miR-944	MI0005769

B

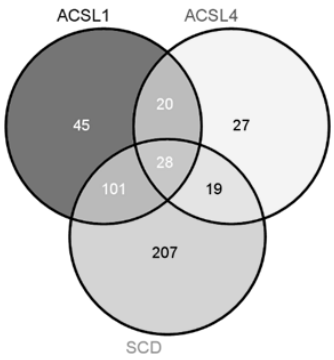

Figure 1: Bioinformatics prediction of common miRNAs regulating *ACSL1*, *ACSL4* and *SCD*

A) MiRanda, PITA, TargetScan and PICTAR5 algorithms were run to predict 31 common miRNAs putatively regulating *ACSL1*, *ACSL4* and *SCD*. A prediction was considered valid whenever co-occurring in at least 2 algorithms. MiRbase ID for all the candidates is also shown. B) Venn diagram showing the intersection of predictions for *ACSL1*, *ACSL4* and *SCD* based on the co-occurrence of at least 3 predicting algorithms

Figure 2

A

	ACSL1 [individual score]	ACSL4 [individual score]	SCD [individual score]	FINAL SCORE
hsa-miR-544-a	-0,385	-0,503	-0,533	-0,474
hsa-miR-142	-0,421	-0,250	-0,577	-0,416
hsa-miR-19b-1	-0,298	-0,295	-0,468	-0,354
hsa-miR-224	-0,252	-0,274	-0,371	-0,299
hsa-miR-106a	-0,343	-0,416	-0,088	-0,282
hsa-miR-31	-0,277	-0,204	-0,344	-0,275
hsa-miR-20b	-0,324	-0,178	-0,246	-0,249
hsa-miR-20a	-0,325	-0,297	-0,120	-0,248
hsa-miR-342	-0,332	-0,212	-0,179	-0,241
hsa-miR-205	-0,261	-0,504	0,149	-0,205
hsa-miR-449b	-0,231	0,224	-0,588	-0,198
hsa-miR-26b	0,115	-0,342	-0,361	-0,196
hsa-miR-548b	-0,349	-0,161	-0,044	-0,185
hsa-miR-199b	0,201	-0,134	-0,511	-0,148
hsa-miR-106b	-0,252	0,078	-0,269	-0,148
hsa-miR-548a-3	-0,267	-0,017	-0,104	-0,129
hsa-miR-515-1	-0,240	-0,009	-0,035	-0,095
hsa-miR-519d	-0,262	-0,238	0,237	-0,088
hsa-miR-19a	-0,266	-0,177	0,617	0,058
hsa-miR-195	-0,011	0,257	0,075	0,107
hsa-miR-556	0,277	-0,016	0,065	0,109
hsa-miR-186	0,055	0,048	0,281	0,128
hsa-miR-369	0,103	-0,003	0,315	0,138
hsa-miR-17	0,083	0,267	0,094	0,148
hsa-miR-578	0,610	-0,029	-0,103	0,160
hsa-miR-34c	0,532	0,160	0,516	0,403
hsa-miR-93	0,130	0,972	0,309	0,471
hsa-miR-875	0,223	0,887	0,484	0,531
hsa-miR-548c	0,626	0,305	0,720	0,551
hsa-miR-940	0,634	0,447	0,761	0,614
hsa-miR-944	1,508	0,613	0,318	0,813

B

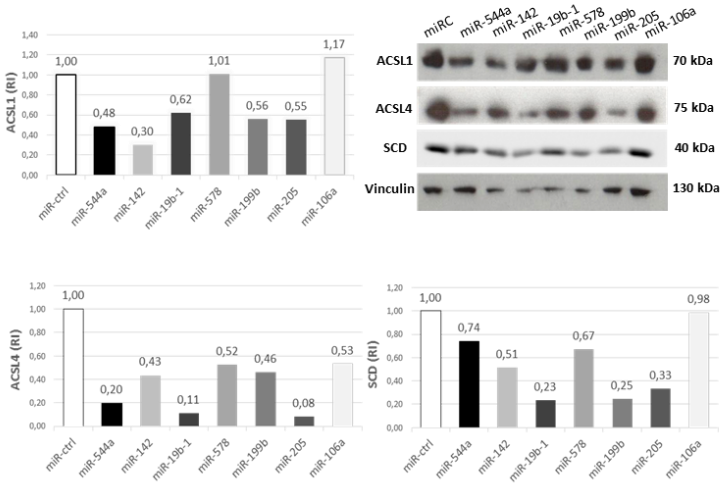

C

miRbase ID	miRNA	Target gene	Conservation	Alignment score	Seed category	Energy	mirSVR score
MIMAT0000433	hsa-miR-142-5p	ACSL1	0,618	162	7	-12,94	-0,5849
MIMAT0000434	hsa-miR-142-3p	ACSL1	0,7484	145	7	-15,34	-1,2218
MIMAT0003164	hsa-miR-544a	ACSL1	0,5128	125	0	-9,67	-1,0027
MIMAT0004491	hsa-miR-19b-1-5p	ACSL1	0,7484	120	6	-6,7	-0,4816
MIMAT0000074	hsa-miR-19b-3p	ACSL1	0,7484	120	6	-11,04	-0,4482

miRbase ID	miRNA	Target gene	Conservation	Alignment score	Seed category	Energy	mirSVR score
MIMAT0000434	hsa-miR-142-3p	ACSL4	0,663	159	7	-11,79	-0,8754
MIMAT0003164	hsa-miR-544a	ACSL4	0,662	151	7	-13,44	-0,8116
MIMAT0004491	hsa-miR-19b-1-5p	ACSL4	0,6486	139	0	-12,2	-0,102
MIMAT0000074	hsa-miR-19b-3p	ACSL4	0,662	151	7	-9,39	-0,5031

miRbase ID	miRNA	Target gene	Conservation	Alignment score	Seed category	Energy	mirSVR score
MIMAT0000433	hsa-miR-142-5p	SCD	0,5288	160	7	-8,63	-0,0652
MIMAT0000434	hsa-miR-142-3p	SCD	0,5651	155	7	-18,02	-0,1429
MIMAT0003164	hsa-miR-544a	SCD	0,5457	140	7	-10,41	-0,0129
MIMAT0000074	hsa-miR-19b-3p	SCD	0,5695	143	7	-9,77	-0,0112

D

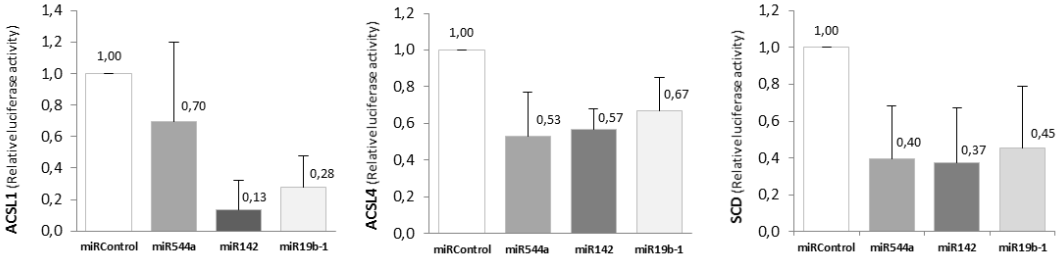

Figure 2. Validation of the predicted miRNAs evidences 3 selected miRNAs: miR-142, miR-544a and miR-19b-1

A) Interaction scoring method: Individual scores (IS) and final scores (FS) from miRNA-gene interactions upon performing RT-QPCR. IS was obtained by subtracting the RT-QPCR replicas mean (2-ΔΔCt) for each interaction by the global mean (2-ΔΔCt average among the 31 miRNAs for each gene). FS represents the average of the 3 individual scores. B) Western blotting showing *ACSL1*, *ACSL4* and *SCD* protein depletion upon treatment with mimic miRNAs for selected candidates from previous RT-QPCR experiments: miR-578, miR-199-b, miR-205, miR-106a, miR-142, miR-544a and miR-19b-1. A negative mimic miRNA control without any known target was used as a control. RI: Relative intensity of protein bands compared to controls. C) MiRanda/mirSVR scoring schema of mRNA-miRNA interactions: *ACSL1*, *ACSL4* and *SCD* and the selected miRNAs [miR-544a, miR-142 (miR-142-3p and miR-142-5p) and miR-19b-1 (miR-19b-1-5p and miR-19b-3p)], based on three different scores generated by miRanda (alignment, thermodynamic, and conservation scores) and the mirSVR machine-learning based score. D) Relative luciferase activity of *ACSL1* (left graph), *ACSL4* (middle graph) or *SCD* (right graph) 3'UTR psiCHECK™-2 vectors upon treatment with the selected miRNAs (miR-142, miR-544a and miR-19b-1). The relative luciferase activity (Renilla luminescence/ firefly luminescence) was determined 48 hours after transfection representing the translational repression of the proteins upon binding to their 3′UTR of candidate miRNAs. A miRNA with no predictive target was used as a negative control. Results represent the fold-change mean ±SD (n= 3).

Figure 3

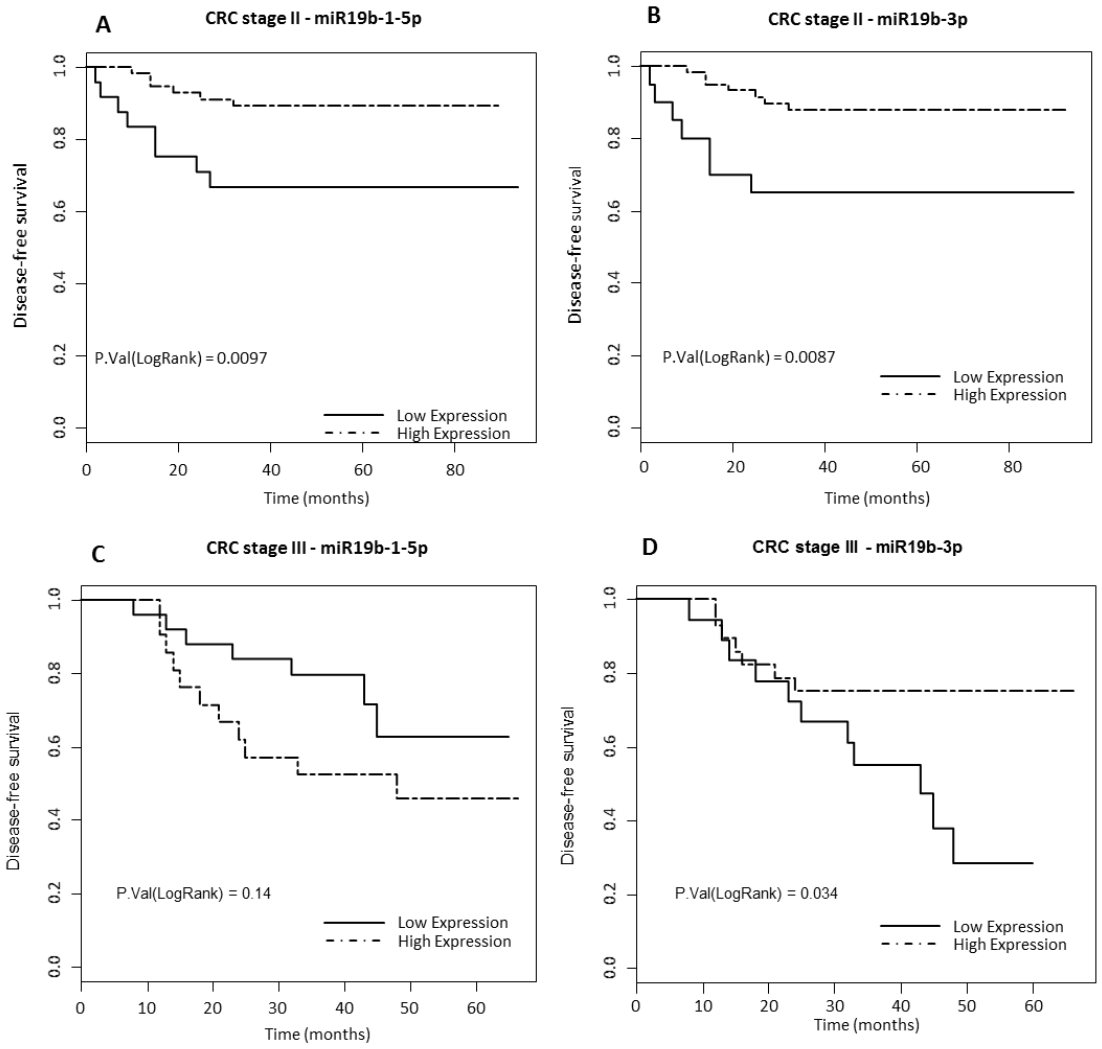

E

	CRC stage II				CRC stage III			
	Unadjusted		Adjusted#		Unadjusted		Adjusted#	
Variable	HR(95% CI)	P	HR(95% CI)	P	HR(95% CI)	P	HR(95% CI)	P
miR-19b-1-5p	0,27 (0,09-0,78)	0,016	0,22 (0,07-0,74)	0,011	2,02 (0,78-5,23)	0,142	2,18 (0,81-5,85)	0,115
miR-19b-1-3p	0,27 (0,09-0,77)	0,018	0,25 (0,08-0,78)	0,017	0,37 (0,14-0,97)	0,039	0,37 (0,14-0,98)	0,041

Abbreviations: HR (95% CI), hazard ratio and corresponding 95% confidence interval from adjusted or unadjusted Cox regression analyses; P, p value from adjusted or unadjusted Cox regression analyses.

Figure 3. Prognostic value of miR-19b-1 in CRC stage II patients

Kaplan-Meier survival curves for colorectal cancer (CRC) patients showing correlation between disease free survival (DFS) in stage II patients and the expression levels of miR19b-1-5p (A) or miR19-b-3p (B); or in stage III patients and the expression levels of miR19b-1-5p (C) or miR19-b-3p (D). E) Univariate and multivariate Cox regression analyses. (CRC stage II patients n=80; 17,50% of recurrence: CRC stage III patients n=46; 39.13% of recurrence).

Figure 4

A

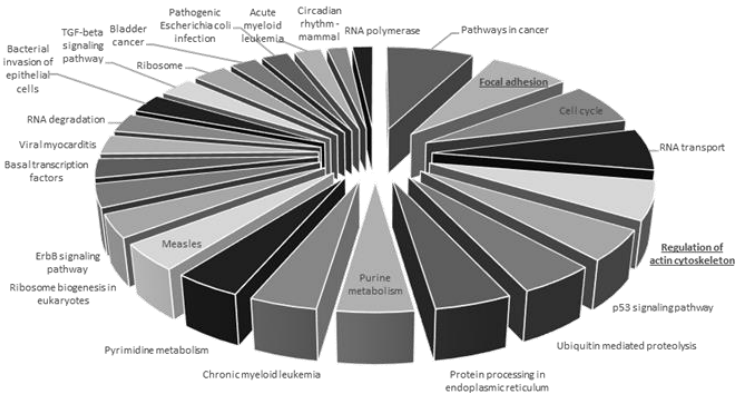

B

Pathway name	Genes	Hyp	Hyp_c	
Cell cycle	CDK6 MDM2 YWHAQ CCND2 CCND1 CDKN2C ORC4 SKP1 CDKN1A ANAPC7 SMAD4	1,77E-06	2,31E-04	***
p53 signaling pathway	CDK6 MDM2 CCND2 CASP8 CCND1 RRM2B CDKN1A ZMAT3	5,36E-06	3,51E-04	***
RNA transport	EIF2B3 SRRM1 THOC7 NMD3 PABPC4 EIF3A THOC1 XPO1 XPOT EIF4G2 NUPL1	8,74E-06	3,82E-04	***
Focal adhesion	CAV2 BIRC2 CCND2 CCND1 KDR ACTB COL6A2 ITGAV ITGB8 VEGFA CRKL PIP5K1C	3,16E-05	1,03E-03	**
Regulation of actin cytoskeleton	ARPC5 GNA12 NCKAP1 ACTB ITGAV IQGAP1 ITGB8 CRKL PIP5K1C FGFR2	9,59E-04	1,14E-02	*
Pathways in cancer	CDK6 MDM2 NCOA4 BIRC2 CASP8 CCND1 CDKN1A ITGAV SMAD4 VEGFA STAT5B CRKL FGFR2	9,26E-04	1,21E-02	*

C

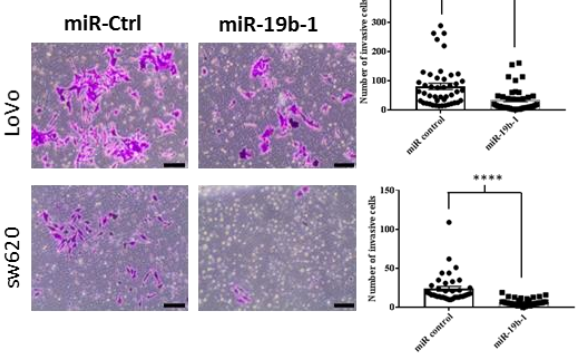

D

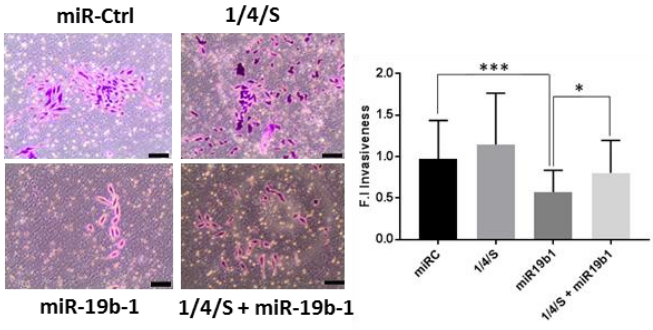

E

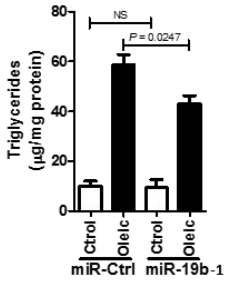

F

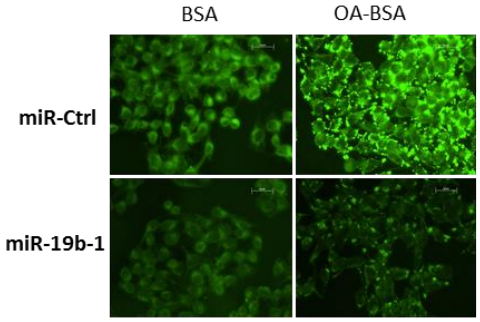

G

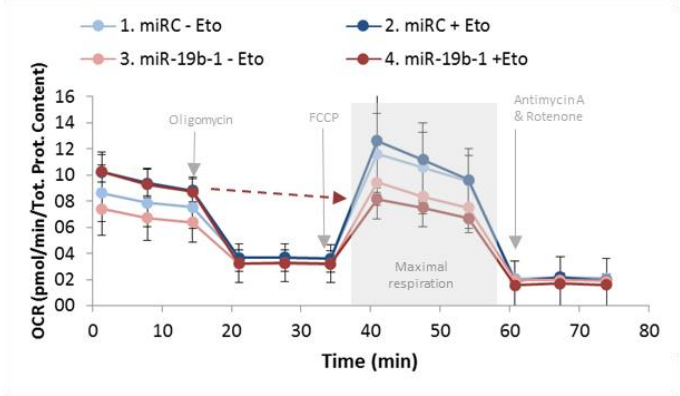

H

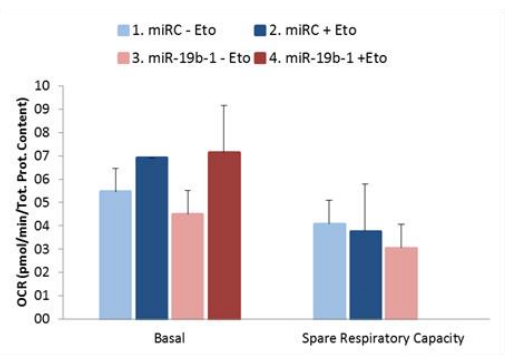

Figure 4. MiR-19b-1 implication in cell invasion and lipid metabolism

A) Biological processes elicited by miR-19b-1 obtained from Genecodis 3 [29]. The chart is ordered according to the increasing number of genes involved in each process (Hyp_c <0,05). The corrected hypergeometric test (Hyp c), *P-value* obtained from the hypergeometric test, determines the significance of the biological process. For miRNA hsa-miR-19b-1, due to its promiscuity, targets were limited to the ones experimentally validated and were retrieved from TarBase database. B) Genes involved in each biological predicted process elicited by miR-19-b1 and ordered by corrected hypergeometric test (Hyp c). C) Boyden chamber transwell assay of invasion through matrigel. miR-19b-1 or a control miRNA with no predicting binding site in the 3′UTR of *ACSL1*, *ACSL4* or *SCD* were electroporated into SW620 or LoVo cells. D) Boyden chamber transwell assay for invasion through matrigel. As a rescue experiment, vectors expressing ACSL1, ACSL4, and SCD were transfected together with mimic miR-19b-1 (miR-19b-1) or a control miRNA (miR-Ctrl) in SW620 cells. The positive invasion controls miR-Ctrl alone and (1/4/S) were also included. In both cases (C, D), after 72h with chemoattractant (10%FBS), inserts were fixed and stained with crystal violet. Non-migrated cells were removed using cotton swabs and images were captured using an Olympus CKX41 microscope (Olympus, Tokyo, Japan) with a 20X LCAch objective and registered using analysis getIT software (Olympus). Scale bars, 50µm. Results represent the number of migrated cells found in six random microscope fields in two independent inserts in three independent experiments ± standard error of the mean (SEM) (n= 3). *, $p<0.05$, **, $p<0.01$, ***, $p<0.001$, ****, $p<0.0001$. E) TG analysis content in DLD-1 cells transfected with mimic miR-19b-1 or a mimic miRNA control upon a 0,5mM Oleic acid-BSA or Fatty acid free BSA (vehicle control) input. Lipids content was expressed as µg TG/mg

of protein in two independent experiments ± standard error of the mean (SEM) (n= 2). *, $p<0.05$. F) Representative immunofluorescence images of the fluorophore Bodipy distribution in DLD-1 cells transfected with mimic miR-19b-1 or a mimic miRNA control, upon a 0,5mM Oleic acid-BSA or Fatty acid free BSA (vehicle control) input. Images were captured using a Leica DM IL microscope from a representative experiment, with a 40X Plan Fluotar objective and registered using Leica Application Suite (LAS) (n=2). G) Bioenergetic profile (oxygen consumption rate) of cells transfected with miR-19b-1 or a mimic miRNA control with or without Etomoxir addition. Injection schema (oligomycin, FCCP, Antimycin A/Rotenone) and key parameters assayed (basal respiration, maximal respiration and spare capacity) are also indicated. H) Basal respiration and spare respiratory capacity quantification of cells transfected with miR-19b-1 or a mimic miRNA control with or without Etomoxir addition. Both results show a representative experiment of two independent experiments with at least 6 replicates per condition ± standard error of the replicates mean (SEM) (n= 2).

Supplementary Figures and Tables

Figure S1

A

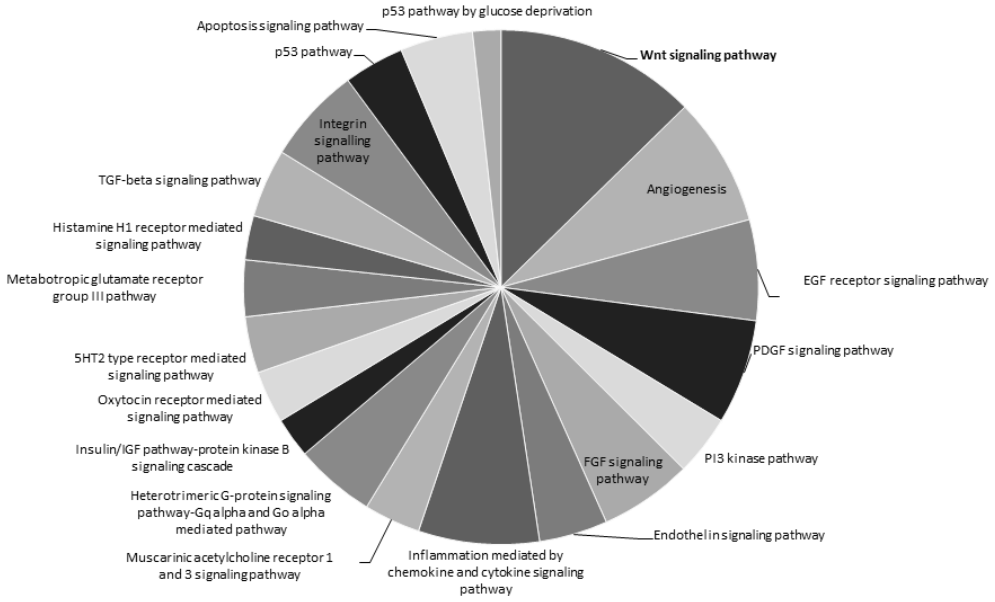

B

Pathway name	Genes	Hyp	Hyp_c
Wnt signaling pathway	PRKCI SMAD4 PCDH18 DKK1 CDH13 SIAH1 PCDH19 CTBP2 GNB4 PCDH7 PRKCE CDHR1 PCDH11Y NFATC4 TBL1XR1 CELSR3 AXIN2 ADSS CCND1 PCDHA9 LRP6 PRKCQ GNB1 PCDH11X CDH5 CDH2 FAT3 FZD3 PPP3CA FZD7 PPP2R5C EP400 PPP2CA SMARCD1 ITPR2 CDH1 DKK2 PRKCA PYGO2 GNG2 TGFBR1 TBL1X CTNNA2 GNG12 SMARCC1 WNT5A HDAC2 ACVR1C PLCB4 PLCB1	6,5E-11	6,6E-09
Angiogenesis	PRKCI FGFR1 PDGFB PIK3R1 NOTCH2 AKT3 PDGFRB PRKCE KRAS AXIN2 PAK2 SOS1 PIK3C2A STAT3 NOTCH1 PDGFRA PRKCQ PTPRB FZD3 JAG1 MAPK1 CRKL DLL1 F3 PRKCA WNT5A HIF1A FGF2 PIK3R3 FRS2 BIRC5 NR1I2	3,3E-09	1,7E-07
EGF receptor signaling pathway	TGFA RASAL2 PRKCI RRAS2 YWHAB AKT3 NF1 SPRY4 PRKCE KRAS SOS1 PIK3C2A STAT3 RAC1 PRKCQ ERBB4 CBL MAP3K3 PPP2R5C MAPK1 PPP2CA MAP3K2 PRKCA RHOQ EREG	6,2E-08	2,1E-06
PDGF signaling pathway	PDGFB RPS6KC1 PIK3R1 ARHGAP5 EHF RPS6KB1 KRAS SOS1 ERG STAT3 DLC1 ARHGAP26 SRGAP1 PDPK1 VAV3 MAPK1 MAP3K2 ITPR2 PRKCA RPS6KA3 NIN GABPA STARD13 PKN2 PIK3R3 SRGAP3	1,7E-07	4,4E-06
PI3 kinase pathway	INSR PIK3R1 FOXO3 AKT3 GNB4 RPS6KB1 KRAS CCND1 SOS1 CCND2 GNB1 PDPK1 FOXO1 FOXO4 PIK3R3	5E-07	8,4E-06
FGF signaling pathway	FGF9 PRKCI FGFR1 FGF5 YWHAB AKT3 SPRY4 PRKCE KRAS SOS1 PIK3C2A FGF7 RAC1 PRKCQ MAP3K3 PPP2R5C MAPK1 PPP2CA MAP3K2 FGF12 PRKCA FGF2 FRS2	4,3E-07	8,7E-06
Endothelin signaling pathway	PRKCI PIK3R1 ADCY9 AKT3 PRKCE PIK3C2A PRKCQ ADCY1 MAPK1 ITPR2 PRKCA PRKACB EDNRA ADCY2 PIK3R3 PLCB4 PLCB1	2,7E-06	3,8E-05
p53 pathway	SIRT1 SIAH1 PIK3R1 AKT3 PIK3C2A HMGB1 TP63 TNFRSF10B SUMO1 PDPK1 ATM PPP2CA PML PIK3R3 SERPINE1	0,00013	0,00073

Figure S1. Biological processes predictably elicited by selected miRNAs: 142-3p, 544a, 19b-1

A) Panther pathways analysis showing biological processes predictably elicited by 142-3p, 544a, 19-b1 miRNAs jointly. The chart is ordered according to the increasing number of genes involved in each process (Hyp_c <0,001). B) Table showing predicted genes involved in each biological predicted process elicited by 142-3p, 544a, 19b-1 miRNAs jointly and ordered by corrected hypergeometric test (Hyp c), the corrected *P-value* obtained from the hypergeometric test.

Gene name	Forward primer	Reverse primer
ACSL1	ACATTATGTTCCTGGGCCCA	AGTCAGAAGGCCATTGTCGA
ACSL4	GGCACAACAGAAAGGGGTAG	GGTTCCTCAGCTCCTTCCTT
SCD-1	TGCCCACCACAAGTTTTCAG	CATCAGCAAGCCAGGTTTGT
GAPDH	TGGTATCGTGGAAGGACTCATGAC	ATGCCAGTGAGCTTCCCGTTCAGC

Supplementary Table 1: Primers used for quantitative real-time PCR

miRBase ID	Cat No
hsa-miR-19b-1-5p	4427975
hsa-miR-19b-3p	4427975
hsa-miR-142-3p	4427975
hsa-miR-142-5p	4427975
hsa-miR-544a	4427975
U6 snRNA	4427975

Supplementary Table 2: Probes from TaqMan® MicroRNA Assays (ThermoFisher) used for quantitative real-time PCR

Name	Origin	Working dilution
ACSL1 Rabbit Polyclonal Antibody	Cell Signaling (Cat No 4047)	1:500
ACSL4 Rabbit Polyclonal Antibody	Dr. Stephen Prescott and Dr. Diana Stafforini [Supplementary methods]	1:2000
SCD Rabbit Polyclonal Antibody	Dr. Jean-Baptiste Demoulin [Supplementary methods]	1:2000
Vinculin Mouse Monoclonal Antibody	Sigma (Cat No V9131)	1:5000
Goat Anti-Rabbit IgG Antibody, (H+L) HRP conjugate	Millipore (Cat No AP307P)	1:20000
Goat Anti-Mouse IgG & IgM Antibody, HRP conjugate	Millipore (Cat No AP130P)	1:40000

Supplementary Table 3: Commercial antibodies used in this study

	Stage II CRC		Stage III CRC	
Characteristics	**nº of Patients**	**(%)**	**nº of Patients**	**(%)**
Total sample size (n)	80	(100)	46	(100)
Age at Diagnosis (years)				
Mean	73.55		63.26	
Median	75		62.5	
<70	24	30	33	71.74
≥70	56	70	13	28.26
Gender				
Female	28	35	26	56.52
Male	52	65	20	43.48
Stage				
IIA (T3 N0 M0)	68	85	26	56.52
IIB (T4 N0 M0)	12	15	20	43.48
Total Lymph Nodes Resected				
Mean Lymph nodes resected	15.75		17.04	
≤12	30	37.5	20	43.48
>12	50	62.5	26	56.52
Location of Primary				
Cecum and Ileocecal Valve	7	8.75	4	8.7
Acending colon and Hepatic flexure	15	18.75	9	19.57
Transverse colon	3	3.75	3	6.52
Splenic flexure and Descending colon	15	18.75	6	13.04
Sigmoid colon and rectosigmoid junction	40	50	24	52.17
Grade/Differentiation				
Well	5	6.41	9	19.57
Moderately	72	92.31	29	63.04
Poor	1	1.28	8	17.39
Bowel Obstruction/Perforation				
Yes	17	21.25	32	69.57
No	63	78.75	14	30.43
Other Histological Features				
Perineural invasion	15	18.75	19	41.3
Vascular invasion	22	27.5	15	32.61
Adjuvant treatment				
Xelox/Folox	32	40	46	100
No treatment	48	60	0	0
Disease-free survival				
Patients with recurrence	14	17.5	18	39.13
Overall survival				
nº of Exitus	18	22.5	8	17.39

Inclusion criteria: Age ≥18, completely resected rectal cancer or colon adenocarcinoma located at ≥15 cm of the anal verge as determined by endoscopy or above the peritoneal reflection in the surgical resection, confirmed Stage II AJCC/UICC primary CRC and follow-up of at least 36 months. **Exclusion criteria**: death within 30 days after surgery, other cancers in previous 5 years and inflammatory bowel disease or specific gene-related cancer.

Supplementary Table 4: Detailed clinical and histopathological characteristics of patients included in the study.

ACSL1	2^(-ΔΔCt) replicate 1	2^(-ΔΔCt) replicate 2	ACSL4	2^(-ΔΔCt) replicate 1	2^(-ΔΔCt) replicate 2	SCD	2^(-ΔΔCt) replicate 1	2^(-ΔΔCt) replicate 2	ACSL1 replicate mean	SD	Downregulation percentage (%)	ACSL4 replicate mean	SD	Downregulation percentage (%)	SCD replicate mean	SD	Downregulation percentage (%)
hsa-miR-544-a	0,528	0,172	hsa-miR-544-a	0,232	0,090	hsa-miR-544-a	0,615	0,299	0,350	0,25	64,98	0,161	0,10	83,88	0,457	0,22	54,31
hsa-miR-142	0,328	0,300	hsa-miR-142	0,414	0,414	hsa-miR-142	0,473	0,354	0,314	0,02	68,59	0,414	0,00	58,60	0,413	0,08	58,65
hsa-miR-19b-1	0,670	0,204	hsa-miR-19b-1	0,543	0,196	hsa-miR-19b-1	0,780	0,264	0,437	0,33	56,29	0,370	0,25	63,04	0,522	0,37	47,79
hsa-miR-224	0,737	0,230	hsa-miR-224	0,567	0,213	hsa-miR-224	0,834	0,405	0,483	0,36	51,68	0,390	0,25	60,97	0,620	0,30	38,05
hsa-miR-106a	0,448	0,337	hsa-miR-106a	0,277	0,220	hsa-miR-106a	0,987	0,817	0,393	0,08	60,74	0,249	0,04	75,15	0,902	0,12	9,79
hsa-miR-31	0,679	0,238	hsa-miR-31	0,645	0,275	hsa-miR-31	0,898	0,395	0,458	0,31	54,19	0,460	0,26	53,97	0,647	0,36	35,35
hsa-miR-20b	0,635	0,188	hsa-miR-20b	0,708	0,265	hsa-miR-20b	1,027	0,460	0,412	0,32	58,84	0,486	0,31	51,35	0,744	0,40	25,62
hsa-miR-20a	0,629	0,190	hsa-miR-20a	0,545	0,189	hsa-miR-20a	1,240	0,501	0,410	0,31	59,04	0,367	0,25	63,30	0,870	0,52	12,97
hsa-miR-342	0,585	0,221	hsa-miR-342	0,649	0,256	hsa-miR-342	1,125	0,498	0,403	0,26	59,69	0,452	0,28	54,79	0,811	0,44	18,87
hsa-miR-205	0,752	0,196	hsa-miR-205	0,246	0,076	hsa-miR-205	1,674	0,604	0,474	0,39	52,62	0,161	0,12	83,92	1,139	0,76	-13,91
hsa-miR-449b	0,633	0,375	hsa-miR-449b	1,020	0,757	hsa-miR-449b	0,473	0,330	0,504	0,18	49,62	0,889	0,19	11,13	0,402	0,10	59,82
hsa-miR-26b	1,400	0,299	hsa-miR-26b	0,449	0,196	hsa-miR-26b	0,864	0,394	0,850	0,78	15,03	0,323	0,18	67,74	0,629	0,33	37,10
hsa-miR-548b	0,596	0,176	hsa-miR-548b	0,702	0,306	hsa-miR-548b	1,349	0,544	0,386	0,30	61,39	0,504	0,28	49,63	0,946	0,57	5,36
hsa-miR-199b	1,035	0,836	hsa-miR-199b	0,589	0,471	hsa-miR-199b	0,555	0,403	0,936	0,14	6,43	0,530	0,08	46,99	0,479	0,11	52,10
hsa-miR-106b	0,568	0,398	hsa-miR-106b	0,749	0,736	hsa-miR-106b	0,830	0,614	0,483	0,12	51,71	0,743	0,01	25,75	0,722	0,15	27,84
hsa-miR-548a-3	0,638	0,297	hsa-miR-548a-3	0,864	0,430	hsa-miR-548a-3	1,118	0,655	0,468	0,24	53,23	0,647	0,31	35,28	0,887	0,33	11,33
hsa-miR-515-1	0,709	0,281	hsa-miR-515-1	0,849	0,462	hsa-miR-515-1	1,228	0,682	0,495	0,30	50,48	0,655	0,27	34,46	0,955	0,39	4,52
hsa-miR-519d	0,647	0,299	hsa-miR-519d	0,539	0,313	hsa-miR-519d	1,547	0,907	0,473	0,25	52,70	0,426	0,16	57,37	1,227	0,45	-22,69
hsa-miR-19a	0,577	0,362	hsa-miR-19a	0,551	0,423	hsa-miR-19a	1,839	1,375	0,469	0,15	53,06	0,487	0,09	51,28	1,607	0,33	-60,69
hsa-miR-195	0,557	0,891	hsa-miR-195	0,640	1,203	hsa-miR-195	0,950	1,181	0,724	0,24	27,63	0,921	0,40	7,88	1,065	0,16	-6,52
hsa-miR-556	0,453	1,571	hsa-miR-556	0,380	0,918	hsa-miR-556	0,753	1,357	1,012	0,79	-1,19	0,649	0,38	35,12	1,055	0,43	-5,49
hsa-miR-186	0,657	0,924	hsa-miR-186	0,514	0,909	hsa-miR-186	1,067	1,475	0,790	0,19	20,98	0,712	0,28	28,81	1,271	0,29	-27,13
hsa-miR-369	1,268	0,408	hsa-miR-369	0,976	0,347	hsa-miR-369	1,869	0,742	0,838	0,61	16,20	0,662	0,44	33,84	1,305	0,80	-30,55
hsa-miR-17	0,802	0,834	hsa-miR-17	0,787	1,076	hsa-miR-17	1,020	1,148	0,818	0,02	18,18	0,932	0,20	6,84	1,084	0,09	-8,40
hsa-miR-578	1,552	1,139	hsa-miR-578	0,684	0,588	hsa-miR-578	1,112	0,662	1,346	0,29	-34,56	0,636	0,07	36,42	0,887	0,32	11,30
hsa-miR-34c	1,320	1,215	hsa-miR-34c	0,682	0,967	hsa-miR-34c	1,302	1,711	1,267	0,07	-26,75	0,824	0,20	17,56	1,506	0,29	-50,62
hsa-miR-93	0,632	1,099	hsa-miR-93	1,089	2,185	hsa-miR-93	1,060	1,539	0,865	0,33	13,46	1,637	0,78	-63,69	1,300	0,34	-29,96
hsa-miR-875	0,886	1,031	hsa-miR-875	1,100	2,003	hsa-miR-875	1,162	1,786	0,959	0,10	4,14	1,552	0,64	-55,15	1,474	0,44	-47,40
hsa-miR-548c	1,155	1,568	hsa-miR-548c	0,604	1,336	hsa-miR-548c	1,325	2,097	1,361	0,29	-36,13	0,970	0,52	3,03	1,711	0,55	-71,07
hsa-miR-940	0,709	2,029	hsa-miR-940	0,530	1,692	hsa-miR-940	0,844	2,659	1,369	0,93	-36,92	1,111	0,82	-11,13	1,752	1,28	-75,16
hsa-miR-944	1,574	2,912	hsa-miR-944	0,590	1,965	hsa-miR-944	1,054	1,561	2,243	0,95	-124,33	1,278	0,97	-27,76	1,308	0,36	-30,77

	ACSL1 total mean	ACSL4 total mean	SCD total mean
Global mean	0,7561	0,6915	1,0077
SD	0,4250	0,3569	0,3741

	ACSL1 [individual score]	ACSL4 [individual score]	SCD [individual score]	FINAL SCORE
hsa-miR-544-a	-0,406	-0,530	-0,551	-0,496
hsa-miR-142	-0,442	-0,277	-0,594	-0,438
hsa-miR-19b-1	-0,319	-0,322	-0,486	-0,376
hsa-miR-224	-0,273	-0,301	-0,388	-0,321
hsa-miR-106a	-0,364	-0,443	-0,106	-0,304
hsa-miR-31	-0,298	-0,231	-0,361	-0,297
hsa-miR-20b	-0,345	-0,205	-0,264	-0,271
hsa-miR-20a	-0,346	-0,324	-0,137	-0,269
hsa-miR-342	-0,353	-0,239	-0,196	-0,263
hsa-miR-205	-0,282	-0,531	0,131	-0,227
hsa-miR-449b	-0,252	0,197	-0,606	-0,220
hsa-miR-26b	0,094	-0,369	-0,379	-0,218
hsa-miR-548b	-0,370	-0,188	-0,061	-0,206
hsa-miR-199b	0,180	-0,161	-0,529	-0,170
hsa-miR-106b	-0,273	0,051	-0,286	-0,169
hsa-miR-548a-3	-0,288	-0,044	-0,121	-0,151
hsa-miR-515-1	-0,261	-0,036	-0,053	-0,117
hsa-miR-519d	-0,283	-0,265	0,219	-0,110
hsa-miR-19a	-0,287	-0,204	0,599	0,036
hsa-miR-195	-0,032	0,230	0,058	0,085
hsa-miR-556	0,256	-0,043	0,047	0,087
hsa-miR-186	0,034	0,020	0,264	0,106
hsa-miR-369	0,082	-0,030	0,298	0,117
hsa-miR-17	0,062	0,240	0,076	0,126
hsa-miR-578	0,589	-0,056	-0,121	0,138
hsa-miR-34c	0,511	0,133	0,498	0,381
hsa-miR-93	0,109	0,945	0,292	0,449
hsa-miR-875	0,203	0,860	0,466	0,510
hsa-miR-548c	0,605	0,278	0,703	0,529
hsa-miR-940	0,613	0,420	0,744	0,592
hsa-miR-944	1,487	0,586	0,300	0,791

Supplementary Table 5: Detailed data from RT-QPCR experiment for miRNA-gene interaction

Left panel shows 2-ΔΔCt data (fold change) from 2 independent experiments for each miRNA-gene interaction as well as the mean of both replicas with their corresponding downregulation percentages and the global mean of the 31 miRNAs interactions for each gene (overall mean value of the whole interactions panel). Negative downregulation percentages mean overexpression instead of downregulation. Right panel shows the replicas mean of each interaction subtracted by the global mean (IS) ensuring only the best interactions within each gene. Final score (FS) is defined as the average of the 3 individual scores.

PUBLICATION IV

A more physiological approach to lipid metabolism alterations in cancer: CRC-like organoids assessment

Silvia Cruz-Gil, Dr. Ruth Sánchez-Martínez, Sonia Wagner-Reguero, Dr. Daniel Stange, Dr. Sebastian Schölch, Dr. Kristin Werner and Dr. Ana Ramírez de Molina

DOI: (submitted for publication)

PUBLICATION IV SUMMARY

A more physiological approach to lipid metabolism alterations in cancer: CRC-like organoids assessment

(submitted for publication)

Organoids represent excellent physiological tools for the development of new CRC personalized treatments. In this way, we decided to get a more *in vivo* approach for the analysis of the lipid metabolism-related axis ACSL/SCD, by employing genetically engineered intestinal mouse models. These organoids have the relevant mutations acquired throughout the different CRC stages ($APC^{fl/fl}$, $KRAS^{G12D/WT}$, $P53^{R172H/WT}$ and $Smad4^{fl/fl}$; corresponding to stages I to IV) named CRC-like organoids.

To check the status of the axis in CRC-like organoids, we measured the mRNA levels of the ACSL/SCD network integrants. ACSL4 mRNA levels clearly augmented throughout the organoid stages, correlating with increased aggressiveness of the organoid. Conversely, ACSL1 levels were stable over the series, and SCD levels increased from the third stage henceforth.

In the case of miRNAs, miR-19b-1-3p expression was decreased in a stage-dependent manner, maintaining its good prognosis role. The rest of the candidate miRNAs were also measured though no statistically significant differences were found in its expression. Therefore, miR-19b-1-3p preserved its protective role, reflecting ACSL/SCD axis involvement on CRC progression.

Since Metformin, an AMPK activator used as antidiabetic treatment that has been associated to increased survival of cancer patients, was able to rescue the epithelial phenotype from the mesenchymal process caused by the overexpression of ACSL/SCD in CRC cells; we wondered what this drug effect would be through the different stages in tumor progression. Using MTT assays, a colorimetric assay to assess viability, we compared Metformin action with the current chemotherapeutic drugs 5-FU upon 48h treatment. Metformin was able to decrease CRC-like organoids viability of all stages at the same rate as 5-FU, without affecting wild-type (WT) organoids viability.

To further check the treatments scope, we analyzed not only the effect but also the potential reversibility of the treatment. We assessed the organoids recovery capacity after 48h treatment plus the subsequent recovery of 72 additional hours in their growing media. Metformin treatment organoids recovery was significantly lower compared to 5-FU in first stages organoids, but a greater recovery was observed in WT organoids; suggesting Metformin potential use as a chemotherapy drug in the first tumor phases. Along the rest of the stages, 5-FU performed a major effect, with lower

recovery rates. Furthermore, we proved that Metformin was able to downregulate the crypt stem cell biomarker LGR5 and the Wnt target genes expression in all CRC-like organoid stages, reaffirming its potential use in intestinal cancers. Metformin action was also stronger on ACSL4 and SCD-overexpressing first stages organoids, diminishing these axis components mRNA levels. This is in accordance with Metformin greater action on this first stage. Finally, we observed that Metformin action in CRC organoids was not related to a Warburg-effect impairment, since L-lactate levels were even higher in Metformin treated CRC-like organoids despite its antitumor progression effect. This increase was especially higher in stage I organoids, coincident with the higher sensitivity to the drug in this stage of CRC-like organoids.

PUBLICATION IV CONCLUSIONS

1. **ACSL4** is progressively overexpressed throughout CRC-like organoids stages; while **miR-19b-1-3p** preserves its protective role, reflecting the role of ACSL/SCD axis action on CRC progression. Besides, Metformin action is stronger on ACSL4 and SCD-overexpressing first stages organoids, agreeing with Metformin greater action on this stage.

Metformin treatment is further proved as an efficient drug in CRC:

2. It is able to decrease CRC-like organoids viability at the same rate as current chemotherapy (5-FU) but that it does not affect to WT organoids.
3. Metformin treatment recovery is significantly inferior compared to 5-FU in **first stages organoids**, but with a greater recovery in WT organoids; becoming an appealing chemotherapy drug in first tumor phases.
4. Metformin downregulates the stem cell biomarker LGR5 and Wnt target genes expression in all CRC-like organoid stages, reaffirming its potential use in intestinal cancers.
5. Metformin action in CRC organoids is not related to a Warburg-effect impairment, presuming that other metabolisms rather than Warburg should be targeted to complete the cancer progression obstruction

My personal contribution to this project was complete. I first enjoyed a research stage in Germany under Dr. Stange supervision, where I learned organoids technology and further implement in our lab. I performed the majority of the experiments and the project approach, always under my supervisors guide.

A more physiological approach to lipid metabolism alterations in cancer: CRC-like organoids assessment

Silvia Cruz-Gil[1], Dr. Ruth Sanchez-Martinez[1], Sonia Wagner-Reguero[1], Dr. Daniel Stange[2], Dr. Sebastian Schölch[3,4,5], Dr. Kristin Werner[2] and Dr. Ana Ramirez de Molina[1,*].

[1] Molecular Oncology Group/ IMDEA Food Institute, CEI UAM + CSIC, Ctra. De Cantoblanco, 8 E-28049 Madrid, Spain.

[2] Department of Gastrointestinal, Thoracic and Vascular Surgery, University Hospital Carl Gustav Carus, Technische Universität Dresden, Fetscherstraße 74, 01307 Dresden, Germany.

[*]Correspondence to Dr. Ana Ramirez de Molina. (E-mail: ana.ramirez@imdea.org).

Running head

Handling organoids for an optimal lipid metabolism-related CRC analysis.

ABSTRACT

Precision medicine might be the response to the recent questioning of the use of metformin as an anticancer drug in colorectal cancer (CRC). Thus, in order to establish properly its benefits, its application need to be assayed on the different progression stages of CRC. In this way, organoids imply a more physiological tool, representing a new therapeutic opportunity for CRC personalized treatment to assay tumor stage-dependent drugs effects. Since the lipid metabolism-related axis, ACSL/SCD, stimulates colon cancer progression and Metformin is able to rescuing the invasive and migratory phenotype conferred to cancer cells upon this axis overexpression; we checked ACSL/SCD status, its regulatory miRNAs and the effect of Metformin treatment in organoids as a model for specific and personalized treatment. Despite ACSL4 expression is upregulated in CRC-like organoids, Metformin is able to downregulate it, especially in the first stages. Besides, organoids are clearly more sensitive in this first stage (Apc mutated) to Metformin than current chemotherapeutic drugs such as fluorouracil (5-FU). Metformin performs an independent "Warburg effect" blockade to cancer progression and is able to reduce crypt stem cell markers expression such as Lgr5+. These results suggest a putative increased efficiency of the use of Metformin in the first stages of CRC than in advanced disease.

Keywords: CRC-like organoids, colorectal cancer, ACSL/SCD axis, lipid metabolism, acyl-CoA synthetases, Stearoyl-CoA desaturase, Metformin, LGR5+, non-Warburg metabolism, personalized medicine.

Abbreviations: ACSL1: Acyl-CoA synthetase 1; ACSL4: Acyl-CoA synthetase 4; CRC: Colorectal cancer; EMT: Epithelial-mesenchymal transition; 5-FU: Fluorouracil; MiRNAs/ miR: MicroRNAs; MTT: 3-(4, 5-dimethylthiazol-2-yl)-2, 5-diphenyltetrazolium bromide; OAA: Oxaloacetate; SCD: Stearoyl-CoA desaturase; TCA: Tricarboxylic Acid cycle; 2D: 2-dimensional; 3D: 3-dimensional.

Introduction

Colorectal cancer (CRC) is the third most common cancer in men (10% of the total), after lung and prostate cancer, and the second in women (9.2% of the total), after breast cancer (1). Most of the CRC cases are sporadic (70-80%), which consists of the acquisition of somatic mutations and in which there is no family history or genetic predisposition. The remaining cases (20-30%) are those among close relatives, which are divided into inherited or familial CRC, (2). Genetically, sporadic CRC development is due to the abnormalities accumulation in tumor suppressor genes and oncogenes (3). Previous research postulated the adenoma-carcinoma transition theory, in which specific somatic mutations promoting tumorigenesis are acquired; proposed by Fearon and Vogelstein (Vogelgram). The Vogelgram proposes that the adenoma-carcinoma sequence model would start with loss of the *APC* gene, followed by mutations in *KRAS* or *BRAF* genes, mutations or loss of *TP53* gene and of SMAD family member 4 (*SMAD4*) (4).

Over the last decade, the interest in metabolic research with respect to cancer has been expansively increased. The first and most characterized tumor metabolism event to be described is the exacerbated glucose uptake and glycolysis utilization; which even in normoxic condition, are not used for maximal ATP generation via mitochondrial respiration. This phenomenon is denoted as the "Warburg effect".

Even though lipid-associated pathways are functionally dependent on glucose and glutamine catabolic pathways, are now a well-recognized and frequently described cancer metabolic feature with a key role in their tumorigenesis. This is the case for the ACSL/SCD axis (5), a lipid metabolism-related network described to promote tumorigenesis through an epithelial-mesenchymal transition (EMT) program that promotes migration and invasion of colon cancer cells. The mesenchymal phenotype produced upon overexpression of these enzymes is reverted through reactivation of AMPK signaling performed by the well-known anti-diabetic drug, Metformin. Though its mechanism of action is not fully understood, Metformin has shown a robust anti-proliferative effect on several types of cancer such as colon, pancreatic, breast,

ovarian, prostate and lung cancer cells (6). Furthermore, Metformin has been recently associated with improved survival of cancer patients, including CRC, though its use as an antitumoral agent has not been established yet (7)

The ACSL/SCD axis pro-tumorigenic activity has been also described to be post-transcriptionally regulated by miRNAs. miR-544a, miR-142, and miR-19b-1 has been proposed as major regulators of the ACSL/SCD network and the miR-19b-1-3p isoform decreased expression associated with a poorer survival rate in CRC patients, consistently with ACSL/SCD involvement in patients relapse (8).

To get insight into the metabolic implication on CRC progression with a special focus on the ACSL/SCD axis and the effect of metformin in each case, more personalized and physiological tools are needed since most of the available data rely on traditional studies using cancer cell lines cultures. In this way, the organoid culture system opens a new methodological door for *ex vivo* studies.

Adult tissue-derived epithelial organoids, also called “mini guts” (9) are stereotypic tissue-like structures derived from digestive healthy tissues or tumors which mimics *in vitro* the tissue composition and morphology of their *in vivo* counterparts (10). This methodology was first established in long-term primary culture from mouse small intestinal crypts to generate epithelial organoids with crypt- and villus-like epithelial domains representing both progenitor and differentiated cells (11).

The organoids technology takes advantage of the intestinal epithelium self-renewing capacity. Organoids starts from LGR5+ gut epithelial stem cells forming symmetric cyst structures, which finally will form budding structures resembling intestinal crypts. These budding structures are formed by these LGR5+ stem cells flanked by differentiated daughter cells (9).

Organoids are currently employed in colorectal cancer studies and chemotherapy assessment (12, 13). Along with intestinal organoids, similar epithelial organoids culture conditions for other

mouse and human digestive epithelial tissues have been also adapted (14–17) including tumor-derived organoids from cancer patients. Importantly, organoids grow as pure epithelial cultures without any contamination of vessels, immune cells or non-transformed mesenchymal which leads to an accurate sequencing or expression profiling (10).

Materials and Methods

CRC-like organoids: culture and maintenance

Mice: Mutant intestinal murine organoids were obtained from the Universitätsklinikum Carl Gustav Carus, Dresden. All procedures involving animals were conducted strictly in accordance with FELASA regulations and approved by the animal welfare committees of the Technische Universität Dresden and the Landesdirektion Sachsen prior to initiation of the experiments.

Mice with conditional mutations in Apc, Kras, Tp53 and Smad4 were obtained from the NCI Mouse Repository (Apc, Kras Tp53) or the Jackson Laboratory (Smad4) and interbred to obtain compound mutant mice. The CRC-like organoid model represents the adenoma-carcinoma sequence with the most common acquired mutations in a sporadic CRC: $APC^{fl/fl}$, $KRAS^{G12D/WT}$, $P53^{R172H/WT}$ and $Smad4^{fl/fl}$ (corresponding to stages I to IV) (Table 1). The parental mouse lines were described in Table 2.

Murine organoids mutagenesis is conditioned by the Cre/loxP system. Adenoviral infections were performed as explained in (18)to provide active mutations.

Crypt isolation and organoid culture: Crypts were isolated from the murine small intestine by incubation for 30 min at 4°C in PBS containing 2 mM EDTA as previously reported (11, 19). Isolated crypts were seeded in Matrigel (Corning® Matrigel® Matrix). The basic culture medium (Advanced Dulbecco's modified Eagle Medium DMEM/F12 complemented with penicillin/streptomycin, 10 mmol/L HEPES, 1x Glutamax [Gibco], named ADF +++) was supplemented with: 100 ng/ml Noggin (Peprotech), R-spondin (conditioned medium, 10% final volume), 1x B27 (Invitrogen), 1x N2 (Invitrogen), 1,25 mM N-acetylcysteine (Sigma-Aldrich), 100 µg/mL Primocin TM (InvivoGen) and 50 ng/mL mEGF (Thermofisher). The complete media is named supplemented ADF +++ media. For passaging, organoids were removed from Matrigel and mechanically dissociated with a glass pipette, pelleted and then transferred to fresh Matrigel

(11, 14, 20). Splitting was performed twice a week in a 1:3 split ratio. Cultures were kept at 37 °C, 5% CO2 in humidity.

Drugs treatment - viability assays

Cell viability was determined by counting and seeding 1000 crypts in 60% of Matrigel in 48-well plates. After 2 days of culture, organoids were exposed 48 hours to 10 µM Metformin (Sigma) or 10, 100 or 150 µM 5-FU (Sigma) in supplemented ADF +++ media, as indicated in the figures. At this point, organoids were collected, split and reseeded for recovery experiments over 72 hours in supplemented ADF +++ media.

Upon treatments (48h) or recovery assays (post-72h), organoids were incubated 3 hours with 3-(4,5-dimethyl-thyazol-2-yl)-2,5-diphenyl-tetrazolium (MTT, Sigma). After discarding the media, 20 µl of 2% SDS (Sigma) solution in H2O was added to solubilize Matrigel (2 h, 37 °C). The resultant formazan was dissolved in 100 µl of DMSO for 1 h (37 °C). The absorbance was measured on the microplate reader (Asys UVM 340, Isogen life science) at 562 nm.

Untreated organoids were defined as 100% viable. Data were expressed as the fold change of viable cells from treated organoids compared to the non-treated organoids.

RNA isolation and RT-QPCR

For RNA isolation, organoids were released from Matrigel (Corning) with cold Dispase (Corning) and pelleted by centrifugation. The supernatant was removed and pelleted organoids were carefully resuspended in Trizol (Qiagen), and storage at -80ºC. RNA was isolated according to the supplier's protocol (Invitrogen) and the concentration and purity (A260/A280 ratio) were determined by spectrophotometric analysis (NanoDrop 2000 Spectrophotometer ThermoScientific). 20 ng/µl RNA was reverse-transcribed using the High Capacity RNA-to-cDNA kit (ThermoFisher), according to manufacturer's instructions. Relative gene expression was measured using VeriQuest Fast SYBR Green qPCR Master Mix (2X) (Isogen). Primers used

are listed in Supplemental Table S1. Regarding miRNAs, their expression was monitored using TaqMan® MicroRNA Reverse Transcription Kit (ThermoFisher Scientific) and Taq-man miRNA probes for RT-qPCR (Supplemental Table S2). RT-QPCRs were performed on the QuantStudio 12K Flex (Applied Biosystems) and the $2^{-\Delta\Delta Ct}$ method was applied to calculate the relative gene or miRNA expression.

L-Lactate quantification

Organoids were seeded at a density of 1000 crypts per well in a 48-well plate. After 48 hours, the medium was changed to PBS, 10 mM of Metformin or 10 µM 5-FU in supplemented ADF +++ media overnight at 37°C before quantification. Using Cayman's Glycolysis cell-based assay (Cayman, Ann Arbor, MI, USA, 600450) extracellular L-Lactate was measured by determining absorbance at 490 nm. L-Lactate measurements (mM) were normalized to total protein concentration (mg) x100.

Statistical analysis

All statistical analyses were performed using the Graph Pad Prism software (Ver. 7.03) (GraphPad Software, San Diego, CA, USA). Significance between groups was determined by *t*-test analyses (unpaired Student's t-tests). Data with $P < 0.05$ were considered statistically significant (ns, $P > 0.05$; *, $P \leq 0.05$; **, $P \leq 0.01$; ***, $P \leq 0.001$; ****, $P \leq 0.0001$). All reported *p* values were two-sided. All values are reported as mean ± S.D.

Results

ACSL4 is overexpressed throughout CRC-like organoids stages

ACSL4 has been previously reported to be overexpressed in malignant tumors, and together with ACSL1 and SCD form an axis involved in CRC progression. ACSL1, ACSL4, and SCD mRNA expression was measured in CRC-like organoids. ACSL4 mRNA was very significantly augmented in more aggressive stages compared to WT (Figure 1A). It is shown an intermediate expression pattern in Apc-mutated organoids, with a significantly differential expression (*p-value:* **) compared to the following second stage (Apc, Kras mutated stage) henceforth. Conversely, ACSL1 and SCD levels were maintained or increased from the third stage henceforth, respectively (Supplemental Figure S1).

Interestingly, organoids in more advanced stages (III and IV) presented a genetic misbalance in ACSL4 expression (Figure 1A) with huge differences in their fold inductions ranges in the same stage, though with a similar tendency.

MiR-19b-1-3p keeps its protective role in CRC-like organoids

MiRNAs expression was assayed in 3 different RNA extractions over time. Previous results from our group pointed toward a correlation between miR-19b-1-3p lower expression and a poorer prognosis in CRC patients (which might have a putative high clinical interest due to its potential to be assed in plasma as a non-invasive biomarker); very likely through its involvement in cell invasion and lipid metabolism regulation (8). In the case of CRC-like organoids, this tendency was maintained and miR-19b-1-3p expression was decreased in a stage-dependent manner (Figure 1B).

Together with miR-19b-1-3p, miR-142 (3p and 5p isoforms) and miR-544a (without murine isoform) were also involved on targeting ACSL/SCD axis (8). Hence, the previous mentioned

miRs plus miR-19b-1-5p isoform was measured though no statistically significant differences were found in its expression (Supplemental Figure S2)

Metformin decreases CRC-like organoids viability to the same extent as current chemotherapy without significant effects on WT organoids

Since Metformin treatment, an AMPK activator used as antidiabetic treatment that has been recently associated to increased survival of cancer patients, was able to rescue the epithelial phenotype from the EMT process caused by the overexpression of ACSL/SCD in CRC cells (5); we wondered what this drug effect would be through the different stages in tumor progression. CRC-like organoids were treated with PBS, 10 µM of Metformin or with the commonly used chemotherapeutic agent 5-FU; and the organoids viability was examined by MTT assays 48 hours upon treatment. None of the drugs affected significantly the viability of WT organoids (Figure 2A), while they were able to cause a decrease of about 50% in the viability of mutated organoids corresponding to the most aggressive phenotypes (Figure 2B-E). 5-FU higher concentrations (100 µM and 150 µM) showed the same effects than the lower concentration (10 µM) in mutated organoids, while they had stronger effects on WT ones (Supplemental Figure S3A-E).

Metformin treatment recovery is significantly lower compared to 5FU in first stages organoids while WT organoids present an opposite behavior

To further check the treatments scope, and analyzing not only the effect but also the potential reversibility of the treatment in normal and tumoral cells in different stages, organoids viability was assayed upon 48 hours treatment (PBS, Metformin or 5-FU) plus the subsequent recovery of 72 additional hours in their growing media. In this case, WT organoids showed differential recovery sensitivity to the treatment. Metformin treated and recovered WT organoids presented almost similar measurements than only treated organoids. Nonetheless, 5FU treated WT organoids recoveries are noteworthy more sensitive and upon 72h recovery time their viability was quite significant reduced (*p-value:* ***) (Figure 3A). In Apc mutated organoids the recovery

is very significantly lower upon Metformin treatment (*p-value:* ****) than 5-FU (*p-value:* *), compared to PBS recovery control; making these Apc mutated organoids the most responsive to the Metformin treatment compared to 5-FU (Figure 3B). Regarding organoids corresponding to stages II-III (Figures 3C-D), both treatments presented almost similar recovery effects, while in stage IV organoids, 5-FU presented a stronger effect shown by the lower recovery of these 5-FU treated organoids (Figures 3E). Again 5-FU higher concentrations (100 µM and 150 µM) had nearly the same recovery effects than the lower concentration (10 µM) (Supplemental Figure S4A-E).

Since WT organoids require more time to achieve their size and their crypt-like phenotype (Figure 3F), the recovery measures are lesser than the mutated organoids. On the other hand, WT organoids recovered upon Metformin treatment presented a higher size than the ones treated with 5-FU (Figure 3F). On the contrary, stage I (Apc mutated) organoids recovered upon Met treatment showed an evident reduced size compared with the control and the 5-FU treated ones. In accordance with viability assays results, this effect is lost in further stages; where Metformin is less effective and Metformin treated recovered organoids presented a bigger size than the ones treated with 5-FU.

By way of clarification, all mutated organoids presented Apc mutated since is the first gene in the adenocarcinoma sequence. Apc completed deletion provokes a hyperactive Wnt signaling. This aberration makes an organoids phenotype switch, losing their crypt-like structure and adopting a cystic morphology (17, 21)

Metformin action is stronger on ACSL4 and SCD overexpressing first stages organoids

Since stage I organoids seemed to present a differential sensitivity to metformin compared to other stages, together with a differential expression of ACSL4, we aimed to analyze the possible link between Metformin and ACSL/SCD axis in intestinal organoids.

To this aim, ACSL4 expression was measured, as well as the other enzymes of the ACSL/SCD metabolic network (ACSL1 and SCD) upon 10 μM Metformin treatment. ACSL4 mRNA expression was strongly reduced by this drug compared to their non-treated controls in stage I and II organoids. By contrast, stage III and IV presented no significance in their reduction or a slight significance, respectively. WT organoids also presented a slight reduction of ACSL4 mRNA upon Metformin treatment (Figure 4B). In addition, SCD expression levels were clearly decreased by Metformin in WT and stage I organoids, while a less marked tendency was found for stage III and IV organoids (Figure 4C). ACSL1 mRNA analysis showed less significant results (Figure 4A) upon Metformin treatment.

The expression of these enzymes was also measured upon 10 μM 5-FU treatment. This drug was able to significantly downregulate ACSL4 and SCD mRNA in most of the stages, though no differences were showed between the effects in initial and later stages such as the case for Metformin treatment (Supplemental Figures S5A-C).

Metformin, but not 5-FU, downregulates stem cell biomarker LGR5 and Wnt target genes expression in all organoid stages

To further assay whether Metformin treatment was targeting the organoids crypts stem cell marker, LGR5; we analyzed its expression together with two other Wnt target genes, Axin2 and Ctnnb-1. Importantly, LGR5 expression was significantly diminished in the whole CRC-like organoids series upon Metformin treatment (Figure 4C) as well as Axin-2 (Figure 4D) and Ctnnb-1 (Figure 4E) mRNAs. Surprisingly, this pattern was not maintained when organoids were treated with 10 μM 5-FU (Supplemental Figures S5D-F).

Metformin action in CRC-like organoids is not related to a Warburg-effect impairement

The avidity to perform glycolysis even in the presence of oxygen, known as the Warburg effect, is one of the hallmarks of tumors. For this reason, we measured the levels of L-lactate, the end product of glycolysis. CRC-like organoids presented increased glycolysis compared to WT

organoids, reflecting an increasing Warburg effect throughout the stages, as expected. Even though 5-FU treatment caused a slight decrease in the glycolytic performance of the mutant organoids (Figure 5), Metformin treatment caused an opposite effect, increasing the glycolytic capacity in all stages, especially in stage I, the most sensitive to the drug. Thus, it seems that Metformin effect on CRC-like organoids viability relies in mechanisms other than preventing pro-tumorigenic Warburg effect, likely through the regulation of lipid metabolism.

Discussion

Organoids seem to represent a good tool to study lipid metabolism (22) and previous studies employing intestinal organoids have linked the critical role of fatty acid metabolism to the intestinal epithelial integrity *in vivo* (23). Therefore, we propose this system to get insight into cancer progression mechanisms in regards to fatty acid metabolism and therefore, to assay ACSL/SCD protumorigenic axis action in CRC.

We showed that ACSL4 augmented while miR-19b-1-3p diminished its expression, both progressively, in murine CRC-like organoids. Metformin action compared to the chemotherapeutic agent 5-FU, in terms of viability reduction, was similar; although no significant reduction was found in WT organoids viability with any treatment. Stage I organoids were the most susceptible to Metformin action compared to 5-FU; while further stages presented similar or stronger sensitivity to 5-FU, including WT organoids. Besides, Metformin was able to reduce the intestinal crypt stem cell marker LGR5 in all the stages, together with two other Wnt downstream targets, Ctnnb-1 and Axin-2. Finally, we showed that even though the CRC-organoids series present a growing Warburg effect through the stages consistent with increased L-lactate levels; Metformin action on CRC organoids viability was not related to an ablation of Warburg effect.

The individual role of ACSL isoform 1 (24, 25) and 4 (24, 26) as well as SCD (27–31) in CRC has been extensively reported. Surprisingly, while ACSL4 mRNA levels are clearly increased through the stages in this organoids model, this was not the case for ACSL1, and SCD was only overexpressed in advanced stages. These results differ from previous ones using human CRC cells which can be due to differential expression in murine tissues compared to human 2D cultures (5) (8). Nevertheless, the use of murine organoids allows their genetic engineering and to accurately control the mutations for a better mechanistic characterization, rather than patient tumor-derived

biopsies with the high variability that each tumor represent. Thus, our CRC model mimics a sporadic colorectal tumor with the common mutations acquired during the progression of this cancer. Due to the organoids results, the overexpression of the three enzymes could be only present in some punctual tumors. However, the overexpression of ACSL4 is preserved in murine organoids with the acquired CRC most common mutations (Figure 1A), indicating a predominant role of this ACSL/SCD component in these cancer progression aspects. The ACSL4 mRNA huge range of expression considering the most mutated stages (Figure 1A) could be explained since stages III and IV in real tumors present an uncontrolled genetic variability with the accumulation of other undetermined mutations. Organoids would be mimicking these uncontrolled stages, compared to the homogeneity presented in 2D cultures. Conversely, ACSL1 static role (Supplemental Figure S1A) could be due to a lesser implication in tumor development in this system which can be also explained by the fact that the rodent protein is one residue longer (699 amino acids) than the human protein (698 amino acids), making it necessary to study the extent of this dissimilarity. For its part, SCD overexpression has been mainly reported in mesenchymal tissues, rather than epithelial ones, which are the only scaffold for organoids (32, 33) giving a reason for the distinctive results found in these epithelial systems among the first stages (Supplemental Figure S1B).

Regarding miRs expression, miR-19b-1-3p kept its tumor-suppressor role in murine CRC-like organoids, also reported as a good prognosis miRNA, able to target the axis (8). The immature isoform of miR-19b-1-3p, miR-19b, and other members of the miR-17-92 cluster, where this miRNA is involved, regulate the self-renewal ability of gastric cancer stem cells (34). The miR-17-92 cluster role is controversial and dependent on the cancer type (35, 36). However, it is interesting the reported role of this miRNA in digestive cancer stem cells, and its role in CRC stem cells may be a potential line of research henceforth. In line with our results, miR-19b was also reported to downregulate suppressor of cytokine signaling 3 (SOC3), modulating chemokine production in intestinal epithelial cells and thereby avoiding intestinal inflammation in Crohn's disease, which may ultimately prevent the derived disease, CRC (37).

Since Metformin was able to revert the ACSL/SCD EMT phenotype, we tried to gain insight on this process using organoid cultures resembling the different stages of a CRC progression. Metformin treatment seems to be more efficient than 5-FU only during first tumor stages, making organoids recovery harder compared to the ones treated with 5-FU. We propose that Metformin therapies could be an appealing alternative in those cases when the tumor is detected in very early stages rather than 5-FU treatments. However, some studies of Metformin treatment in CRC patients points to stage III to be the most likeable to present an effect (38). Since CRC is very improbable to detect on its very early stages, known as one of the most silent and deadly cancer; we wonder whether these studies with a low number of candidates in stage I are enough representative.

As well, Metformin therapies has been proposed alone or in combination with other drugs, in CRC. For example, Metformin has been recently combined with aspirin to treat middle stages in non-diabetic CRC patients.(II and III stages) (39). Furthermore, it exists a Phase 2 Trial for the study of Metformin and 5-Fluorouracil combination in metastatic CRC (40) ,concluded with a longstanding cancer control. An older report also claimed the benefits of this combination, but they also reported that Metformin alone has antineoplastic activity *per se* in colon cancer cells, and enhanced the activity of 5-FU, oxaliplatin and irinotecan in cells previously treated (41).

Previous reports hypothesized that the inhibition of mitochondrial complex I was the main mechanism of action for Metformin. However, recent studies suggest that cancer progression is compromised upon Metformin treatment, by decreasing the TCA cycle´s anaplerosis. Metformin decreases the flow of glucose- and glutamine-derived metabolic intermediates into the TCA cycle, decreasing the citrate output of the mitochondria and leading to a reduction of acetyl-CoA (Ac-CoA) and oxaloacetate (OAA) in the cytoplasm and therefore a reduction in de novo FA synthesis (42). This way, Metformin could be targeting lipid metabolism through ACSL/SCD axis. ACSL4 downregulation in the presence of Metformin is clearly evident and the results are larger significant in first stages (I, II) (Figure 4A). Maybe, the reduced overexpression of ACSL4 in the first stages (Figure 1A) increases the sensitivity to Metformin action (Figure 4A); while in more

advanced stages, the overexpression is so high that Metformin action could appear to be less effective. This would not be the case for SCD, which showed no overexpression in the first stages and enhanced overexpression in III and IV stages, though it is significantly reduced upon Metformin exposure again in the first stages (Figure 4B). On the other hand, it has been reported that variations in the types and amounts of fatty acids, are able to modify intracellular ACSLs expression (43), thus, this conditions could be also affecting ACSL/SCD components expression besides that the network connection between those enzymes could make them present coordinated effects upon Metformin treatment, reducing its expression due to the lack of their substrate. Metformin was also previously reported to downregulate ACSL expression, lowering fatty acid synthesis and normalizing lipid profile in diabetic rats (44); as well as limiting its products, 18-carbon chain length fatty acids, in skeletal muscle insulin resistant rats (45), suggesting in this case that metformin is increasing FAs mitochondrial channeling due to the reduction of CPT1 inhibition by malonyl-CoA and therefore decreasing 18-carbon acyl-chain-derived bioactive lipids in the cytoplasm (45), This action of Metformin could be additional to the aforementioned, detoxifying ACSLs probable over activity.

Metformin seems also to target cancer stem cells of different cancer types (46). However, we have described for the first time the LGR5 downregulation in CRC-like organoids upon Metformin treatment; consistent with previous reports using 2D CRC cultures (47). LGR5 was diminished in the whole CRC-like organoids series to minimum levels, an indicative that Metformin action is affecting the stem cells of the crypt, responsible for the progression of the organoids lineage. Curiously, Metformin treated organoids do not present apoptosis or even necrosis, but they kept at a minimum size compared to other treatments, where the organoids layer disappeared and the cells appeared apoptotic in the lumen (Supplemental Figure S6), showing that cell membrane biogenesis is somehow blocked, mostly built by *de novo* lipogenesis routes.

Finally, Metformin treated CRC organoids exhibit a greater compensatory increase in aerobic glycolysis. Since ATP levels are diminished due to complex I inhibition, the metabolic sensor

AMPK is activated, inhibiting mTOR and proliferative events; and promoting glycolysis as an alternative ATP source (48). We found that even though the CRC-organoids serie presented an increasing glycolysis with the stages, (Figure 5); Metformin was able to increase more this glycolytic phenotype, especially in stage I organoids, coincident with the higher sensitivity to the drug in this organoids. These results point towards Metformin targeting different metabolic routes other that Warburg effect to perform its effect on CRC organoids viability.

Even though the Warburg effect is a priority for current drugs, each day the evidence grows that other metabolic pathways should be targeted for cancer progression ablation. CRC is a leading cause of death in the developed world, though yet simplistic preclinical models that mimic the usual stages of CRC progression are lacking (13). In this way, organoids further analysis need to be included as the tool of choice for stage-dependent drugs screening.

Conclusions

General conclusion

1. Organoids display a precise platform to assay **tumor stage-dependent drugs** being suitable for **personalized medicine**, constituting an invaluable tool due to their relatively low costs, animal saving suffering and their ease and legibility to genetically manipulate.

Metformin-related conclusions

2. **Metformin** treatment is further proved as an efficient drug in CRC:

   -It is able to decrease CRC-like organoids viability at the same rate as current chemotherapy (5-FU) but it does not affect to WT organoids.

   -Metformin treatment recovery is significantly inferior compared to 5-FU in **first stages organoids**, but with a greater recovery in WT organoids; becoming an appealing chemotherapy drug in first tumor phases.

   -Metformin downregulates the stem cell biomarker LGR5 and Wnt target genes expression in all CRC-like organoid stages, reaffirming its potential use in intestinal cancers.

-Metformin action in CRC organoids is not related to a Warburg-effect impairment, presuming that other metabolisms rather than Warburg should be targeted to complete the cancer progression obstruction

ACSL/SCD-related conclusions

3. **ACSL4** is progressively overexpressed throughout CRC-like organoids stages; while **miR-19b-1-3p** preserves its protective role, reflecting the role of ACSL/SCD axis action on CRC progression. Besides, Metformin action is stronger on ACSL4 and SCD-overexpressing first stages organoids, agreeing with Metformin greater action on this stage.

Acknowledgment

We kindly thank Dr. Daniel Stange and Dr. Schölch for providing the CRC-like organoids and to the whole Department of Gastrointestinal, Thoracic and Vascular Surgery at University Hospital Carl Gustav Carus for its continuous support .The research stay on this lab was kindly financed with the assistance of a Boehringer Ingelheim Fonds travel grant.

Conflict of interest statement

Authors declare no potential conflict of interest.

Source of funding

This work was supported by Ministerio de Economía y Competitividad del Gobierno de España (MINECO, Plan Nacional I+D+i AGL2016-76736-C3), Gobierno regional de la Comunidad de Madrid (P2013/ABI-2728, ALIBIRD-CM) and EU Structural Funds.

References

1. Ferlay, J., I. Soerjomataram, R. Dikshit, S. Eser, C. Mathers, M. Rebelo, D. M. Parkin, D. Forman, and F. Bray. 2015. Cancer incidence and mortality worldwide: sources, methods and major patterns in GLOBOCAN 2012. *Int. J. Cancer*. **136**: E359-386.

2. Müller, M. F., A. E. K. Ibrahim, and M. J. Arends. 2016. Molecular pathological classification of colorectal cancer. *Virchows Arch.* **469**: 125–134.

3. Yamagishi, H., Kuroda, H., Imai, Y., & Hiraishi, H. (2016). Molecular pathogenesis of sporadic colorectal cancers. Chinese Journal of Cancer, 35, 4. http://doi.org/10.1186/s40880-015-0066-y

4. Fearon, E. R., and B. Vogelstein. 1990. A genetic model for colorectal tumorigenesis. *Cell*. **61**: 759–767.

5. Sánchez-Martínez, R., S. Cruz-Gil, M. Gómez de Cedrón, M. Álvarez-Fernández, T. Vargas, S. Molina, B. García, J. Herranz, J. Moreno-Rubio, G. Reglero, M. Pérez-Moreno, J. Feliu, M. Malumbres, and A. Ramírez de Molina. 2015. A link between lipid metabolism and epithelial-mesenchymal transition provides a target for colon cancer therapy. *Oncotarget*. **6**: 38719–38736.

6. Nasri, H., and M. Rafieian-Kopaei. 2014. Metformin: Current knowledge. *J. Res. Med. Sci. Off. J. Isfahan Univ. Med. Sci.* **19**: 658–664.

7. Baglia, M. L., Y. Cui, T. Zheng, G. Yang, H. Li, M. You, L. Xu, H. Murff, Y.-T. Gao, W. Zheng, Y.-B. Xiang, and X.-O. Shu. 2018. Diabetes Medication Use in Association with Survival among Patients of Breast, Colorectal, Lung, or Gastric Cancer. *Cancer Res. Treat. Off. J. Korean Cancer Assoc.*

8. Cruz-Gil, S., R. Sanchez-Martinez, M. Gomez de Cedron, R. Martin-Hernandez, T. Vargas, S. Molina, J. Herranz, A. Davalos, G. Reglero, and A. Ramirez de Molina. 2018. Targeting the lipid metabolic axisACSL/SCDin colorectal cancer progression by therapeutic miRNAs: miR-19b-1 role. *J. Lipid Res.* **59**: 14–24.

9. Sato, T., and H. Clevers. 2015. SnapShot: Growing Organoids from Stem Cells. *Cell*. **161**: 1700–1700.e1.

10. Werner, K., J. Weitz, and D. E. Stange. 2016. Organoids as Model Systems for Gastrointestinal Diseases: Tissue Engineering Meets Genetic Engineering. *Curr. Pathobiol. Rep.* **4**: 1–9.

11. Sato, T., R. G. Vries, H. J. Snippert, M. van de Wetering, N. Barker, D. E. Stange, J. H. van Es, A. Abo, P. Kujala, P. J. Peters, and H. Clevers. 2009. Single Lgr5 stem cells build crypt-villus structures in vitro without a mesenchymal niche. *Nature*. **459**: 262–265.

12. Golovko, D., D. Kedrin, Ö. H. Yilmaz, and J. Roper. 2015. Colorectal cancer models for novel drug discovery. *Expert Opin. Drug Discov.* **10**: 1217–1229.

13. O'Rourke, K. P., E. Loizou, G. Livshits, E. M. Schatoff, T. Baslan, E. Manchado, J. Simon, P. B. Romesser, B. Leach, T. Han, C. Pauli, H. Beltran, M. A. Rubin, L. E. Dow, and S. W. Lowe. 2017. Transplantation of engineered organoids enables rapid generation of metastatic mouse models of colorectal cancer. *Nat. Biotechnol.* **35**: 577–582.

14. Barker, N., M. Huch, P. Kujala, M. van de Wetering, H. J. Snippert, J. H. van Es, T. Sato, D. E. Stange, H. Begthel, M. van den Born, E. Danenberg, S. van den Brink, J. Korving, A. Abo, P. J. Peters, N. Wright, R. Poulsom, and H. Clevers. 2010. Lgr5(+ve) stem cells drive self-renewal in the stomach and build long-lived gastric units in vitro. *Cell Stem Cell*. **6**: 25–36.

15. Boj, S. F., C.-I. Hwang, L. A. Baker, I. I. C. Chio, D. D. Engle, V. Corbo, M. Jager, M. Ponz-Sarvise, H. Tiriac, M. S. Spector, A. Gracanin, T. Oni, K. H. Yu, R. van Boxtel, M. Huch, K. D. Rivera, J. P. Wilson, M. E. Feigin, D. Öhlund, A. Handly-Santana, C. M. Ardito-Abraham, M. Ludwig, E. Elyada, B. Alagesan, G. Biffi, G. N. Yordanov, B. Delcuze, B. Creighton, K. Wright, Y. Park, F. H. M. Morsink, I. Q. Molenaar, I. H. Borel Rinkes, E. Cuppen, Y. Hao, Y. Jin, I. J. Nijman, C. Iacobuzio-Donahue, S. D. Leach, D. J. Pappin, M. Hammell, D. S. Klimstra, O. Basturk, R. H. Hruban, G. J. Offerhaus, R. G. J. Vries, H. Clevers, and D. A. Tuveson. 2015. Organoid models of human and mouse ductal pancreatic cancer. *Cell*. **160**: 324–338.

16. Huch, M., C. Dorrell, S. F. Boj, J. H. van Es, V. S. W. Li, M. van de Wetering, T. Sato, K. Hamer, N. Sasaki, M. J. Finegold, A. Haft, R. G. Vries, M. Grompe, and H. Clevers. 2013. In vitro expansion of single Lgr5+ liver stem cells induced by Wnt-driven regeneration. *Nature*. **494**: 247–250.

17. Sato, T., D. E. Stange, M. Ferrante, R. G. J. Vries, J. H. Van Es, S. Van den Brink, W. J. Van Houdt, A. Pronk, J. Van Gorp, P. D. Siersema, and H. Clevers. 2011. Long-term expansion of epithelial organoids from human colon, adenoma, adenocarcinoma, and Barrett's epithelium. *Gastroenterology*. **141**: 1762–1772.

18. Seidlitz, T., S. R. Merker, A. Rothe, F. Zakrzewski, C. von Neubeck, K. Grützmann, U. Sommer, C. Schweitzer, S. Schölch, H. Uhlemann, A.-M. Gaebler, K. Werner, M. Krause, G. B. Baretton, T. Welsch, B.-K. Koo, D. E. Aust, B. Klink, J. Weitz, and D. E. Stange. 2018. Human gastric cancer modelling using organoids. *Gut*.

19. Barker, N., M. Huch, P. Kujala, M. van de Wetering, H. J. Snippert, J. H. van Es, T. Sato, D. E. Stange, H. Begthel, M. van den Born, E. Danenberg, S. van den Brink, J. Korving, A. Abo, P. J. Peters, N. Wright, R. Poulsom, and H. Clevers. 2010.

Lgr5(+ve) stem cells drive self-renewal in the stomach and build long-lived gastric units in vitro. *Cell Stem Cell*. **6**: 25–36.

20. Farin, H. F., J. H. Van Es, and H. Clevers. 2012. Redundant sources of Wnt regulate intestinal stem cells and promote formation of Paneth cells. *Gastroenterology*. **143**: 1518–1529.e7.

21. Andersson-Rolf, A., R. C. Mustata, A. Merenda, J. Kim, S. Perera, T. Grego, K. Andrews, K. Tremble, J. C. R. Silva, J. Fink, W. C. Skarnes, and B.-K. Koo. 2017. One-step generation of conditional and reversible gene knockouts. *Nat. Methods*. **14**: 287–289.

22. Bijsmans, I. T. G. W., A. Milona, N. Ijssennagger, E. C. L. Willemsen, J. M. Ramos Pittol, J. W. Jonker, K. Lange, G. J. E. J. Hooiveld, and S. W. C. van Mil. 2017. Characterization of stem cell-derived liver and intestinal organoids as a model system to study nuclear receptor biology. *Biochim. Biophys. Acta*. **1863**: 687–700.

23. Ciorba, M. A. 2015. Scap and the intestinal epithelial stem cell niche: new insights from lipid biology. *J. Lipid Res.* **56**: 1381–1382.

24. Chen, W.-C., C.-Y. Wang, Y.-H. Hung, T.-Y. Weng, M.-C. Yen, and M.-D. Lai. 2016. Systematic Analysis of Gene Expression Alterations and Clinical Outcomes for Long-Chain Acyl-Coenzyme A Synthetase Family in Cancer. *PLoS ONE*. **11**. [online] https://www.ncbi.nlm.nih.gov/pmc/articles/PMC4865206/ (Accessed January 10, 2018).

25. Heimerl, S., C. Moehle, A. Zahn, A. Boettcher, W. Stremmel, T. Langmann, and G. Schmitz. 2006. Alterations in intestinal fatty acid metabolism in inflammatory bowel disease. *Biochim. Biophys. Acta*. **1762**: 341–350.

26. Cao, Y., K. B. Dave, T. P. Doan, and S. M. Prescott. 2001. Fatty acid CoA ligase 4 is up-regulated in colon adenocarcinoma. *Cancer Res.* **61**: 8429–8434.

27. Roongta, U. V., J. G. Pabalan, X. Wang, R.-P. Ryseck, J. Fargnoli, B. J. Henley, W.-P. Yang, J. Zhu, M. T. Madireddi, R. M. Lawrence, T. W. Wong, and B. A. Rupnow. 2011. Cancer cell dependence on unsaturated fatty acids implicates stearoyl-CoA desaturase as a target for cancer therapy. *Mol. Cancer Res. MCR*. **9**: 1551–1561.

28. Igal, R. A. 2016. Stearoyl CoA desaturase-1: New insights into a central regulator of cancer metabolism. *Biochim. Biophys. Acta*. **1861**: 1865–1880.

29. Chen, L., J. Ren, L. Yang, Y. Li, J. Fu, Y. Li, Y. Tian, F. Qiu, Z. Liu, and Y. Qiu. 2016. Stearoyl-CoA desaturase-1 mediated cell apoptosis in colorectal cancer by promoting ceramide synthesis. *Sci. Rep.* **6**: 19665.

30. Ran, H., Y. Zhu, R. Deng, Q. Zhang, X. Liu, M. Feng, J. Zhong, S. Lin, X. Tong, and Q. Su. 2018. Stearoyl-CoA desaturase-1 promotes colorectal cancer metastasis in response to glucose by suppressing PTEN. *J. Exp. Clin. Cancer Res. CR*. **37**: 54.

31. Qiu, Y., G. Cai, B. Zhou, D. Li, A. Zhao, G. Xie, H. Li, S. Cai, D. Xie, C. Huang, W. Ge, Z. Zhou, L. X. Xu, W. Jia, S. Zheng, Y. Yen, and W. Jia. 2014. A distinct metabolic signature of human colorectal cancer with prognostic potential. *Clin. Cancer Res. Off. J. Am. Assoc. Cancer Res.* **20**: 2136–2146.

32. Lu, Y., Z. Zhou, J. Tao, B. Dou, M. Gao, and Y. Liu. 2014. Overexpression of stearoyl-CoA desaturase 1 in bone marrow mesenchymal stem cells enhance the expression of induced endothelial cells. *Lipids Health Dis.* **13**: 53.

33. Tao, J., J. Shi, Y. Lu, B. Dou, Z. Zhou, M. Gao, and Z. Zhu. 2013. Overexpression of stearoyl-CoA desaturase 1 in bone-marrow mesenchymal stem cells increases osteogenesis. *Panminerva Med.* **55**: 283–289.

34. Wu, Q., Z. Yang, F. Wang, S. Hu, L. Yang, Y. Shi, and D. Fan. 2013. MiR-19b/20a/92a regulates the self-renewal and proliferation of gastric cancer stem cells. *J. Cell Sci.* **126**: 4220–4229.

35. Xiang, J., and J. Wu. 2010. Feud or Friend? The Role of the miR-17-92 Cluster in Tumorigenesis. *Curr. Genomics*. **11**: 129–135.

36. Zhang, K., L. Zhang, M. Zhang, Y. Zhang, D. Fan, J. Jiang, L. Ye, X. Fang, X. Chen, S. Fan, M. Chao, and C. Liang. 2017. Prognostic value of high-expression of miR-17-92 cluster in various tumors: evidence from a meta-analysis. *Sci. Rep.* **7**: 8375.

37. Cheng, X., X. Zhang, J. Su, Y. Zhang, W. Zhou, J. Zhou, C. Wang, H. Liang, X. Chen, R. Shi, K. Zen, C.-Y. Zhang, and H. Zhang. 2015. miR-19b downregulates intestinal SOCS3 to reduce intestinal inflammation in Crohn's disease. *Sci. Rep.* **5**. [online] https://www.ncbi.nlm.nih.gov/pmc/articles/PMC4441154/ (Accessed July 26, 2018).

38. Lee, J. H., T. I. Kim, S. M. Jeon, S. P. Hong, J. H. Cheon, and W. H. Kim. 2012. The effects of metformin on the survival of colorectal cancer patients with diabetes mellitus. *Int. J. Cancer*. **131**: 752–759.

39. De Monte, A., D. Brunetti, L. Cattin, F. Lavanda, E. Naibo, M. Malagoli, G. Stanta, and S. Bonin. 2018. Metformin and aspirin treatment could lead to an improved survival rate for Type 2 diabetic patients with stage II and III colorectal adenocarcinoma relative to non-diabetic patients. *Mol. Clin. Oncol.* **8**: 504–512.

40. Miranda, V. C., M. I. Braghiroli, L. D. Faria, G. Bariani, A. Alex, J. E. Bezerra Neto, F. C. Capareli, J. Sabbaga, J. F. Lobo Dos Santos, P. M. Hoff, and R. P. Riechelmann. 2016. Phase 2 Trial of Metformin Combined With 5-Fluorouracil in Patients With Refractory Metastatic Colorectal Cancer. *Clin. Colorectal Cancer*. **15**: 321–328.e1.

41. Effect of metformin alone and in combination with 5-fluorouracil (5FU), oxaliplatin (O) and irinotecan (I) on human colon cancer cell lines.: Journal of Clinical Oncology: Vol 29, No 15_suppl. [online] http://ascopubs.org/doi/abs/10.1200/jco.2011.29.15_suppl.e13041 (Accessed July 26, 2018).

42. Griss, T., E. E. Vincent, R. Egnatchik, J. Chen, E. H. Ma, B. Faubert, B. Viollet, R. J. DeBerardinis, and R. G. Jones. 2015. Metformin Antagonizes Cancer Cell Proliferation by Suppressing Mitochondrial-Dependent Biosynthesis. *PLoS Biol.* **13**: e1002309.

43. Yan, S., X.-F. Yang, H.-L. Liu, N. Fu, Y. Ouyang, and K. Qing. 2015. Long-chain acyl-CoA synthetase in fatty acid metabolism involved in liver and other diseases: an update. *World J. Gastroenterol.* **21**: 3492–3498.

44. Ghadge, A., A. Harsulkar, M. Karandikar, V. Pandit, and A. Kuvalekar. 2016. Comparative anti-inflammatory and lipid-normalizing effects of metformin and omega-3 fatty acids through modulation of transcription factors in diabetic rats. *Genes Nutr.* **11**. [online] https://www.ncbi.nlm.nih.gov/pmc/articles/PMC4968436/ (Accessed July 26, 2018).

45. Zabielski, P., M. Chacinska, K. Charkiewicz, M. Baranowski, J. Gorski, and A. U. Blachnio-Zabielska. 2017. Effect of metformin on bioactive lipid metabolism in insulin-resistant muscle. *J. Endocrinol.* **233**: 329–340.

46. Metformin and Cancer Stem Cells: Old Drug, New Targets | Cancer Prevention Research. [online] http://cancerpreventionresearch.aacrjournals.org/content/5/3/351 (Accessed July 30, 2018).

47. Mogavero, A., M. V. Maiorana, S. Zanutto, L. Varinelli, F. Bozzi, A. Belfiore, C. C. Volpi, A. Gloghini, M. A. Pierotti, and M. Gariboldi. 2017. Metformin transiently inhibits

colorectal cancer cell proliferation as a result of either AMPK activation or increased ROS production. *Sci. Rep.* **7**: 15992.

48. Andrzejewski, S., S.-P. Gravel, M. Pollak, and J. St-Pierre. 2014. Metformin directly acts on mitochondria to alter cellular bioenergetics. *Cancer Metab.* **2**: 12.

Figures

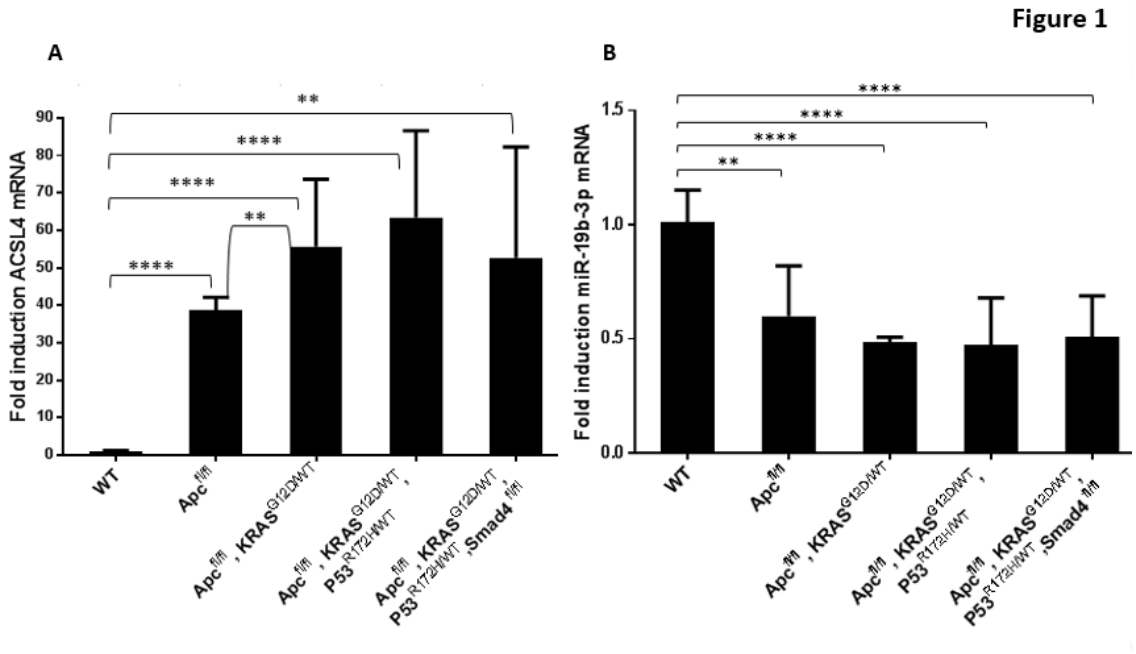

Figure 1: ACSL4 is overexpressed throughout CRC-like organoids stages while miR-19b-1-3p preserves its protective role.

A) RT-QPCR analysis showing ACSL4 mRNA expression levels throughout CRC-like organoids stages. B) RT-QPCR analysis showing miR-19b-1-3p mRNA expression levels throughout CRC-like organoids stages. Results represent the fold-change mean ±SD (n = 4) in plots A, (n = 3) in plots B. (ns, $P > 0.05$; *, $P \leq 0.05$; **, $P \leq 0.01$; ***, $P \leq 0.001$; ****, $P \leq 0.0001$)

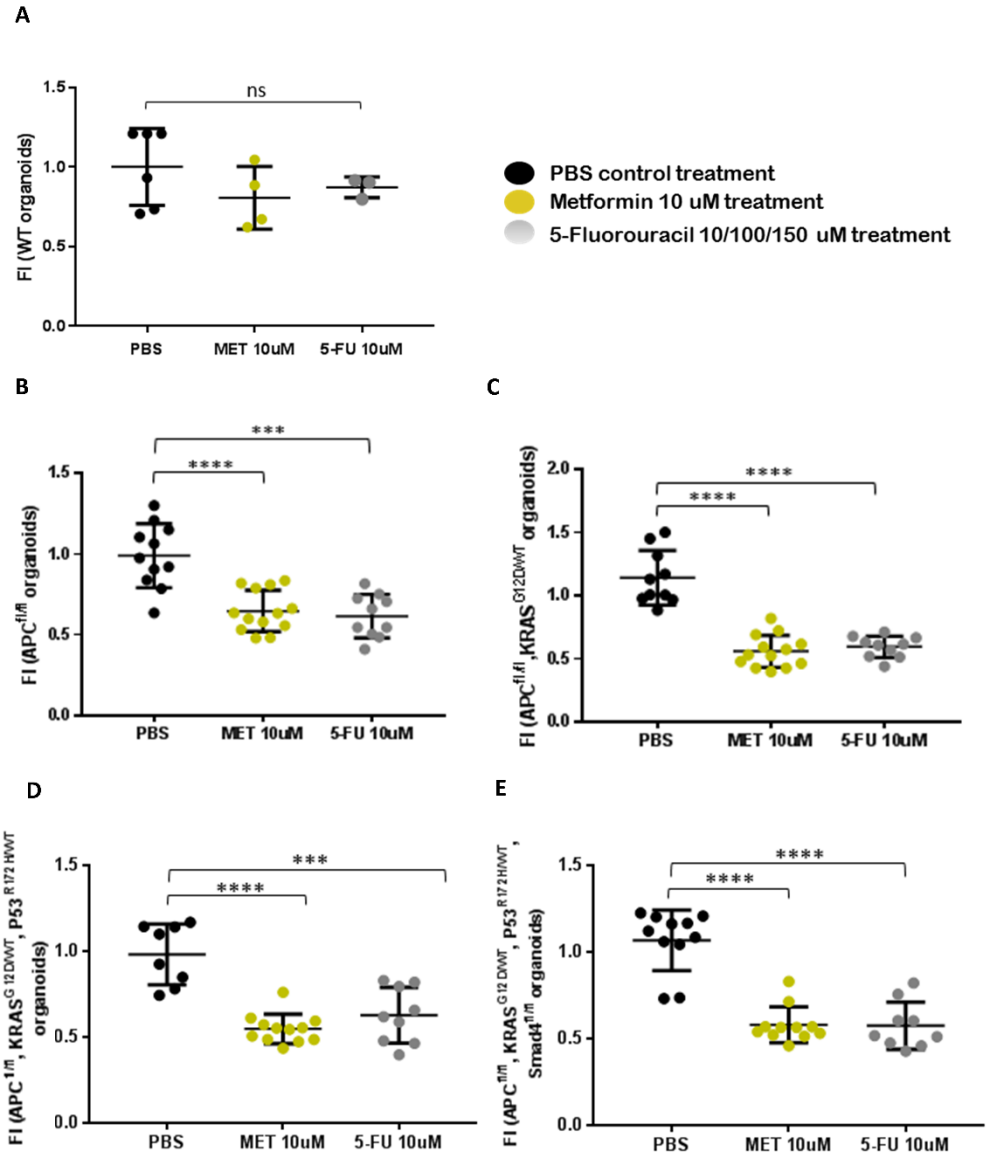

Figure 2: Metformin decreases CRC-like organoids viability to the same extent as current chemotherapy without significant effects on WT organoids

MTT cell viability assays upon 48 hours treatments with Metformin or 5-FU in the different CRC-like organoids representative stages (A) WT organoids; (B) *APC*$^{fl/fl}$ organoids resembling stage I; (C) *APC*$^{fl/fl}$, *KRAS*$^{G12D/WT}$ organoids resembling stage II; (D) *APC*$^{fl/fl}$, *KRAS*$^{G12D/WT}$,*P53*$^{R172H/WT}$ organoids resembling stage III; (E) *APC*$^{fl/fl}$, *KRAS*$^{G12D/WT}$,*P53*$^{R172H/WT}$,Smad4$^{fl/fl}$ organoids

resembling stage IV. Data are represented by the fold-change mean ±SD (n = 3) in all the plots except A: (n=2). (ns, $P > 0.05$; *, $P \leq 0.05$; **, $P \leq 0.01$; ***, $P \leq 0.001$; ****, $P \leq 0.0001$).

Figure 3

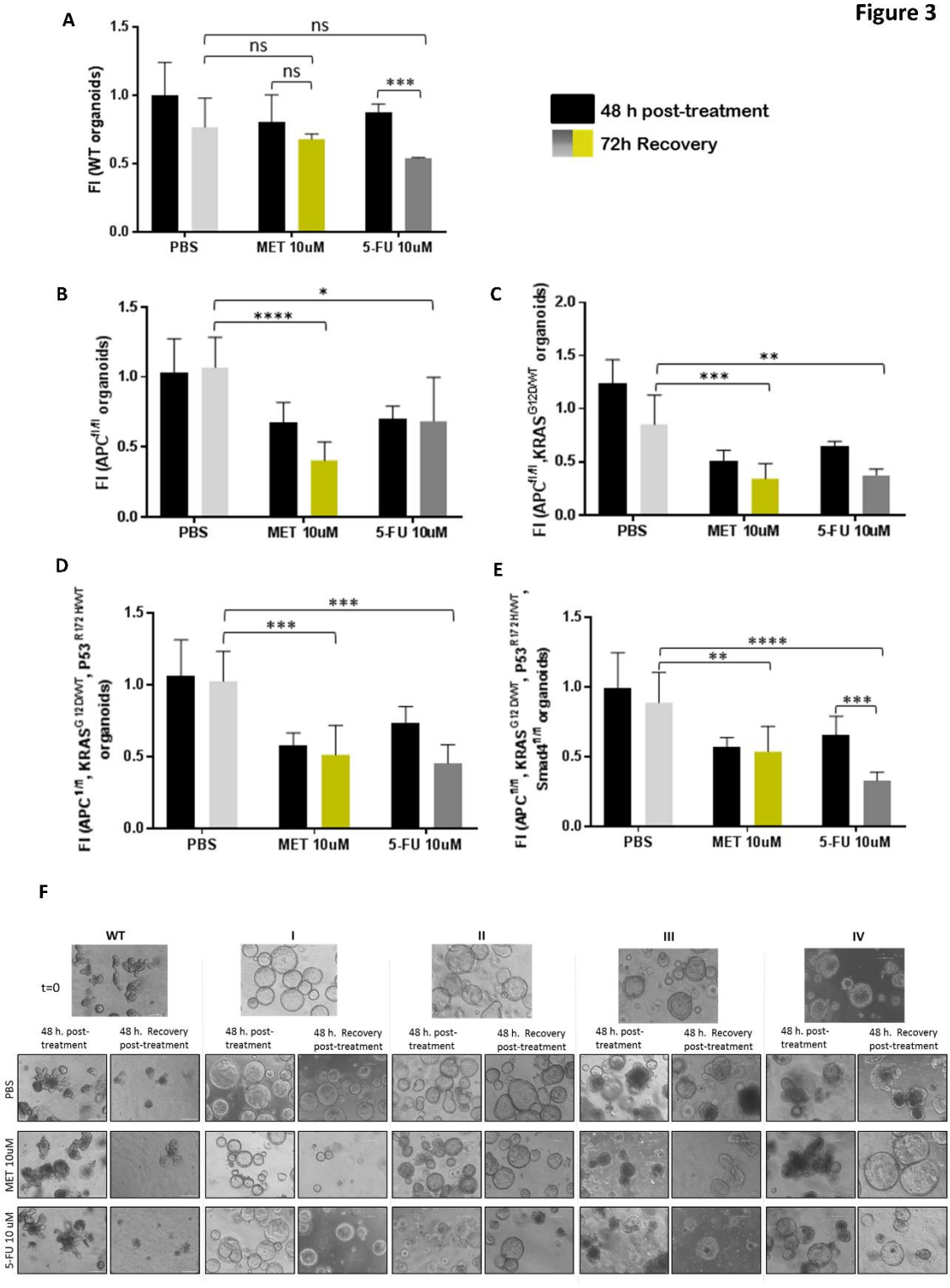

Figure 3: Metformin treatment recovery is significantly lower compared to 5FU in first stages organoids while WT organoids present an opposite behavior

MTT cell viability assays upon 48 hours treatments (black bars) and upon extra 72h post-treatment recovery with PBS (light grey bars) Metformin (yellow bars) or 5-FU (dark grey bars) in the different CRC-like organoids representative stages (A) WT organoids; (B) $APC^{fl/fl}$ organoids resembling stage I; (C) $APC^{fl/fl}$, $KRAS^{G12D/WT}$ organoids resembling stage II; (D) $APC^{fl/fl}$, $KRAS^{G12D/WT}$,$P53^{R172H/WT}$ organoids resembling stage III; (E) $APC^{fl/fl}$, $KRAS^{G12D/WT}$,$P53^{R172H/WT}$,$Smad4^{fl/fl}$ organoids resembling stage IV. Data are represented by the fold-change mean ±SD (n = 3) in all the plots. (ns, $P > 0.05$; *, $P \leq 0.05$; **, $P \leq 0.01$; ***, $P \leq 0.001$; ****, $P \leq 0.0001$). (F) Organoids pictures with PBS, Metformin or 5-FU, upon 48 hours treatments and upon extra 72h post-treatment recovery as indicated. Pictures were captured using the × 10 objective, in bright field. Leica microscope (Leica microsystems).

Figure 4

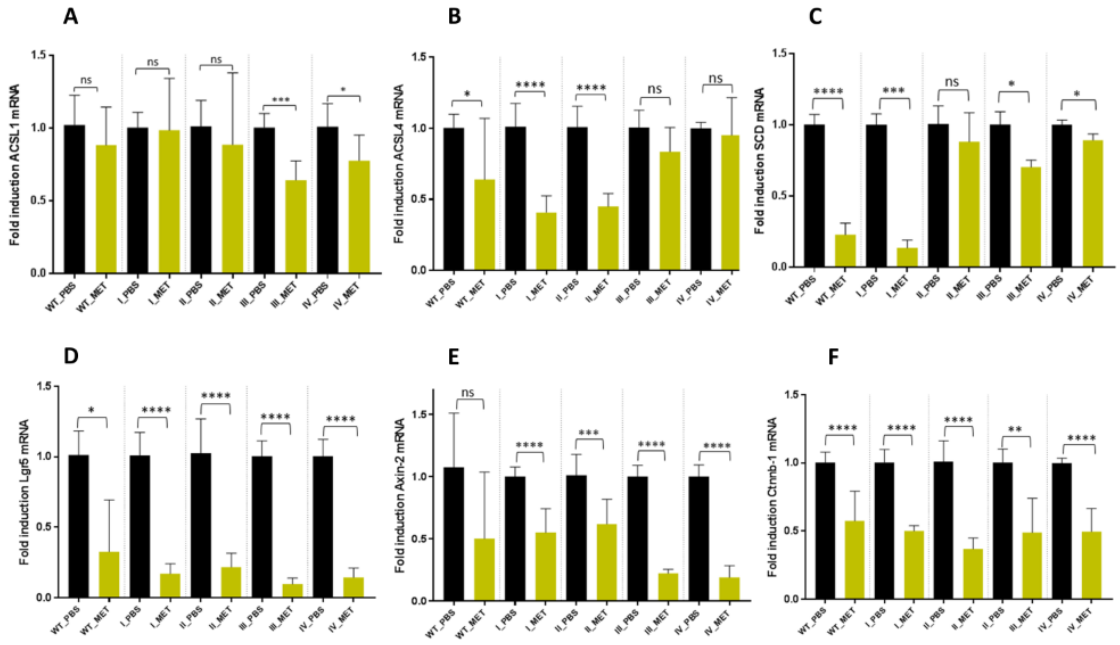

Figure 4: Metformin action is stronger on ACSL4 and SCD overexpressing first stages organoids and downregulates stem cell biomarker LGR5 and Wnt target genes expression in all organoid stages.

mRNA expression levels of enzymes related to the ACSL/SCD axis, ACSL4 (A), SCD (B), by RT-QPCR; and expression levels of different stem cell markers, Lgr5 (C), Axin-2 (D) and Ctnnb-1 (E) by RT-QPCR upon PBS (black bars) and 10 uM Metformin (yellow bars). Data are represented by the fold-change mean to each PBS control ±SD (n = 3). (ns, P> 0.05; *, $P \leq 0.05$; **, $P \leq 0.01$; ***, $P \leq 0.001$; ****, $P \leq 0.0001$).

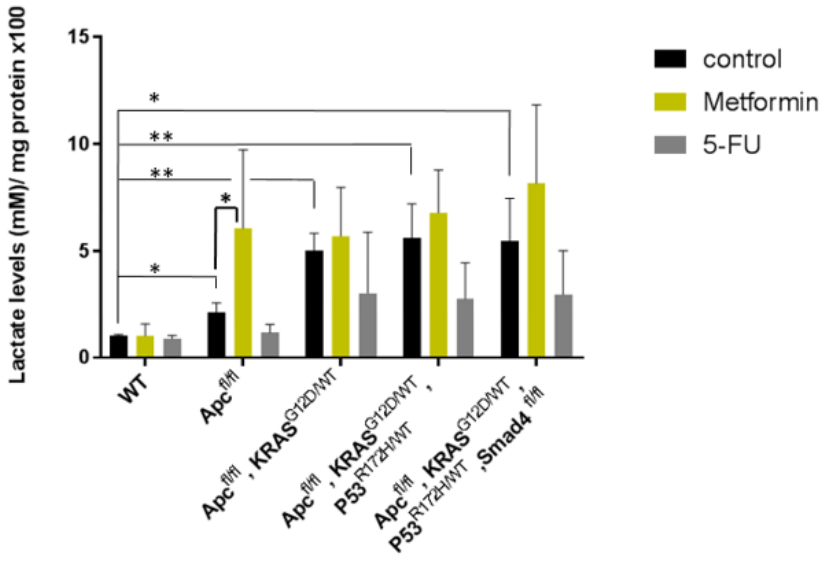

Figure 5: Metformin action in CRC organoids is not related to a Warburg-effect impairement

Bars represent the extracellular L-lactate production upon overnight PBS treatment (black bars), Metformin treatment (yellow bars) and 5-FU treatment (grey bars) using the Cayman's Glycolysis cell-based assay. L-lactate production measurement is normalized by total protein content (x100). Data are represented by the fold-change mean ±SD (n = 3) in all the plots. (ns, P> 0.05; *, $P \leq$ 0.05; **, $P \leq 0.01$; ***, $P \leq 0.001$; ****, $P \leq 0.0001$).

Tables

Table 1: CRC-like organoids with the acquired mutations related to the stage.

Organoid mutation	CRC-like stage
WT	-
***APC*$^{fl/fl}$**	I
***APC*$^{fl/fl}$, *KRAS*$^{G12D/WT}$**	II
***APC*$^{fl/fl}$, *KRAS*$^{G12D/WT}$,*P53*$^{fl/R172H}$**	III
***APC*$^{fl/fl}$, *KRAS*$^{G12D/WT}$,*P53*$^{fl/R172H}$,Smad4$^{fl/fl}$**	IV

Table 2: Parental cell lines and publication´s PMID of the mutations in the organoids

Mutation	Parental mouse line	PMID
APC	C57BL/6 males	17002498
***KRAS* G12D**	C57BL/6 males	11323676
P53 floxed	C57BL/6 males	11694875
***P53* R172H**	C57BL/6 males	15607980
Smad4 floxed	C57BL/6 males	11857783

Supplemental Figures and Tables

Supplemental Figure S1

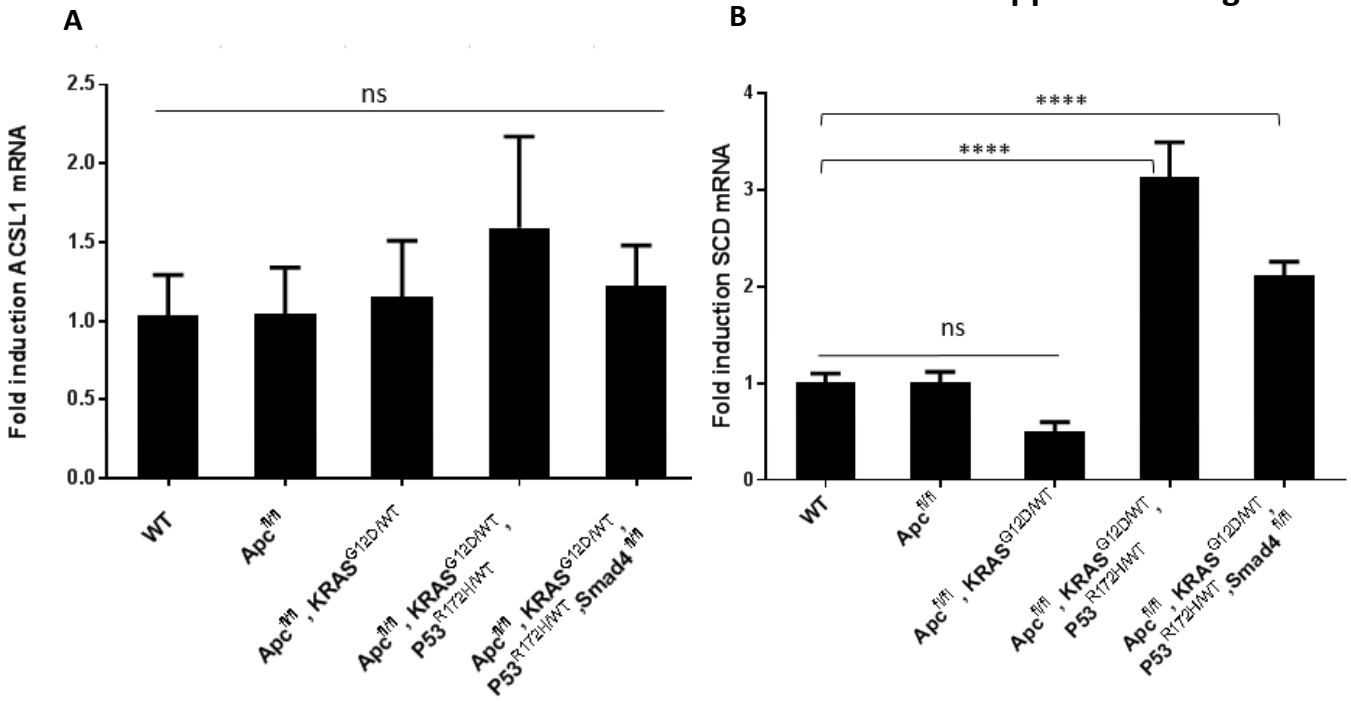

Supplemental Figure S1: ACSL1 and SCD mRNA expression throughout CRC-like organoids stages;

RT-QPCR analysis showing ACSL1 (A) and SCD (B) mRNA expression levels throughout CRC-like organoids stages. Results represent the fold-change mean ±SD (n = 3) (ns, $P > 0.05$; *, $P \leq 0.05$; **, $P \leq 0.01$; ***, $P \leq 0.001$; ****, $P \leq 0.0001$)

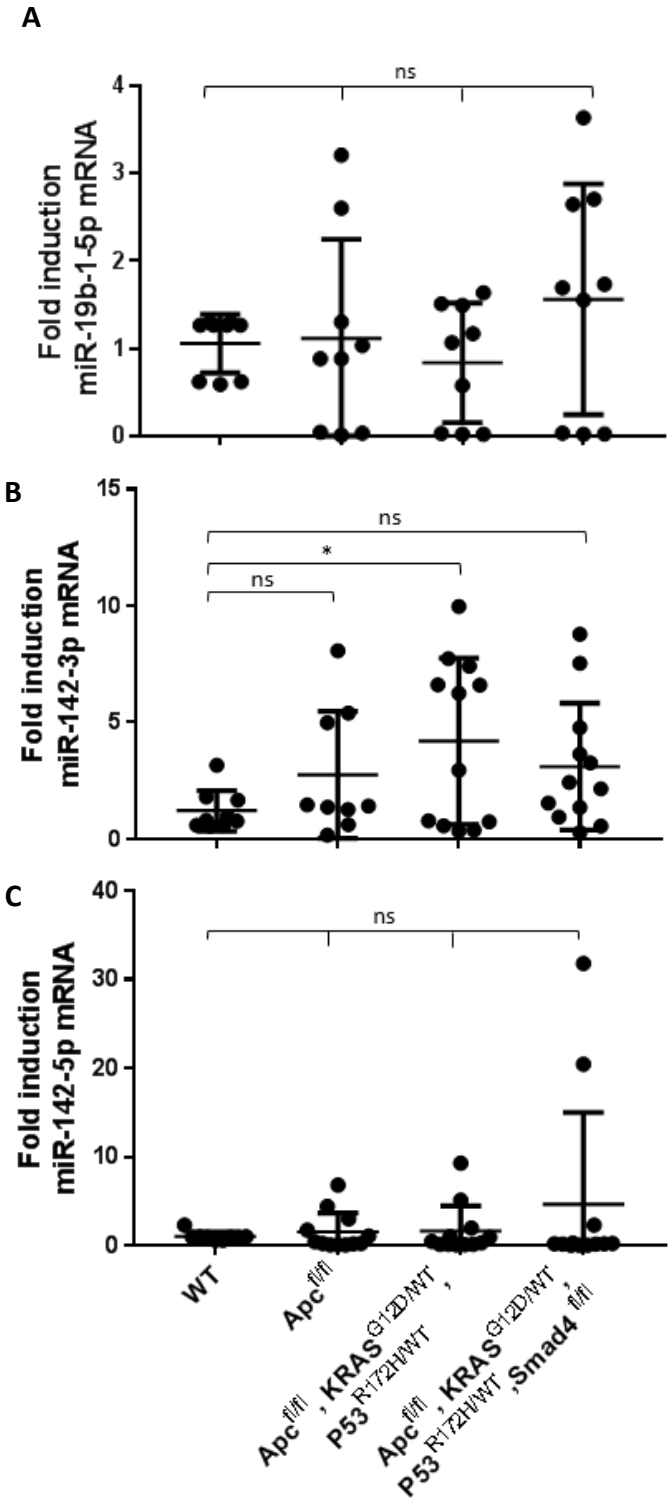

Supplemental Figure S2: ACSL/SCD regulatory miRNAs expression in CRC-like organoids

RT-QPCR analysis showing mRNA expression levels throughout CRC-like organoids stages of different ACSL/SCD regulatory miRNAS: miR-19b-1-5p (A), miR-142-3p (B), miR-142-5p (C). Results represent the fold-change mean ± SD (n = 3). (ns, P> 0.05; *, $P \leq 0.05$; **, $P \leq 0.01$; ***, $P \leq 0.001$; ****, $P \leq 0.0001$).

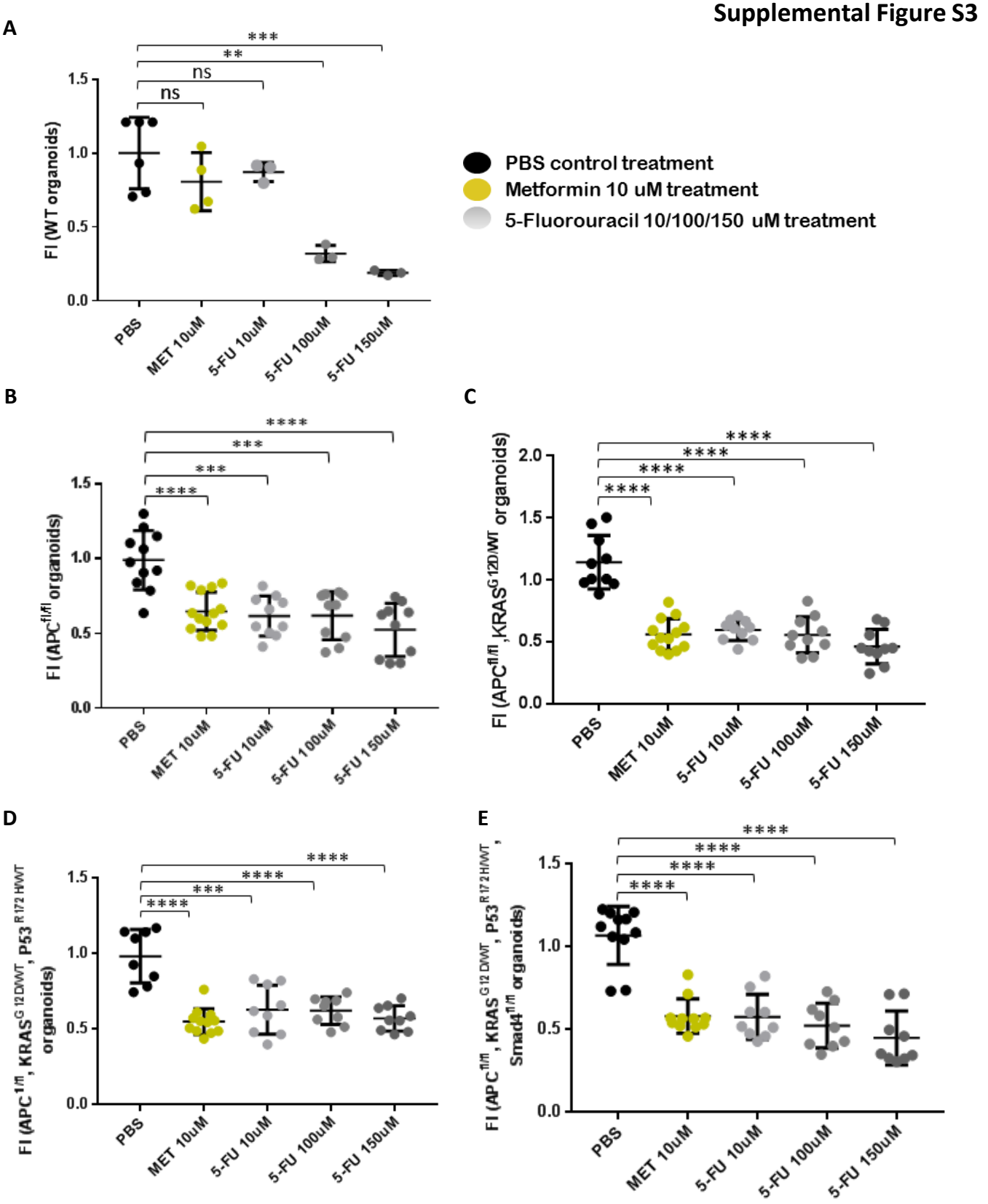

Supplemental Figure S3: Metformin and 5-FU effect in CRC-like organoids.
MTT cell viability assays upon 48 hours treatments with PBS (black bars), 10 uM Metformin (yellow bars) or 10, 100 and 150 uM 5-FU (grey bars) in the different CRC-like organoids representative stages: WT organoids (A); *APC*$^{fl/fl}$ organoids resembling stage I (B); *APC*$^{fl/fl}$, *KRAS*$^{G12D/WT}$ organoids resembling stage II (C); *APC*$^{fl/fl}$, *KRAS*$^{G12D/WT}$,*P53*$^{R172H/WT}$ organoids resembling stage III (D); *APC*$^{fl/fl}$, *KRAS*$^{G12D/WT}$,*P53*$^{R172H/WT}$,Smad4$^{fl/fl}$ organoids resembling stage IV (E). Data are represented by the fold-change mean ±SD (n = 3) in all the plots. (ns, $P > 0.05$; *, $P \leq 0.05$; **, $P \leq 0.01$; ***, $P \leq 0.001$; ****, $P \leq 0.0001$).

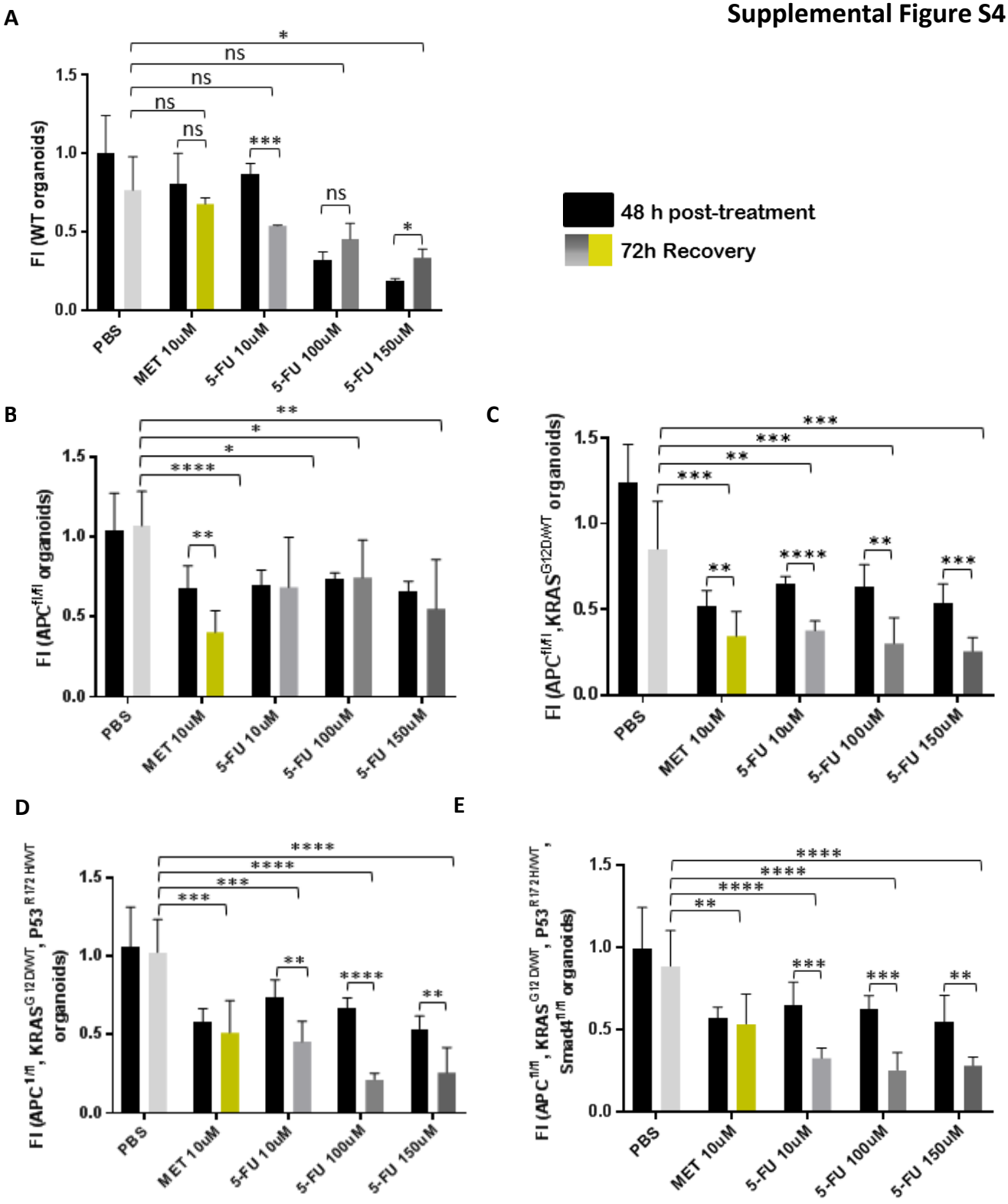

Supplemental Figure S4: Metformin and 5-FU recovery effect in CRC-like organoids.

MTT cell viability assays upon 48 hours treatments (black bars) and upon extra 72h post-treatment recovery with PBS (light grey bars), 10 uM Metformin (yellow bars) or 10, 100 and 150 uM 5-FU (dark grey bars) in the different CRC-like organoids representative stages:: WT organoids (A); *APC*$^{fl/fl}$ organoids resembling stage I (B); *APC*$^{fl/fl}$, *KRAS*$^{G12D/WT}$ organoids resembling stage II (C); *APC*$^{fl/fl}$, *KRAS*$^{G12D/WT}$,*P53*$^{fl/R172H}$ organoids resembling stage III (D); *APC*$^{fl/fl}$, *KRAS*$^{G12D/WT}$,*P53*$^{fl/R172H}$,Smad4$^{fl/fl}$ organoids resembling stage IV (E). Data are represented by the fold-change mean ±SD (n = 3) in all the plots. (ns, $P > 0.05$; *, $P \leq 0.05$; **, $P \leq 0.01$; ***, $P \leq 0.001$; ****, $P \leq 0.0001$).

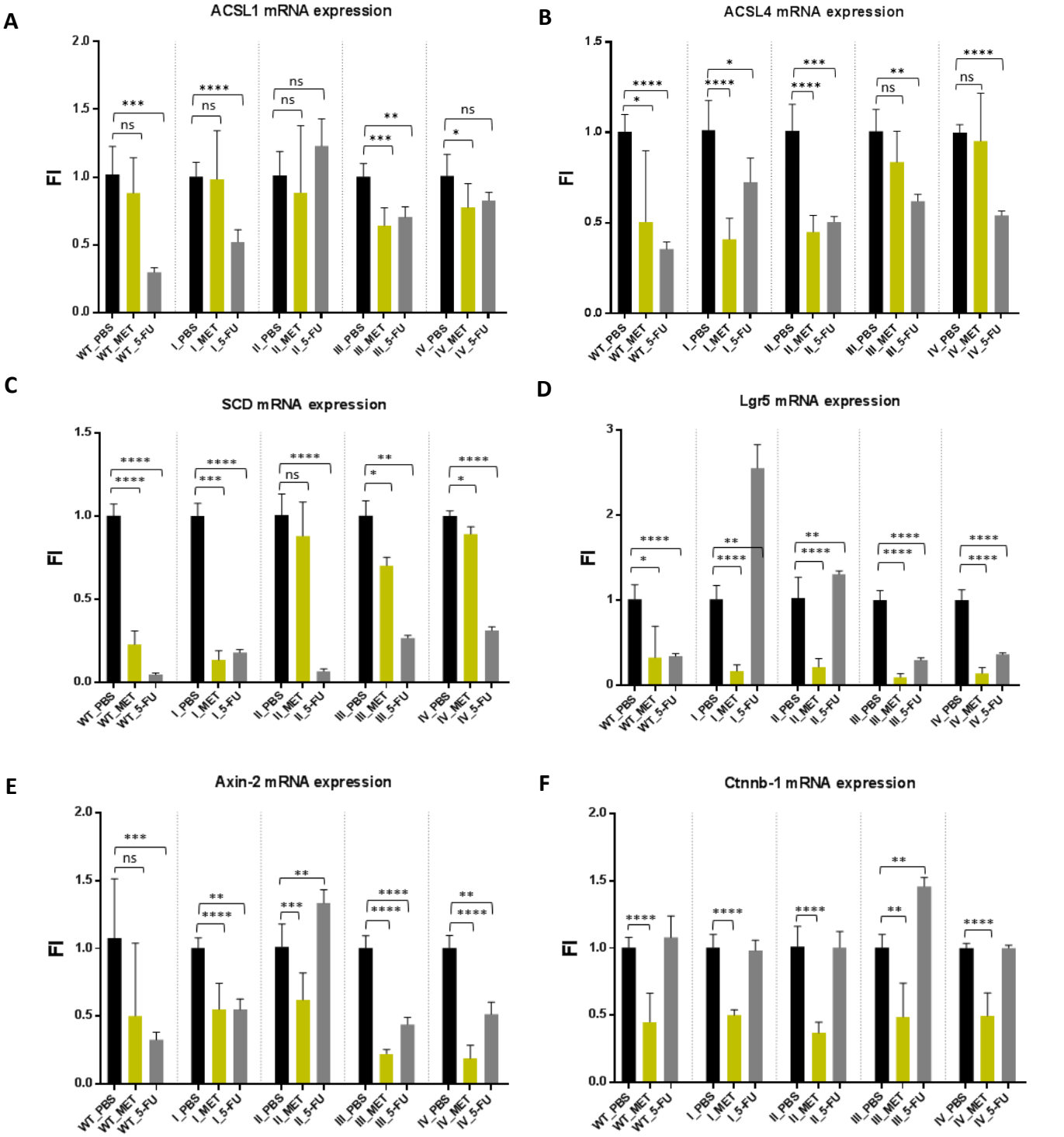

Supplemental Figure S5: ACSL/SCD axis and stem cell markers expression (Lgr5, Axin-2 and Ctnnb-1) upon Metformin and 5-FU treatment

Expression leveles of enzymes related to the ACSL/SCD axis, ACSL1 (A), ACSL4 (B) and SCD (C) by RT-QPCR; and expression levels of different stem cell markers, Lgr5 (D), Axin-2 (E) and Ctnnb-1 (F) by RT-QPCR; upon PBS (black bars), 10 uM Metformin (yellow bars) or 10, 100 and 150 uM 5-FU (grey bars). Data are represented by the fold-change mean ±SD (n = 3). (ns, P> 0.05; *, $P \leq 0.05$; **, $P \leq 0.01$; ***, $P \leq 0.001$; ****, $P \leq 0.0001$).

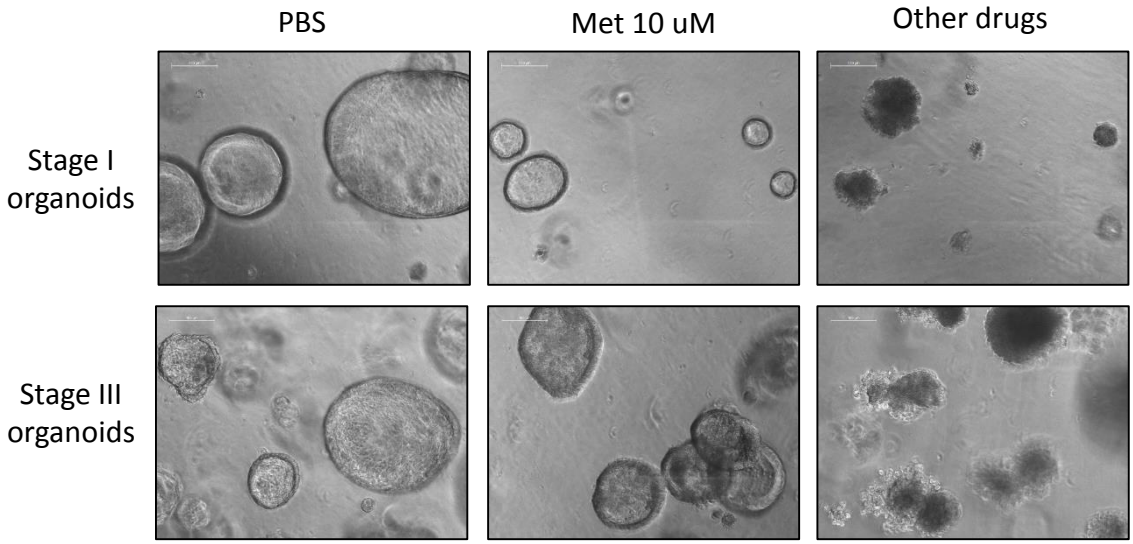

Supplemental Figure S6: Comparative organoids morphology between Metformin and other oncologic treatments.

Organoids (stage I and III) representative pictures with DMSO, Metformin and other metabolic drugs against CRC progression, upon 48 hours treatments plus upon extra 72h post-treatment recovery. Pictures were captured using the × 10 objective, in bright field. Leica microscope (Leica microsystems).

Supplemental Table S1: Primers´ sequences (Invivogen) used for quantitative real-time PCR.

ACSL1	TGACCTCTCCATGCAGTCAG/ AGCCTATGCACTCAGCCAGT
ACSL4	CACCATTGCCATTTTCTGTG/ GCCTTCAGTTTGCTTTCCAG
SCD	TTCTTACACGACCACCACCA/ GCAGGAGGGAACCAGTATGA
CTNNB1	TAACTATCAGGATGACGCGG/ TTAACTACCACCTGGTCCTC
AXIN-2	GGACTGGGGAGCCTAAAGGT/ AAGGAGGGACTCCATCTACGC
LGR5	GGACCAGATGCGATACCGC/ CAGAGGCGATGTAGGAGACTG
B2M	AGACTGATACATACGCCTGC/ ATCACATGTCTCGATCCCAG

Supplemental Table S2: Probes from TaqMan® MicroRNA Assays (ThermoFisher) used for quantitative real-time PCR.

miRBase ID	Cat No
mmu-miR-19b-3p	4427975
mmu-miR-19b-1-5p	4427975
mmu-miR-142a-3p	4427975
mmu-miR-142a-5p	4427975
U6 snRNA	4427975

DISCUSSION

Considering the axis ACSL/SCD as a work team

The research reported in this Doctoral Thesis contribute to elucidate the role in cancer progression of the joint overexpression of three enzymes involved in FA metabolism: ACSL1, ACSL4 and SCD. We propose this metabolic switch in FA metabolism as an example of metabolic reprogramming that can be used by malignant cells to increase their tumorigenicity, and therefore an appealing and hot point to target. Here we describe how their overexpression stimulates cell plasticity accompanied with increased migratory and invasive properties but not proliferation, in CRC cells. Therefore, the axis would be producing other altered metabolisms rather than the Warburg effect, characterized by pro-proliferative events and aerobic glycolysis. In fact, ACSL/SCD cells show a decrease in lactate production. Other metabolic enzymes overexpression have been linked to cancer migration and invasion before; such as a monoacylglycerol lipase [88] or ACLY, involved in metastasis [221]. ACSL/SCD overexpressed cells present also an upgraded energetic status characterized by elevated creatine and phosphocreatine levels together with lower basal respiration levels and decreased OCR. Besides, the number of differential metabolites are incremented in ACSL/SCD cells compared to their individual overexpressions. Indeed, they show same metabolic features than other well-known metastatic cells. CRC patients which present elevated levels of ACSL1, ACSL4 and SCD simultaneously show an increased risk of relapse compared to other CRC patients in the same clinical stage. All the facts above mentioned evidence the aggressive phenotype provoked exclusively upon the three metabolic enzymes overexpression.

The abnormal metabolism performed by ACSL/SCD is driven by an impaired AMPK signaling since the original epithelial phenotype is recovered through Metformin, an AMPK activator. AMPK could be regulating EMT via Akt-MDM2-Foxo3 signaling axis, linked to EMT suppression [222]. Although this fact is in agreement with the increased Akt signaling observed in x3 cells; an Akt inhibitor fails to revert the mesenchymal features, suggesting that additional pathways affected by AMPK are also needed for a complete rescue. Accordingly, SCD downregulation was reported to activate AMPK [163,223] and since free FA are able to activate AMPK [224], ACSL overexpression could prevent this activation through the conversion of fatty acids into Acyl-CoAs. Regarding Akt signaling, inhibition of SCD decreases the synthesis of PIP_3, crucial for Pi3K/Akt signaling; and SCD's main product, oleic acid, activates Akt [223]. In addition, AA, ACSL4 preferred substrate, is one of the most common fatty acids of PIP_3 [129], evidencing the contribution of the axis enzymes to this pathway, highly linked to cell cycle progression and survival, key to cancer progression [225].

Even though the complete phenotype is achieved upon x3 overexpression; either of the enzymes show a specific and partial function to the whole axis contribution. **ACSL1** seems to be the initiator of mesenchymal-promoting genes stimulation and acquisition of invasion capabilities accompanied by a decreased in basal OCR. In ACSL1 overexpressed cells, acylcarnitines were showed elevated. Upregulated acylcarnitines could be also associated with a fatty acid oxidation (FAO) reduction in the mitochondria, accompanied by decreased Acetyl-CoA. This could be connected to the lower basal OCR [226]. In line with this, the ACSL1 deficiency was reported to promote β-oxidation and the synthesis of PL species in hepatic cells [227]. Besides, acylcarnitines could be mediating the invasive capabilities important for cancer progression since FAO intermediates levels have been found dramatically upregulated in several malignancies [228–230].

ACSL4 display the most epithelial-like behavior, probably taking part in the reversion of the epithelial phenotype in the metastasis establishment [231]. As well, ACSL4 overexpressed cells present a tendency to induce proliferation; together with a more glycolytic phenotype compared to control or ACSL1 cells. ACSL4 also presents reduced PUFA levels corresponding to a greater utilization to synthesize complex lipids, such as the phospholipids required for membrane biogenesis, crucial for cancer cells [232]. Although not directly involved in invasion or migration, we wonder whether ACSL4 substrate preference for AA is contributing to prostaglandin production and inflammatory mediators for EMT action [233,234]. ACSL4 has been previously reported to promote AA conversion into PE, PI, and TG; metabolic building blocks and energy storage for the cell as well as lipooxygenated and cyclooxygenated metabolites, inflammatory mediators, known to trigger tumor aggressiveness in several cancers, including CRC [121,129,130]. Besides, intestinal organoids technology, a new platform bridging *in vitro* and patient results, keep the poor prognosis potential of ACSL4 overexpression along the organoids staging increase; despite its murine origin. The axis status results differ from previous ones using human CRC cells in ACSL1 static expression, which can be due to differential expression in murine tissues compared to human 2D cultures but also by the fact that the rodent protein is one residue longer (699 amino acids) than the human protein (698 amino acids), making it necessary to study the extent of this dissimilarity

Several shreds of evidence makes ACSLs family of enzymes a productive network for the progression of cancer. ACSL1 catalyzes and activates FAs from 16:0-20:0 carbons; and also unsaturated FAs from 16:1-22:6 carbons. For its part, ACSL4 catalyzes preferentially FAs of 20:4 and 20:5 carbons [235]. With both enzymes overexpressed most of the FAs activation needed for the tumor progression is covered. On the other hand, each isoform is located in different cell compartments covering again a wide physical space, though they can share some subcellular

locations [122]. ACSL1 is mainly found in mitochondria and lipid droplets. However, ACSL4 is a peripheral protein which moves from ER to peroxisomes [235], where it is probably the only ACSL isoform located [123]. Covering the majority of the subcellular locations, the overexpression of these two enzymes allows the tumor to take control over FAs different fates: storage, β-oxidation…

SCD might maintain the network through different signaling pathways activation such as Erk and Akt, allowing GSK3β inactivation, β-catenin degradation impairment and allowing EMT signaling as a consequence, reported also by Ha, G.H. *et al.* [236]. Accordingly, SCD knock-down has been described to cause EMT in breast cancer cells [237]. Naturally, SCD overexpression implies MUFA levels upregulation, which is not the case for x3 cells, with lower MUFA levels reflecting its incorporation in complex lipids. Low proliferation tendencies are presented by SCD and x3, in agreement with Erk and Akt activation of both cells. Globally, SCD could help to provide an appropriate MUFA/PUFA ratio, essential for the membrane integrity. Regarding organoids results, SCD augments significantly its expression but only in higher stages (III and IV). We postulate if this late overexpression is due to the lipotoxic accumulation regarding ACSL4 overexpression from first stages.

As previously mentioned, the complete aggressive phenotype is only achieved upon x3 overexpression though is not the sum of individual enzymes effects. These cells are also depicted by upregulated complex lipids such as phospholipids and sphinganine-derived ceramides and sphingolipids, reported to alter signaling pathways like Akt [238–240], over-activated in x3 cells. Curiously, other non-lipid metabolism related pathways were altered in x3 cells such us urea cycle and glycolysis. Urea metabolites upregulation, such as polyamines, probably mediated by increased Acetyl-CoA levels, have been previously reported in cancer malignancies, [219,220,241,242]. Interestingly, polyamines could suppose a metastatic biomarker since we have also reported elevated levels in a CRC metastatic line compared to its primary tumor. The elevated levels of creatine and phosphocreatine found in x3 cells, represent an advantageous energetic status to the aim of invasion, as reported in liver metastasis upon phosphocreatine elevation [243]. The lower basal respiration levels and decreased OCR is also part of the energetically efficient status of ACSL/SCD cells

These features characterized as well metastatic CRC cells when compared to their parental cell line. We hypothesize that x3 cells lower basal OCR together with elevated creatine that could be partly fed by ACSL1-drived increased FAO and maintained by further phospholipid signaling supported by ACSL4 and SCD increased PUFA and MUFA products, respectively.

Although other reports point toward the simultaneous overexpression of ACSL and SCD, this is the first time reporting their joint action. For example, in a previous study from melanoma patients genes involved in the synthesis of FAs (SCD) and complex lipids (ACSL3) among other 16 genes involved in the FAs metabolism have been found to be upregulated [244] in these tumors. ACSL1 and ACSL4, together with ACSL5 were previously reported overexpressed in a breast cancer type, the estrogen receptor-negative type [245].

All in all, an increased FA synthesis caused by ACSL overexpression, together with an enriched MUFA content and lipotoxicity detoxification upon SCD upregulation, an improved energetic capacity and invasive and migratory properties could generate the perfect context for the progression of cancer and might represent a new therapeutic opportunity for CRC treatment.

Therapies and prognosis of the axis

The ACSL/SCD metabolic axis could be highly considered from a therapeutic point of view. First for being involved in the last steps of FA activation and therefore the previous critical intermediates crucial for other routes could follow its fate, avoiding undesirable side effects. ACS enzymes are also involved in the first step when considering the uptake of extracellular FAs. Thus ACS inhibition leads to the blockade of FAs entrance to the routes. ACS is also considered the first enzyme in TG synthesis [246]. Lipid droplets, composed by TG, could also play a role in cancer as described in the introduction section. The activation by ACS and the following FAs desaturation by SCD suppose a key point in the partition of FAs into different routes. For those reasons, we consider this axis an interesting strategic point in terms of therapeutics.

The combination of two specific ACSL/SCD inhibitors, Triacsin C and A939572 synergistically decreases CRC cells viability without affecting colon normal cells. Both drugs, A939572 [159] and Triacsin C [247] separately have significantly delayed CRC tumor growth in previous reports. Additionally, this is also effective in CRC cells resistant to conventional chemotherapy (5-FU). In fact, it has been reported also that Triacsin C is able to increase 5-FU activity in CRC cell lines, despite cell-death resistance provoked by LD accumulation [248]. Therefore, the combination of ACSL and SCD inhibitors might represent a new way for targeting tumor metabolism.

Remarkable antitumorigenic results were also obtained upon Metformin, initially used as an antidiabetic treatment. Metformin, able to revert the ACSL/SCD invasive phenotype, greatly decreases the viability of first stages CRC-like organoids compared to current chemotherapeutic drugs (5-FU), without affecting WT organoids. Metformin is also proved to reduce ACSL/SCD expression levels in organoids, as well as stem cells markers (LGR5). Despite we found that CRC-

organoids show increased glycolysis throughout the stages; upon Metformin treatment glycolysis experimented an increase in this glycolytic phenotype, especially in stage I organoids, coincident with the higher sensitivity to the drug in this organoids. Hence, Metformin could be targeting different metabolic routes other than Warburg effect to perform its effect on CRC organoids viability, such as ACSL/SCD axis impairment. Considering that it has been proved as a drug for CRC in previous studies [249], Metformin based therapies could also be an appealing alternative in those cases when the tumor is detected in very early stages rather than 5-FU treatments. Our results using Metformin are very promising and extend the list of the increasing studies over its use in CRC [249]. However, some reports point to CRC stage III patients to be the most likeable stage to present a greater Metformin response [250], though with a low number of candidates in stage I, not enough representative. As well, further studies with combination doses of Metformin with 5-FU in different stages would be of great interest. Remarkably, it exists a Phase 2 Trial for the study of Metformin and 5-FU combination in metastatic CRC [251], concluded with a longstanding cancer control. Metformin therapies in combination with other drugs are also an appealing approach such as Metformin combined with aspirin to treat middle stages in non-diabetic CRC patients (stages II and III) [252].

CRC patient's great difficulty lies on the absence of symptoms until the tumor is in advanced stages, leading to a reduction of the treatments efficacy. Early diagnosis pursuit might be an appealing focus in the clinics. In this way, ACSL/SCD axis could be considered a prognostic value in stage II-CRC patients since the joint overexpression of ACSL1/ACSL4/SCD show a poorer outcome and higher risk of relapse when compared to the upregulation of the individual genes. This suggests an augmented aggressiveness of tumors displaying ACSL/SCD network overexpression. Together with this potential clinical biomarker, we consider the possibility of non-invasive biomarkers such as miRNAs. In this way, miR-19b-1 lower expression in stage II and III CRC patients correspond with a poorer prognosis suggesting also a protective role for this miRNA in CRC. Both prognostic values could comprise a tandem of clinical biomarkers.

MiRs comprehend a vast group of inter regulations among genes and they sometimes are encountered in polycistronic miRNA "clusters", where a single primary transcript generates multiple miRNA genes. Contradictorily, miR-19b-1, a member of the miR-17-92 cluster is frequently accepted as an oncomiR [253] associated to CRC [254] among other cancers [255]. However, it exists a wide controversy among this cluster with several studies suggesting the anti-tumorigenic role of some of its members [256,257]; evidencing that miR-17-92 cluster role needs to be further investigated. Probably these miRNAs roles and expression may be tissue and tumor stage

dependent [258]. As a noninvasive biomarker, it could be interesting to further study its circulating levels in serum, plasma or urine as previously described for other types of cancer [257].

Apart from the prognostic value of this miRNA, studying miRNAs regulating mechanisms over the axis supposes a great strategy to propose effective cancer therapies. Here we propose novel interaction scoring approaches for a more convenient bioinformatics screening, selecting best miRNA candidates for a combination of targets. We also proved the combination of two important bioinformatic tools (miRanda/mirSVR) to detect canonical and non-canonical interaction sites, often filtered out by most algorithms. Through these screening tools we get the best candidates simultaneously targeting ACSL1, ACSL4 and SCD; which are miR-142, miR-544a and miR-19b-1. We finally proved miR-19b-1, the best prognosis candidate, involvement in cell invasion and lipid metabolism regulation. In accordance with previous findings describing the ACSL/SCD to promote invasion and migration, miR-19b-1 was able to inhibit CRC cells invasion. *In silico* analysis were an effective method to discover this miRNA implication in processes like focal adhesions and regulation of actin cytoskeleton, which regulate cellular behaviors such as cell proliferation, migration, and invasion [259,260]. MiR-19b-1 was further related to lipid metabolism accordingly to the condition of lipid metabolism enzymes of its targets. We postulate that miR-19b-1 could act by inhibiting *de novo* lipogenesis by targeting fatty acid (FA) activating enzymes (ACSLs and SCD), and therefore the previous steps to TG synthesis, leading to less accumulation of lipid droplets. Furthermore, respiratory analysis suggested that miR-19b-1 compromises the respiratory capacity of cells. Inhibiting ACSL-mediated FA activation by miR-19b-1 would lead to a reduced β-oxidation, limiting maximal mitochondrial respiration and impaired spare capacity.

Wnt route was the most represented biological pathway common to the 3 candidate miRNAs designated by Panther analysis. Wnt pathway was demonstrated to be activated by ACSL/SCD mediated GSK3β phosphorylation [261]. Therefore, it would be interesting to study these miRNAs role over this network through Wnt regulation. Previous reports linked Wnt routes with our candidate miRNAs: miR-544a in gastric and lung cancer [262,263] or miR-142-3p in CRC [264]. Wnt over active route is also present in all Apc mutated organoids from stage I to stage IV, since Apc is the first gene in the adenocarcinoma sequence. Apc completed deletion provokes a hyperactive Wnt signaling [208,265]. Remarkably, the best candidate, miR-19b-1, preserves its protective role again in murine CRC-like organoids showing a steady decline throughout the increasing aggressive stages. A deeper study of the effect of this miRNA over Wnt pathway in CRC-like organoids would be of great interest. As well, it is interesting the reported role of miR-19b-1 in digestive cancer stem cells, and also its role in CRC stem cells may be a prospective line of research [266].

miR-19b-1 was also reported to modulate chemokine production avoiding intestinal inflammation in Crohn's disease, which may ultimately prevent the derived disease, CRC [267], in line with our results. Regarding the other miRNA candidates, no statistically significant results were obtained in organoids. However, miR-142-3p was reported to target cancer stem cell markers such as the Wnt target, LGR5, in CRC cells [264]. Targeting LGR5 could be the main mechanism of action for miR-142-3p since ACSL/SCD are positively enriched in this stem cell marker, among others.

Regarding the previous discussion, miR-19b-1 could be considered not only a good prognosis marker but a promising therapeutic miRNA inhibiting CRC cells invasion. miRNA replacement therapy, as exemplified by the use of miR-34 for other types of human neoplasias [268] or miRNA dietary modulation as described for miR-19b-1 low protein diet in piglets [269] are examples of succesful miRNAs therapies.

Organoids bounties

Organoids were previously reported to represent a useful tool to study lipid metabolism [270] and previous studies have linked the critical role of FA metabolism to the intestinal epithelial integrity *in vivo* employing intestinal organoids [271]. We suggest organoids as a great platform to get insight into fatty acid metabolic anomalies in cancer progression and therefore, to assay ACSL/SCD protumorigenic axis action in CRC.

In this work we decided to employ murine organoids, which allow their genetic engineering and accurate control of the mutations for a better mechanistic characterization. Using patient tumor-derived biopsies would lead with the management of high variability that each tumor represents. Thus, our next step is to stablish paired organoids (tumor biopsies and its normal counterparts), where we will be able to assess ACSL/SCD status as well as doing drug testing, evidencing personalized medicine as a great tool to give an accurate prognosis and therapy.

We suggest the use of organoids as great platforms to study drug screening in controlled stages, as it was done in stages of prostate cancer looking for different Vitamin E effects [272]. Apart from the above-mentioned boundaries to use organoids as a precise platform to assay tumor stage-dependent drugs being suitable for personalized medicine, they also constitute an invaluable tool due to their relatively low costs. On one hand, because we can save in animal facilities costs but also to test High-Priced Drugs before administering it to a patient [273]. Moreover, from an ethical point of view, animal saving suffering could be reduced to minimal levels, once the pertinent analysis are fine tuned to minimal variables in organoids.

CONCLUSIONS

GENERAL CONCLUSIONS

1. ACSL/SCD network is a relevant metabolic axis for colon cancer progression able to confer cancer stem cells properties, increase cellular migration and invasion, stimulate several survival pathways and to present an upgraded energetic status and differential metabolomic phenotype that cannot be explained by additive functions of each enzyme separately.

2. ACSL/SCD network is susceptible to be targeted by different inhibitors.

-Specific ACSLs/SCD pharmacological inhibitors, A939572 and Triacsin C, affect cancer cell viability in a synergistic manner without showing an effect in normal colonocytes.

-Metformin becomes an appealing chemotherapy drug in first tumor phases, where it present a stronger downregulation on ACSL and SCD levels.

-MiR-19b-1 inhibits cancer cells invasion, counteracting the opposite effect exerted by its targets from the ACSL/SCD axis.

3. ACSL/SCD simultaneous overexpression represents an increased aggressiveness in a CRC tumor with an increased risk of relapse and disfavored outcomes in patients; while miR-19b-1 is postulated as a protective miRNA correlating with a better prognosis in CRC patients, evidencing a possible tandem of clinical biomarkers.

4. Organoids display a precise platform to assay tumor stage-dependent drugs being suitable for personalized medicine.

CONCLUSIONES

CONCLUSIONES GENERALES

1. La red ACSL/SCD se postula como un eje metabólico relevante para la progresión del cáncer de colon confiriendo propiedades de células madre del cáncer, a la vez que aumenta la invasión y la migración celular, estimula varias vías de supervivencia, presenta un estado energético mejorado y un fenotipo metabólico diferencial que no se puede explicar por las funciones aditivas de cada enzima por separado.

2. La red ACSL / SCD es susceptible de ser regulada por diferentes inhibidores:

- La combinación de dos inhibidores farmacológicos específicos de ACSL/SCD, denominados A939572 y Triacsin C, afectan a la viabilidad de las células cancerosas de manera sinérgica sin mostrar un efecto en los colonocitos normales.
-La Metformina se convierte en un fármaco antitumoral favorable en las primeras fases del tumor, donde presenta una regulación negativa sobre los niveles de ACSL y SCD.
-MiR-19b-1 inhibe la invasión de células cancerosas, contrarrestando el efecto opuesto ejercido por sus dianas ACSL/SCD.

3. La sobreexpresión simultánea de ACSL/SCD en un tumor de CCR supone un aumento de la agresividad con un mayor riesgo de recaída y un pronóstico desfavorable en los pacientes; mientras que el miR-19b-1 se postula como un miRNA protector cuya sobreexpresión se correlaciona con un mejor pronóstico en pacientes con CCR, lo que evidencia un posible tándem de biomarcadores clínicos.

4. 4. Los organoides suponen una plataforma de precisión para el análisis de fármacos dependientes de la etapa del tumor como medio para una medicina más personalizada.

REFERENCES

1. Ferlay, J. *et al.* Cancer incidence and mortality worldwide: sources, methods and major patterns in GLOBOCAN 2012. *Int. J. Cancer* **136,** E359-386 (2015).
2. International Agency for Research on Cancer. Global Cancer Observatory-Home.
3. Galceran, J. *et al.* Cancer incidence in Spain, 2015. *Clin. Transl. Oncol. Off. Publ. Fed. Span. Oncol. Soc. Natl. Cancer Inst. Mex.* **19,** 799–825 (2017).
4. Torre, L. A., Siegel, R. L., Ward, E. M. & Jemal, A. Global Cancer Incidence and Mortality Rates and Trends--An Update. *Cancer Epidemiol. Biomark. Prev. Publ. Am. Assoc. Cancer Res. Cosponsored Am. Soc. Prev. Oncol.* **25,** 16–27 (2016).
5. Esposito, K. *et al.* Colorectal cancer association with metabolic syndrome and its components: a systematic review with meta-analysis. *Endocrine* **44,** 634–647 (2013).
6. Bardou, M., Barkun, A. N. & Martel, M. Obesity and colorectal cancer. *Gut* **62,** 933–947 (2013).
7. Jochem, C. & Leitzmann, M. Obesity and Colorectal Cancer. *Recent Results Cancer Res. Fortschritte Krebsforsch. Progres Dans Rech. Sur Cancer* **208,** 17–41 (2016).
8. Armstrong, B. & Doll, R. Environmental factors and cancer incidence and mortality in different countries, with special reference to dietary practices. *Int. J. Cancer* **15,** 617–631 (1975).
9. Burkitt, D. P. Epidemiology of cancer of the colon and rectum. *Cancer* **28,** 3–13 (1971).
10. Bouvard, V. *et al.* Carcinogenicity of consumption of red and processed meat. *Lancet Oncol.* **16,** 1599–1600 (2015).
11. Terry, P. *et al.* Fruit, vegetables, dietary fiber, and risk of colorectal cancer. *J. Natl. Cancer Inst.* **93,** 525–533 (2001).
12. Ghafari, M., Mohamadian, M., Valipour, A. A. & Mohammadian-Hafshejani, A. Physical Activity and Colorectal Cancer. *Iran. J. Public Health* **45,** 1673–1674 (2016).
13. Slattery, M. L. Physical activity and colorectal cancer. *Sports Med. Auckl. NZ* **34,** 239–252 (2004).

14. Walter, V., Jansen, L., Hoffmeister, M. & Brenner, H. Smoking and survival of colorectal cancer patients: systematic review and meta-analysis. *Ann. Oncol. Off. J. Eur. Soc. Med. Oncol.* **25,** 1517–1525 (2014).

15. Varela-Rey, M., Woodhoo, A., Martinez-Chantar, M.-L., Mato, J. M. & Lu, S. C. Alcohol, DNA Methylation, and Cancer. *Alcohol Res. Curr. Rev.* **35,** 25–35 (2013).

16. Ballester, V., Rashtak, S. & Boardman, L. Clinical and molecular features of young-onset colorectal cancer. *World J. Gastroenterol.* **22,** 1736–1744 (2016).

17. Johns, L. E. & Houlston, R. S. A systematic review and meta-analysis of familial colorectal cancer risk. *Am. J. Gastroenterol.* **96,** 2992–3003 (2001).

18. Lynch, H. T. & de la Chapelle, A. Hereditary colorectal cancer. *N. Engl. J. Med.* **348,** 919–932 (2003).

19. Siegel, R. L., Miller, K. D. & Jemal, A. Cancer statistics, 2016. *CA. Cancer J. Clin.* **66,** 7–30 (2016).

20. Siegel, R. L., Miller, K. D. & Jemal, A. Cancer statistics, 2017. *CA. Cancer J. Clin.* **67,** 7–30 (2017).

21. Large intestine | Britannica.com. Available at: https://www.britannica.com/science/large-intestine. (Accessed: 20th September 2018)

22. Crosnier, C., Stamataki, D. & Lewis, J. Organizing cell renewal in the intestine: stem cells, signals and combinatorial control. *Nat. Rev. Genet.* **7,** 349–359 (2006).

23. Ponz de Leon, M. & Di Gregorio, C. Pathology of colorectal cancer. *Dig. Liver Dis. Off. J. Ital. Soc. Gastroenterol. Ital. Assoc. Study Liver* **33,** 372–388 (2001).

24. Colorectal Cancer Center - Johns Hopkins Medicine.

25. Fleming, M., Ravula, S., Tatishchev, S. F. & Wang, H. L. Colorectal carcinoma: Pathologic aspects. *J. Gastrointest. Oncol.* **3,** 153–173 (2012).

26. Amin, M. B. *et al. AJCC Cancer Staging Manual. American Joint Committee on Cancer. Colon and Rectum.* (Springer International Publishing, 2017).

27. Amin, M. B. *et al.* The Eighth Edition AJCC Cancer Staging Manual: Continuing to build a bridge from a population-based to a more 'personalized' approach to cancer staging. *CA. Cancer J. Clin.* **67,** 93–99 (2017).

28. American Cancer Society. *Cancer Facts & Figures 2018 | American Cancer Society*. (Atlanta, Ga: American Cancer Society, 2018).

29. Libutti, S., Salz, L., Willett, C. & Levine, R. Chapter 57: Cancer of the colon. in *Cancer: Principles and Practice of Oncology* (2015).

30. Libutti, S., Salz, L., Willett, C. & Levine, R. Chapter 58: Cancer of the rectum. in *Cancer: Principles and Practice of Oncology* (2015).

31. Prenen, H., Vecchione, L. & Van Cutsem, E. Role of targeted agents in metastatic colorectal cancer. *Target. Oncol.* **8,** 83–96 (2013).

32. Müller, M. F., Ibrahim, A. E. K. & Arends, M. J. Molecular pathological classification of colorectal cancer. *Virchows Arch.* **469,** 125–134 (2016).

33. Bogaert, J. & Prenen, H. Molecular genetics of colorectal cancer. *Ann. Gastroenterol.* **27,** 9–14 (2014).

34. Munkholm, P. Review article: the incidence and prevalence of colorectal cancer in inflammatory bowel disease. *Aliment. Pharmacol. Ther.* **18 Suppl 2,** 1–5 (2003).

35. Yamagishi, H., Kuroda, H., Imai, Y. & Hiraishi, H. Molecular pathogenesis of sporadic colorectal cancers. *Chin. J. Cancer* **35,** (2016).

36. Grady, W. M. & Carethers, J. M. Genomic and epigenetic instability in colorectal cancer pathogenesis. *Gastroenterology* **135,** 1079–1099 (2008).

37. Herman, J. G. *et al.* Incidence and functional consequences of hMLH1 promoter hypermethylation in colorectal carcinoma. *Proc. Natl. Acad. Sci. U. S. A.* **95,** 6870–6875 (1998).

38. Toyota, M. *et al.* CpG island methylator phenotype in colorectal cancer. *Proc. Natl. Acad. Sci. U. S. A.* **96,** 8681–8686 (1999).

39. Fearon, E. R. & Vogelstein, B. A genetic model for colorectal tumorigenesis. *Cell* **61,** 759–767 (1990).

40. Walther, A. *et al.* Genetic prognostic and predictive markers in colorectal cancer. *Nat. Rev. Cancer* **9,** 489–499 (2009).

41. Budinska, E. *et al.* Gene expression patterns unveil a new level of molecular heterogeneity in colorectal cancer. *J. Pathol.* **231,** 63–76 (2013).

42. Marisa, L. *et al.* Gene expression classification of colon cancer into molecular subtypes: characterization, validation, and prognostic value. *PLoS Med.* **10,** e1001453 (2013).

43. Roepman, P. *et al.* Colorectal cancer intrinsic subtypes predict chemotherapy benefit, deficient mismatch repair and epithelial-to-mesenchymal transition. *Int. J. Cancer* **134,** 552–562 (2014).

44. Sadanandam, A. *et al.* A colorectal cancer classification system that associates cellular phenotype and responses to therapy. *Nat. Med.* **19,** 619–625 (2013).

45. Schlicker, A. *et al.* Subtypes of primary colorectal tumors correlate with response to targeted treatment in colorectal cell lines. *BMC Med. Genomics* **5,** 66 (2012).

46. The Cancer Genome Atlas Home Page. *The Cancer Genome Atlas - National Cancer Institute* (2011). Available at: https://cancergenome.nih.gov/. (Accessed: 17th September 2018)

47. Network, T. C. G. A. Comprehensive molecular characterization of human colon and rectal cancer. *Nature* **487,** 330–337 (2012).

48. Guinney, J. *et al.* The Consensus Molecular Subtypes of Colorectal Cancer. *Nat. Med.* **21,** 1350–1356 (2015).

49. Hanahan, D. & Weinberg, R. A. The hallmarks of cancer. *Cell* **100,** 57–70 (2000).

50. Hanahan, D. & Weinberg, R. A. Hallmarks of cancer: the next generation. *Cell* **144,** 646–674 (2011).

51. Currie, E., Schulze, A., Zechner, R., Walther, T. C. & Farese, R. V. Cellular Fatty Acid Metabolism and Cancer. *Cell Metab.* **18,** 153–161 (2013).

52. Warburg, O. On the origin of cancer cells. *Science* **123,** 309–314 (1956).

53. Altman, B. J., Stine, Z. E. & Dang, C. V. From Krebs to clinic: glutamine metabolism to cancer therapy. *Nat. Rev. Cancer* **16,** 619–634 (2016).

54. DeBerardinis, R. J. & Chandel, N. S. Fundamentals of cancer metabolism. *Sci. Adv.* **2,** (2016).

55. Metallo, C. M. *et al.* Reductive glutamine metabolism by IDH1 mediates lipogenesis under hypoxia. *Nature* **481,** 380–384 (2011).

56. Carracedo, A., Cantley, L. C. & Pandolfi, P. P. Cancer metabolism: fatty acid oxidation in the limelight. *Nat. Rev. Cancer* **13,** 227–232 (2013).

57. Mashima, T., Seimiya, H. & Tsuruo, T. De novo fatty-acid synthesis and related pathways as molecular targets for cancer therapy. *Br. J. Cancer* **100,** 1369–1372 (2009).

58. Medes, G., Thomas, A. & Weinhouse, S. Metabolism of neoplastic tissue. IV. A study of lipid synthesis in neoplastic tissue slices in vitro. *Cancer Res.* **13,** 27–29 (1953).

59. Ookhtens, M., Kannan, R., Lyon, I. & Baker, N. Liver and adipose tissue contributions to newly formed fatty acids in an ascites tumor. *Am. J. Physiol.* **247,** R146-153 (1984).

60. Haven, F. L., Bloor, W. R. & Randall, C. The nature of the fatty acids of rats growing Walker carcinoma 256. *Cancer Res.* **11,** 619–623 (1951).

61. Baenke, F., Peck, B., Miess, H. & Schulze, A. Hooked on fat: the role of lipid synthesis in cancer metabolism and tumour development. *Dis. Model. Mech.* **6,** 1353–1363 (2013).

62. Röhrig, F. & Schulze, A. The multifaceted roles of fatty acid synthesis in cancer. *Nat. Rev. Cancer* **16,** 732–749 (2016).

63. Zaidi, N. *et al.* Lipogenesis and lipolysis: the pathways exploited by the cancer cells to acquire fatty acids. *Prog. Lipid Res.* **52,** 585–589 (2013).

64. Daniëls, V. W. *et al.* Cancer cells differentially activate and thrive on de novo lipid synthesis pathways in a low-lipid environment. *PloS One* **9,** e106913 (2014).

65. Kuo, C.-Y. & Ann, D. K. When fats commit crimes: fatty acid metabolism, cancer stemness and therapeutic resistance. *Cancer Commun. Lond. Engl.* **38,** 47 (2018).

66. Deshmukh, A., Deshpande, K., Arfuso, F., Newsholme, P. & Dharmarajan, A. Cancer stem cell metabolism: a potential target for cancer therapy. *Mol. Cancer* **15,** 69 (2016).

67. Vanni, S. Intracellular Lipid Droplets: From Structure to Function. *Lipid Insights* **10,** (2017).

68. Fujimoto, T. & Ohsaki, Y. Cytoplasmic lipid droplets: rediscovery of an old structure as a unique platform. *Ann. N. Y. Acad. Sci.* **1086,** 104–115 (2006).

69. Koizume, S. & Miyagi, Y. Lipid Droplets: A Key Cellular Organelle Associated with Cancer Cell Survival under Normoxia and Hypoxia. *Int. J. Mol. Sci.* **17,** (2016).

70. de Gonzalo-Calvo, D. *et al.* Intratumor cholesteryl ester accumulation is associated with human breast cancer proliferation and aggressive potential: a molecular and clinicopathological study. *BMC Cancer* **15,** 460 (2015).

71. Yue, S. *et al.* Cholesteryl ester accumulation induced by PTEN loss and PI3K/AKT activation underlies human prostate cancer aggressiveness. *Cell Metab.* **19,** 393–406 (2014).

72. Cheng, M., Bhujwalla, Z. M. & Glunde, K. Targeting Phospholipid Metabolism in Cancer. *Front. Oncol.* **6,** (2016).

73. Agarwal, A. K. Lysophospholipid acyltransferases: 1-acylglycerol-3-phosphate O-acyltransferases. From discovery to disease. *Curr. Opin. Lipidol.* **23,** 290–302 (2012).

74. Takeuchi, K. & Reue, K. Biochemistry, physiology, and genetics of GPAT, AGPAT, and lipin enzymes in triglyceride synthesis. *Am. J. Physiol. Endocrinol. Metab.* **296,** E1195-1209 (2009).

75. Marchan, R. *et al.* Glycerol-3-phosphate Acyltransferase 1 Promotes Tumor Cell Migration and Poor Survival in Ovarian Carcinoma. *Cancer Res.* **77,** 4589–4601 (2017).

76. He, J. *et al.* Lipin-1 regulation of phospholipid synthesis maintains endoplasmic reticulum homeostasis and is critical for triple-negative breast cancer cell survival. *FASEB J. Off. Publ. Fed. Am. Soc. Exp. Biol.* **31,** 2893–2904 (2017).

77. Song, L. *et al.* Silencing LPAATβ inhibits tumor growth of cisplatin-resistant human osteosarcoma in vivo and in vitro. *Int. J. Oncol.* **50,** 535–544 (2017).

78. Bagnato, C. & Igal, R. A. Overexpression of diacylglycerol acyltransferase-1 reduces phospholipid synthesis, proliferation, and invasiveness in simian virus 40-transformed human lung fibroblasts. *J. Biol. Chem.* **278,** 52203–52211 (2003).

79. Mitra, R., Le, T. T., Gorjala, P. & Goodman, O. B. Positive regulation of prostate cancer cell growth by lipid droplet forming and processing enzymes DGAT1 and ABHD5. *BMC Cancer* **17,** 631 (2017).

80. Luo, X. *et al.* Emerging roles of lipid metabolism in cancer metastasis. *Mol. Cancer* **16,** (2017).

81. Tirinato, L. *et al.* An Overview of Lipid Droplets in Cancer and Cancer Stem Cells. *Stem Cells Int.* **2017,** (2017).

82. Zagani, R., El-Assaad, W., Gamache, I. & Teodoro, J. G. Inhibition of adipose triglyceride lipase (ATGL) by the putative tumor suppressor G0S2 or a small molecule inhibitor attenuates the growth of cancer cells. *Oncotarget* **6,** 28282–28295 (2015).

83. Al-Zoughbi, W. *et al.* Loss of adipose triglyceride lipase is associated with human cancer and induces mouse pulmonary neoplasia. *Oncotarget* **7,** 33832–33840 (2016).

84. Vegliante, R., Leo, L. D., Ciccarone, F. & Ciriolo, M. R. Hints on ATGL implications in cancer: beyond bioenergetic clues. *Cell Death Dis.* **9,** 316 (2018).

85. Tomin, T. *et al.* Deletion of Adipose Triglyceride Lipase Links Triacylglycerol Accumulation to a More-Aggressive Phenotype in A549 Lung Carcinoma Cells. *J. Proteome Res.* **17,** 1415–1425 (2018).

86. Das, S. K. *et al.* Adipose triglyceride lipase contributes to cancer-associated cachexia. *Science* **333,** 233–238 (2011).

87. Baba, Y. *et al.* Expression of monoacylglycerol lipase as a marker of tumour invasion and progression in malignant melanoma. *J. Eur. Acad. Dermatol. Venereol. JEADV* **31,** 2038–2045 (2017).

88. Nomura, D. K. *et al.* Monoacylglycerol lipase regulates a fatty acid network that promotes cancer pathogenesis. *Cell* **140,** 49–61 (2010).

89. Melone, M. A. B. *et al.* The carnitine system and cancer metabolic plasticity. *Cell Death Dis.* **9,** (2018).

90. Gu, J.-J. *et al.* Mitochondrial carnitine palmitoyl transferase-II inactivity aggravates lipid accumulation in rat hepatocarcinogenesis. *World J. Gastroenterol.* **23,** 256–264 (2017).

91. Liu, P.-P. *et al.* Elimination of chronic lymphocytic leukemia cells in stromal microenvironment by targeting CPT with an antiangina drug perhexiline. *Oncogene* **35,** 5663–5673 (2016).

92. Chmurzyńska, A. The multigene family of fatty acid-binding proteins (FABPs): function, structure and polymorphism. *J. Appl. Genet.* **47,** 39–48 (2006).

93. Guaita-Esteruelas, S., Gumà, J., Masana, L. & Borràs, J. The peritumoural adipose tissue microenvironment and cancer. The roles of fatty acid binding protein 4 and fatty acid binding protein 5. *Mol. Cell. Endocrinol.* **462,** 107–118 (2018).

94. Thompson, K. J. *et al.* Altered fatty acid-binding protein 4 (FABP4) expression and function in human and animal models of hepatocellular carcinoma. *Liver Int. Off. J. Int. Assoc. Study Liver* (2017). doi:10.1111/liv.13639

95. Kim, S., Lee, Y. & Koo, J. S. Differential expression of lipid metabolism-related proteins in different breast cancer subtypes. *PloS One* **10,** e0119473 (2015).

96. Hui, X. *et al.* Adipocyte fatty acid-binding protein modulates inflammatory responses in macrophages through a positive feedback loop involving c-Jun NH2-terminal kinases and activator protein-1. *J. Biol. Chem.* **285,** 10273–10280 (2010).

97. Terra, X. *et al.* FABP 4 is associated with inflammatory markers and metabolic syndrome in morbidly obese women. *Eur. J. Endocrinol.* **164,** 539–547 (2011).

98. Shu, L. *et al.* A-FABP mediates adaptive thermogenesis by promoting intracellular activation of thyroid hormones in brown adipocytes. *Nat. Commun.* **8,** (2017).

99. Gnoni, G. V., Priore, P., Geelen, M. J. H. & Siculella, L. The mitochondrial citrate carrier: metabolic role and regulation of its activity and expression. *IUBMB Life* **61,** 987–994 (2009).

100. Kolukula, V. K. *et al.* SLC25A1, or CIC, is a novel transcriptional target of mutant p53 and a negative tumor prognostic marker. *Oncotarget* **5,** 1212–1225 (2014).

101. Ozkaya, A. B., Ak, H., Atay, S. & Aydin, H. H. Targeting mitochondrial citrate transport in breast cancer cell lines. *Anticancer Agents Med. Chem.* **15,** 374–381 (2015).

102. Khwairakpam, A. D. *et al.* ATP Citrate Lyase (ACLY): A Promising Target for Cancer Prevention and Treatment. *Current Drug Targets* (2015). Available at: http://www.eurekaselect.com/127128/article. (Accessed: 14th March 2018)

103. Zaidi, N., Swinnen, J. V. & Smans, K. ATP-citrate lyase: a key player in cancer metabolism. *Cancer Res.* **72,** 3709–3714 (2012).

104. Wellen, K. E. *et al.* ATP-citrate lyase links cellular metabolism to histone acetylation. *Science* **324,** 1076–1080 (2009).

105. Pietrocola, F., Galluzzi, L., Bravo-San Pedro, J. M., Madeo, F. & Kroemer, G. Acetyl coenzyme A: a central metabolite and second messenger. *Cell Metab.* **21,** 805–821 (2015).

106. Wang, C. *et al.* The acetyl-CoA carboxylase enzyme: a target for cancer therapy? *Expert Rev. Anticancer Ther.* **15,** 667–676 (2015).

107. Yahagi, N. *et al.* Co-ordinate activation of lipogenic enzymes in hepatocellular carcinoma. *Eur. J. Cancer Oxf. Engl. 1990* **41,** 1316–1322 (2005).

108. Milgraum, L. Z., Witters, L. A., Pasternack, G. R. & Kuhajda, F. P. Enzymes of the fatty acid synthesis pathway are highly expressed in in situ breast carcinoma. *Clin. Cancer Res. Off. J. Am. Assoc. Cancer Res.* **3,** 2115–2120 (1997).

109. Chajès, V., Cambot, M., Moreau, K., Lenoir, G. M. & Joulin, V. Acetyl-CoA carboxylase alpha is essential to breast cancer cell survival. *Cancer Res.* **66,** 5287–5294 (2006).

110. Flavin, R., Peluso, S., Nguyen, P. L. & Loda, M. Fatty acid synthase as a potential therapeutic target in cancer. *Future Oncol. Lond. Engl.* **6,** 551–562 (2010).

111. Kuhajda, F. P. Fatty acid synthase and cancer: new application of an old pathway. *Cancer Res.* **66,** 5977–5980 (2006).

112. Menendez, J. A. & Lupu, R. Oncogenic properties of the endogenous fatty acid metabolism: molecular pathology of fatty acid synthase in cancer cells. *Curr. Opin. Clin. Nutr. Metab. Care* **9,** 346–357 (2006).

113. Menendez, J. A. & Lupu, R. Fatty acid synthase and the lipogenic phenotype in cancer pathogenesis. *Nat. Rev. Cancer* **7,** 763–777 (2007).

114. Menendez, J. A., Lupu, R. & Colomer, R. Targeting fatty acid synthase: potential for therapeutic intervention in her-2/neu-overexpressing breast cancer. *Drug News Perspect.* **18,** 375–385 (2005).

115. Swinnen, J. V., Brusselmans, K. & Verhoeven, G. Increased lipogenesis in cancer cells: new players, novel targets. *Curr. Opin. Clin. Nutr. Metab. Care* **9,** 358–365 (2006).

116. Menendez, J. A. & Lupu, R. Fatty acid synthase (FASN) as a therapeutic target in breast cancer. *Expert Opin. Ther. Targets* **21,** 1001–1016 (2017).

117. Horton, J. D., Goldstein, J. L. & Brown, M. S. SREBPs: activators of the complete program of cholesterol and fatty acid synthesis in the liver. *J. Clin. Invest.* **109,** 1125–1131 (2002).

118. Shao, W. & Espenshade, P. J. Expanding roles for SREBP in metabolism. *Cell Metab.* **16,** 414–419 (2012).

119. Huang, W.-C., Li, X., Liu, J., Lin, J. & Chung, L. W. K. Activation of androgen receptor, lipogenesis, and oxidative stress converged by SREBP-1 is responsible for regulating growth and progression of prostate cancer cells. *Mol. Cancer Res. MCR* **10,** 133–142 (2012).

120. Bao, J. *et al.* SREBP-1 is an independent prognostic marker and promotes invasion and migration in breast cancer. *Oncol. Lett.* **12,** 2409–2416 (2016).

121. Yan, S. *et al.* Long-chain acyl-CoA synthetase in fatty acid metabolism involved in liver and other diseases: an update. *World J. Gastroenterol.* **21,** 3492–3498 (2015).

122. Grevengoed, T. J., Klett, E. L. & Coleman, R. A. Acyl-CoA Metabolism and Partitioning. *Annu. Rev. Nutr.* **34,** 1–30 (2014).

123. Soupene, E. & Kuypers, F. A. Mammalian long-chain acyl-CoA synthetases. *Exp. Biol. Med. Maywood NJ* **233,** 507–521 (2008).

124. Kanter, J. E., Tang, C., Oram, J. F. & Bornfeldt, K. E. Acyl-CoA synthetase 1 is required for oleate and linoleate mediated inhibition of cholesterol efflux through ATP-binding cassette transporter A1 in macrophages. *Biochim. Biophys. Acta* **1821,** 358–364 (2012).

125. Grevengoed, T. J. *et al.* Acyl-CoA synthetase 1 deficiency alters cardiolipin species and impairs mitochondrial function. *J. Lipid Res.* **56,** 1572–1582 (2015).

126. Poppelreuther, M. *et al.* The N-terminal region of acyl-CoA synthetase 3 is essential for both the localization on lipid droplets and the function in fatty acid uptake. *J. Lipid Res.* **53,** 888–900 (2012).

127. Lewin, T. M., Kim, J. H., Granger, D. A., Vance, J. E. & Coleman, R. A. Acyl-CoA synthetase isoforms 1, 4, and 5 are present in different subcellular membranes in rat liver and can be inhibited independently. *J. Biol. Chem.* **276,** 24674–24679 (2001).

128. Kang, M.-J. *et al.* A novel arachidonate-preferring acyl-CoA synthetase is present in steroidogenic cells of the rat adrenal, ovary, and testis. *Proc. Natl. Acad. Sci. U. S. A.* **94,** 2880–2884 (1997).

129. Golej, D. L. *et al.* Long-chain acyl-CoA synthetase 4 modulates prostaglandin E_2 release from human arterial smooth muscle cells. *J. Lipid Res.* **52,** 782–793 (2011).

130. Cooke, M., Orlando, U., Maloberti, P., Podestá, E. J. & Maciel, F. C. Tyrosine phosphatase SHP2 regulates the expression of acyl-CoA synthetase ACSL4. *J. Lipid Res.* **52,** 1936–1948 (2011).

131. Tang, Y., Zhou, J., Hooi, S. C., Jiang, Y.-M. & Lu, G.-D. Fatty acid activation in carcinogenesis and cancer development: Essential roles of long-chain acyl-CoA synthetases. *Oncol. Lett.* **16,** 1390–1396 (2018).

132. Chen, W.-C. *et al.* Systematic Analysis of Gene Expression Alterations and Clinical Outcomes for Long-Chain Acyl-Coenzyme A Synthetase Family in Cancer. *PLoS ONE* **11,** (2016).

133. Soupene, E., Dinh, N. P., Siliakus, M. & Kuypers, F. A. Activity of the acyl-CoA synthetase ACSL6 isoforms: role of the fatty acid Gate-domains. *BMC Biochem.* **11,** 18 (2010).

134. Lopes-Marques, M., Cunha, I., Reis-Henriques, M. A., Santos, M. M. & Castro, L. F. C. Diversity and history of the long-chain acyl-CoA synthetase (Acsl) gene family in vertebrates. *BMC Evol. Biol.* **13,** 271 (2013).

135. Van Horn, C. G. *et al.* Characterization of recombinant long-chain rat acyl-CoA synthetase isoforms 3 and 6: identification of a novel variant of isoform 6. *Biochemistry (Mosc.)* **44,** 1635–1642 (2005).

136. Heimerl, S. *et al.* Alterations in intestinal fatty acid metabolism in inflammatory bowel disease. *Biochim. Biophys. Acta* **1762,** 341–350 (2006).

137. Kim, E. R. & Chang, D. K. Colorectal cancer in inflammatory bowel disease: The risk, pathogenesis, prevention and diagnosis. *World J. Gastroenterol. WJG* **20,** 9872–9881 (2014).

138. Pei, Z. *et al.* Very long-chain acyl-CoA synthetase 3: overexpression and growth dependence in lung cancer. *PloS One* **8,** e69392 (2013).

139. Marques, R. B. *et al.* Modulation of androgen receptor signaling in hormonal therapy-resistant prostate cancer cell lines. *PloS One* **6,** e23144 (2011).

140. Cao, Y., Pearman, A. T., Zimmerman, G. A., McIntyre, T. M. & Prescott, S. M. Intracellular unesterified arachidonic acid signals apoptosis. *Proc. Natl. Acad. Sci. U. S. A.* **97,** 11280–11285 (2000).

141. Cao, Y., Dave, K. B., Doan, T. P. & Prescott, S. M. Fatty acid CoA ligase 4 is up-regulated in colon adenocarcinoma. *Cancer Res.* **61,** 8429–8434 (2001).

142. Sung, Y. K. *et al.* Regulation of cell growth by fatty acid-CoA ligase 4 in human hepatocellular carcinoma cells. *Exp. Mol. Med.* **39,** 477–482 (2007).

143. Sun, X.-J. & Xu, G.-L. Overexpression of Acyl-CoA Ligase 4 (ACSL4) in Patients with Hepatocellular Carcinoma and its Prognosis. *Med. Sci. Monit. Int. Med. J. Exp. Clin. Res.* **23,** 4343–4350 (2017).

144. Wu, X. *et al.* ACSL4 promotes prostate cancer growth, invasion and hormonal resistance. *Oncotarget* **6,** 44849–44863 (2015).

145. Ye, X., Zhang, Y., Wang, X., Li, Y. & Gao, Y. Tumor-suppressive functions of long-chain acyl-CoA synthetase 4 in gastric cancer. *IUBMB Life* **68,** 320–327 (2016).

146. Pitule, P. *et al.* Differential expression and prognostic role of selected genes in colorectal cancer patients. *Anticancer Res.* **33,** 4855–4865 (2013).

147. Mashima, T., Sato, S., Sugimoto, Y., Tsuruo, T. & Seimiya, H. Promotion of glioma cell survival by acyl-CoA synthetase 5 under extracellular acidosis conditions. *Oncogene* **28,** 9–19 (2009).

148. Enoch, H. G., Catalá, A. & Strittmatter, P. Mechanism of rat liver microsomal stearyl-CoA desaturase. Studies of the substrate specificity, enzyme-substrate interactions, and the function of lipid. *J. Biol. Chem.* **251,** 5095–5103 (1976).

149. Igal, R. A. Stearoyl-CoA desaturase-1: a novel key player in the mechanisms of cell proliferation, programmed cell death and transformation to cancer. *Carcinogenesis* **31,** 1509–1515 (2010).

150. Beloribi-Djefaflia, S., Vasseur, S. & Guillaumond, F. Lipid metabolic reprogramming in cancer cells. *Oncogenesis* **5,** e189 (2016).

151. Roongta, U. V. *et al.* Cancer cell dependence on unsaturated fatty acids implicates stearoyl-CoA desaturase as a target for cancer therapy. *Mol. Cancer Res. MCR* **9,** 1551–1561 (2011).

152. Holder, A. M. *et al.* High stearoyl-CoA desaturase 1 expression is associated with shorter survival in breast cancer patients. *Breast Cancer Res. Treat.* **137,** 319–327 (2013).

153. Wood, C. B. *et al.* Increase of oleic acid in erythrocytes associated with malignancies. *Br. Med. J. Clin. Res. Ed* **291,** 163–165 (1985).

154. Igal, R. A. Stearoyl CoA desaturase-1: New insights into a central regulator of cancer metabolism. *Biochim. Biophys. Acta* **1861,** 1865–1880 (2016).

155. Arous, C., Naïmi, M. & Van Obberghen, E. Oleate-mediated activation of phospholipase D and mammalian target of rapamycin (mTOR) regulates proliferation and rapamycin sensitivity of hepatocarcinoma cells. *Diabetologia* **54,** 954–964 (2011).

156. Sadowski, M. C. *et al.* The fatty acid synthase inhibitor triclosan: repurposing an anti-microbial agent for targeting prostate cancer. *Oncotarget* **5,** 9362–9381 (2014).

157. Vinciguerra, M. *et al.* Unsaturated fatty acids promote hepatoma proliferation and progression through downregulation of the tumor suppressor PTEN. *J. Hepatol.* **50,** 1132–1141 (2009).

158. Peck, B. *et al.* Inhibition of fatty acid desaturation is detrimental to cancer cell survival in metabolically compromised environments. *Cancer Metab.* **4,** 6 (2016).

159. Chen, L. *et al.* Stearoyl-CoA desaturase-1 mediated cell apoptosis in colorectal cancer by promoting ceramide synthesis. *Sci. Rep.* **6,** 19665 (2016).

160. Ran, H. *et al.* Stearoyl-CoA desaturase-1 promotes colorectal cancer metastasis in response to glucose by suppressing PTEN. *J. Exp. Clin. Cancer Res. CR* **37,** 54 (2018).

161. Qiu, Y. *et al.* A distinct metabolic signature of human colorectal cancer with prognostic potential. *Clin. Cancer Res. Off. J. Am. Assoc. Cancer Res.* **20,** 2136–2146 (2014).

162. Vargas, T. *et al.* ColoLipidGene: signature of lipid metabolism-related genes to predict prognosis in stage-II colon cancer patients. *Oncotarget* **6,** 7348–7363 (2015).

163. Scaglia, N., Chisholm, J. W. & Igal, R. A. Inhibition of StearoylCoA Desaturase-1 Inactivates Acetyl-CoA Carboxylase and Impairs Proliferation in Cancer Cells: Role of AMPK. *PLOS ONE* **4,** e6812 (2009).

164. Li, L. O., Klett, E. L. & Coleman, R. A. Acyl-CoA synthesis, lipid metabolism and lipotoxicity. *Biochim. Biophys. Acta* **1801,** 246–251 (2010).

165. Goodridge, A. G. Regulation of the activity of acetyl coenzyme A carboxylase by palmitoyl coenzyme A and citrate. *J. Biol. Chem.* **247,** 6946–6952 (1972).

166. Munday, M. R. & Hemingway, C. J. The regulation of acetyl-CoA carboxylase--a potential target for the action of hypolipidemic agents. *Adv. Enzyme Regul.* **39,** 205–234 (1999).

167. Ahmad, N., Haider, S., Jagannathan, S., Anaissie, E. & Driscoll, J. J. MicroRNA theragnostics for the clinical management of multiple myeloma. *Leukemia* **28,** 732–738 (2014).

168. Lee, R. C., Feinbaum, R. L. & Ambros, V. The C. elegans heterochronic gene lin-4 encodes small RNAs with antisense complementarity to lin-14. *Cell* **75,** 843–854 (1993).

169. MacFarlane, L.-A. & Murphy, P. R. MicroRNA: Biogenesis, Function and Role in Cancer. *Curr. Genomics* **11,** 537–561 (2010).

170. Wahid, F., Shehzad, A., Khan, T. & Kim, Y. Y. MicroRNAs: synthesis, mechanism, function, and recent clinical trials. *Biochim. Biophys. Acta* **1803,** 1231–1243 (2010).

171. Bartel, D. P. MicroRNAs: Genomics, Biogenesis, Mechanism, and Function. *Cell* **116,** 281–297 (2004).

172. Ladomery, M. R., Maddocks, D. G. & Wilson, I. D. MicroRNAs: their discovery, biogenesis, function and potential use as biomarkers in non-invasive prenatal diagnostics. *Int. J. Mol. Epidemiol. Genet.* **2,** 253–260 (2011).

173. Pedersen, I. M. *et al.* Interferon modulation of cellular microRNAs as an antiviral mechanism. *Nature* **449,** 919–922 (2007).

174. Triboulet, R. *et al.* Suppression of microRNA-silencing pathway by HIV-1 during virus replication. *Science* **315,** 1579–1582 (2007).

175. Sempere, L. F. *et al.* Expression profiling of mammalian microRNAs uncovers a subset of brain-expressed microRNAs with possible roles in murine and human neuronal differentiation. *Genome Biol.* **5,** R13 (2004).

176. Smirnova, L. *et al.* Regulation of miRNA expression during neural cell specification. *Eur. J. Neurosci.* **21,** 1469–1477 (2005).

177. Johnnidis, J. B. *et al.* Regulation of progenitor cell proliferation and granulocyte function by microRNA-223. *Nature* **451,** 1125–1129 (2008).

178. Sonkoly, E. *et al.* MicroRNAs: novel regulators involved in the pathogenesis of psoriasis? *PloS One* **2,** e610 (2007).

179. Wang, S. *et al.* The endothelial-specific microRNA miR-126 governs vascular integrity and angiogenesis. *Dev. Cell* **15,** 261–271 (2008).

180. da Costa Martins, P. A., Leptidis, S., Salic, K. & De Windt, L. J. MicroRNA regulation in cardiovascular disease. *Curr. Drug Targets* **11,** 900–906 (2010).

181. Güller, I. & Russell, A. P. MicroRNAs in skeletal muscle: their role and regulation in development, disease and function. *J. Physiol.* **588,** 4075–4087 (2010).

182. Leung, A. K. L. & Sharp, P. A. MicroRNA functions in stress responses. *Mol. Cell* **40,** 205–215 (2010).

183. Zhang, C. Novel functions for small RNA molecules. *Curr. Opin. Mol. Ther.* **11,** 641–651 (2009).

184. Di Leva, G., Garofalo, M. & Croce, C. M. microRNAs in cancer. *Annu. Rev. Pathol.* **9,** 287–314 (2014).

185. Zhang, B., Pan, X., Cobb, G. P. & Anderson, T. A. microRNAs as oncogenes and tumor suppressors. *Dev. Biol.* **302,** 1–12 (2007).

186. Leal, J. A., Feliciano, A. & Lleonart, M. E. Stem cell microRNAs in senescence and immortalization: novel players in cancer therapy. *Med. Res. Rev.* **33,** 112–138 (2013).

187. Raza, U., Zhang, J. D. & Sahin, O. MicroRNAs: master regulators of drug resistance, stemness, and metastasis. *J. Mol. Med. Berl. Ger.* **92,** 321–336 (2014).

188. Anand, S. A brief primer on microRNAs and their roles in angiogenesis. *Vasc. Cell* **5,** 2 (2013).

189. Ding, X.-M. MicroRNAs: regulators of cancer metastasis and epithelial-mesenchymal transition (EMT). *Chin. J. Cancer* **33,** 140–147 (2014).

190. Garzon, R., Fabbri, M., Cimmino, A., Calin, G. A. & Croce, C. M. MicroRNA expression and function in cancer. *Trends Mol. Med.* **12,** 580–587 (2006).

191. Paliouras, A. R., Monteverde, T. & Garofalo, M. Oncogene-induced regulation of microRNA expression: Implications for cancer initiation, progression and therapy. *Cancer Lett.* **421,** 152–160 (2018).

192. Calin, G. A. *et al.* MicroRNA profiling reveals distinct signatures in B cell chronic lymphocytic leukemias. *Proc. Natl. Acad. Sci. U. S. A.* **101,** 11755–11760 (2004).

193. Lu, J. *et al.* MicroRNA expression profiles classify human cancers. *Nature* **435,** 834–838 (2005).

194. Mayr, C., Hemann, M. T. & Bartel, D. P. Disrupting the Pairing Between let-7 and Hmga2 Enhances Oncogenic Transformation. *Science* **315,** 1576–1579 (2007).

195. Krek, A. *et al.* Combinatorial microRNA target predictions. *Nat. Genet.* **37,** 495–500 (2005).

196. Gambari, R., Brognara, E., Spandidos, D. A. & Fabbri, E. Targeting oncomiRNAs and mimicking tumor suppressor miRNAs: New trends in the development of miRNA therapeutic strategies in oncology (Review). *Int. J. Oncol.* **49,** 5–32 (2016).

197. Concepcion, C. P., Bonetti, C. & Ventura, A. The miR-17-92 family of microRNA clusters in development and disease. *Cancer J. Sudbury Mass* **18,** 262–267 (2012).

198. Mendell, J. T. miRiad roles for the miR-17-92 cluster in development and disease. *Cell* **133,** 217–222 (2008).

199. Ferland-McCollough, D., Ozanne, S. E., Siddle, K., Willis, A. E. & Bushell, M. The involvement of microRNAs in Type 2 diabetes. *Biochem. Soc. Trans.* **38,** 1565–1570 (2010).

200. De Smaele, E., Ferretti, E. & Gulino, A. MicroRNAs as biomarkers for CNS cancer and other disorders. *Brain Res.* **1338,** 100–111 (2010).

201. Fittipaldi, S. *et al.* miRNA Signature of Hepatocellular Carcinoma Vascularization: How the Controls Can Influence the Signature. *Dig. Dis. Sci.* **62,** 2397–2407 (2017).

202. Xiong, D.-D. *et al.* A nine-miRNA signature as a potential diagnostic marker for breast carcinoma: An integrated study of 1,110 cases. *Oncol. Rep.* **37,** 3297–3304 (2017).

203. Cortez, M. A. *et al.* MicroRNAs in body fluids—the mix of hormones and biomarkers. *Nat. Rev. Clin. Oncol.* **8,** 467–477 (2011).

204. Sato, T. & Clevers, H. SnapShot: Growing Organoids from Stem Cells. *Cell* **161,** 1700–1700.e1 (2015).

205. Werner, K., Weitz, J. & Stange, D. E. Organoids as Model Systems for Gastrointestinal Diseases: Tissue Engineering Meets Genetic Engineering. *Curr. Pathobiol. Rep.* **4,** 1–9 (2016).

206. Sato, T. *et al.* Single Lgr5 stem cells build crypt-villus structures in vitro without a mesenchymal niche. *Nature* **459,** 262–265 (2009).

207. Radtke, F. & Clevers, H. Self-renewal and cancer of the gut: two sides of a coin. *Science* **307,** 1904–1909 (2005).

208. Sato, T. *et al.* Long-term expansion of epithelial organoids from human colon, adenoma, adenocarcinoma, and Barrett's epithelium. *Gastroenterology* **141,** 1762–1772 (2011).

209. Mini Review: Intestinal Organoid Culture. Available at: https://www.stemcell.com/intestinal-organoid-culture-lp.html. (Accessed: 20th September 2018)

210. Mou, H., Brazauskas, K. & Rajagopal, J. Personalized medicine for cystic fibrosis: establishing human model systems. *Pediatr. Pulmonol.* **50 Suppl 40,** S14-23 (2015).

211. Drost, J. *et al.* Sequential cancer mutations in cultured human intestinal stem cells. *Nature* **521,** 43–47 (2015).

212. Koo, B.-K. *et al.* Controlled gene expression in primary Lgr5 organoid cultures. *Nat. Methods* **9,** 81–83 (2012).

213. Matano, M. *et al.* Modeling colorectal cancer using CRISPR-Cas9-mediated engineering of human intestinal organoids. *Nat. Med.* **21,** 256–262 (2015).

214. Schwank, G., Andersson-Rolf, A., Koo, B.-K., Sasaki, N. & Clevers, H. Generation of BAC Transgenic Epithelial Organoids. *PLOS ONE* **8,** e76871 (2013).

215. Barker, N. *et al.* Lgr5(+ve) stem cells drive self-renewal in the stomach and build long-lived gastric units in vitro. *Cell Stem Cell* **6,** 25–36 (2010).

216. Boj, S. F. *et al.* Organoid models of human and mouse ductal pancreatic cancer. *Cell* **160,** 324–338 (2015).

217. Huch, M. *et al.* In vitro expansion of single Lgr5+ liver stem cells induced by Wnt-driven regeneration. *Nature* **494,** 247–250 (2013).

218. van de Wetering, M. *et al.* Prospective derivation of a living organoid biobank of colorectal cancer patients. *Cell* **161,** 933–945 (2015).

219. Russell, D. & Snyder, S. H. Amine synthesis in rapidly growing tissues: ornithine decarboxylase activity in regenerating rat liver, chick embryo, and various tumors. *Proc. Natl. Acad. Sci. U. S. A.* **60,** 1420–1427 (1968).

220. Soda, K. The mechanisms by which polyamines accelerate tumor spread. *J. Exp. Clin. Cancer Res. CR* **30,** 95 (2011).

221. He, Y. *et al.* Nuclear localization of metabolic enzymes in immunity and metastasis. *Biochim. Biophys. Acta* **1868,** 359–371 (2017).

222. Chou, C.-C. *et al.* AMPK reverses the mesenchymal phenotype of cancer cells by targeting the Akt-MDM2-Foxo3a signaling axis. *Cancer Res.* **74,** 4783–4795 (2014).

223. Fritz, V. *et al.* Abrogation of de novo lipogenesis by stearoyl-CoA desaturase 1 inhibition interferes with oncogenic signaling and blocks prostate cancer progression in mice. *Mol. Cancer Ther.* **9,** 1740–1754 (2010).

224. Za'tara, G. *et al.* AMPK activation by long chain fatty acyl analogs. *Biochem. Pharmacol.* **76,** 1263–1275 (2008).

225. Carnero, A. & Paramio, J. M. The PTEN/PI3K/AKT Pathway in vivo, Cancer Mouse Models. *Front. Oncol.* **4,** (2014).

226. Schooneman, M. G., Vaz, F. M., Houten, S. M. & Soeters, M. R. Acylcarnitines. *Diabetes* **62,** 1–8 (2013).

227. Li, L. O. *et al.* Liver-specific loss of long chain acyl-CoA synthetase-1 decreases triacylglycerol synthesis and beta-oxidation and alters phospholipid fatty acid composition. *J. Biol. Chem.* **284,** 27816–27826 (2009).

228. Chughtai, K., Jiang, L., Greenwood, T. R., Glunde, K. & Heeren, R. M. A. Mass spectrometry images acylcarnitines, phosphatidylcholines, and sphingomyelin in MDA-MB-231 breast tumor models. *J. Lipid Res.* **54,** 333–344 (2013).

229. Ganti, S. *et al.* Urinary acylcarnitines are altered in human kidney cancer. *Int. J. Cancer J. Int. Cancer* **130,** 2791–2800 (2012).

230. Wettersten, H. I. *et al.* Grade-Dependent Metabolic Reprogramming in Kidney Cancer Revealed by Combined Proteomics and Metabolomics Analysis. *Cancer Res.* **75,** 2541–2552 (2015).

231. Nieto, M. A. & Cano, A. The epithelial-mesenchymal transition under control: global programs to regulate epithelial plasticity. *Semin. Cancer Biol.* **22,** 361–368 (2012).

232. Sánchez-Martínez, R., Cruz-Gil, S., García-Álvarez, M. S., Reglero, G. & Molina, A. R. Complementary ACSL isoforms contribute to a non-Warburg advantageous energetic status characterizing invasive colon cancer cells. *Sci. Rep.* **7,** 11143 (2017).

233. Wang, H. *et al.* Epithelial-mesenchymal transition (EMT) induced by TNF-α requires AKT/GSK-3β-mediated stabilization of snail in colorectal cancer. *PloS One* **8,** e56664 (2013).

234. Neil, J. R., Johnson, K. M., Nemenoff, R. A. & Schiemann, W. P. Cox-2 inactivates Smad signaling and enhances EMT stimulated by TGF-beta through a PGE2-dependent mechanisms. *Carcinogenesis* **29,** 2227–2235 (2008).

235. Coleman, R. A., Lewin, T. M., Van Horn, C. G. & Gonzalez-Baró, M. R. Do long-chain acyl-CoA synthetases regulate fatty acid entry into synthetic versus degradative pathways? *J. Nutr.* **132,** 2123–2126 (2002).

236. Ha, G.-H., Park, J.-S. & Breuer, E.-K. Y. TACC3 promotes epithelial-mesenchymal transition (EMT) through the activation of PI3K/Akt and ERK signaling pathways. *Cancer Lett.* **332,** 63–73 (2013).

237. Mauvoisin, D., Charfi, C., Lounis, A. M., Rassart, E. & Mounier, C. Decreasing stearoyl-CoA desaturase-1 expression inhibits β-catenin signaling in breast cancer cells. *Cancer Sci.* **104,** 36–42 (2013).

238. Bunney, T. D. & Katan, M. Phosphoinositide signalling in cancer: beyond PI3K and PTEN. *Nat. Rev. Cancer* **10,** 342–352 (2010).

239. Hannun, Y. A. & Obeid, L. M. Principles of bioactive lipid signalling: lessons from sphingolipids. *Nat. Rev. Mol. Cell Biol.* **9,** 139–150 (2008).

240. Wymann, M. P. & Schneiter, R. Lipid signalling in disease. *Nat. Rev. Mol. Cell Biol.* **9,** 162–176 (2008).

241. Bhat, M. *et al.* Targeting the translation machinery in cancer. *Nat. Rev. Drug Discov.* **14,** 261–278 (2015).

242. Mandal, S., Mandal, A., Johansson, H. E., Orjalo, A. V. & Park, M. H. Depletion of cellular polyamines, spermidine and spermine, causes a total arrest in translation and growth in mammalian cells. *Proc. Natl. Acad. Sci. U. S. A.* **110,** 2169–2174 (2013).

243. Loo, J. M. *et al.* Extracellular metabolic energetics can promote cancer progression. *Cell* **160,** 393–406 (2015).

244. Sumantran, V. N., Mishra, P. & Sudhakar, N. Microarray analysis of differentially expressed genes regulating lipid metabolism during melanoma progression. *Indian J. Biochem. Biophys.* **52,** 125–131 (2015).

245. Yen, M.-C. *et al.* Association of long-chain acyl-coenzyme A synthetase 5 expression in human breast cancer by estrogen receptor status and its clinical significance. *Oncol. Rep.* **37,** 3253–3260 (2017).

246. Coleman, R. A., Lewin, T. M. & Muoio, D. M. Physiological and nutritional regulation of enzymes of triacylglycerol synthesis. *Annu. Rev. Nutr.* **20,** 77–103 (2000).

247. Monjazeb, A. M. *et al.* Arachidonic acid-induced gene expression in colon cancer cells. *Carcinogenesis* **27,** 1950–1960 (2006).

248. Cotte, A. K. *et al.* Lysophosphatidylcholine acyltransferase 2-mediated lipid droplet production supports colorectal cancer chemoresistance. *Nat. Commun.* **9,** 322 (2018).

249. Kobiela, J. *et al.* Metformin and Colorectal Cancer - A Systematic Review. *Exp. Clin. Endocrinol. Diabetes Off. J. Ger. Soc. Endocrinol. Ger. Diabetes Assoc.* (2018). doi:10.1055/a-0621-8830

250. Lee, J. H. *et al.* The effects of Metformin on the survival of colorectal cancer patients with diabetes mellitus. *Int. J. Cancer* **131,** 752–759 (2012).

251. Miranda, V. C. *et al.* Phase 2 Trial of Metformin Combined With 5-Fluorouracil in Patients With Refractory Metastatic Colorectal Cancer. *Clin. Colorectal Cancer* **15,** 321–328.e1 (2016).

252. De Monte, A. *et al.* Metformin and aspirin treatment could lead to an improved survival rate for Type 2 diabetic patients with stage II and III colorectal adenocarcinoma relative to non-diabetic patients. *Mol. Clin. Oncol.* **8,** 504–512 (2018).

253. Mo, M.-H., Chen, L., Fu, Y., Wang, W. & Fu, S. W. Cell-free Circulating miRNA Biomarkers in Cancer. *J. Cancer* **3,** 432–448 (2012).

254. Diosdado, B. *et al.* MiR-17-92 cluster is associated with 13q gain and c-myc expression during colorectal adenoma to adenocarcinoma progression. *Br. J. Cancer* **101,** 707–714 (2009).

255. Kandalam, M. M., Beta, M., Maheswari, U. K., Swaminathan, S. & Krishnakumar, S. Oncogenic microRNA 17-92 cluster is regulated by epithelial cell adhesion molecule and could be a potential therapeutic target in retinoblastoma. *Mol. Vis.* **18,** 2279–2287 (2012).

256. YANG, O., HUANG, J. & LIN, S. Regulatory effects of miRNA on gastric cancer cells. *Oncol. Lett.* **8,** 651–656 (2014).

257. Zhang, J. *et al.* Circulating MiR-16-5p and MiR-19b-3p as Two Novel Potential Biomarkers to Indicate Progression of Gastric Cancer. *Theranostics* **5,** 733–745 (2015).

258. Reid, G., Kirschner, M. B. & van Zandwijk, N. Circulating microRNAs: Association with disease and potential use as biomarkers. *Crit. Rev. Oncol. Hematol.* **80,** 193–208 (2011).

259. Wozniak, M. A., Modzelewska, K., Kwong, L. & Keely, P. J. Focal adhesion regulation of cell behavior. *Biochim. Biophys. Acta BBA - Mol. Cell Res.* **1692,** 103–119 (2004).

260. Yamaguchi, H. & Condeelis, J. Regulation of the actin cytoskeleton in cancer cell migration and invasion. *Biochim. Biophys. Acta* **1773,** 642–652 (2007).

261. Sánchez-Martínez, R. *et al.* A link between lipid metabolism and epithelial-mesenchymal transition provides a target for colon cancer therapy. *Oncotarget* **6,** 38719–38736 (2015).

262. Yanaka, Y., Muramatsu, T., Uetake, H., Kozaki, K. & Inazawa, J. miR-544a induces epithelial-mesenchymal transition through the activation of WNT signaling pathway in gastric cancer. *Carcinogenesis* **36,** 1363–1371 (2015).

263. Mo, X.-M., Li, H.-H., Liu, M. & Li, Y.-T. Downregulation of GSK3β by miR-544a to maintain self-renewal ability of lung caner stem cells. *Oncol. Lett.* **8,** 1731–1734 (2014).

264. Shen, W.-W., Zeng, Z., Zhu, W.-X. & Fu, G.-H. MiR-142-3p functions as a tumor suppressor by targeting CD133, ABCG2, and Lgr5 in colon cancer cells. *J. Mol. Med. Berl. Ger.* **91,** 989–1000 (2013).

265. Andersson-Rolf, A. *et al.* One-step generation of conditional and reversible gene knockouts. *Nat. Methods* **14,** 287–289 (2017).

266. Wu, Q. *et al.* MiR-19b/20a/92a regulates the self-renewal and proliferation of gastric cancer stem cells. *J. Cell Sci.* **126,** 4220–4229 (2013).

267. Cheng, X. *et al.* miR-19b downregulates intestinal SOCS3 to reduce intestinal inflammation in Crohn's disease. *Sci. Rep.* **5,** (2015).

268. Beg, M. S. *et al.* Phase I study of MRX34, a liposomal miR-34a mimic, administered twice weekly in patients with advanced solid tumors. *Invest. New Drugs* **35,** 180–188 (2017).

269. Sun, R.-P. *et al.* In low protein diets, microRNA-19b regulates urea synthesis by targeting SIRT5. *Sci. Rep.* **6,** srep33291 (2016).

270. Bijsmans, I. T. G. W. *et al.* Characterization of stem cell-derived liver and intestinal organoids as a model system to study nuclear receptor biology. *Biochim. Biophys. Acta* **1863,** 687–700 (2017).

271. Ciorba, M. A. Scap and the intestinal epithelial stem cell niche: new insights from lipid biology. *J. Lipid Res.* **56,** 1381–1382 (2015).

272. Njoroge, R. N. *et al.* Organoids model distinct Vitamin E effects at different stages of prostate cancer evolution. *Sci. Rep.* **7,** 16285 (2017).

273. Regalado, A. Companies are testing pricey drugs in organoids. *MIT Technology Review* Available at: https://www.technologyreview.com/s/608141/organoids-proposed-to-screen-patients-for-high-priced-drugs/. (Accessed: 13th August 2018)